THÈSE DE DOCTORAT DE LA SORBONNE UNIVERSITÉ

Spécialité

Computational Neuroscience

École doctorale Informatique, Télécommunications et Électronique (Paris)

Présentée par

Jacob HUTH

Pour obtenir le grade de

DOCTEUR de la SORBONNE UNIVERSITÉ

Sujet de la thèse :

Modelling Aging in the Visual System & The `Convis` Python Toolbox

soutenue devant le jury composé de:

M. Angelo ARLEO	Directeur de thèse
M. Timothee MASQUELLIER	Co-Directeur de thèse
M. Simon THORPE	Rapporteur
M. Eduardo ROS	Rapporteur
M. Nicolas THOME	Examinateur
M. Adrien WOHRER	Examinateur
Mme. Evelyne KLINGER	Examinateur
M. Bruno GAS	President du jury

Abstract

In this thesis we investigate aging processes in the visual system from a computational modelling perspective. We give a review about neural aging phenomena, basic aging changes and possible mechanisms that can connect causes and effects. The hypotheses we formulate from this review are: the input noise hypothesis, the plasticity hypothesis, the white matter hypothesis and the inhibition hypothesis. Since the input noise hypothesis has the possibility to explain a number of aging phenomena from a very simple premise, we focus mainly on this theory. Since the size and organization of receptive fields is important for perception and is changing in high age, we developed a theory about the interaction of noise and receptive field structure. We then propose spike-time dependent plasticity (STDP) as a possible mechanism that could change receptive field size in response to input noise.

In two separate chapters we investigate the approaches to model neural data and psychophysical data respectively. In this process we examine a contrast gain control mechanism and a simplified cortical model respectively.

Finally, we present `convis`, a Python toolbox for creating convolutional vision models, which was developed during the studies for this thesis. `convis` can implement the most important models used currently to model responses of retinal ganglion cells and cells in the lower visual cortices (V1 and V2).

Résumé français

Dans cette thèse, nous étudions les processus de vieillissement dans le système visuel à partir d'une perspective de modélisation computationnelle. Nous passons en revue les phénomènes de vieillissement neuronal, les changements fondamentaux du vieillissement et les mécanismes possibles qui peuvent relier les causes et les effets. Les hypothèses que nous formulons à partir de cette revue sont : l'hypothèse de bruit d'entrée, l'hypothèse de plasticité, l'hypothèse de matière blanche et l'hypothèse d'inhibition. Puisque l'hypothèse de bruit d'entrée a la possibilité d'expliquer un certain nombre de phénomènes de vieillissement à partir d'une prémisse très simple, nous nous concentrons principalement sur cette théorie. Puisque la taille et l'organisation des champs récepteurs est importante pour la perception et change à un âge élevé, nous avons développé une théorie sur l'interaction entre le bruit et la structure des champs récepteurs. Nous proposons ensuite la STDP comme mécanisme possible qui pourrait changer la taille du champ récepteur en réponse au bruit d'entrée.

Dans deux chapitres distincts, nous examinons les approches pour modéliser les données neurales et les données psychophysiques respectivement. Dans ce processus, nous examinons respectivement un mécanisme de contrôle du gain de contraste et un modèle cortical simplifié.

Enfin, nous présentons `convis`, une boîte à outils Python pour la création de modèles de vision convolutionnelle, qui a été développée lors de cette thèse. `convis` peut mettre en œuvre les modèles les plus importants utilisés actuellement pour modéliser les réponses des cellules ganglionnaires rétiniennes et des cellules des corticales inférieures (V1 et V2).

Contents

List of Projects

0.1 Introduction

In nordic mythology, the goddess Idunn is the keeper of a wooden box, filled with magical apples. Whenever the gods feel that they grow old, they eat one of her apples and become young again[1]. The wish to not grow old is an ancient one. A more menacing thought from the greek pantheon concerns the three Moirai, who cut the string of life, giving each mortal their destiny and time to live at birth. And even when a mortal is granted immortality, the gods might forget to also give them eternal youth. This thesis is not about mythology, even if this introduction might make it seem this way. It is instead part of the scientific endeavour to "find Idunns apples", to study the aging process in the hope of - if not quite providing complete rejuvenation - at least improving the quality of life in old age.

The increase in life expectancy due to advances in medicine is leading to a larger percentage of the population that reaches high age and faces the problems that come with it.

In this thesis we investigate the neural components of the aging visual system. We use computational modelling to evaluate fundamental hypotheses and to relate theory, neural recordings and psychophysics. From the perspective of aging research, computational models can help to reduce the large variety of aging mechanisms to a small number of causes. For computational neuroscience, the phenomenon of aging gives us the opportunity to test current models of the nervous system.

In this thesis we focus on a small number of hypotheses in the wide field of aging phenomena. We propose that aging effects in neural responses and perception could be mainly caused by (1) changes in input statistics (due to e.g. sensory receptors being more variable), (2) changes in plasticity mechanisms, (3) changes in white matter or (4) changes in cortical inhibition. These hypotheses allow us to slowly advance our understanding of aging phenomena by comparing computational models with observed data from electrophysiology and psychophysics.

In relation to the first aging hypothesis, we examine the change in receptive fields that occur in age. We show that, while increased receptive fields reduce the amount of input noise, increased input noise can induce larger receptive fields through a mechanism as simple as classical spike-time dependent plasticity (STDP). We model the effect of input noise on contrast gain control and variability of neural spike trains and from this can derive an explanation of why the magnocellular and parvocellular pathways are affected to different degrees by aging. In another project, we model the effect of cortical organization on perceptual contrast thresholds. Even if this project is so far not conclusive, the methodology gives us the opportunity to draw conclusions on response properties of large populations of neurons in the sensory cortices without the need for invasive electrophysiology.

As a methodological advance, we present `convis`, a Python modelling toolbox that can compute a wide array of vision models and provides automated differentiation for all models automatically. Even though this tool is not particularly related to aging, it is included in this thesis, since we used it in some of the modelling work and it also comprised a significant proportion of my work as a PhD student.

The toolbox is an answer to the problem that previous modelling tools we used were not capable of using arbitrary, spatio-temporally inseparable filters. Since we assumed that the aging visual system might suffer changes that change the shape of receptive fields away from idealized, compact Gaussian functions to less compact, patchy receptive fields, we wanted to

[1] free after the *Prose Edda*

create a tool that mimics the functions of previous models, but can optionally perform spatio-temporal convolutions with arbitrary receptive field shapes. Since we are using a back-end that was designed mainly with deep- and convolutional-neural-networks in mind (`PyTorch`), we can provide efficient 3d-convolutions that can be performed on a GPU. We also get the added benefit of automated differentiation from using this framework, which makes it possible to use gradient descent methods on models that previously had to be fitted using very computing intense methods such as parameter grid-search or Monte-Carlo simulations.

> Old age isn't so bad when you consider the alternative.
>
> *Maurice Chevalier*

0.2 Contributions

The thesis is divided into five chapters and distinct *projects* are highlighted in each chapter, most of which tackle a specific hypothesis or problem. Two of these projects were done in collaboration with master students. I want to use this opportunity to give them credit for their work, which for the sake of completeness I summarize at the appropriate point in the thesis without the intention to appropriate it. I also want to stress that supervising the students was the most rewarding work I have done during my PhD.

Section 3.5.2 presents the work of Emilie Mayer who joined the team for a 6 month internship in 2016. After completing her Master studies at the Ecole de Mines ParisTech, she enrolled in a medical school and is now on the path of becoming a great practitioner. During the internship she modified the VirtualRetina software and performed a set of simulations and analysis investigating the different reactions to noisy input of M- and P-pathway cells.

In section 4.7.1 the results of Atle Eskeland Rimehaug's internship project are presented. Atle has a Bachelors degree in Cognitive Psychology, then changed studies to Physics and wanted to complete an internship in our group in spring 2018 to gain experience since he wanted to apply for PhD positions in neuroscience. Starting from a model I created some time earlier and modified for this project, he had the task of running the stimulation with a range of parameter pairs, analyse the results and relate his findings to our hypotheses and available literature.

My personal contributions start with a review of aging mechanisms, which I wrote up and presented to the lab after my first 6 months in the team. I since extended the review, which now comprises chapter 1, to be more centred on aging mechanisms that relate to neural mechanisms resulting in a set of neural aging hypotheses, which set the framework for most of the following considerations. We aim to publish this chapter in a modified version as a review paper.

Chapter 2 builds on the hypothesis that receptive fields adapt to compensate for input noise and discusses theoretical considerations and evidence that could be collected to confirm or refute this hypothesis. While I do not claim to having the initial idea, all extensions presented in this chapter are my own. I simulated a small neural network to prove that STDP can be a possible mechanism for this adaptation. The connection between STDP, input variability and receptive field size has not been studied extensively so far, so we aim at submitting a paper about this novel proof of concept and the theoretical considerations soon.

In chapter 3, I concentrate on methods that relate directly to neural signals. I present a number of established methods and present a novel spike pseudo-distance that avoids correlating with the information content due to firing rate differences. In section 3.4.2 I discuss my analysis of multi-electrode array (MEA) recorded retinal ganglion cell (RGC) data. The data was collected by Vidhya Krishnamoorty and colleagues in the Lab of Tim Gollisch in Göttingen. The goal of my analysis was to estimate how many successful recordings are necessary to confirm hypothesized changes in RGC receptive fields with age. Specifically I want to thank Vidhyasankar Krishnamoorthy, Fernando Rozenblit, Norma Kühn, Mohammad Hossein Khani, Helene-Marianne Schreyer, Jian Liu, Michael Weick and of course Tim Gollisch for welcoming me in their laboratory and discussing the state-of-the-art methods and problems of large scale retinal recordings which I outline in section 3.4.2.1. The results of the analysis suggest that a direct measurement of RGC receptive field change in age requires either a large amount of experiments or novel methods as the stochasticity of the recording process and random sampling of cells make it hard to find significant differences even if we assume a relatively large change of 10% in receptive fields size.

The differential aging in M and P pathways then directly leads to project 3.5.2 that Emilie executed during her internship which became her Master Thesis, so the simulations and analysis presented in that section were performed by her under my supervision. Project 3.5.3 then contains my follow up analysis that was again my own work. We show that gain control could indeed be the defining difference that makes the magnocellular pathway more resistant to noise and thus aging effects.

Chapter 4 is in contrast to the previous chapter more concerned with what we can learn from psychophysics and how we can use the perceptual thresholds of neuromorphic models to test theories about contrast thresholds at different spatial frequencies and noise levels. I created a very simple cortical model to test the effects of receptive field size, number of cells and lateral inhibition. Atles project was to run a version of the model with varying receptive field sizes and cell numbers. In addition to presenting his findings in section 4.7.1, I also extend the analysis to the effect of lateral inhibition and present it in section 4.7.2. With the combined results we aim to create a simple computational model of the aging visual system, which is verified not by electrophysiological data, but simple, psychophysical measurements.

The last chapter presents `convis`, the Python toolbox for convolutional vision models I built during my PhD. This work has been published as Huth, Masquelier, and Arleo 2018. The toolbox contains my reimplementations of vision models from the retina (Wohrer 2008, Mcintosh et al. 2016 and Real et al. 2017), primary visual cortex and even secondary visual cortex (Rowekamp and Sharpee 2017). In addition to the initial release presented in the paper, I also discuss fitting procedures and spiking mechanisms in more detail.

0.3 List of Conference Attendances and Oral Presentations

Date	Conference Attendance, Posters and Oral Presentations	Location
2015	**Joining the Team as Assistant Researcher**	
April 2-3	European Institute For Theoretical Neuroscience (EITN) SP9 Workshop	EITN, Paris

Date	Conference Attendance, Posters and Oral Presentations	Location
June 17	1er Symposium des Neurosciences Computationelles a l'UPMC	UPMC, Paris
June 22	Visiting the Group of Tim Gollisch in Göttingen **Oral Presentation:** "Characterizing Noise that Causes Deteriorating Vision During Aging"	EITN, Paris
Oct. 1-3	European Retina Meeting	Brighton, UK
Dec. 14-15	Sensory Encoding by Neural Systems Workshop	ENS, Paris
2016	**Official Start of the PhD:** 16th of January 2016	
Jan. 19-20	EITN Modelling the visual system Meeting	EITN, Paris
Jan. 28-29	Neuroscience Workshop Saclay (NEWS) **Poster Presentation:** "Modeling the Visual System with Respect to Aging"	Campus Paris-Saclay
Feb. 4 - March 11	Spring School: Interdisciplinary College **Poster Presentation:** "Modeling the Visual System with Respect to Aging"	Günne/Lake Möhne, Germany
May 9	Seminar of the Department of Visual Information Processing **Oral Presentation:** "Modelling aging in the early visual system"	IdV, Paris
May 20-21	pyData	Berlin
Sept. 7	Emilie Mayer's Master Thesis Defense	Ecole de Mines, Paris
Sept. 20-25	Bernstein Conference of Computational Neuroscience **Poster Presentation:** "Using Equivalent Internal Noise as a Constraint on Vision Models"	Berlin
2017	**2nd Year**	
March 22-24	École des Neurosciences Paris - ENP Days	Collège des St. Bernadins, Paris
April 26	Full-day TensorFlow training by Google	Paris
May 31	2eme Symposium des Neurosciences Computationnelles à l'UPMC **Poster Presentation:** "The convis framework - Simulation of the Visual System with Automatic Differentiation using theano"	UPMC, Paris
June 12-13	PyParis	Paris-Courbevoie
July 15-20	CNS 2017 **Poster Presentation:** "The convis framework - Simulation of the Visual System with Automatic Differentiation using theano"	Antwerp, Belgium
July 31 - Aug. 4	G-node Summerschool Neural Data Analysis	Munich, Germany

Date	Conference Attendance, Posters and Oral Presentations	Location
Aug. 25-27	VSAC 2017 **Poster Presentation:** "The convis framework - Simulation of the Visual System with Automatic Differentiation using theano"	FU Berlin
Sept. 12-17	Bernstein Conference 2017 **Poster Presentation:** "The convis framework - Simulation of the Visual System with Automatic Differentiation using theano" (v2)	University Göttingen
Sept. 25	Essilor Internal Poster Presentations **Poster Presentation:** "The convis framework - Simulation of the Visual System with Automatic Differentiation using theano" (v2)	IdV, Paris
Oct. 5-7	European Retina Meeting 2017 **Poster Presentation:** "Effects of Noise on Contrast Gain Control" **Poster Presentation:** "The convis framework - Simulation of the Visual System with Automatic Differentiation using theano" (v2)	Paris
Dec. 18	Essilor Research & Science Interaction **Poster Presentation:** "The convis framework - Simulation of the Visual System with Automatic Differentiation using theano" (v2)	Essilor Créteil
2018	**3rd Year**	
Feb. 5-6	EITN workshop on Cortical Codes	EITN, Paris
Feb. 27	Cognitive Computation Symposium: Thinking Beyond Deep Learning	City University, London
March 13	Visiting the Instituto de Microelectrónica de Sevilla **Oral Presentation:** "What has deep learning ever done for us?"	IMSE, Seville
April 12	IdV Methods Day 2018 **Poster Presentation:** "What has Deep Learning ever done for us? - Simulating the Visual System with convis" (v1)	IdV, Paris
May 15	NeuroComp @ Paris 2018 **Poster Presentation:** "What has Deep Learning ever done for us? - Simulating the Visual System with convis" (v2)	UPMC, Paris
June 26	Visit to Centre de Recherche Cerveau et Cognition **Oral Presentation:** "What has deep learning ever done for us?"	CerCo, Toulouse
July 7-11	Forum of the European Neuroscience Society (FENS 2018) **Poster Presentation:** "What has Deep Learning ever done for us? - Simulating the Visual System with convis" (v3)	City Cube, Berlin

UPMC: Université Pierre et Marie Curie, now Sorbonne Université, Paris

IdV: Institut de la vision, Paris

EITN: European Institute For Theoretical Neuroscience, Paris

Chapter 1

Aging Effects on Neural Mechanisms

> And it came to pass, that Isaac was old, and his eyes were dim.
>
> *Genesis, Chapter 27, Verse 1*

1.1 Introduction

Aging is a complicated, multifaceted process. The workings of the nervous system are complex at its best and perplexing in the many aspects in which it is still opaque to our scientific investigations. We think that the combination of these two areas of study, aging research and neuroscience, can help us to understand which neural mechanisms are vital to perception and cognition and conversely which aging processes can be influenced and which work in fact to compensate for other, detrimental changes. As a more narrow field of investigation we chose the visual system, as it provides a range of investigative tools and also has a strong impact on well being. In this chapter, I will summarize important aging processes that affect the visual system and develop hypotheses how neural mechanisms and aging mechanisms could interact in section 1.9.

Neurons are not only subject to the general aging mechanisms as all other cells (be it programmed or accumulated damage), but also to very specific break downs unique to neural function and specific effects of general processes (e.g. Calcium buffering). The sensory modalities, in specific the visual system, have to deal with specific problems in addition to that. The brain is plastic and adapts to its environment and usage. In the aging process this is relevant at two fronts: 1) neural adaptation can compensate or aggravate aging processes and 2) if the adaptation itself is subject to changes induced by aging, the brain might be unable to adapt to changing circumstances - whether induced by aging or not.

1.2 How Old is Old?

To investigate aging scientifically, it is necessary for some methods of analysis to separate subjects into age groups, so that the observations made about each group can be observed. While the definition of aging itself is open to various interpretations (Sacher 1982), at least

the definition of age is established and can be used as a proxy. But since aging is a stochastic process, it is hard to separate participants in a study into *young* and *old* groups based solely on a single age threshold. There are large inter-individual differences in the aging process that can mask significant aging effects. Many studies in humans, but also other animals, separate their *young* and *old* groups by a broad margin, e.g. for human studies a *young* group of participants between 19 and 25 years old and an *old* group of 65 years and older. This is convenient for recruitment, as the *young* age group corresponds to the age of university students which can be easily recruited for experiments as well as for a clean separation of the two populations: The probability that a fast aging 25 year old will show stronger aging effects than a slow aging 65 year old are a lot smaller than when comparing e.g. 35 and 55 year olds. But this method excludes a large portion of population where the dynamics and variability of aging is the most heterogeneous but where individual differences might give insight into mechanisms for successful aging. Table 1.1 gives an overview of commonly used age group ranges (with a more detailed table found in Appendix 7.1). It is notable that the longest human life span reported (122 years) is twice the lower bound of the *old* age group (60 years in some studies). The group of *oldest old* for humans is defined as subjects older than either 80 or 85 years (depending on the study) and also has been studied extensively (e.g. in Gussekloo et al. 2005; Andersen-Ranberg et al. 2005; Arai et al. 2015). Correlation studies and longitudinal studies use a more fine grained analysis where they plot their data over the age of the participants, which also allows to investigate the speed of aging at different ages and the spread of the population. But these studies require a larger amount of participants and data than studies that rely on group comparison.

Table 1.1: Age limits of different species summarized from a range of scientific studies. A table listing the studies considered and the corresponding age ranges can be found in Appendix 7.1

Animal	Young Age	"Early Aging"	Old age	Expected Lifespan	Max. Reported Lifespan
Human	20-60 years		60 or more years	72 years[a]	122 years[a]
Monkeys					
- Rhesus Monkey	5-15.2 years	21-22 years	17.5-32 years	40 years	
Mouse					4.3 years
- C57BL/6	10 months		25 months	27 months	3.3 years
- wild derived[a]				34 months	4.0 years
Rat					
- Norway Rat	7-8 m.		27-35 m.		46 months
Aplysia caifornica	< 240 days		>240 days		

[a] WHO 2016.

[a] Whitney 1997.

[a] Miller et al. 2002.

1.3 Which Changes in Age Do We Want to Explain?

To set the scope of the topics discussed in this review we will start with the resulting effects that are observed, but not fully explained, which we will try to connect to the low level changes discussed in Sections 1.5, 1.6, 1.7 and 1.8. The explananda we discuss focus mainly on visual psychophysics, but also include observations about executive functions and neurological changes.

1.3.1 Visual Perception

In terms of visual perception, the most notable change is a decrease in contrast sensitivity (CS) and acuity in general. One might think that these changes can be readily explained by optical factors and we review the optical changes in the eye and their immediate consequences in Section 1.7.1, but even if these changes are accounted for, there are still differences between young and old subjects (Owsley 2011).

Changes in *Flicker Fusion* show that the speed of visual processing is decreased. Brozek and Keys 1945 and Mewborn et al. 2015 found that age adjusted *critical Flicker Fusion* was predictive of a shifting attention task. Bennett, Sekuler, and Sekuler 2007 found a decrease in motion direction sensitivity for short stimuli.

According to Spear et al. 1994, the magnocellular and parvocellular pathways show different aging effects psychophysically. We discuss this in more detail in section 3.2.2.1.

1.3.2 Psychophysical Inhibition, Attention and Executive Functions

One concern is a decline in visual attention while driving a car, which can lead to an increased chance of accidents (Kline et al. 1992). Older subjects show a deterioration in the *Useful Field of View* (Sekuler, Bennett, and Mamelak 2000), which the authors conceptualized as subjects being less able to extract information from a cluttered scene.

Executive functions like the capacity for attentional inhibition are also altered in age and give rise to its very own aging theory (Dempster 1992): The resistance to interference is a major factor in aging ("Interference Theory"). This theory supposes changes in the frontal cortex, which enables suppression of stimuli that are not relevant for the task which also gave it another name: "Frontal Aging Hypothesis".

In a auditory-visual distraction task Andrés, Parmentier, and Escera 2006 found that old subjects were less able to filter out irrelevant auditory information. Kramer, Humphrey, et al. 1994 and Faubert and Bellefeuille 2002 found no differences between the distractability of young and old subjects.

As neuroscientists, we usually have a different definition of inhibition, namely inhibitory synaptic connections. Later we will present electrophysiological studies showing that neural inhibition is decreased in age as well. But already with psychophysical methods, the effect of neural inhibition can be seen. In visual motion processing the center-surround antagonism is reduced (Betts et al. 2005), which means that lateral inhibition in the visual cortex must be reduced. This mechanism, although it is a very low-level neurological effect, it has consequences that can be observed psychophysically. It is easier to judge the motion direction of a small, high contrast stimulus than an increasingly larger one. This is because the high-contrast stimulus activates the lateral surround inhibition that usually enhances contrast for

small stimuli. A similar effect is psychophysical crowding (e.g. Manassi, Sayim, and Herzog 2012), where perceptions of one stimulus can be prevented by adding other visual stimuli in its vicinity. This suppression seemed diminished for old subjects in the task of Betts et al. 2005 and also Karas and McKendrick 2009, as it took them significantly less time to give an answer than young subjects. Schefrin, Bieher, and Werner 1997 found that the area of complete spatial summation enlarges with age, also hinting at reduced inhibition. Finally, Syka 2010 used a rat model to investigate auditory senescence. Since the auditory hair cells themselves were intact, they explained the increased thresholds with reduced GABA inhibition.

1.3.3 Neurological

Using *EEG* to measure visual evoked potentials (VEPs) shows strong age effects as well in amplitude as well as latency Tobimatsu et al. 1993. A similar result was found by Yao et al. 2015 in cats and Schmolesky et al. 2000; Leventhal et al. 2003; Yu 2005 in macaque monkeys, when they recorded directly from neurons in the visual cortices and found that visual signals arrive with a delay. Xi et al. 1999 found conductance speeds of pyramidal axons themselves to be slower.

In the middle temporal visual area (V5 or MT) of aged macaque, direction selectivity is reduced (Liang et al. 2010), as well as stimulus selectivity in *V1* (Schmolesky et al. 2000). The surround suppression of cells in the primary visual cortex of old macaque monkeys was found to be reduced as well and is probably related to selectivity (Fu et al. 2010). Similarly, Zhou et al. 2011 found decreased intracortical inhibition that resulted in decreased contrast sensitivity in the neurons of aged cats visual cortex. In human primary motor cortex, inhibition is also reduced, as found with a EMG/TMS paired-pulse paradigm by Peinemann et al. 2001.

In terms of cortical organization, the visual system is restructuring itself drastically (Brewer and Barton 2011): In humans, the overall area of the visual cortices shrinks and the size of population receptive fields (pRFs) increases. We further discuss the changes to population RFs in section 2.3.1.

1.4 General Aging Theories

According to Lipsky and King 2015 there are more than 300 aging theories. In addition, the definition of aging is itself open to various interpretations (Weinert and Timiras 2003). In greek mythology, the cruel irony has already been noted, that delaying death is not the same as stopping aging:

The greek goddess Eos fell in love with Tithonus of Troy and asked Zeus for the gift of immortality for her lover, which he grudgingly granted. But since Eos did not ask for eternal youth, Tithonus grew older and weaker, but he could not die. In the end he shrunk, such that only his voice remained.[1]

Still, a number of aging studies define aging as the progressive changes that are linked to increased risk of disease and ultimately death e.g. Harman 1981 or Liochev 2015. The main goal of these studies is extending human life span, which is why they measure lifespan in animal models as the defining characteristic of delayed aging. But the alternative definition

[1] free after the Homeric Hymn to Aphrodite

of aging, the one we are more interested in, is about the quality of life in old age. When longevity rises, the scientific community still expects the onset of age-related neural diseases to remain fixed (World Health Organization 2015), leading to an increased morbidity, not a decrease. The aging factors that are correlated with longevity can very well be different than the ones associated with neural aging. There might still be common causes and processes that behave similarly, which is why it can be helpful to also take a survey of (longevity-) aging science as these studies gathered a lot of data about what happens in old age in a number of species.

Aging theories can be sorted into two groups: those that believe that the primary changes in due to age are *programmed* and those that believe that the changes are accumulative *damage* or *errors*. Later, we will also talk about changes that are possible secondary changes, i.e. responses to aging changes, which can be *compensatory* or *exacerbatory*.

1.4.1 Programmed Aging

Theories of *programmed* aging assume that part of our DNA evolved specifically to govern the behaviour of protein expression in old age. While some programmed changes definitely exist, such as menopause as a programmed change in the neuroendocrine system (or puberty as an earlier example of programmed, age dependent hormone expression). The change in the neuroendocrine system of both men and women in high age could thus be an age-dependent, programmed process. Hormone replacement therapy is indeed used as anti-aging strategies by physicians (Boccardi and Herbig 2012). Twin studies estimate that about 20-30% of the variability in lifespan variability can be explained by genetics (Cournil and Kirkwood 2001; Barzilai et al. 2012) and genes are being investigated that are associated with aging or even cause premature aging (progeria or progeroid syndromes). An example for a progeric gene in a model organism is the *klotho* mutant mouse Vanhooren and Libert 2013, which exhibits reduced life span, decreased activity, infertility, osteoporosis, arteriosclerosis and atrophy of the skin similar to aged mice, all from the alteration of a single gene.

Another interpretation of *programmed* aging is “antagonistic pleiotropy”: the idea that some genes that are beneficial in young age might pose a disadvantage at a later stage in life (Williams 1957). As an example, muscle effectiveness might be evolutionarily enhanced by oxidative processes, that increase the amount of free radicals beyond sustainable and repairable levels. Increased levels of testosterone increase the risk of atherosclerosis in the long run, but might give short term benefits. A question these theories raise is whether aging is subject to evolutionary forces or not and there are theories on both sides of the debate.

1.4.2 Damage Theories vs. Usage Theories

In the 1920s, Pearl 1924 stated that the amount of heavy labour done after the age of 45 is proportional to a decrease in life span. Even if we ignored that prior to 1920, heavy labour was in all likelihood also related to exposure to industrial chemicals, dusts, etc., the fact remains that e.g. arthritis is exacerbated by increased stress on the joints and similar changes can be correlated to more activity. The accumulation of damages from usage, accidents, diseases, etc. then would lead to a decreased functioning, loss of cells and aging phenotypes. One of the byproducts of this damage - *lipofuscin*[2] - correlates with oxidative enzymes and

[2]lipofuscin: from latin "fuscus": dark; and greek "lipos": fat

activity, which shows according to Friede 1962 that activity leads to wear, which is reflected in the amount of oxidative metabolism. However, living organisms possess repair mechanisms for many of the damages that stochastically occur over the course of a life time. Wang, Michelitsch, et al. 2009 updated the wear-and-tear theory to a theory of misrepair: since repair mechanisms also work stochastically, their action might introduce the actual aging effects.

Swaab 1991 contrasts "wear and tear" with "use it or lose it", stating that while in non-neural cells, increased activity usually is associated with an increased rate of aging, neurons require regular activation. The author even speculated that the activation of neurons could stimulate protective mechanisms such as DNA repair.

As we will discuss later in section 1.8.4, this is especially true for the synaptic connections between neurons. On a behavioural level Salthouse 2006 states that while many studies have found a positive relation between training, expertise or mental activity and cognitive functioning, very few studies found an interactive effect of age and mental activity on cognitive function. So, while mental exercise will definitely provide positive effects (in old and young) that will also counter aging processes, a lack of exercise is so far not proven to be a cause of age related cognitive decline.

1.5 Cell Specific Aging Mechanisms

I will start this review of aging mechanisms with cellular mechanisms that apply to all or most cells in mammals. In the following sections I will then talk more specifically about neurons and supporting brain cells and finally neurons of the visual system specifically.

The general cell aging mechanisms I will discuss are specifically the shortening of telomeres (1.5.1), changes in the life cycle of cells and the cells' reaction to ROS induced stress (1.5.2) and changes in calcium dynamics (1.5.2.1). While each of these phenomenons are undoubtedly linked to aging and are heavily investigated, currently, there are no clear mechanistic consequences that we can causally link to behaviour or well being other than by a generic assumption that cells are disturbed in their function. A link that I will later discuss with neural function is the change in calcium dynamics (see section 1.8.3) that could influence neural plasticity.

1.5.1 Telomeres

In many organisms we can find physical correlates to the aging process on a cellular level that might enable us to objectify at least some components of the aging process so that they can be compared to the actual age as well as to the fitness of the individual. One such marker stems from the way our cells replicate. During mitosis, the DNA in a cell is copied, however at each replication, the ends of each DNA strand gets slightly shorter. To preserve the integrity of the information stored in the DNA, each strand starts and ends with replications of the pattern *TTAGGG*, that are called the *telomeres* (from the greek for "end part") that also tell the replicating machinery to stop copying. While this portion of the DNA might serve many purposes, it is relevant for us that at each shortening of the DNA, for many replications only parts of the telomeres are lost, which has no negative impact on the DNA itself. But as soon as the telomeres are removed completely, the cell fails to copy the DNA. This creates a natural

count-down, starting with 11.000 base pairs at birth declining to less than 4.000 base at 75 years or older (Arai et al. 2015).

The idea of this clock ticking down inevitably and creating a hard limit on lifespan is pretty scary and parallels the greek myth of the three fates spinning the thread that represents life and cutting it to its allotted length. A number of research projects work on investigating the dynamics of telomeres and work on therapies that can reverse the shortening of telomeres. Telomerase, a protein that preservese telomere length during copying can be an important ingredient in this endavour. But it might be questionable if decreased telomere shortening is desirable as it might be a protective mechanism. Boccardi and Herbig 2012 pose the theory that this hard limit on cell replications is a protection against cancerous cells - similar to a computer program, that prevents infinite looping by including a iteration counter. The data from (Arai et al. 2015) shows a strong decline in telomere length, but not a complete loss of telomeres even in very advanced age. It is plausible that cells that divide often will lose their telomeres earlier which might mean that certain cell populations might fail a lot earlier than the decline mentioned above which was measured in DNA extracted from whole blood prepartions.

Since mouse telomeres are very long (40-60kb) and they exhibit telomerase, the replication limit or mouse fibroblasts - although it looks similar human fibroblast aging - is believed to not depend on telomere shortening, but governed by an external process such as oxidative stress (Itahana, Campisi, and Dimri 2004). Nevertheless, when telomerase was deleted in a gene modified mouse model, after a few generations a disappearance of telomeres could be observed which lead to early aging phenotypes and skin-cancer resistance (for sources see Itahana, Campisi, and Dimri 2004).

It should be mentioned, that Arai et al. 2015 found no correlation between length of telomeres and performance in cognitive tests. They even found a paradoxical increase in telomere length when comparing 100 year old participants with participants aged 110 and older - which could be e.g. explained by survivor bias.

The impact of telomere loss on cells might be very similar to cell loss due to any other kind of cause, with the added complication that also no new cells can be created. In section 1.5.3 we assess whether there is evidence for reduced cell genesis in aging.

My cautious conclusion on the current state of research about telomeres in high age is that neither human longevity nor cognitive performance are primarily limited by the shortening of telomeres.

1.5.2 Oxidative Stress and Changes in the Cell Life Cycle

Since it was shown that in rodents telomeres were not the limiting factor on life span as they have much longer telomeres than humans and express telomere extending proteins, alternative explanations were sought to explain why rodents show signs of senescence as well and their fibroblast cells also have a finite number of replication cycles in laboratory conditions (Itahana, Campisi, and Dimri 2004). Instead of showing decreased telomeres, the fibroblast cells of mice that stopped replicating showed signs of increased oxidative stress and oxidative DNA damage. However, the cells were kept at air oxygen levels, which is many times higher than the physiological conditions these cells normally encounter. Mouse fibroblast cells that were then cultured in lower oxygene concentrations did not show senescence. Through cancer detecting proteins, one of which being the retinoblastom protein *Rb*, oxida-

tive stress causes an arrest of cell division or apoptosis to prevent potential cancerous cells from spreading. The senescence in mouse fibroblast cells looks so similar to human fibroblast cell senescence, since both activate *Rb*, leading to similar consequences. That processes in the metabolism could be responsible for aging has been formulated more than a century ago (Rubner 1908), out of observations that the speed of aging is related to the speed of metabolism. Since then, it has been shown in multiple species that restricted caloric intake has a positive influence on longevity Ristow and Zarse 2010. The *caloric restriction* paradigms consist of providing a diet that contains a certain percentage of calories compared to the *ad libidum* consumption that would be typical for the animal. E.g. a mouse would recieve 70% of the food it would normally eat in a day, or would receive less calorie dense food.

Oxidative stress occurs when aerobic metabolism creates large quantities of reactive oxygen species (ROS), such as $O_2 \cdot^-$, H_2O_2 or $\cdot OH$. These highly reactive molecules can attack lipids, proteins and DNA. In this process *lipofuscin* is created as a byproduct. It was found to correlate so strongly with age that it has been called the *age pigment* Harman 1981.

Cells use energy and their demand of energy has to be regulated strictly. A sensor for energy consumption in eukaryotic cells is AMP-activated protein kinase (AMPK). This sensor is intricately linked into the cell cycle and even neural functions, such as membrane excitability (Hardie, Ross, and Hawley 2012) and plasticity (Potter et al. 2010).

Early theories about the effect of free radicals assumed that more metabolic activity will lead to more free radicals, especially in the mitochondira (Harman 1981), leading to damage and thus aging. This was first confirmed by experiments linking caloric restriction to longevity, but it is (now) in stark opposition to these experiments, as it was shown that caloric restriction *increases* oxidative stress rather than relieves it (Ristow and Zarse 2010). In fact the whole story around anti-oxidants was turned on its head. While previously it was thought that oxidative stress in cells has only detrimental effects and anti-oxidants can relieve that stress and counter all negative effects, it seems to be the case that the defence mechanisms of cells use oxidative stress as a promoter for many maintenance processes, including binding ROS, but also initiating *DNA* repair, which antioxidants by themselves don't. In this shift Mittler 2017 published a paper titled "ROS are good" describing that ROS are even necessary for cell proliferation and differentiation. Caloric restriction survived this shift since it is a fairly reliable effect in rodent models, only the mechanism was inverted from caloric restriction preventing metabolism and thus reducing ROS, to caloric restriction shifting between different forms of metabolism, leading to more ROS, which promotes e.g. cell repair.

As bottom line we want to conclude that there certainly is something interesting going on that in the end will also have strong effects on neurons (which have a notoriously high energy demand), but so far these intracellular mechanisms were not shown to interfere with neural function in a predictable way. They might possibly be a causal mechanism for studies that showed a link between physical exercise and neuro-genesis (for a review see Kramer, Bherer, et al. 2004), as the proliferation could be mediated by oxidative stress.

1.5.2.1 Change in Cell Calcium Dynamics

In aging, two mechanisms for Ca^{2+} clearance are disturbed: buffering and removal. Ca^{2+} buffering binds Ca^{2+} intra-cellularly, such that it can be made available if needed, but is otherwise inactivated for any chemical processes. In aging the amount of Ca^{2+} that can be

buffered is greatly reduced (Duckles, Tsai, and Buchholz 1996; Villa et al. 1994). If Ca^{2+} can not be bound internally and disturbs cellular function, it must be removed from the cell, e.g. by Ca^{2+} channels in the membrane which form an integral part of the activity dynamics of many neurons. That this mechanism is also disturbed can be observed in neurons having a prolonged recovery time after they experienced an influx of Ca^{2+}. This can be measured as a strong after hyper polarization (AHP), which in old animals was found to be greatly increased (Toescu and Verkhratsky 2000).

We will examine in section 1.8.3 the effect changes in Calcium Dynamics have on plasticity.

1.5.3 Evidence of Cell Loss and Genesis

It has long been believed that we lose neurons in aging (Shefer 1973) and that neuro-genesis ceases in adult organisms. While e.g. in Alzheimers and other neuro-degenerative diseases there is a significant loss of neurons (Coleman and Flood 1987), it is now fairly certain, that in healthy aging there is no significant cell loss - with a few specialized exceptions. Rather, previous reports of loss were affected by methodological problems (Peters, Morrison, et al. 1998), such as a differential change in the volume of the collected tissue. With advances of methodology and an increasing number of studies, this myth could be disproven. At most a localized loss of up to 10% in sub-populations of neurons would be possible according to Peters, Morrison, et al. 1998, however if these sub-populations serve an important function, even this could play an important role.

One group of cells that was shown to be diminished are sensory receptors such as photoreceptors (see section 1.7.1.2), hair cells in the auditory system (Engle, Tinling, and Recanzone 2013) and mechanoreceptors (Stevens 1992). These cells do have an important function since they connect our nervous system with the outside world. But since they have to be exposed to photochemical and mechanic activity, they are also under increased risk of malfunctioning and cell death.

The idea that the nervous system is fixed after development and no new neurons are generated in adult organisms has also been held for a long time. But starting with Altman 1962, evidence was found that new neurons are born constantly in the striatum and dentate gyrus of the hippocampus (Eriksson et al. 1998), countering potential neural loss. Kannangara et al. 2011 found that in laboratory mice exercise can even enhance neurogenesis and also reduce stress hormones. Since the methods for labeling and tracking progenitor cells is very invasive, the data on human neurogenesis is less certain than e.g. in rodents. Sorrells et al. 2018 even found no neuro-genesis comparable to other studied organisms in humans at all, but it must be noted that they base their observation on post-mortem histological analysis and not on carbon dating as e.g. Ernst and Frisén 2015 or on labeling and tracking actual neuron migration of newly generated neurons such as Altman 1962. But even if we trust their data, it can hardly be thought of as an effect of old age, as they found neuro-genesis to cease already at 13 years of age.

Overall, general neural cell loss can be said to be characteristic only of neuro-degenerative disease, not general aging. We would expect neuro-genesis to still operate in adult organisms, despite counter evidence, however this is not crucial to any of our arguments since neuronal cell count seems stable and cells that do exhibit losses due to age, such as photoreceptors, do not have pathways for neural progenitors to migrate to them, and are only developed during

a specific critical period during development.

1.6 Neuro Specific Aging

Neurons carry and produce the activity patterns that allow us to perceive and act, which makes them very important cells, but due to their complex intracellular activity and ability to rewire subject to detrimental aging effects.

Aging effects on neurons have been observed in specific regions and in specific mechanisms.

Myelin sheaths of long-range white matter axons begin to decay in age (Schmidt et al. 2011). Specialized glial cells, s.c. Oligodenrocytes, form isolating layers which wrap many times around the axons crossing larger distances in the central nervous system. This isolation creates a larger membrane resistance which allows neural signals to be transmitted faster and at a lower energetic cost. In age, and even more so in diseases such as Alzheimer, these sheaths loosen and pockets of extracellular medium ("balloons") can be found between the different layers (Peters, Sethares, and Killiany 2001). The disruption of the isolating function of the myelin sheaths results in slower conductance velocities. Ultimately this process leads to a loss of myelinated nerve fibres (Marner et al. 2003).

Neural inhibition was found to be altered in age as well. Peinemann et al. 2001 reported a decrease in the excitability of intracortical inhibitory networks in human motorcortex using *TMS*. Cheng and Lin 2013 also found a decrease in cortical inhibition mostly in the primary somatosensory cortex, but not in the secondary somatosensory cortex, revealing that there might be area specific differences. Luebke, Chang, et al. 2004 found an increase in inhibitory currents in patch clamped prefrontal cortex cells of rhesus monkeys.

The effect of intracellular Ca^{2+} dynamics on neurons causes primarily changes in plasticity, as we will discuss in section 1.8.3.

1.7 Vision Specific

Being exposed to light is dangerous for any cell, since light induces chemical reactions by adding energy. Skin cells developed to be resistant to light exposure, but the components of our eye and the receptors and neurons in our retina have to be exposed to light to give us information about the world.

In addition the retinal diseases that cause drastic changes, some pathologies are so common, that they can be counted as normal aging processes: presbyopia and cataracts being very common issues which we today know how to treat. Even though the exact number is contested, it was unanimously found that the number of photoreceptors diminish in age and that the retina is remodelling in so far poorly understood ways.

1.7.1 Normal Aging of the Eye

1.7.1.1 Presbyopia and Cataracts

Coming from the greek roots of $\pi\rho\epsilon\sigma\beta\upsilon\varsigma$ (old) and $\omega\psi$ (eye/sight), the term *presbyopia* has been used by scholars for more than two millenia [3] to describe age related loss of sharp vision. Today presbyopia is a precisely defined condition characterized by difficulty to focus on close objects caused by the decrease of the lenses ability to accommodate to the distance of objects due to the natural hardening of the lens. It can be corrected with refractive glasses, often bifocal lenses, or with accommodative, intra-ocular implants.

The effects of presbyopia do not per se affect acuity, but only the ability to change the plane of focus to near and far locations, so high acuity vision is still possible and common at the appropriate distance. This is important to us since a general decrease in acuity would also have neural consequences (as discussed in Chapter 2).

A stronger influence the changes in the lens have on visual function are cataracts. Due to accumulation of proteins and pigments, the optical qualities of the lens changes, leading to yellowing and ultimately clouding of the lens. The link between cataracts and age is not as close as presbyopia, as smoking, diabetes and sunlight exposure increase the risk of cataracts. Even before cataracts can be diagnosed, retinal illumination and light scatter differ between young and old due to the changes in the lens of the eye.

Weale 1987 answer their own suggestive title of "Senescent vision: is it all the fault of the lens?" in the negative. In the following sections we will therefore look at other changes in the aging eye.

1.7.1.2 Loss of Photoreceptors

Rod loss in humans slows over life time, starting with ~ 1000 per mm^2 per year under 40, slowing to 300 per mm^2 per year at the age of 80 (Gao and Hollyfield 1992) with the total numbers dropping by $\sim 40\%$ from 140.000 to 80.000 per mm^2. The loss of cones is almost constant at ~ 16 cones per mm^2 per year. Over the life time the observed mean of total cones per mm^2 drops from over 5000 to about 4000, giving a loss of 20% over the whole lifetime. Gao and Hollyfield 1992 argue that for any notable reduction in visual performance at least 20% of cells need to be lost between measurements.

While neurogenesis of photoreceptors has been observed in zebrafish adult retinas (Cameron 2000), it is unclear whether a similar process can happen in mammals and specifically in humans. In any case the observed loss can be expected to have some influence on perception, but not a drastic one as e.g. is the case in retinal pathologies (see section 1.7.2). The loss of rods, even though it is quite significant over the lifespan, might be even hard to notice perceptually in the periphery where rods are most frequent and ganglion cells sum over thousands of photoreceptors. The reduction of cones in the central retina could have a stronger effect since they are important for acuity and color vision. However, the changes to the lens of the eye also impact acuity and color vision. Whether these effects mask or exacerbate each other is also not clear.

[3] 100 A.C. in "Symposiacs" by Lucius Mestrius Plutarchus or 400 BC in the writings of Aristotle

1.7.1.3 Loss of Retinal Ganglion Cells

The loss of retinal ganglion cells (RGC) in general follows the loss of cone photoreceptors (Gao and Hollyfield 1992). In the fovea 16% of cells are lost between age 20 and 60. More peripherally around 50%, however these cells follow the logarithmic loss of rods with the largest decrease below age 40 and only a slow decline afterwards.

Melanopsin RGCs Some retinal ganglion cells are themselves reactive to light through their expression of melanopsin (Sanes and Masland 2015). In many animals these cells are involved in the circadian rhythm. In old age melanopsin RGCs are more affected by cell loss than other ganglion cell populations. Also the circadian rhythm is more and more disturbed and it has been theorized that the loss of melanopsin RGCs is connected to the change in circadian rhythm (Lazzerini Ospri, Prusky, and Hattar 2017). Samuel et al. 2011 found melanopsin cells in their mouse retina preparations, but did not comment on the frequency.

1.7.1.4 Increase of Photoreceptor Noise

A definite change in the retina that is part of the normal aging process is the accumulation of debris in the photoreceptor layer of the retina (Leger et al. 2011). As mentioned before, being exposed to light is pretty dangerous for a cell, so photoreceptors are constantly regenerating themselves and shed discs that were destroyed by photochemical processes. The accumulation of cellular debris in the retinal pigment epithelium (RPE) can also slow the transfer of nutrients from blood-vessels through Bruch's membrane into the RPE (Jackson, Owsley, and Curcio 2002), changing the responsiveness of photoreceptors (for a schematic of the retina including Bruch's membrane see Figure 3.2.1, Bruch's membrane is labelled **BM**).

1.7.1.5 Retinal Remodelling

In addition to the increased functional variability at the level of photoreceptors, the natural loss of ganglion cells (Gao and Hollyfield 1992) and the onset of retinal diseases which we will discuss in the next section, the circuitry of the retina undergoes a systematic change in disease-free aging that is quite puzzling.

Across multiple species it has been found that horizontal and bipolar cells develop cellular processes that grow outside of the outer plexiform layer, growing into the *ONL* (see Figures 1.7.3 for mouse and Figures 1.7.1 and 1.7.2 for human). Eliasieh, Liets, and Chalupa 2007 counted this process as evidence for preserved plasticity. The dendritic tree of ganglion cells was in contrast found to decrease slightly. In combination with the increase in retina area in mice, Samuel et al. 2011 predicted a decrease in the receptive field coverage of the retina. However, it is unclear whether the more extensive bipolar receptive field and the reduced ganglion cell receptive field would cancel each other out.

Regus-Leidig 2018 investigated synaptic markers in aged mice and confirmed that the synapses created by the ectopic processes are indeed functional.

It would be very odd if the extensive restructuring of the retina would be without functional consequences. Samuel et al. 2011 did some rudimentary assessment of ganglion cell functions and concluded that the function in old ganglion cells (if they respond) is preserved. The expected change of 5% reduced receptive field (RF) size could not be verified since the

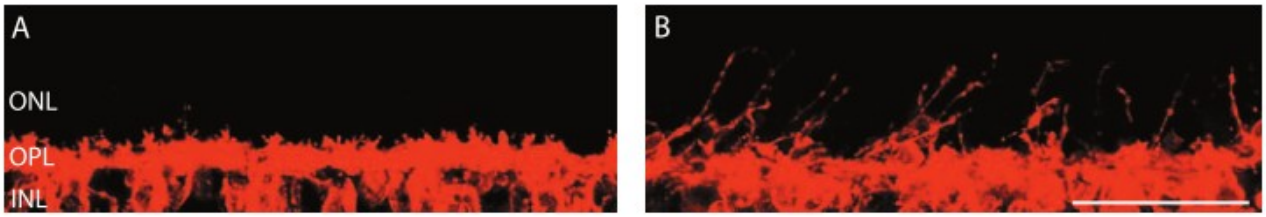

Figure 1.7.1: **Retinal Sprouting**: visual assessment. **A** in a young retina, the labeled horizontal cells are constrained to their layer vs **B** in an retina preparation from an old subject the dendrites of the horizontal and bipolar cells are increasing in length but leave their designated layer. From Eliasieh, Liets, and Chalupa 2007

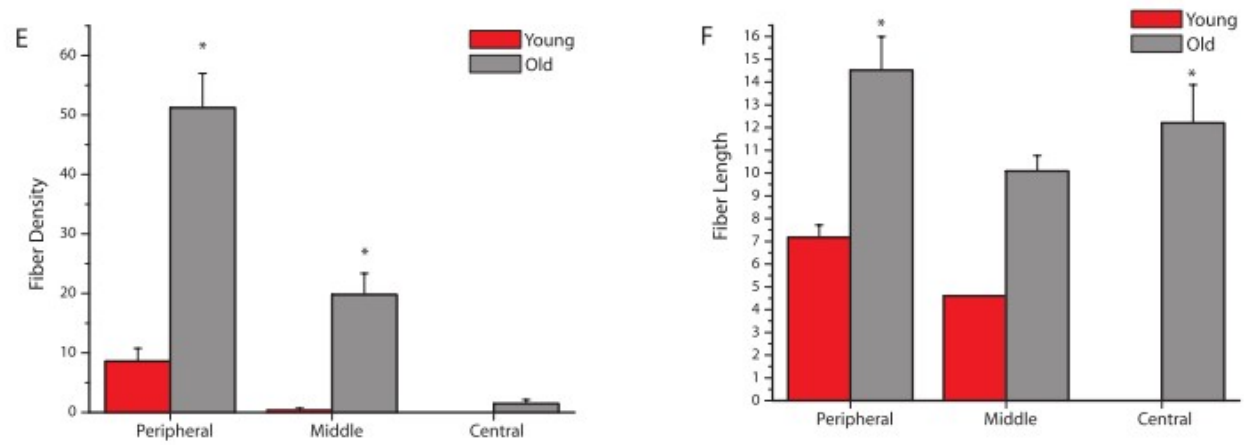

Figure 1.7.2: **Retinal Sprouting**: quantitative assessment. While long fibres do occur in young subjects, they are strictly found in the periphery. In old subjects fibre length and density increases throughout the retina. From Eliasieh, Liets, and Chalupa 2007

variability between ganglion cells was orders of magnitude larger than the expected difference. In section 3.4.2 we did some calculations on whether large scale multi-electrode array (MEA) recordings could give conclusive answers about functional changes in old retinas.

1.7.2 Retinal Diseases

In addition to normal aging related loss, the diseases of AMD, Stargardt disease and RP are characterized by up to total loss of specific groups of photoreceptors.

1.7.2.1 Age-Related Macular Degeneration (AMD) and Stargardt Disease

Age-related macular degeneration (AMD) is a family of age related diseases that all lead to the progressive loss of central vision (Bonnel, Mohand-Said, and Sahel 2003). The disorder is accompanied with abnormalities in the retinal pigment epithelium (RPE) and the accumulation of soft drusen in the macular area. Two main types of AMD are dry AMD, which shows degeneration of RPE and the neural layers of the retina, and the rarer wet (neovascular or exudative) AMD which also shows growth of blood vessels which can lead to a loss of almost 50% of ganglion cells (Medeiros and Curcio 2001).

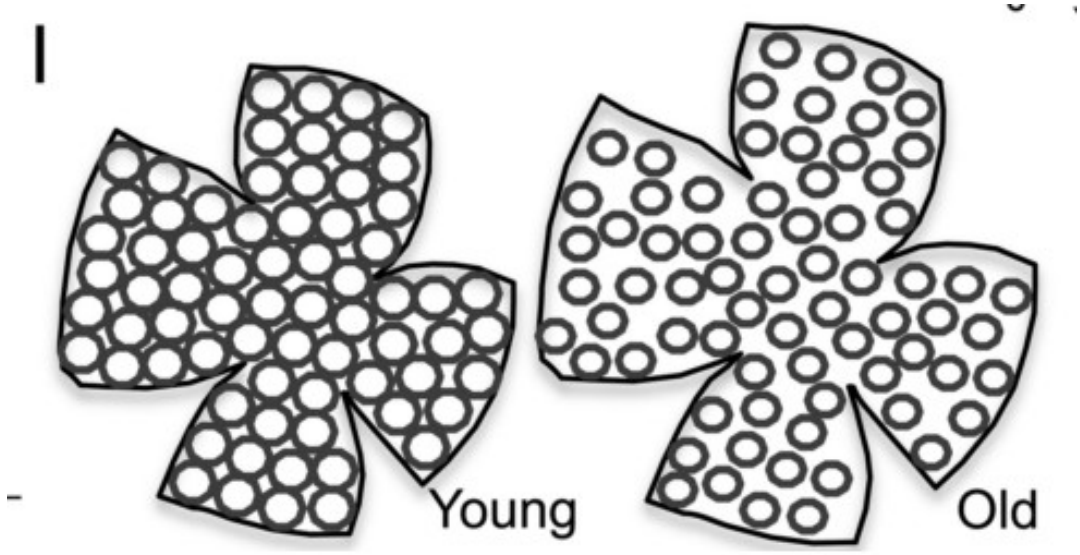

Figure 1.7.3: **Decrease of retinal cell coverage in aged mice**: The combination of slightly shrinking receptive fields (due to RGC dendritic trees shrinking) and an increase in retinal area, the receptive fields of old mice RGCs cover less of the visual field. From Samuel et al. 2011

Stargardt disease affects like AMD central vision but is not related to old age and instead a heritable disease related to the phototransduction cascade. The effects of Stargardt and AMD are comparable in that they attack photoreceptors in the central retina while the periphery stays mostly intact, but both have a high interpersonal variability.

1.7.2.2 Retinitis Pigmentosa (RP)

Retinitis Pigmentosa (RP) can be thought as the complementary disorder to AMD and Stargardt disease, as it is also characterized through a region specific vision loss, but primarily in the periphery, not the center of the retina. contrast sensitivity (CS) in RP can vary from unimpeded to a three-fold decline in contrast sensitivity (Jason McAnany et al. 2013).

Ferreira et al. 2017 found that patients with RP had significant visual cortex remapping that correlated with the decrease in visual field. Cortical representations were expanded or shifted to cortical regions that had reduced retinal input, consistent with other studies about plasticity (see Section 1.8.1).

1.8 Adaptation and Plasticity

Neural connections are plastic and adapt to their usage. In the aging process this is relevant at two fronts: (1) neural adaptation can compensate or aggravate other aging processes (section 1.8.1) and (2) if the adaptation itself is subject to changes induced by aging, the brain might be unable to adapt to changing circumstances - whether induced by aging or not (section 1.8.2).

The brain developed to allow adaptive behaviour in changing environments. Even though mammals live in diverse environments with very different goals, the structure of their brains is remarkably similar. Even cortical regions in one individual that handle different tasks are for the most part comprised of similar neurons organized in similar structures.

The difference between compensation and maladaptation can be slim. In most cases it is plausible that processes that compensate some function that was impacted by aging do this at the cost of other functions. We will argue that the increase in receptive field sizes throughout the visual system is a compensatory mechanism, even though it does impact spatial resolution.

1.8.1 Plasticity "When All Is Well"

There are a number of experiments that illustrate the effect of input dependent plasticity very nicely. Most of these experiments were done in rodents, most commonly rats and mice, since they grow up (and also age) rapidly and have well studied sensorimotor areas, such as e.g. the barrel cortex in which the strictly organized cortical representations of single whiskers can be distinguished optically by staining for *cytochrome c oxidase* (Hardingham et al. 2003). When whiskers are cut, the barrel cortex reorganizes over time by shrinking the area that is responsible for the cut whisker and using the neurons in that area instead for processing the sensory stimuli of the neighbouring whiskers. Deprivation experiments like these have been used to investigate plasticity over the life span of the animals.

1.8.2 Changes in Plasticity in Aging

Berardi, Pizzorusso, and Maffei 2000 found that monocular deprivation leads to cortical reorganization in the visual cortex in young rats, but not in adult rats, being in agreement with the long standing, but now heavily refuted idea that plasticity is turned off in the adult organism.

1.8.2.1 Relating Human and Rodent Studies

In humans we observe similar effects in blind Braille readers or musicians (Pantev et al. 1998; Elbert et al. 1997; Sterr et al. 1998; Pascual-Leone and Torres 1993) where sensorimotor representations are enlarged, using a larger area of the surface to represent sensory information. More so, the relation between competence and cortical representation is roughly proportional (Elbert et al. 1997; Pascual-Leone and Torres 1993). And we can also observe that the visual cortex of blind people can be used for completely different functions such as sound discrimination (Kujala et al. 1995) or verbal processing (Amedi 2004; Röder et al. 2002). Even though we should not replicate the deprivation experiments performed with rats in humans, there were non-invasive measurements of the size of cortical representations when patients had to have an ankle immobilized (Liepert, Tegenthoff, and Malin 1995; Dinse et al. 2003). These similarities let us hope that the studies on plasticity done in animal models can be transferred to knowledge about the human neurosystem, since many of the more complicated experimental paradigms (which most aging studies are) can not be replicated with human subjects. Even in non-human primates, aging studies take many times longer than in rodents as the example of a longitudinal study from the 90s shows (Liepert, Tegenthoff, and

Malin 1995), who will publish the effect of their intervention on longevity in the year 2020. In the light of these complications, we will continue in summarizing literature on rodents, but want to make clear that we can expect differences between rodent and primate aging and can only hope that some of the specific processes discussed are transferable.

1.8.2.2 Evidence Against Loss of Plasticity

One of the challengers of the idea of plasticity turning off in old age, (Scali et al. 2012), showed plasticity could be restored when senescent rats (> 20 months old) were exposed to "enriched environments" in contrast to the scientific standard which are isolated, square cages. These enriched environments featured a running wheel, multiple floors, multiple food dispensers, weekly changed novel shape objects and social interaction in groups of 6 animals. Any single one of these factors can play a role in the recovery of plasticity, as e.g. physical exercise, mental exercise and social interaction are all recommended for a healthy aging process (Fratiglioni, Paillard-Borg, and Winblad 2004). The deficits in plasticity in old age of laboratory animals could possibly not be related to age at all, but to the amount of time spent in laboratory conditions.

1.8.3 Calcium and Neural Aging

A theory put forward in Ashok and Foster 2007 relates the change in Calcium dynamics to plasticity. Normally, the intracellular Calcium levels depend on spiking activity and can induce LTD as well as LTP (Graupner and Brunel 2012). For very low levels (no activity at all) there is no change. Low frequency stimulation induces low levels of intracellular Calcium and weakens synaptic connections while high frequency stimulation increases intracellular Calcium concentration and strengthens the synapses. In old age a number of intracellular messengers change their expression, extruding and buffering less Calcium, such that the intracellular concentration of Calcium is generally increased, and specifically so during low frequency stimulation. However, the increased concentration of Calcium also changes the membrane potential resulting in a measurably increased after hyper polarization (AHP) as reported by multiple studies (Toescu and Verkhratsky 2000; Ashok and Foster 2007; Kumar and Foster 2005; Bodhinathan, Kumar, and Foster 2010; Oh, Oliveira, and Disterhoft 2010). The AHP makes it harder to elicit further spikes and thus prevents the activity to reach a regime that would potentate the strength of the synapses.

1.8.4 Usage Dependent Plasticity

Dinse 2006 reported that the sensory as well as the motor-representations of rats' hind legs - but not front legs - change dramatically with age. The specific changes are very interesting, as is the probable cause for the change. While in young rats, the sensory receptive fields are very small and allow a precise mapping between points on the foot and locations on the cortex, in old rats, the cortical representation maps to larger, more diffuse receptive fields encompassing multiple toes instead of just a specific part of a single toe. The overall cortical area mapping the complete paw shrinks. In the motor-cortex the changes were similar. The authors compared the electrophysiology of mechanoreceptors in front and hind paws and found that while there was an increase in response latency, they both showed similar changes,

even though the representation of front paws was indistinguishable from young rats. An explanation for the differences can be the change in paw usage: while old rats tend to lift their feet less and instead drag them along, they still use their front paws for feeding and cleaning. Hence they experience many distinct touch sensations on their front paws and only diffuse touch on their hind paws. This can be compared to an experiment done by Allard et al. 1991 in which they sewed two fingers of an owl monkey together and observed a fusing of representation - not because of neural connections between the fingers, but soley due to the input statistics of the two fingers coinciding. If the cortex notices a similarity in its inputs, it will organize the representations accordingly. In the case of the old rats in (Dinse 2006), the toes of the paw are not used individually, so their representation fuses, receptive fields get larger and the overall representation needs less cortical space.

If instead of giving correlated sensory information, the signal-to-noise ratio of the environmental stimuli is reduced, the cortex takes longer or even fail to develop a topographic organization (Chang and Merzenich 2003). When they reared rats in an environment subjected to continuous auditory noise, they found that the critical developmental period of the auditory cortex was delayed and an unusually large area of the cortex as sensitive to very high auditory frequencies. It is unclear what effects a non-mature, unstructured sensory cortex with shifting representations has on perception or higher cognitive functions.

1.8.5 Changes in Behaviour and Sensory Information

While it has been shown that physical, mental and social activity is beneficial for cognitive function and might even have protective effects against dementia (Fratiglioni, Paillard-Borg, and Winblad 2004), staying active in any of these three areas becomes harder with age (Salthouse 2006). Stine-Morrow 2007 even goes as far as to ask whether our pattern of choices to engage in intellectual challenges contribute more to cognitive vitality than the (biological) senescence process.

1.8.6 Reduction of Columnar Structure

Cruz et al. 2004 found that the micro-structure in monkey prefrontal cortex declines in age and similar results were found by Chance et al. 2006. The specific kind of structure Cruz et al. 2004 investigated was the spatial correlation of cells which normally shows a clear columnar organization: laterally cells are either very close or spaced in equal distances, horizontally cells are more likely to be directly above each other creating a very characteristic spatial crosscorrelogram, which they parameterized and found a significant decrease in columnar strength. Possible causes could be dendritic and axonal atrophy that causes minimal local displacement of a few micrometers, which can lead to the observed changes. In terms of consequences it is not clear how the displacement of cortical cells could impact cognition. The authors conjectured that the loss of specificity of features that are coded by the microcolumn, such as e.g. orientation (see Luebke, Barbas, and Peters 2010), could be linked to the integrity of microcolumnar structure. Since they did their analysis in layer III, they also link their findings to cotrico-cortical connectivity.

1.9 Our Theories About Aging in the Visual System

In addition to the established aging theories we want to highlight the following hypotheses which to us seem like good starting points for a scientific program to investigate aging mechanisms. Our goal is to gain insight into the aging phenomenon by neuro-computational modelling, so our hypotheses focus on the mechanisms with which neurons communicate and process information. We chose the hypotheses that aging effects are mainly caused (1.9.1) by input statistics of sensory stimuli, (1.9.2) by changes in plasticity mechanisms, (1.9.3) by de-myelination of white matter tracts and (1.9.4) by changes in cortical inhibition. We formulate the hypotheses here in the strong form of being "the main cause", which in all likelihood will not be true as aging is certainly a mix of different processes which might interact. But a strong, simple hypothesis can encourage scientists to consider novel view points: if you currently believe that de-myelination is the main aging mechanism, considering that a change in input statistics could be enough to create the aging effects observed can be more helpful to develop new ideas than to add the changing input statistics hypothesis to your current favourite theory and to try to juggle all the complexity that comes with it.

1.9.1 Mainly Due to Input Statistics

We discussed a number of reasons why we think it's plausible that sensory input in old age differs from sensory input in young subjects. In both the visual and the auditory system the receptors lose sensitivity and become less reliable (Bonnel, Mohand-Said, and Sahel 2003; Wayne and Johnsrude 2015). Cataracts and yellowing of the lens reduce retinal illumination which further increases randomness while the ability of the eye to adapt both to the distance of attended objects and the light level decreases.

The effect of increased variability at the sensory input can propagate through the sensory system if there are no noise suppressing mechanisms. We investigate two possible noise reduction mechanisms in chapter 3: gain control and (spatial) summation.

All of these changes do not only have a negative effect on the general quality of the sensory information (reducing acuity or decreasing the signal-to-noise-ratio (SNR)), they also cause the sensory cortices to adapt to the new statistics. As discussed, Chang and Merzenich 2003 found that at least the primary auditory cortex is not very good at developing under the presence of noisy input. So we might suspect that if the visual input would become more noisy and change input statistics enough to cause cortical reorganization (as found e.g. by Brewer and Barton 2011, discussed in section 2.3.1), that this re-organization might not even produce a stable representation.

Consequences: One effect of noisy sensory input is certainly broader tuning curves, which were observed (see Section 1.3.3), reduced cortical representations (Brewer and Barton 2011), increased cortical latency. In chapter 2 we also investigate the connection between input noise and receptive field size. As larger receptive fields filter noise, it is possible that the increase in receptive field size observed, e.g. in Schefrin, Bieher, and Werner 1997, is a compensatory mechanism. We also give a possible plasticity mechanism that could implement this function.

1.9.2 Mainly Due to Changed Plasticity

Since the aging effects happening at the level of the cell cycle and Calcium buffering ability of the cells are already hard to ignore, it is also very plausible that plasticity mechanisms themselves change. Ignoring all other effects of aging, the change in plasticity can depend on the specific type of neuron and how its plasticity mechanisms relate to intracellular Calcium levels.

As discussed in section 1.8.3, Ashok and Foster 2007 put forward a nice theory on how changes in Calcium dynamics change both the threshold for synapse modification and the excitability of the neuron. For young animals the dynamics cause LTD and LTP to be in perfect balance, while for old animals plasticity shifts to favour LTD over LTP.

Consequences: A change in plasticity, specifically a bias towards depression will first of all be noticable in a loss of synapses and dendrites. It is possible that a loss of synapses will lead to less activity in downstream neurons, however it is equally likely that other synapses compensate for the input by increasing their efficacy. A loss of dendritic spines has actually been observed and even if other synapses compensate for the loss in input, this will inevitably lead to a simplification of neural network structure which might be the cause of many age-related changes in cognitive functions (Dickstein et al. 2007).

1.9.3 Mainly Due to White Matter Tracts

In old age, there is a significant amount of demyelination (Davis et al. 2009). Demyelination causes white matter tracts to loose speed, specificity and can even lead to the complete loss of single connections (Peters 2002; Atilla et al. 2006; Barrick et al. 2010). The loss of long-range connections has an effect on the amount of information that can be passed from one brain region to another. E.g. if already the optic nerve loses $2/3$ of its nerve fibres as reported in Sandell and Peters 2001, acuity and contrast sensitivity suffers drastically, causing cortical representations to shrink and becoming broader. If we add to this that the remaining fibres might become increasingly unreliable in transmission and latency, we get similar effects as discussed in our input hypothesis 1.9.1, but with variability added at each transmission stage. Also there is some similarity to our plasticity hypothesis 1.9.2, but the loss of myelin function is limited to long-range white matter tracts and the only change possible is a gradual loss of connectivity.

Consequences: Demyelination causes a general increase in noisy activity and increased cortical delays as was found by Yao et al. 2015. Price et al. 2017 found sensory evoked responses in the visual system to be delayed by changes in the white matter structure. A decrease in neural activity as could be expected from less input is as far as we know not observed.

1.9.4 Mainly Due to Inhibition

Neural inhibition decreases during aging (Pleger et al. 2016; Cheng and Lin 2013; Peinemann et al. 2001).

A change in lateral inhibition has effects on the shape of receptive fields as we will discuss in section 2.5. Inhibition can also function as a anti-noise mechanism, sharpening tuning curves or implementing a soft winner-take-all function as we do in 4.7.2. The loss of surround suppression, characterized e.g. by Fu et al. 2010, is one example where inhibition is measurably reduced. The decrease of contrast sensitivity of visual cortical cells in old cats is also related to a reduction of intracortical inhibition according to Zhou et al. 2011.

Pleger et al. 2016 managed to restore tactile acuity through perceptual learning, but their neural field model explaining their fMRI data suggests that old subjects have weaker lateral inhibition and perceptual learning - instead of reversing this effect - further weakens intracortical inhibition and thus restores acuity.

Consequences: With a decrease in inhibition, spontaneous activity of neurons will certainly increase. This has been found across the neural system (e.g. Wang, Yao, et al. 2014). Consequences of increased spontaneous activity is a lowered signal-to-noise-ratio (SNR).

Since inhibition plays an important role in shaping RFs, the shape and specificity of receptive fields can be expected to be changed if inhibition is reduced.

Neural inhibition is also possibly related to executive functions and attentional inhibition. We outlined some deficits in attentional inhibition in section 1.3.2. The capacity for task shifting and attentional inhibition was found by Zhang et al. 2015 to be correlated to spontaneous eye blinks, which are both mediated by the central dopamine system, which involves inhibitory synapses between the striatum and the globus pallidus.

1.10 Summary: Aging Effects on Neural Mechanisms

In this chapter we aimed at characterizing aging effects that can be explained with computational theories. We presented these theories as changes mainly due to (1) input, (2) plasticity, (3) white matter and (4) inhibition. We chose to not pursue the theory that there is just a general increase in noise within each neuron, since this hypothesis is much too broad and the observed increased variability in neurons can be explained with any of our four candidate theories. Similarly, we do not assume that wide-spread neural cell loss is a natural process in healthy aging, although we do explore the change in the number of cells in Chapter 4 as a possible factor in our model.

At least some of the neurological and psychophysical findings we discussed can be explained with each of these hypotheses and we believe it is worth considering the full consequences of each hypothesis in isolation, even though in reality none of our theories in isolation will be able to fully explain all aging phenomena.

In the following chapters we will test mainly consequences of the input hypothesis, since it has not been explored much before and our modelling approach enables us to propagate the effect of increased input noise through a model system and analyse what consequences this single change can have.

The plasticity hypothesis has a lot of merit for computational modelling. In section 2.6.1.3 we sketch out how an aging plasticity model could be investigated. Since we found input noise to affect the weight distribution of an artificial neural network with spike-time dependent plasticity (STDP), we would be interested in future projects to combine these two approaches.

Since the hypothesis that white matter changes (sec 1.9.3) can give rise to some aging phenomena can locally look like either the input noise hypothesis (if we assume the viewpoint of the cells in the cortex that receive the white matter connections), or a change in plasticity, we believe that investigating the two more basic hypothesis first makes it easier to argue about this more specialized, but certainly important factor in aging.

Inhibition is an important tool for neural networks. It can sharpen tuning curves, evaluate conflicting percepts and convert signals into sparser signals via lateral inhibition. The balance between between excitation and inhibition is crucial for a neural networks functioning. If inhibition changes even only a little with old age, many properties of cortical computation will change. In section 3.5.1 we examine the function of gain control (which builds on inhibition) as an anti-noise mechanism. We also investigated the role of inhibition as a signal-enhancing, soft winner-take-all mechanism in section 4.7.2. But there are many ways how this hypothesis can be used to generate predictions that we have not touched upon. The cortico-thalamic interaction itself being a well modelled dynamical system that has interest for any modality as well as pre-frontal functions since it provides an almost universal feedback mechanism which also links into attention.

Even with these very limited and simplified hypotheses, a large number of computational approaches are possible to test our knowledge of the nervous system and to generate new predictions to be tested in further experiments. The following chapters of this thesis are barely a start on this journey.

1.11 References

Allard, T. et al. (1991). "Reorganization of somatosensory area 3b representations in adult owl monkeys after digital syndactyly". In: *Journal of Neurophysiology* 66.3, pp. 1048–1058. ISSN: 0022-3077. DOI: 10.1152/jn.1991.66.3.1048. URL: http://www.physiology.org/doi/10.1152/jn.1991.66.3.1048.

Altman, J (1962). "Are new neurons formed in the brains of adult mammals?" In: *Science (New York, N.Y.)* 135.3509, pp. 1127–1128. ISSN: 0036-8075. DOI: 10.1126/science.135.3509.1127. URL: https://doi.org/10.1126/science.135.3509.1127.

Amedi, Amir (2004). "Visual and multisensory processing and plasticity in the human brain". In: *Nature neuroscience* 7.11, pp. 1266–70. ISSN: 1097-6256. DOI: 10.1038/nn1328. URL: http://www.ncbi.nlm.nih.gov/pubmed/15467719.

Andersen-Ranberg, K et al. (2005). *Who are the oldest-old?*

Andrés, Pilar, Fabrice B R Parmentier, and Carles Escera (2006). "The effect of age on involuntary capture of attention by irrelevant sounds: A test of the frontal hypothesis of aging". In: *Neuropsychologia* 44.12, pp. 2564–2568. ISSN: 00283932. DOI: 10.1016/j.neuropsychologia.2006.05.005.

Arai, Yasumichi et al. (2015). "Inflammation, But Not Telomere Length, Predicts Successful Ageing at Extreme Old Age: A Longitudinal Study of Semi-supercentenarians". In: *EBioMedicine* 2.10, pp. 1549–1558. ISSN: 23523964. DOI: 10.1016/j.ebiom.2015.07.029. URL: http://dx.doi.org/10.1016/j.ebiom.2015.07.029.

Ashok, Kumar and Thomas C Foster (2007). "Neurophysiology of Old Neurons and Synapses". In: *Brain Aging: Models, Methods, and Mechanisms*, pp. 1–19. URL: http://www.ncbi.nlm.nih.gov/books/NBK3882/.

Atilla, Huban et al. (2006). "Pattern electroretinography and visual evoked potentials in optic nerve diseases". In: *Journal of Clinical Neuroscience* 13.1, pp. 55–59. ISSN: 09675868. DOI: 10.1016/j.jocn.2005.02.007.

Barrick, Thomas R. et al. (2010). "White matter structural decline in normal ageing: A prospective longitudinal study using tract-based spatial statistics". In: *NeuroImage* 51.2, pp. 565–577. ISSN: 10538119. DOI: 10.1016/j.neuroimage.2010.02.033. URL: http://dx.doi.org/10.1016/j.neuroimage.2010.02.033.

Barzilai, Nir et al. (2012). "The place of genetics in ageing research". In: *Nature Reviews Genetics* 13.8, pp. 589–594. ISSN: 14710056. DOI: 10.1038/nrg3290. URL: http://dx.doi.org/10.1038/nrg3290.

Bennett, Patrick J, Robert Sekuler, and Allison B Sekuler (2007). "The effects of aging on motion detection and direction identification." In: *Vision research* 47.6, pp. 799–809. ISSN: 0042-6989. DOI: 10.1016/j.visres.2007.01.001. URL: http://www.ncbi.nlm.nih.gov/pubmed/17289106.

Berardi, Nicoletta, Tommaso Pizzorusso, and Lamberto Maffei (2000). "Critical periods during sensory development". In: *Current Opinion in Neurobiology* 10.1, pp. 138–145. ISSN: 09594388. DOI: 10.1016/S0959-4388(99)00047-1.

Betts, Lisa R. et al. (2005). "Aging Reduces Center-Surround Antagonism in Visual Motion Processing". In: *Neuron* 45.3, pp. 361–366. ISSN: 08966273. DOI: 10.1016/j.neuron.2004.12.041. URL: http://linkinghub.elsevier.com/retrieve/pii/S0896627305000139.

Boccardi, Virginia and Utz Herbig (2012). "Telomerase gene therapy: A novel approach to combat aging". In: *EMBO Molecular Medicine* 4.8, pp. 685–687. ISSN: 17574676. DOI: 10.1002/emmm.201200246.

Bodhinathan, Karthik, Ashok Kumar, and Thomas C Foster (2010). "Redox sensitive calcium stores underlie enhanced after hyperpolarization of aged neurons: role for ryanodine receptor mediated calcium signaling." In: *Journal of neurophysiology* 104.5, pp. 2586–93. ISSN: 1522-1598. DOI: 10.1152/jn.00577.2010. URL: http://www.pubmedcentral.nih.gov/articlerender.fcgi?artid=2997029%7B%5C&%7Dtool=pmcentrez%7B%5C&%7Drendertype=abstract.

Bonnel, Sébastien, Saddek Mohand-Said, and José Alain Sahel (2003). "The aging of the retina". In: *Experimental Gerontology* 38.8, pp. 825–831. ISSN: 05315565. DOI: 10.1016/S0531-5565(03)00093-7.

Brewer, a. and B. Barton (2011). "Aging and dementia in human visual cortex: Visual field map organization and population receptive fields". In: *Journal of Vision* 11.15, pp. 28–28. ISSN: 15525260. DOI: 10.1167/11.15.28.

Brozek, J. and A. Keys (1945). "Changes in flicker-fusion frequency with age." In: *Journal of Consulting Psychology* 9.2, pp. 87–90. ISSN: 0095-8891. DOI: 10.1037/h0053488. URL: http://content.apa.org/journals/ccp/9/2/87.

Cameron, David A. (2000). "Cellular proliferation and neurogenesis in the injured retina of adult zebrafish". In: *Visual Neuroscience* 17.5, pp. 789–797. ISSN: 09525238. DOI: 10.1017/S0952523800175121.

Chance, Steven a. et al. (2006). "Minicolumn thinning in temporal lobe association cortex but not primary auditory cortex in normal human ageing". In: *Acta Neuropathologica* 111.5, pp. 459–464. ISSN: 00016322. DOI: 10.1007/s00401-005-0014-z.

Chang, Edward F. and Michael M. Merzenich (2003). "Environmental noise retards auditory cortical development". In: *Science* 300.5618, pp. 498–502. ISSN: 00368075. DOI: 10.1126/science.1082163.

Cheng, Chia Hsiung and Yung Yang Lin (2013). "Aging-related decline in somatosensory inhibition of the human cerebral cortex". In: *Experimental Brain Research* 226.1, pp. 145–152. ISSN: 00144819. DOI: 10.1007/s00221-013-3420-9.

Coleman, Paul D. and Dorothy G. Flood (1987). "Neuron numbers and dendritic extent in normal aging and Alzheimer's disease". In: *Neurobiology of Aging* 8.6, pp. 521–545. ISSN: 01974580. DOI: 10.1016/0197-4580(87)90127-8. URL: http://linkinghub.elsevier.com/retrieve/pii/0197458087901278.

Cournil, Amandine and Thomas Kirkwood (2001). "If you would live long, choose your parents well". In: *Trends in Genetics* 17.5, pp. 233–235. ISSN: 01689525. DOI: 10.1016/S0168-9525(01)02306-X.

Cruz, Luis et al. (2004). "Age-related reduction in microcolumnar structure in area 46 of the rhesus monkey correlates with behavioral decline." In: *Proceedings of the National Academy of Sciences of the United States of America* 101.45, pp. 15846–15851. ISSN: 0027-8424. DOI: 10.1073/pnas.0407002101.

Davis, Simon W. et al. (2009). "Assessing the effects of age on long white matter tracts using diffusion tensor tractography". In: *NeuroImage* 46.2, pp. 530–541. ISSN: 10538119. DOI: 10.1016/j.neuroimage.2009.01.068. URL: http://dx.doi.org/10.1016/j.neuroimage.2009.01.068.

Dempster, F N (1992). "The rise and fall of the inhibitory mechanism: Toward a unified theory of cognitive development and aging". In: *Developmental Review* 12.1, pp. 45–75. ISSN: 02732297. DOI: 10.1016/0273-2297(92)90003-K. URL: http://www.sciencedirect.com/science/article/pii/027322979290003K%7B%5C%7D5Cnpapers3://publication/uuid/6BC6D23F-18C5-4937-8B16-7DD8F917B430.

Dickstein, Dara L et al. (2007). "Changes in the structural complexity of the aged brain." In: *Aging cell* 6.3, pp. 275–84. ISSN: 1474-9718. DOI: 10.1111/j.1474-9726.2007.00289.x. URL: http://www.pubmedcentral.nih.gov/articlerender.fcgi?artid=2441530%7B%5C&%7Dtool=pmcentrez%7B%5C&%7Drendertype=abstract.

Dinse, Hubert R. (2006). "Chapter 5 Cortical reorganization in the aging brain". In: *Progress in Brain Research* 157.06. ISSN: 00796123. DOI: 10.1016/S0079-6123(06)57005-0.

Dinse, Hubert R et al. (2003). "Pharmacological Modulation of Perceptual Learning and Associated Cortical Reorganization TL - 301". In: *Science* 301 VN -.5629, pp. 91–94. ISSN: 0036-8075. DOI: 10.1126/science.1085423. URL: http://dx.doi.org/10.1126/science.1085423.

Duckles, Sue Piper, Henry Tsai, and John N. Buchholz (1996). "Evidence for decline in intracellular calcium buffering in adrenergic nerves of aged rats". In: *Life Sciences* 58.22, pp. 2029–2035. ISSN: 00243205. DOI: 10.1016/0024-3205(96)00194-4.

Elbert, Thomas et al. (1997). "Input-increase and input-decrease types of cortical reorganization after upper extremity amputation in humans". In: *Experimental Brain Research* 117.1, pp. 161–164. ISSN: 00144819. DOI: 10.1007/s002210050210.

Eliasieh, Kasra, Lauren C. Liets, and Leo M. Chalupa (2007). "Cellular reorganization in the human retina during normal aging". In: *Investigative Ophthalmology and Visual Science* 48.6, pp. 2824–2830. ISSN: 01460404. DOI: 10.1167/iovs.06-1228.

Engle, James R., Steve Tinling, and Gregg H. Recanzone (2013). "Age-Related Hearing Loss in Rhesus Monkeys Is Correlated with Cochlear Histopathologies". In: *PLoS ONE* 8.2. ISSN: 19326203. DOI: 10.1371/journal.pone.0055092.

Eriksson, P S et al. (1998). "Neurogenesis in the adult human hippocampus". In: *Nat Med* 4.11, pp. 1313–1317. ISSN: 1078-8956. DOI: 10.1038/3305. arXiv: arXiv:1011.1669v3. URL: http://www.ncbi.nlm.nih.gov/pubmed/9809557%7B%5C%%7D5Cnhttp://www.nature.com/nm/journal/v4/n11/pdf/nm1198_1313.pdf.

Ernst, Aurélie and Jonas Frisén (2015). "Adult Neurogenesis in Humans- Common and Unique Traits in Mammals". In: *PLoS Biology* 13.1, pp. 1–12. ISSN: 15457885. DOI: 10.1371/journal.pbio.1002045.

Faubert, Jocelyn and Anne Bellefeuille (2002). "Aging effects on intra- and inter-attribute spatial frequency information for luminance, color, and working memory". In: *Vision Research* 42.3, pp. 369–378. ISSN: 00426989. DOI: 10.1016/S0042-6989(01)00292-9.

Ferreira, Sónia et al. (2017). "Primary visual cortical remapping in patients with inherited peripheral retinal degeneration". In: *NeuroImage: Clinical* 13, pp. 428–438. ISSN: 22131582. DOI: 10.1016/j.nicl.2016.12.013. URL: http://dx.doi.org/10.1016/j.nicl.2016.12.013.

Fratiglioni, Laura, Stephanie Paillard-Borg, and Bengt Winblad (2004). "An active and socially integrated lifestyle in late life might protect against dementia". In: *Lancet Neurology* 3.6, pp. 343–353. ISSN: 14744422. DOI: 10.1016/S1474-4422(04)00767-7.

Friede, Reinhard L. (1962). "The relation of the formation of lipofuscin to the distribution of oxidative enzymes in the human brain". In: *Acta Neuropathologica* 2.2, pp. 113–125. ISSN: 00016322. DOI: 10.1007/BF00685170.

Fu, Y. et al. (2010). "The effects of aging on the strength of surround suppression of receptive field of V1 cells in monkeys". In: *Neuroscience* 169.2, pp. 874–881. ISSN: 03064522. DOI: 10.1016/j.neuroscience.2010.05.015. arXiv: NIHMS150003. URL: http://linkinghub.elsevier.com/retrieve/pii/S0306452210007335.

Gao, H and J G Hollyfield (1992). "Aging of the human retina." In: *Investigative ophthalmology & visual science* 33.1, pp. 1–17. ISSN: 0146-0404. URL: http://www.ncbi.nlm.nih.gov/pubmed/1730530.

Graupner, M. and N. Brunel (2012). "Calcium-based plasticity model explains sensitivity of synaptic changes to spike pattern, rate, and dendritic location". In: *Proceedings of the National Academy of Sciences* 109.10, pp. 3991–3996. ISSN: 0027-8424. DOI: 10.1073/pnas.1109359109. URL: http://www.pnas.org/cgi/doi/10.1073/pnas.1109359109.

Gussekloo, Jacobijn et al. (2005). "Sensory impairment and cognitive functioning in oldest-old Subjects: The leiden 85+ study". In: *American Journal of Geriatric Psychiatry* 13.9, pp. 781–786. ISSN: 15457214. DOI: 10.1097/00019442-200509000-00006.

Hardie, D. Grahame, Fiona a. Ross, and Simon a. Hawley (2012). "AMPK: a nutrient and energy sensor that maintains energy homeostasis". In: *Nature Reviews Molecular Cell Biology* 13.4, pp. 251–262. ISSN: 1471-0072. DOI: 10.1038/nrm3311. URL: http://dx.doi.org/10.1038/nrm3311.

Hardingham, Neil et al. (2003). "Neocortical long-term potentiation and experience-dependent synaptic plasticity require alpha-calcium/calmodulin-dependent protein kinase II autophosphorylation." In: *The Journal of neuroscience : the official journal of the Society for Neuroscience* 23.11, pp. 4428–4436. ISSN: 1529-2401. DOI: 23/11/4428[pii].

Harman, D (1981). "The aging process." In: *Proceedings of the National Academy of Sciences of the United States of America* 78.11, pp. 7124–8. ISSN: 0027-8424. DOI: 10.1073/pnas.78.11.7124. URL: http://www.pubmedcentral.nih.gov/articlerender.fcgi?artid=349208%7B%5C&%7Dtool=pmcentrez%7B%5C&%7Drendertype=abstract.

Itahana, Koji, Judith Campisi, and Goberdhan P. Dimri (2004). "Mechanisms of cellular senescence in human and mouse cells". In: *Biogerontology* 5.1, pp. 1–10. ISSN: 13895729. DOI: 10.1023/B:BGEN.0000017682.96395.10.

Jackson, Gregory R., Cynthia Owsley, and Christine a. Curcio (2002). "Photoreceptor degeneration and dysfunction in aging and age-related maculopathy". In: *Ageing Research Reviews* 1.3, pp. 381–396. ISSN: 15681637. DOI: 10.1016/S1568-1637(02)00007-7.

Jason McAnany, J. et al. (2013). "Equivalent intrinsic noise, sampling efficiency, and contrast sensitivity in patients with retinitis pigmentosa". In: *Investigative Ophthalmology and Visual Science* 54.6, pp. 3857–3862. ISSN: 01460404. DOI: 10.1167/iovs.13-11789.

Kannangara, Timal S. et al. (2011). "Running reduces stress and enhances cell genesis in aged mice". In: *Neurobiology of Aging* 32.12, pp. 2279–2286. ISSN: 01974580. DOI: 10.1016/j.neurobiolaging.2009.12.025. arXiv: 15334406. URL: http://linkinghub.elsevier.com/retrieve/pii/S0197458010000102.

Karas, Renee and Allison M McKendrick (2009). "Aging alters surround modulation of perceived contrast." In: *Journal of vision* 9.5, pp. 11.1–9. ISSN: 1534-7362. DOI: 10.1167/9.5.11. URL: http://www.ncbi.nlm.nih.gov/pubmed/19757889.

Kline, D W et al. (1992). "Vision, aging, and driving: the problems of older drivers." In: *Journal of gerontology* 47.1, P27–P34. ISSN: 0022-1422. DOI: 10.1093/geronj/47.1.P27.

Kramer, a F, L Bherer, et al. (2004). "Environmental influences on cognitive and brain plasticity during aging". In: *The journals of gerontology.Series A, Biological sciences and medical sciences* 59.9, pp. M940–57. ISSN: 1079-5006; 1079-5006. DOI: 10.1093/gerona/59.9.M940.

Kramer, a F, D G Humphrey, et al. (1994). "Aging and inhibition: beyond a unitary view of inhibitory processing in attention." In: *Psychology and aging* 9.4, pp. 491–512. ISSN: 0882-7974. DOI: 10.1037/0882-7974.9.4.491.

Kujala, Teija et al. (1995). "Visual cortex activation in blind humans during sound discrimination". In: *Neuroscience Letters* 183.1-2, pp. 143–146. ISSN: 03043940. DOI: 10.1016/0304-3940(94)11135-6.

Kumar, Ashok and Thomas C. Foster (2005). "Intracellular calcium stores contribute to increased susceptibility to LTD induction during aging". In: *Brain Research* 1031.1, pp. 125–128. ISSN: 00068993. DOI: 10.1016/j.brainres.2004.10.023.

Lazzerini Ospri, Lorenzo, Glen Prusky, and Samer Hattar (2017). "Mood, The Circadian System, and Melanopsin Retinal Ganglion Cells". In: *Annual Review of Neuroscience* 40.1, annurev–neuro–072116–031324. ISSN: 0147-006X. DOI: 10.1146/annurev-neuro-072116-031324. URL: http://www.annualreviews.org/doi/10.1146/annurev-neuro-072116-031324.

Leger, François et al. (2011). "Protein aggregation in the aging retina." In: *Journal of neuropathology and experimental neurology* 70.1, pp. 63–68. ISSN: 0022-3069. DOI: 10.1097/NEN.0b013e31820376cc.

Leventhal, Audie G et al. (2003). "GABA and its agonists improved visual cortical function in senescent monkeys." In: *Science (New York, N.Y.)* 300.5620, pp. 812–815. ISSN: 00368075. DOI: 10.1126/science.1082874. URL: http://www.ncbi.nlm.nih.gov/pubmed/12730605.

Liang, Zhen et al. (2010). "Aging affects the direction selectivity of MT cells in rhesus monkeys". In: *Neurobiology of Aging* 31.5, pp. 863–873. ISSN: 01974580. DOI: 10.1016/j.neurobiolaging.2008.06.013. URL: http://dx.doi.org/10.1016/j.neurobiolaging.2008.06.013.

Liepert, J, M Tegenthoff, and J.-P Malin (1995). "Changes of cortical motor area size during immobilization". In: *Elecfroencephalography and clinical Neurophysiology* 97, pp. 382–386. ISSN: 0924980X. DOI: 10.1016/0924-980X(95)00194-P.

Liochev, Stefan (2015). "Which Is the Most Significant Cause of Aging?" In: *Antioxidants* 4.4, pp. 793–810. ISSN: 2076-3921. DOI: 10.3390/antiox4040793. URL: http://www.mdpi.com/2076-3921/4/4/793.

Lipsky, Martin S. and Mitch King (2015). "Biological theories of aging". In: *Disease-a-Month* 61.11, pp. 460–466. ISSN: 00115029. DOI: 10.1016/j.disamonth.2015.09.005. URL: http://dx.doi.org/10.1016/j.disamonth.2015.09.005%20https://www.karger.com/Article/FullText/270885%20http://linkinghub.elsevier.com/retrieve/pii/S0011502915001467.

Luebke, J I, Y-M Chang, et al. (2004). "Normal aging results in decreased synaptic excitation and increased synaptic inhibition of layer 2/3 pyramidal cells in the monkey prefrontal cortex." In: *Neuroscience* 125.1, pp. 277–88. ISSN: 0306-4522. DOI: 10.1016/j.neuroscience.2004.01.035. URL: http://www.ncbi.nlm.nih.gov/pubmed/15051166.

Luebke, Jennifer, Helen Barbas, and Alan Peters (2010). *Effects of normal aging on prefrontal area 46 in the rhesus monkey*. DOI: 10.1016/j.brainresrev.2009.12.002. arXiv: NIHMS150003.

Manassi, M., B. Sayim, and M. H. Herzog (2012). "Grouping, pooling, and when bigger is better in visual crowding". In: *Journal of Vision* 12.10, pp. 13–13. ISSN: 1534-7362. DOI: 10.1167/12.10.13. URL: http://jov.arvojournals.org/Article.aspx?doi=10.1167/12.10.13.

Marner, Lisbeth et al. (2003). "Marked loss of myelinated nerve fibers in the human brain with age". In: *Journal of Comparative Neurology* 462.2, pp. 144–152. ISSN: 00219967. DOI: 10.1002/cne.10714.

Medeiros, N E and C A Curcio (2001). "Preservation of ganglion cell layer neurons in age-related macular degeneration". In: *Invest Ophthalmol.Vis.Sci.* 42.3, pp. 795–803. ISSN: 0146-0404.

Mewborn, Catherine et al. (2015). "Critical Flicker Fusion Predicts Executive Function in Younger and Older Adults". In: *Archives of Clinical Neuropsychology*, acv054. ISSN: 0887-6177. DOI: 10.1093/arclin/acv054. URL: http://acn.oxfordjournals.org/lookup/doi/10.1093/arclin/acv054.

Miller, Richard A et al. (2002). "Longer life spans and delayed maturation in wild-derived mice." In: *Experimental biology and medicine (Maywood, N.J.)* 227.7, pp. 500–8. ISSN: 1535-3702. DOI: 10.1258/ebm.2010.010f11. URL: http://www.ncbi.nlm.nih.gov/pubmed/12094015.

Mittler, Ron (2017). "ROS Are Good". In: *Trends in Plant Science* 22.1, pp. 11–19. ISSN: 13601385. DOI: 10.1016/j.tplants.2016.08.002. arXiv: arXiv:1011.1669v3.

Oh, M Matthew, Fernando a Oliveira, and John F Disterhoft (2010). "Learning and aging related changes in intrinsic neuronal excitability." In: *Frontiers in aging neuroscience* 2.February, p. 2. ISSN: 1663-4365. DOI: 10.3389/neuro.24.002.2010. URL: http://www.pubmedcentral.nih.gov/articlerender.fcgi?artid=2874400%7B%5C&%7Dtool=pmcentrez%7B%5C&%7Drendertype=abstract.

Owsley, Cynthia (2011). "Aging and vision." In: *Vision research* 51.13, pp. 1610–22. ISSN: 1878-5646. DOI: 10.1016/j.visres.2010.10.020. URL: http://www.pubmedcentral.nih.gov/articlerender.fcgi?artid=3049199%7B%5C&%7Dtool=pmcentrez%7B%5C&%7Drendertype=abstract.

Pantev, Christo et al. (1998). "Increased auditory cortical representation in musicians". In: *Nature* 392.6678, pp. 811–814. ISSN: 00280836. DOI: 10.1038/33918.

Pascual-Leone, A and F Torres (1993). "Plasticity of the Sensorimotor Cortex \nRepresentation of the Reading Finger of Braille \nReaders". In: *Brain* 116.September, pp. 39–52.

Pearl, Raymond et al. (1924). "Studies in human biology". In:

Peinemann, a et al. (2001). "Age-related decrease in paired-pulse intracortical inhibition in the human primary motor cortex." In: *Neuroscience letters* 313.1-2, pp. 33–36. ISSN: 0304-3940. DOI: 10.1016/S0304-3940(01)02239-X.

Peters, Alan (2002). "The effects of normal aging on myelin and nerve fibers: A review". In: *Journal of Neurocytology* 31.8-9, pp. 581–593. ISSN: 03004864. DOI: 10.1023/A:1025731309829.

Peters, Alan, John H. Morrison, et al. (1998). "Are neurons lost from the primate cerebral cortex during normal aging?" In: *Cerebral Cortex* 8.4, pp. 295–300. ISSN: 10473211. DOI: 10.1093/cercor/8.4.295.

Peters, Alan, Claire Sethares, and Ronald J. Killiany (2001). "Effects of age on the thickness of myelin sheaths in monkey primary visual cortex". In: *Journal of Comparative Neurology* 435.2, pp. 241–248. ISSN: 00219967. DOI: 10.1002/cne.1205.

Pleger, Burkhard et al. (2016). "A complementary role of intracortical inhibition in age-related tactile degradation and its remodelling in humans". In: *Scientific Reports* 6.April 2015, pp. 1–15. ISSN: 20452322. DOI: 10.1038/srep27388. URL: http://dx.doi.org/10.1038/srep27388.

Potter, Wyatt B. et al. (2010). "Metabolic regulation of neuronal plasticity by the energy sensor AMPK". In: *PLoS ONE* 5.2. ISSN: 19326203. DOI: 10.1371/journal.pone.0008996.

Price, D. et al. (2017). "Age-related delay in visual and auditory evoked responses is mediated by white- and grey-matter differences". In: *Nature Communications* 8.May 2016,

p. 15671. ISSN: 2041-1723. DOI: 10.1038/ncomms15671. URL: http://www.nature.com/doifinder/10.1038/ncomms15671.

Regus-Leidig, Hanna (2018). "Age-associated alterations of photoreceptor synapses in the mouse retina". In: *Poster Fens Forum 2018*.

Ristow, Michael and Kim Zarse (2010). "How increased oxidative stress promotes longevity and metabolic health: The concept of mitochondrial hormesis (mitohormesis)". In: *Experimental Gerontology* 45.6, pp. 410–418. ISSN: 05315565. DOI: 10.1016/j.exger.2010.03.014. URL: http://dx.doi.org/10.1016/j.exger.2010.03.014.

Röder, Brigitte et al. (2002). "Speech processing activates visual cortex in congenitally blind humans". In: *European Journal of Neuroscience* 16.5, pp. 930–936. ISSN: 0953816X. DOI: 10.1046/j.1460-9568.2002.02147.x.

Rubner, Max (1908). *Das Problem der Lebensdauer und seine Beziehungen zu wachstum und ernährung*. Oldenbourg.

Sacher, George A (1982). "Evolutionary theory in gerontology". In: *Perspectives in biology and medicine* 25.3, pp. 339–353.

Salthouse, Timothy A (2006). "Mental Exercise and Mental Aging. Evaluating the Validity of the "Use It or Lose It" Hypothesis". In: *Perspectives on Psychological Science* 1.1, pp. 68–87. ISSN: 1745-6916. DOI: 10.1111/j.1745-6916.2006.00005.x. URL: http://www.ingentaconnect.com/content/bsc/ppsc/2006/00000001/00000001/art00006%7B%5C%%7D5Cnhttp://www3.interscience.wiley.com/cgi-bin/abstract/118600559/ABSTRACT.

Samuel, Melanie a. et al. (2011). "Age-Related Alterations in Neurons of the Mouse Retina". In: *Journal of Neuroscience* 31.44, pp. 16033–16044. ISSN: 0270-6474. DOI: 10.1523/JNEUROSCI.3580-11.2011.

Sandell, JH and Alan Peters (2001). "Effects of age on nerve fibers in the rhesus monkey optic nerve". In: *Journal of Comparative Neurology* 553.August 2000, pp. 541–553. URL: http://onlinelibrary.wiley.com/doi/10.1002/1096-9861(20010122)429:4%7B%5C%%7D3C541::AID-CNE3%7B%5C%%7D3E3.0.CO;2-5/full.

Sanes, Joshua R. and Richard H. Masland (2015). "The Types of Retinal Ganglion Cells: Current Status and Implications for Neuronal Classification". In: *Annual Review of Neuroscience* 38.1, pp. 221–246. ISSN: 0147-006X. DOI: 10.1146/annurev-neuro-071714-034120. URL: http://www.annualreviews.org/doi/abs/10.1146/annurev-neuro-071714-034120.

Scali, Manuela et al. (2012). "A rich environmental experience reactivates visual cortex plasticity in aged rats". In: *Experimental Gerontology* 47.4, pp. 337–341. ISSN: 05315565. DOI: 10.1016/j.exger.2012.01.007. URL: http://dx.doi.org/10.1016/j.exger.2012.01.007.

Schefrin, B. E., M. L. Bieher, and J. S. Werner (1997). "The area of complete spatial summation enlarges with age". In: *Investigative Ophthalmology and Visual Science* 38.4, pp. 340–348. ISSN: 01460404. DOI: 10.1364/JOSAA.15.000340.

Schmidt, Reinhold et al. (2011). "Heterogeneity in age-related white matter changes". In: *Acta Neuropathologica* 122.2, pp. 171–185. ISSN: 00016322. DOI: 10.1007/s00401-011-0851-x.

Schmolesky, M T et al. (2000). "Degradation of stimulus selectivity of visual cortical cells in senescent rhesus monkeys." In: *Nature neuroscience* 3.4, pp. 384–90. ISSN: 1097-6256. DOI: 10.1038/73957. URL: http://www.ncbi.nlm.nih.gov/pubmed/10725929.

Sekuler, a B, P J Bennett, and M Mamelak (2000). "Effects of aging on the useful field of view." In: *Experimental aging research* 26.2, pp. 103–120. ISSN: 0361-073X. DOI: 10.1080/036107300243588.

Shefer, V F (1973). "Absolute number of neurons and thickness of the cerebral cortex during aging, senile and vascular dementia, and Pick's and Alzheimer's diseases". In: *Neuroscience and Behavioral Physiology* 6.4, pp. 319–324.

Sorrells, Shawn F. et al. (2018). "Human hippocampal neurogenesis drops sharply in children to undetectable levels in adults". In: *Nature* 555.7696, pp. 377–381. ISSN: 14764687. DOI: 10.1038/nature25975. URL: http://dx.doi.org/10.1038/nature25975.

Spear, P. D. et al. (1994). "Effects of aging on the primate visual system: spatial and temporal processing by lateral geniculate neurons in young adult and old rhesus monkeys". In: *Journal of Neurophysiology* 72.1, pp. 402–420. ISSN: 0022-3077. DOI: 10.1152/jn.1994.72.1.402. URL: http://www.physiology.org/doi/10.1152/jn.1994.72.1.402.

Sterr, A et al. (1998). "Perceptual correlates of changes in cortical representation of fingers in blind multifinger Braille readers." In: *The Journal of neuroscience : the official journal of the Society for Neuroscience* 18.11, pp. 4417–23. ISSN: 0270-6474. URL: http://www.ncbi.nlm.nih.gov/pubmed/9592118%7B%5C%%7D5Cnhttp://www.jneurosci.org/content/18/11/4417.abstract.

Stevens, J. C. (1992). "Aging and spatial acuity of touch". In: *Journals of Gerontology* 47.1, pp. 35–40. ISSN: 00221422. DOI: 10.1093/geronj/47.1.P35.

Stine-Morrow, Elizabeth A. L. (2007). "The Dumbledore Hypothesis of Cognitive Aging". In: *Current Directions in Psychological Science* 16.6, pp. 295–299. ISSN: 0963-7214. DOI: 10.2307/20183223. URL: http://www.jstor.org/stable/20183223%7B%5C%%7D5Cnhttp://www.jstor.org/stable/pdfplus/20183223.pdf?acceptTC=true.

Swaab, DF (1991). "Brain aging and Alzheimer's disease,"wear and tear" versus "use it or lose it"". In: *Neurobiology of aging* 12.31, pp. 317–324. ISSN: 01974580. DOI: 10.1016/0197-4580(91)90008-8. URL: http://www.sciencedirect.com/science/article/pii/0197458091900088.

Syka, Josef (2010). "The Fischer 344 rat as a model of presbycusis". In: *Hearing Research* 264.1-2, pp. 70–78. ISSN: 03785955. DOI: 10.1016/j.heares.2009.11.003. URL: http://dx.doi.org/10.1016/j.heares.2009.11.003.

Tobimatsu, Shozo et al. (1993). "Age-related changes in pattern visual evoked potentials : differential effects of luminance , contrast and check size". In: 88, pp. 12–19.

Toescu, EC and A Verkhratsky (2000). "Parameters of calcium homeostasis in normal neuronal ageing". In: *Journal of anatomy*, pp. 563–569. URL: http://onlinelibrary.wiley.com/doi/10.1046/j.1469-7580.2000.19740563.x/abstract.

Vanhooren, Valerie and Claude Libert (2013). "The mouse as a model organism in aging research: Usefulness, pitfalls and possibilities". In: *Ageing Research Reviews* 12.1, pp. 8–21. ISSN: 15681637. DOI: 10.1016/j.arr.2012.03.010. URL: http://dx.doi.org/10.1016/j.arr.2012.03.010.

Villa, Antonello et al. (1994). "Cytosolic Ca2+ Binding Proteins during Rat Brain Ageing: Loss of Calbindin and Calretinin in the Hippocampus, with no Change in the Cerebellum". In: *European Journal of Neuroscience* 6.9, pp. 1491–1499. ISSN: 14609568. DOI: 10.1111/j.1460-9568.1994.tb01010.x.

Wang, Jicun, Thomas Michelitsch, et al. (2009). "Aging as a consequence of misrepair – a novel theory of aging". In: pp. 1–9. arXiv: 0904.0575. URL: http://arxiv.org/abs/0904.0575.

Wang, Zhengchun, Zhimo Yao, et al. (2014). "Declined contrast sensitivity of neurons along the visual pathway in aging cats." In: *Frontiers in aging neuroscience* 6, p. 163. ISSN: 1663-4365. DOI: 10.3389/fnagi.2014.00163. URL: http://www.pubmedcentral.nih.gov/articlerender.fcgi?artid=4089086%7B%5C&%7Dtool=pmcentrez%7B%5C&%7Drendertype=abstract.

Wayne, Rachel V. and Ingrid S. Johnsrude (2015). "A review of causal mechanisms underlying the link between age-related hearing loss and cognitive decline". In: *Ageing Research Reviews* 23, pp. 154–166. ISSN: 18729649. DOI: 10.1016/j.arr.2015.06.002. URL: http://dx.doi.org/10.1016/j.arr.2015.06.002.

Weale, R A (1987). "Senescent vision: is it all the fault of the lens?" In: *Eye (London, England)* 1 (Pt 2).2, pp. 217–221. ISSN: 0950-222X. DOI: 10.1038/eye.1987.40. URL: http://www.ncbi.nlm.nih.gov/pubmed/3653435.

Weinert, Brian T and Poala S Timiras (2003). "Invited Review: Theories of aging". In: *Journal of Applied Physiology* 95.4, pp. 1706–1716. ISSN: 8750-7587. DOI: 10.1152/japplphysiol.00288.2003. URL: http://www.physiology.org/doi/10.1152/japplphysiol.00288.2003.

Whitney, Craig R (1997). "Jeanne Calment, World's Elder, Dies at 122". In: *The New York Times*. URL: https://www.nytimes.com/1997/08/05/world/jeanne-calment-world-s-elder-dies-at-122.html.

WHO (2016). "WHO Life expectancy". In: *World Health Organization Website*. URL: http://www.who.int/gho/mortality_burden_disease/life_tables/situation_trends/en/.

Williams, George C. (1957). "Pleiotropy , Natural Selection , and the Evolution of Senescence Author (s): George C . Williams Published by : Society for the Study of Evolution Stable URL : http://www.jstor.org/stable/2406060". In: *Evolution* 11.4, pp. 398–411. URL: http://www.jstor.org/stable/2406060.

World Health Organization (2015). *World Report on Ageing and Health*. ISBN: 9789240694811. URL: http://apps.who.int/iris/bitstream/10665/186463/1/9789240694811_eng.pdf.

Xi, M. C. et al. (1999). "Changes in the axonal conduction velocity of pyramidal tract neurons in the aged cat". In: *Neuroscience* 92.1, pp. 219–225. ISSN: 03064522. DOI: 10.1016/S0306-4522(98)00754-4.

Yao, Z. et al. (2015). "Delayed signal transmission in area 17, area 18 and the posteromedial lateral suprasylvian area of aged cats". In: *Neuroscience* 289, pp. 358–366. ISSN: 03064522. DOI: 10.1016/j.neuroscience.2015.01.004. URL: http://linkinghub.elsevier.com/retrieve/pii/S0306452215000287.

Yu, Shan (2005). "Effects of age on latency and variability of visual response in monkeys". In: *Chin Sci Bull* 50.11, pp. 1163–1165. ISSN: 1001-6538. DOI: 10.1360/982005-572. URL: http://219.238.6.200/article?code=982005-572%7B%5C&%7Djccode=98.

Zhang, Ting et al. (2015). "Dopamine and executive function: Increased spontaneous eye blink rates correlate with better set-shifting and inhibition, but poorer updating". In: *International Journal of Psychophysiology* 96.3, pp. 155–161. ISSN: 18727697. DOI: 10.1016/j.ijpsycho.2015.04.010. URL: http://dx.doi.org/10.1016/j.ijpsycho.2015.04.010.

Zhou, J et al. (2011). "Decreased contrast sensitivity of visual cortical cells to visual stimuli accompanies a reduction of intracortical inhibition in old cats". In: *Dongwuxue Yanjiu* 32.5, pp. 533–539. ISSN: 0254-5853. URL: http://www.ncbi.nlm.nih.gov/entrez/query.fcgi?cmd=Retrieve%7B%5C&%7Ddb=PubMed%7B%5C&%7Ddopt=Citation%7B%5C&%7Dlist_uids=22006807.

Chapter 2

Receptive Fields and Noise

> An inspirational quote about receptive fields is hard to find.
>
> *Anonymous*

2.1 Introduction

In Chapter 1 we formulated the hypothesis that increased noise at the level of sensory receptors is enough to produce wide spread changes in the visual system. Next to the general decrease in signal-to-noise-ratio (SNR) throughout the perceptual systems, we also claim that an increase in receptive field sizes can be a compensatory mechanism against input noise and further that it can be a consequence of increased input noise.

In this chapter we pose a theoretical framework for receptive fields (RFs) and review the evidence of RFs enlarging with age and other possible changes to RFs. We then present our findings that the simple and well established established plasticity mechanism spike-time dependent plasticity (STDP) can be the mechanism that adapts the size of RFs according to input noise.

2.2 Trade-offs in Receptive Fields

The characterization of RFs has been a useful tool for neuroscience since the concept was used by early electrophysiologists like Sherrington 1906. In the visual system the size of RFs differs between cells of different functions, which correspond to the multitude of demands we have towards vision: we might have to discriminate minute details, or judge whether a large object is moving towards or away from us. The most prominent example of divergent receptive field, the magnocellular and parvocellular pathways in the lateral geniculate nucleus (LGN), divide the task of having a high spatial resolution and a high temporal resolution between them. The shape of RFs is always a trade-off, namely in (1) volume, (2) main direction (e.g. temporal or spatial) and (3) complexity.

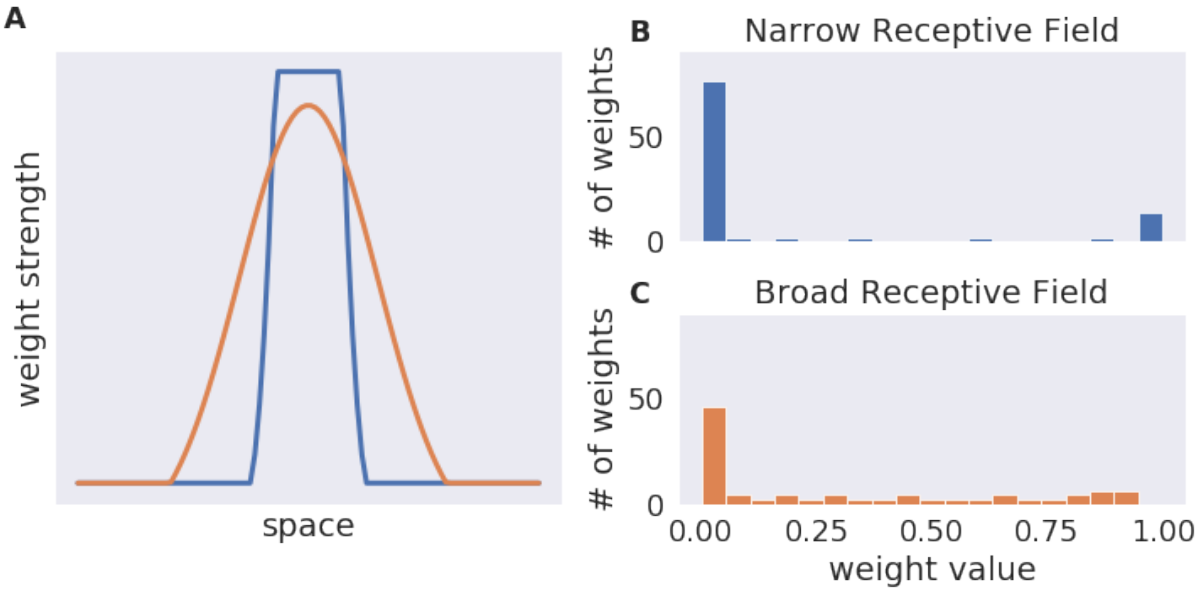

Figure 2.2.1: **A broad and a narrow Receptive Field:** plot **A** shows the profile of two gaussian receptive fields, generated with different standard deviations. The weights are constraint between 0 and a *gmax* value and the sum of the weights is roughly equal between the two receptive fields. **B** shows that the narrow receptive field has a very sparse weight histogram, with many weights being either 0 or 1. **C** shows that the broader receptive field has more intermediate values, since less weights are truncated, and less weights close to 0 or 1.

2.2.1 Volume

A small Receptive Field (RF), that only integrates very few sensory impulses, is subject to a very strong stochasticity and thus also to noise. A very large Receptive Field (RF) (given that it is a perfectly scaled version of the smaller one) will average over a larger portion of sensory information and thus be more noise robust, but it will tell us less about the fine structure of the stimulus, since it will also average over the fine details of the external world. Since for the visual system this is true not only for the spatial dimensions, but also time, we would like to coin the term of the *volume* of receptive fields, rather than the *size*. Taking only the spatial scale of a linear Receptive Field (RF) into account, there would already be an optimal amount of information for a Receptive Field (RF) to capture to get a reliable, but informative signal from the environment. This optimum would depend on the typical scale of external signals.

We can define the *volume* of a Receptive Field (RF) similar to a volume in space, delimiting the spatio-temporal points in the stimulus that can create a perturbation in the response when the response is modelled with a feed-forward LN model. If the stimulus is spatially organized, we can estimate the area that has an effect on the firing rate with different time lags. If there is no spatial structure but we have e.g. in a simulation of a neural network access to the input weight matrix of a neuron, we can count the number of non-zero synaptic weights. Figure 2.2.1 shows a simple schematic of two receptive fields and their weight distribution. The narrower Receptive Field (RF) has a higher number of weights close to zero than the broader Receptive Field (RF).

2.2.2 Temporal vs. Spatial

The distinction between spatial and temporal extent of a Receptive Field (RF) is exemplary of the second trade-off. Scaling in either direction would increase the volume, but it is also possible to keep the volume constant by compensating e.g. a shorter integration time with a larger spatial extent as the magnocellular pathway is doing. Or if we require a high spatial resolution, we can achieve that with the same volume by integrating over a longer time period. To cover both, high spatial and temporal resolution, with only one shape of Receptive Field (RF) would be much less efficient, since even a compromise between spatial and temporal extent would drastically reduce the volume of the Receptive Field (RF). Having these two different visual channels therefore makes a lot of sense, not to mention that integration over space and time can be very different neural processes. [1]

2.2.3 Selectivity

The third trade-off is selectivity. Irrespective of the overall envelope of the Receptive Field (RF), a similar stimulus might elicit different responses e.g. only due to the orientation of the stimulus or some other similar fine scale structure. Neurons can be more or less selective to stimuli inside their Receptive Field (RF), with the least selective being simple spatial integration where a single point stimulus anywhere in the Receptive Field (RF) will excite the neuron. A more selective Receptive Field (RF) could be a center-surround Receptive Field (RF) or a *gabor* patch which is only selective to a certain orientation of the stimulus. The tuning curve of the neuron with respect to the selective feature can vary from a very steep function around the preferred value, or just show a small relative increase. In Section 1.3.3 we discussed electro-physiological studies that showed e.g. a broadening of tuning curves in age.

Multiple integration stages can narrow or widen selectivity, so that selectivity does not increase monotonously in the visual hierarchy. Riesenhuber and Poggio 1999 e.g. modelled *IT* cells, which show a trade-off between invariance to position and scale-changes and object selectivity - either being very scale and position selective or very object selective. A similar observation was made by Zoccolan et al. 2007.

2.2.4 Volume of Receptive Fields Constrained to Form Two Pathways

In the visual system two pathways can be singled out anatomically in the lateral geniculate nucleus (LGN) and by their spatio-temporal selectivity. The two inner layers of the LGN contain large cells, which respond to very large, but fast moving stimuli. Due to their size they are called magnocellular or *M* cells. Layers 3 to 6 contain much smaller, parvocellular or *P* cells, which also have smaller receptive fields, meaning that they can discern more spatial details. However they need a longer temporal integration period. In terms of behavioural relevance, the two pathways seem to correspond well with two very distinct visual skills: reacting to close, fast movement, primarily in the periphery of our visual field, and discerning small details such as writing or objects that are far away. But wouldn't it be advantageous to have a visual pathway that could combine the advantage of both? A pathway that would respond to fast changing stimuli with high visual acuity. We believe this is undesirable not

[1] In the simplest case time can be multiplexed into dendritic space

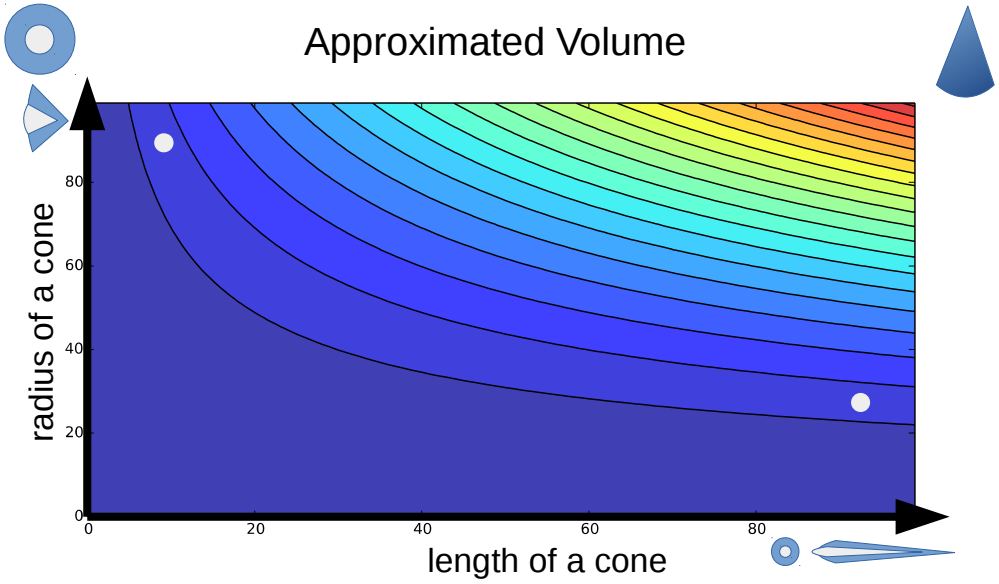

Figure 2.2.2: **Volume of a RF approximated as a cone** The two marked points label very different receptive fields: one is spatially very small, but has a long temporal integration time while the other one has only a short temporal extent but a larger spatial area. In terms of *volume* the two receptive fields are equivalent if we approximate them with a cone.

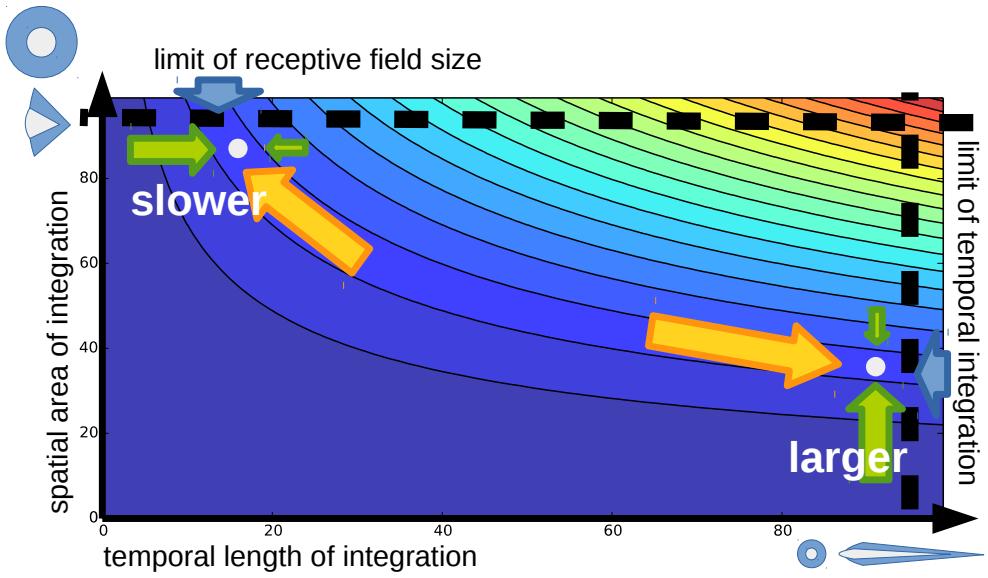

Figure 2.2.3: **Volume of a RF approximated as a cone** In addition to the two points from Figure 2.2.2, four arrows show forces acting on each point. The green arrows act along the gradient of volume and represent the desire to be as precise as possible (towards small receptive fields) and to be noise resistant (towards large receptive fields). The two orange arrows decorrelate the two pathways to minimize redundancy. Finally the blue arrows and black dashed lines postulate a sensible limit for receptive field sizes in a specific direction (e.g. too long of an integration time to be useful)

because e.g. high acuity vision is usually done in a more stationary environment (saccades are important for high acuity vision as well), but because of the *volume* of the visual stimulus that needs to be sampled to get an idea of what is happening. If we think of discrete events that are sparsely sampled to estimate whether a certain visual pattern is present and these events are fired with equal probability anywhere in the visual field, we can gather more events if we are collecting them over a larger area than if we only examine a small area. To be certain of what is happening in the small area, we need to wait longer to accumulate enough events.

Figure 2.2.3 shows two receptive fields that are identical except for their spatial and temporal scaling. They produce characteristics very similar to the responses in the magnocellular and parvocellular pathways respectively[2], one being very motion sensitive, the other allowing for high acuity. It also shows two green arrows per Receptive Field (RF) that signify the forces keeping the balance between a large volume to counter noise and a smaller volume to be as precise as possible. We present an example for a mechanism that can exhibit this behaviour in response to noise in Section 2.6.1. The green arrows act perpendicular to the gradient of the volume.

If sensory noise increases in old age, which we discussed in Section 1.9.1, we can assume this would require the visual system to adapt and change the volume of receptive fields by either increasing Receptive Field (RF) size, or increasing the temporal integration period either all along the pathway or at least at higher levels where visual information is integrated into percepts. In the following sections we discuss evidence for these two processes and a possible neural mechanism.

But to make a more testable hypothesis we can make some additional assumptions: Since we do have these two distinct pathways with distinct functions in our visual system, it seems plausible that they would want to diverge further, such that we can have one pathway that is as motion sensitive as possible and one that has a high acuity. However, there are biological limits to the size of receptive fields and length of temporal integration. In the consideration of Figure 2.2.3 we assume that while the two pathways are driven to diverge (orange arrows), they are fixed in their position by the upper limit of Receptive Field (RF) size for magnocellular cells and for temporal integration for parvocellular cells. We don't necessarily assume a hard biological limit, but rather a limit of usefulness if the receptive fields are too large or integrate for too long.

From this very simplified picture, we can make two predictions what happens if sensory noise increases in age and thus the volume of the receptive fields is increasing: (1) the magnocellular pathway is close to the limit on Receptive Field (RF) size, which will cause it to lose temporal precision and increase its temporal integration while (2) the parvocellular pathway will mainly increase Receptive Field (RF) size.

2.3 Evidence for Increased Receptive Fields in Age

Visual receptive fields can change dynamically due to changes in input statistics, e.g. retinal lesions which cause RFs to increase (Pettet and Gilbert 1992). Similar effects of *use dependent plasticity* is reviewed in section 1.8.4. But is there also evidence of Receptive Field (RF) size increase in age? Zhou et al. 2011 found a shift of *sf* sensitivity to lower spatial frequencies

[2]ignoring for now contrast gain control in the *magnocellular* pathway. We will discuss contrast gain control of the *magnocellular* pathway in Section 3.5.1

and an increase in Receptive Field (RF) size by a factor of 2 in old cats. There are also findings about the surround suppression of V1 neurons decreasing (Fu et al. 2010), which was most apparent in the selectivity of V1 cells.

In humans, evidence of increased receptive fields comes mostly from analysis of *population receptive fields*. The temporal response can be assessed with *EEG* by measuring the (VEP).

2.3.1 Population Receptive Fields

A number of studies have investigated the change in receptive fields in advanced age. One method to assess receptive fields non-invasively is to analyse the responses of fMRI or EEG when showing patterned stimuli to map visual to cortical locations. This method is of course very coarse and does not allow to find an actual receptive field of a single cell, it is said to instead measure population receptive fields (pRFs): the cumulative area of all receptive fields of the neurons in a specific voxel. Brewer and Barton 2011 investigated these population RFs using patterned stimuli and fMRI on human subjects to investigate the cortical representation of visual information in different visual areas. They found a general increase in pRF size in V1, V2, V3 and hV4, and an even more pronounced increase in the central 3 degrees of the visual field, which normally exhibit very small receptive fields for high acuity vision. They found the overall cortical area of each functionally measured visual cortex to be reduced, which strengthens the hypothesis that the cortex response to some change in input with considerable reorganization.

When interpreting population RFs, it is important to keep in mind that the population Receptive Field (RF) of a voxel can change size in two ways: the single receptive fields of individual neurons can change in size or the spacing-relation between the visual locations and their representation in the cortex can change (see Figure 2.3.1). One can expect those two quantities to vary together, but the increase of population RFs sizes is no direct evidence for the enlargement of the individual RFs. The spacing-relations between the RFs can vary as a simple consequence of general enlargement if the cortex tries to keep the overlap between receptive fields constant. But it is also possible that individual RFs stay constant, but either there are fewer RFs or the representation in the cortex is less “redundant”, resulting in a smaller area of the cortex that represents the visual space. A possible reason for decreased redundant positions of receptive fields could be that cells are less selective to features such as ocularity, spatial frequency or orientation (as found in macaque (Leventhal et al. 2003)), resulting in redundant responses which reorganize into a smaller cortical representation.

An alternative explanation for the change in population RFs is that the coverage of the visual field with receptive fields could be reduced, yet each Receptive Field (RF) stays constant in size. Figure 2.3.1 compares the two interpretations of the results visually.

2.3.2 Change in Temporal Dynamics

The temporal aspect of receptive fields can be hard to capture in an experiment. Even though the methods to estimate the temporal aspect of receptive fields differ from the ones used to estimate them spatially, there is some evidence of changes in temporal integration. E.g. flicker fusion and response latency can be taken as proxies for the temporal extent of single cell receptive fields, both of which were found to be increased (Brozek and Keys 1945; Emmerson-Hanover et al. 1994). Wang et al. 2005 found the visual system in general more sluggish, with

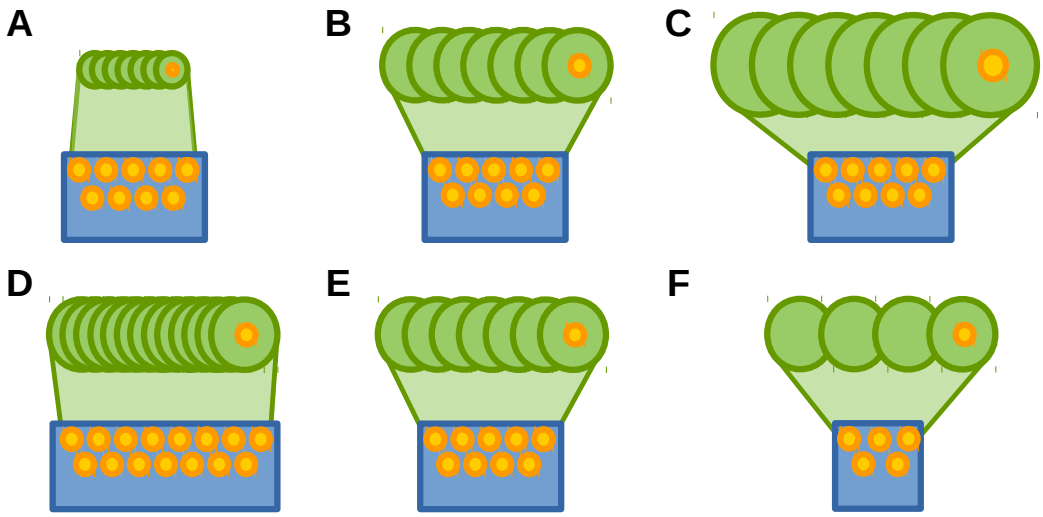

Figure 2.3.1: **Population Receptive Fields** The possible relations between visual space (green) and cortical space (blue) when population receptive fields are reported to change in size. **Upper row:** the same cortical area represents a larger visual area due to the increase in size and coverage of the individual receptive fields. **Lower row:** without change in the receptive fields, the cortex represents the same visual information in a smaller cortical area.

an increase in latencies throughout the visual system and an increasing spread of latencies with each subsequent hierarchical layer. They measured the response of many neurons to a visual stimulus and concluded that in old monkeys, some signals arrive in V1 roughly at the same time as for young monkeys, however a large portion of V1 responses are delayed by $\approx 20ms$. For V2, all responses were delayed significantly and it can be expected that throughout the visual system, the delay would further accumulate.

2.4 Evidence for Broadened Tuning Curves

So far we examined evidence for a change in receptive field size and temporal dimension. But there is also a change in complexity, as tuning curves of neural responses change due to age. Liang et al. 2010 foung the direction selectivity of middle temporal visual area (V5 or MT) cells in rhesus monkeys to decrease. The center-surround antagonism, which gives rise to the relative difficulty to perceive large, high contrast moving stimuli (as opposed to small ones), is reduced in old subjects Betts et al. 2005, showing a simplification of the response.

2.5 Inhibition Shaping Receptive Fields

It is tempting to equate the excitatory regions of the Receptive Field (RF) to the dendritic field of a neuron that integrates different points of the stimulus. But the actual shape of the Receptive Field (RF) is also mediated by e.g. the contrast of the stimulus that can change the size of the Receptive Field (RF) (Wielaard and Sajda 2005) or the spatio-temporal frequency

content of the stimulus (Galli et al. 1988), or they can depend on the activity of other cortical columns around them, leading to crowding effects in higher visual areas. Receptive fields are therefore *dynamic* and not static and a large part of their dynamics come from inhibitory inputs, which can be feed-forward or lateral, feature-specific or unspecific.

2.6 Noise Shaping Receptive Fields

2.6.1 Project 1: Noise Adaptive Receptive Fields Can Emerge From STDP

→ see also List of Projects

Even though it is clear that the size of RFs can reduce input noise by averaging over more input samples, it remains to be shown that there could be actual mechanisms that change the Receptive Field (RF) size in response to the input. In this simulation we want to show that a simple formulation of STDP can already produce similar changes, so the existence of plasticity behaving similarly in biological synapses is plausible.

2.6.1.1 Methods

We simulated a small network of integrate and fire neurons in *brian2* (Goodman and Brette 2009) with classical all-to-all STDP (Song, Miller, and Abbott 2000). 100 input neurons projected to 10 output neurons. On each pre-synaptic spike, the conductance of the output neurons will be adjusted according to the synaptic weight and the synaptic spike will be reduced according to the time since each previous post-synaptic spikes. On every post-synaptic spike the weight is increased depending on the time since each previous pre-synaptic spikes and all other output neurons are inhibited to decorrelate the weight convergence (Masquelier, Guyonneau, and Thorpe 2009). The change in synapse weight depending on the temporal difference between pre- and post-synaptic spikes can be seen in Figure 2.6.1. Weights are bounded between 0 and a value g_{max}. We introduced a slight bias for depression over facilitation.

The input was a continuous repeat of a frozen spike pattern on half of the inputs and random Poisson spike trains on the other half. To make the input pattern more salient for human observers, we used not only random activity for the frozen pattern, but added a cascade of spikes starting at input neuron 0 to 20, firing 1ms later than the previous neuron. When replaying the pattern, each spike was jittered according to a *noise level* parameter. Similar to Masquelier 2017, we expected the weights to converge to match the recurring spikes of the pattern. Since the first output neurons response also creates inhibition on all output neurons, each output neuron will become selective to a specific portion of the temporal input pattern.

The parameters of the simulation were:

Table 2.1: parameters of the simulation

Parameter	value	Description
tau_m	10ms	Time constant of the LIF model
tau_{pre}	40ms	Time constant of pre-synaptic STDP memory

Parameter	value	Description
tau_{post}	40ms	Time constant of post-synaptic STDP memory
E_e	0mV	Excitatory current equilibirum
v_t	-54mV	Spiking Threshold
v_r	-60mV	Reset membrane time constant
E_l	-74mV	Leak current equilibirum
tau_e	5ms	Time constant of excitatory current
g_{max}	.08	Synapse scale
dA_{pre}	.01	Synaptic decrease (relative to g_{max})
dA_{post}	.0105	Synaptic increase (relative to g_{max})
I_{inh}	.05 mV	Lateral Inhibition

We varied the jitter of the input from $< 1ms$ up to $100ms$ and recorded the statistics of the spiking output and weight distribution.

2.6.1.2 Results

We observed similar behaviour as Masquelier, Guyonneau, and Thorpe 2009: each output neuron responded selectively to a time point within the pattern for all noise levels.

Our input stimuli did not have any spatial structure, so we took the number of non-zero weights to stand in for the "size" of the Receptive Field (RF). What we observe is that with increasing noise level, less weights are driven to the extremes 0 and g_{max}. Instead there are more weights contributing for each output neuron spike. In Figure 2.6.2 we show the number of weights < 0.01, which does fall with increasing noise level from about 7% to 2%. When examining the weight evolution over time, the low-noise simulations converge faster to fixed weights while the more noisy simulations either take longer to converge.

Because of lateral inhibition, the firing rate stays constant (usually within 1Hz for all simulations of the same parameters, e.g. between 30 and 31Hz for the results in Figure 2.6.3) for all noise levels as each output neuron spikes once per pattern repetition. An exception were parameters that lead the synaptic weights to shrink below a critical value. Without inhibition, the parameters for the neuron threshold and the maximal synaptic weight g_{max} have to be adjusted to precise values to keep the simulation in a biologically plausible range.

2.6.1.3 Discussion

The results show that a simple synaptic mechanism can cause a neuron that receives noisy input to maintain synapses to more input sources, while each synapse becomes weaker. In a structure that receives spatially correlated input, we can assume that these synapses will tend to come from correlated input sources. This will lead to broader receptive fields under increased input noise.

The simulation was very simplistic and did create a large number of excitatory synapses, but we show in Appendix 7.2 that for other synaptic parameters, e.g. favouring facilitation over depression similar results will be observed. We did not include spatial patterns in the activity (e.g. movement). Each neuron was wired independently to the input. This makes the simulation applicable to a wider range of phenomena besides vision (e.g. touch or auditory stimuli). While in this simulation the time constants of all neurons was similar and so no

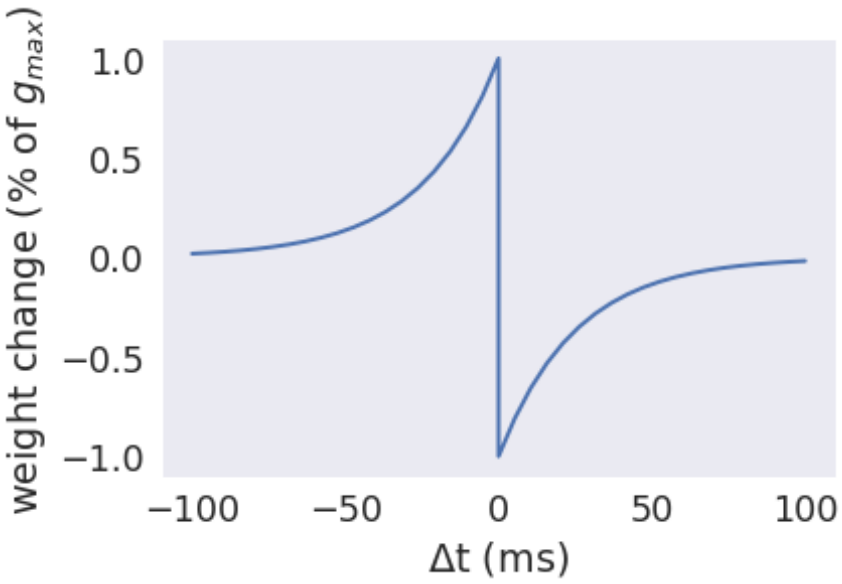

Figure 2.6.1: **The STDP rule.** If the difference between the spikes is negative (the pre-synaptic spike arrived before the post-synaptic spike), the connection is strengthened. If the post-synaptic spike precedes the pre-synaptic spike, it can be assumed that the pre-synaptic neuron did not contribute to the cell firing and the connection is weakened. If the spikes arrive shortly after each other, the change is large while a longer pause between the spikes will only lead to a small change.

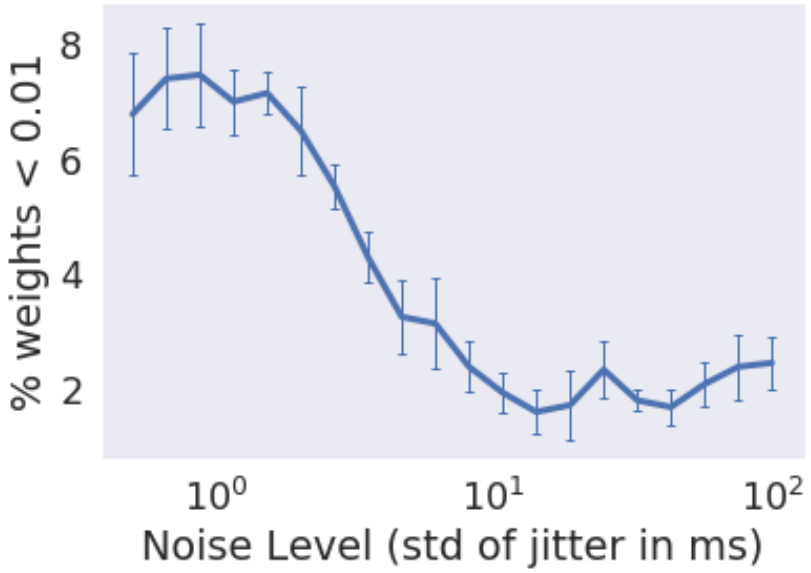

Figure 2.6.2: **Resulting weights.** With increasing noise level the number of small weights drops. A more detailed plot is visible in Figure 2.6.3.

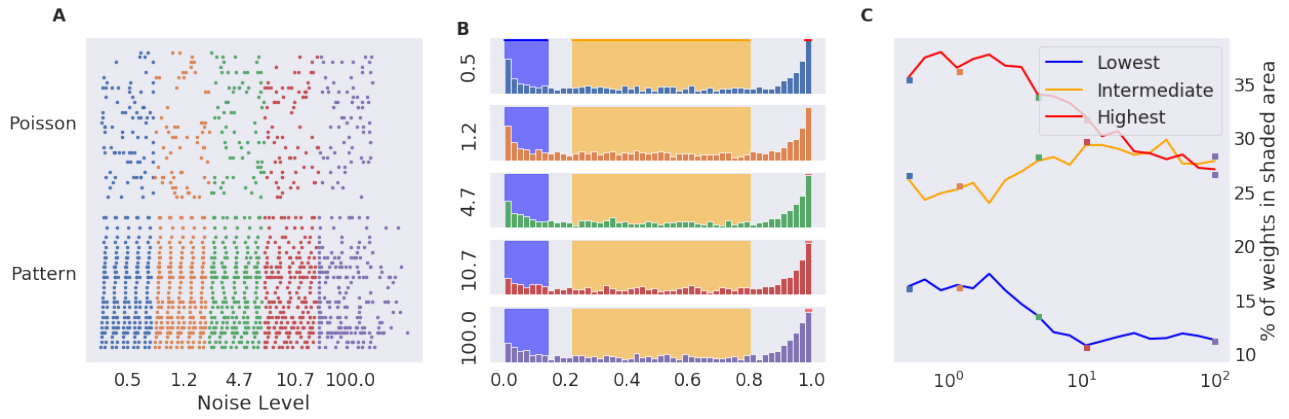

Figure 2.6.3: **Spike Patterns and Resulting Weights:** The raster plot in **A** shows the same repeating spike pattern being distorted by different levels of jitter noise. The pattern is clearly visible for up to 1.2ms jitter, then the repetitions of the pattern look more and more dissimilar. **B** shows resulting weight profiles for the selected simulations. with some areas shaded (see C) **C** shows the sum of weights of the 7 lowest bins (blue), 28 intermediate bins (orange) and the top bin (red) over noise levels (the bins were chosen for the lines to have comparable scale while still showing the trend). It is apparent that the lower bins and highest bins drop while the intermediate bins gain more weights. The square markers correspond to the weight distributions in B.

change in the temporal sensitivity of the neurons can be expected, we assume that in a biologically plausible situation, the input to a neuron already provides temporally diverse representations of a stimulus since the same signal can arrive at different times through different neural connections. With this interpretation, the spread of synaptic weights is also a spread in time for the Receptive Field (RF).

An area that is interesting to investigate in future projects is the effect of changed plasticity dynamics on the shown effect. In section 1.8.3 we summarize the theory that increased intracellular Ca^{2+} can shift neural plasticity into a regime of LTD. With a detailed model that relates Ca^{2+} to plasticity, such as e.g. Graupner and Brunel 2012, it would be interesting to see whether this shift even increases the effect, or if it counters it as LTD removes active synapses. We have found for our simulation in the Appendix in Figure 7.2.2, which mimics a longer intracellular Ca^{2+} signal, that this single change increases the effect, however it also corresponds to a general increase in LTP over LTD. To replicate the exact changes predicted by Ashok and Foster 2007, we need to use a more detailed STDP model in which Ca^{2+} has the two divergent functions of plasticity signal and hyper-polarization.

2.7 Summary: Receptive Fields and Noise

In this chapter we discussed the theoretical background to a possible aging theory. Under the sole assumption of increased input noise, what changes do we expect to occur in the receptive fields of the sensory system? We introduced the idea that the volume of a Receptive Field (RF) is a trade-off between spatial and temporal precision and noise robustness. Looking at the parvocellular and magnocellular pathway in the visual system, we concluded that their response to increased input noise will result in differential changes: parvocellular cells lose

acuity and magnocellular cells lose temporal precision. Next, we related the measurement of population RFs, which are found to increase specifically in the central visual field by Brewer and Barton 2011, to receptive field size. We also discussed the notion that inhibition plays a large role in shaping receptive fields, which is the basis of another, alternative aging theory. Factually, the two mechanisms (receptive field changes due to noise and due to changes in inhibition) are likely to interact and facilitate each other.

Finally we showed that a dynamic increase of receptive field sizes as a response to noise can be achieved with a mechanism as simple as STDP.

References

Ashok, Kumar and Thomas C Foster (2007). "Neurophysiology of Old Neurons and Synapses". In: *Brain Aging: Models, Methods, and Mechanisms*, pp. 1–19. URL: http://www.ncbi.nlm.nih.gov/books/NBK3882/.

Betts, Lisa R. et al. (2005). "Aging Reduces Center-Surround Antagonism in Visual Motion Processing". In: *Neuron* 45.3, pp. 361–366. ISSN: 08966273. DOI: 10.1016/j.neuron.2004.12.041. URL: http://linkinghub.elsevier.com/retrieve/pii/S0896627305000139.

Brewer, a. and B. Barton (2011). "Aging and dementia in human visual cortex: Visual field map organization and population receptive fields". In: *Journal of Vision* 11.15, pp. 28–28. ISSN: 15525260. DOI: 10.1167/11.15.28.

Brozek, J. and A. Keys (1945). "Changes in flicker-fusion frequency with age." In: *Journal of Consulting Psychology* 9.2, pp. 87–90. ISSN: 0095-8891. DOI: 10.1037/h0053488. URL: http://content.apa.org/journals/ccp/9/2/87.

Emmerson-Hanover, R. et al. (1994). "Pattern reversal evoked potentials: Gender differences and age-related changes in amplitude and latency". In: *Electroencephalography and Clinical Neurophysiology - Evoked Potentials* 92.2, pp. 93–101. ISSN: 01685597. DOI: 10.1016/0168-5597(94)90049-3.

Fu, Y. et al. (2010). "The effects of aging on the strength of surround suppression of receptive field of V1 cells in monkeys". In: *Neuroscience* 169.2, pp. 874–881. ISSN: 03064522. DOI: 10.1016/j.neuroscience.2010.05.015. arXiv: NIHMS150003. URL: http://linkinghub.elsevier.com/retrieve/pii/S0306452210007335.

Galli, L. et al. (1988). "The organization of receptive fields in area 18 neurones of the cat varies with the spatio-temporal characteristics of the visual stimulus". In: *Experimental Brain Research* 71.1, pp. 269–276. ISSN: 0014-4819. DOI: 10.1007/BF00247517. URL: http://link.springer.com/10.1007/BF00247517.

Goodman, Dan F M and Romain Brette (2009). "The brian simulator". In: *Frontiers in Neuroscience* 3.SEP, pp. 192–197. ISSN: 16624548. DOI: 10.3389/neuro.01.026.2009.

Graupner, M. and N. Brunel (2012). "Calcium-based plasticity model explains sensitivity of synaptic changes to spike pattern, rate, and dendritic location". In: *Proceedings of the National Academy of Sciences* 109.10, pp. 3991–3996. ISSN: 0027-8424. DOI: 10.1073/pnas.1109359109. URL: http://www.pnas.org/cgi/doi/10.1073/pnas.1109359109.

Leventhal, Audie G et al. (2003). "GABA and its agonists improved visual cortical function in senescent monkeys." In: *Science (New York, N.Y.)* 300.5620, pp. 812–815. ISSN: 00368075. DOI: 10.1126/science.1082874. URL: http://www.ncbi.nlm.nih.gov/pubmed/12730605.

Liang, Zhen et al. (2010). "Aging affects the direction selectivity of MT cells in rhesus monkeys". In: *Neurobiology of Aging* 31.5, pp. 863–873. ISSN: 01974580. DOI: 10.1016/j.neurobiolaging.2008.06.013. URL: http://dx.doi.org/10.1016/j.neurobiolaging.2008.06.013.

Masquelier, Timothée (2017). "STDP allows close-to-optimal spatiotemporal spike pattern detection by single coincidence detector neurons". In: *Neuroscience*, pp. 1–8. ISSN: 18737544. DOI: 10.1016/j.neuroscience.2017.06.032. arXiv: 1610.07355.

Masquelier, Timothée, Rudy Guyonneau, and Simon J Thorpe (2009). "Competitive STDP-based spike pattern learning." In: *Neural Computation* 21.5, pp. 1259–1276. URL: http://www.ncbi.nlm.nih.gov/pubmed/19718815.

Pettet, M W and C D Gilbert (1992). "Dynamic changes in receptive-field size in cat primary visual cortex." In: *Proceedings of the National Academy of Sciences of the United States of America* 89.17, pp. 8366–70. ISSN: 0027-8424. DOI: 10.1073/pnas.89.17.8366. URL: http://www.pubmedcentral.nih.gov/articlerender.fcgi?artid=49919%7B%5C&%7Dtool=pmcentrez%7B%5C&%7Drendertype=abstract.

Riesenhuber, Maximilian and Tomaso L B - Riesenhuber.Natureneuro.2.1999.1019 Poggio (1999). "Hierarchical models of object recognition in cortex". In: *Nature Neuroscience* 2, pp. 1019–1025. ISSN: 1097-6256. DOI: 10.1038/14819.

Sherrington, C S (1906). *The integrative action of the nervous system. C. Scribner's Sons, New York. See also: 1961 reprint of the original edition*.

Song, Sen, Kenneth D. Miller, and L. F. Abbott (2000). "Competitive Hebbian learning through spike-timing-dependent synaptic plasticity". In: *Nature Neuroscience* 3.9, pp. 919–926. ISSN: 10976256. DOI: 10.1038/78829.

Wang, Yongchang et al. (2005). "Degradation of signal timing in cortical areas V1 and V2 of senescent monkeys." In: *Cerebral cortex (New York, N.Y. : 1991)* 15.4, pp. 403–8. ISSN: 1047-3211. DOI: 10.1093/cercor/bhh143. URL: http://www.ncbi.nlm.nih.gov/pubmed/15749984.

Wielaard, J and P Sajda (2005). "Neural mechanisms of contrast dependent receptive field size in V1". In: *Advances in Neural Information Processing Systems*, pp. 1505–1512. ISSN: 10495258. URL: http://www.scopus.com/inward/record.url?eid=2-s2.0-34047188647%7B%5C&%7DpartnerID=40%7B%5C&%7Dmd5=4ea587d59d197056fa70f57054b4e7f9.

Zhou, J et al. (2011). "Decreased contrast sensitivity of visual cortical cells to visual stimuli accompanies a reduction of intracortical inhibition in old cats". In: *Dongwuxue Yanjiu* 32.5, pp. 533–539. ISSN: 0254-5853. URL: http://www.ncbi.nlm.nih.gov/entrez/query.fcgi?cmd=Retrieve%7B%5C&%7Ddb=PubMed%7B%5C&%7Ddopt=Citation%7B%5C&%7Dlist_uids=22006807.

Zoccolan, D. et al. (2007). "Trade-Off between Object Selectivity and Tolerance in Monkey Inferotemporal Cortex". In: *Journal of Neuroscience* 27.45, pp. 12292–12307. ISSN: 0270-6474. DOI: 10.1523/JNEUROSCI.1897-07.2007. URL: http://www.jneurosci.org/cgi/doi/10.1523/JNEUROSCI.1897-07.2007.

Chapter 3

Investigating Aging by Modelling Neural Activity

> Everything we do, every thought we've ever had, is produced by the human brain. But exactly how it operates remains one of the biggest unsolved mysteries, and it seems the more we probe its secrets, the more surprises we find.
>
> *Neil deGrasse Tyson*

> "The seat of sensations is in the brain. This contains the governing faculty. All the senses are connected in some way with the brain; consequently they are incapable of action if the brain is disturbed. The power of the brain to synthesize sensations makes it also the seat of thought: The storing up of perceptions gives memory and belief and when these are stabilized you get knowledge."
>
> Alcmaeon of Croton (5th century BC) from Gross, Charles G. (1987), "Early History of Neuroscience"

3.1 Introduction

As we discussed in Chapter 1, aging has a range of effects on the nervous system that are still not well understood. The changes that were found still have to be explained in a coherent

theory of neural aging. The approach to test possible explanations which we have chosen is computational modelling, in which we build models according to the current understanding of neural processes, e.g. in the visual system, and draw conclusions from their behaviour in simulated experiments. In this way, we can try to reduce the wealth of observations made about the aging process to a few, simple mechanisms. The differential aging effects on the magnocellular and parvocellular pathway in the visual system gives us an opportunity to test one of our aging theories on the fairly established model of lateral geniculate nucleus (LGN) responses. We simplify the differences between the two pathways to a few parameters, such that we can pin-point the exact mechanisms involved.

This chapter will introduce the idea to investigate the visual system by comparing neural activity. When we want to determine how well the visual system can tell stimuli apart, we can look at the differences in firing rate, the signal to noise ratio, spike distances, decoding and mutual information. We applied these methods to synthetic data generated by a model of retinal ganglion cells or LGN cells.

In a collaboration with the group of Tim Gollisch in Göttingen, we also looked at mouse retinal ganglion cell (RGC) activity to estimate the feasibility of performing exploratory experiments to determine the size of receptive fields of RGCs. We intended to run a quick run of experiments to establish if already at the retinal level aging effects change the properties of visual information, since the retina is fairly easily accessible in contrast to e.g. the LGN. To judge the number of experiments we would have to perform, we used the spread of receptive field sizes and recording quality to estimate the probability of finding a true positive result, assuming a change in receptive field size of 10%. The results suggest that a large number of experiments or the use of more complicated recording technology is necessary to find even this generous change.

3.2 A Short Introduction to the Neural Visual System

3.2.1 The Retina

The retina is the first neural stage of the visual system. The output of the retina is the optic nerve, which is comprised of the axons of retinal ganglion cells (RGCs) (**G** and **Ax** in Figure 3.2.1). There are around 50 different types of RGC classes in each species (Masland 2001; Sanes and Masland 2015), characterizable by their response properties, genetic markers and connectivity to other cell types. While for some RGC types, we have some idea of the circuitry they are involved in, others remain completely obscure. In the following, we will describe a very rough sketch of the connectivity in the retina.

The retina contains rod and cone photorecpetors (**R** and **C** in Figure 3.2.1) which respond to light with a change in their membrane potential. Rod photoreceptors respond to a wide range of wavelengths and are found predominantly in the periphery. Cone photoreceptor are larger than rods, less light sensitive, found mostly in the central areas of the retina and can be colour sensitive. The types of cones expressed in a species determine which colours can be distinguished. Humans and some other animals possess a fovea which exclusively contains densely packed cones for high-acuity colour vision. The activity of photoreceptors is mediated by horizontal cells (**H** in Figure 3.2.1), which laterally connect photoreceptors and inhibits them depending on the activity of others.

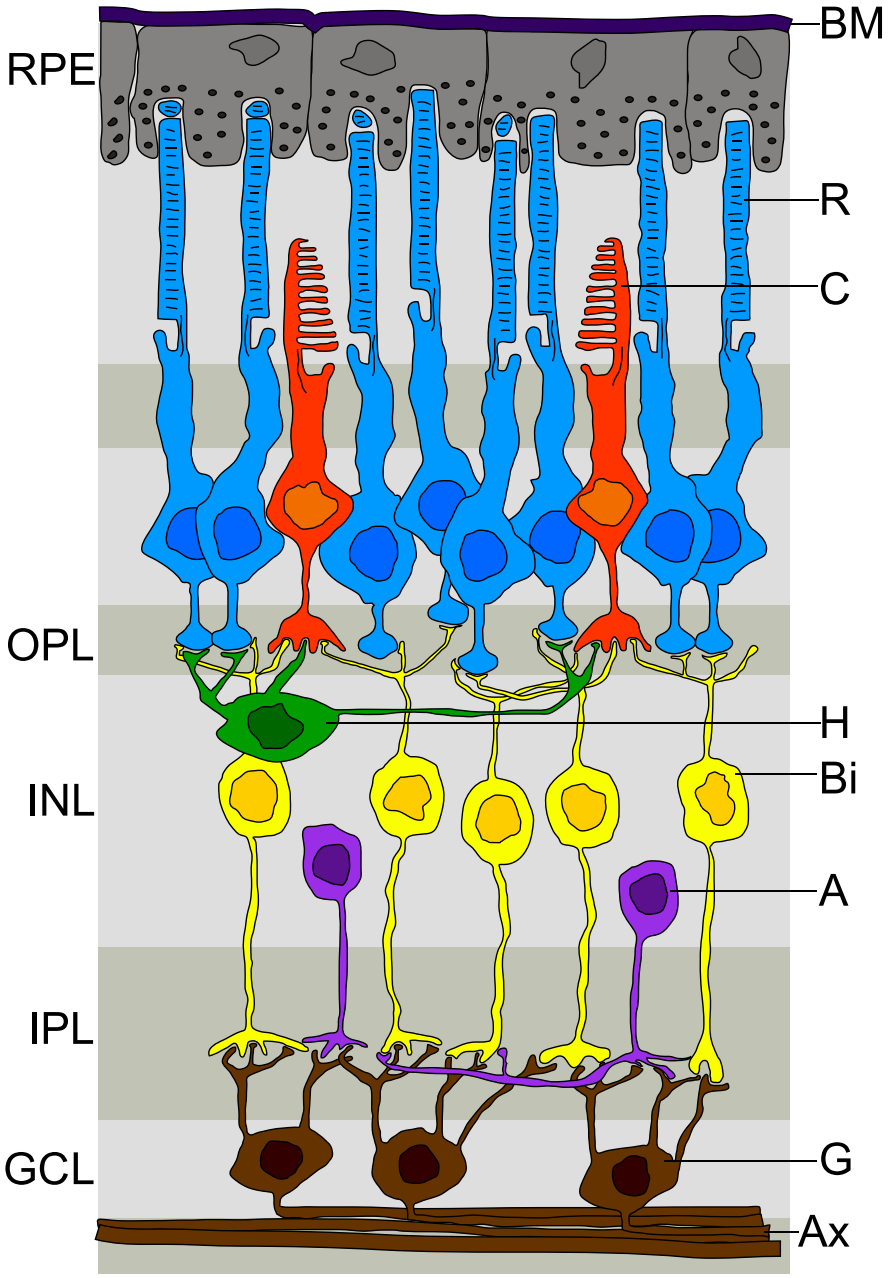

Figure 3.2.1: **Schematic Structure of the Retina.** The cells mentioned in section 3.2.1 are: Rod (**R**) and Cone (**C**) photoreceptors, Horizontal cells (**H**), Biploar cells (**Bi**), Amacrine cells (**A**) and Ganglion Cells (**G**). The top of the image is oriented towards the outside of the eye, ending with the RPE and Bruch's membrane (**BM**). The light enters the retina through the ganglion cells at the bottom. The layers labelled are: retinal pigment epithelium (RPE), outer plexiform layer (OPL), inner nuclear layer (INL), inner plexiform layer (IPL) and the Ganglion cell layer (GCL). Modified from: https://commons.wikimedia.org/wiki/File:Retina_layers.svg

Bipolar cell dendrites also connect to the photoreceptors. How many photoreceptors connect to one bipolar cell depends on the type of the bipolar cell as well as the eccentricity and can range from as few a single photoreceptor in the fovea to multiple thousands in the periphery. While photoreceptors and horizontal cells only appear as one of two structural types each, bipolar cell types are diverse. As with horizontal cells for photoreceptors, there is also a lateral inhibition mechanism for bipolar cells. Amacrine cells (**A** in Figure 3.2.1) - just as bipolar cells - have diverse morphology and mediate the output of bipolar cells with a range of different methods. Some amacrine cells connect directly onto bipolar cells (similar to horizontal cells), others form triadic synapses with a bipolar and a ganglion cell and only act on that specific connection. One possible effect of these inhibitory mechanisms is gain control acting on the contrast of the signal, as the luminance was already normalized locally. Bipolar cells connect very specifically to ganglion cells of matching (sub-)types. The depth at which they connect within the retina gives a spectrum of phasic and transient responses, as well as two polarities of bipolar cells.

In contrast to other neurons in the retina, ganglion cells transmit their activity as discrete spikes in membrane potential that can efficiently travel along the axon at a rapid speed.

3.2.2 The LGN

Most ganglion cells terminate in the lateral geniculate nucleus (LGN), where they connect onto relay neurons which project into the primary visual cortex. In the LGN there is another gain control mechanism, inhibiting activity laterally. Not every spike from an RGC is transmitted, reducing noise and overall firing rate of the projections into the visual cortex. The RGCs that do not project to the LGN, project directly to the superior colliculus (SC) to give tight feedback on eye movements and reflex behaviour.

3.2.2.1 The Magnocellular and Parvocellular Pathway

The visual system can be divided into two parallel pathways, which already diverge in the retina and ultimately reach very different parts of the brain. Since their different characteristics are most prominently found in the LGN, where they are separated into distinct layers, they are named for the appearance of the cells in the LGN:

The magnocellular pathway is named for the relatively large cell bodies found in the first two layers of the LGN compared to layer 3-6. The term M cell is used for both the LGN cells in the magnocellular layers and retinal parasol ganglion cells, which provide the input for the LGN cells. M cells respond rapidly to strong contrasts in the low spatial frequencies.

The parvocellular pathway recieves their input from midget cells. They offer a much better spatial resolution as well as color sensitivity than the magnocellular pathway, but they are slower.

Spear et al. 1994 found that magnocellular neurons have a higher signal-to-noise ratios than parvocellular neurons in aged rhesus monkeys.

3.2.3 The Primary Visual Cortex and Higher Visual Cortices

In the visual cortices, columns of neurons orthogonal to the cortical surface are processing a specific feature at a specific location. For the primary visual cortex (called V1 in humans),

these features correspond to Gabor patches of varying orientation and spatial frequency. While simple cells only respond to a bright stimulus in the excitatory portions of their receptive field, while the suppressive regions should receive as little light as possible, complex cells respond to multiple patterns, most commonly a Gabor patch and its inverse. From the primary cortex, visual information is further forwarded onto other areas, forming more complex features which become more location invariant.

3.3 Methods for Comparing Neural Activity

3.3.1 Firing Rates

One of the simplest ways to compare spiking activity either between cells or between different stimulus conditions is to count the number of action potentials recorded. Normalized over time the firing rate can be used to classify the cell by its activity relative to the stimulus. In the retina there are for example cells that respond to bright-to-dark transitions (OFF cells) and others that respond to dark-to-bright transitions (ON cells). The cells that differ in response type also differ in their neural circuitry and genetic markers (Masland 2001).

3.3.2 Signal to Noise Ratio

Neurons usually respond to some aspect of a stimulus specifically. But they can also exhibit spontaneous activity. So the firing rate alone is less informative than the firing rate relative to the spontaneous (baseline) activity of the neuron.

3.3.3 Spike Train Distances

Spikes are events on a time line with theoretically infinite precision and so if we want to compare two spike trains we have a range of different options in weighing the importance of temporal accuracy, removal or addition of spike events. The firing-rate difference (FRD) can be thought of as the most coarse timescale in which we can compare two spike trains: no matter when the spikes occur, their number is what distinguishes one response from another. But in many cases the temporal structure of the response will be just as or even more important than the overall firing rate.

3.3.3.1 Binned Euclidean Distance and Word Coding

If we break up each spike train into smaller, equal sized bins of a specific length (e.g. $10ms$ or even $100ms$), we can also take into account the temporal structure by counting the spikes that fall in each bin, or to create a binary time series: if at least one spike fell inside the bin. These discretized vectors can then be compared by either using euclidean distance resulting in exact matches have a distance of 0, coding the same *binary word*, while all others have some distance > 0 (see e.g. Strong et al. 1998). The bin width is an important parameter for this approach as for smaller time-bins the distance of similar, but non-identical spike trains will grow, while for very large time-bins the metric will tend to the firing rate distance - or in the case of binary words will only code if at least one spike was fired.

3.3.3.2 Victor Purpura Distance

The Victor-Purpura Distance (VPD) (Victor and Purpura 1996) is defined as the minimal cost of transforming one spike train into another using three rules: adding a spike has a cost of 1, removing a spike has a cost of 1 and moving a spike by a certain amount has a cost of q (e.g. per second). Without the third rule, this metric would give the same result as the firing rate difference. But if the cost of moving a spike is smaller than the cost of removing the old spike and adding a new spike, we get a notion of similarity that rewards spike trains with similar temporal structure. The reciprocal of the parameter q determines the temporal granularity of the metric, ranging from a pure firing rate comparison to a constraint of a spike having to be within 50ms, 10ms or even 1ms of a corresponding spike in the other spike train to be counted as the same. This allows to find the temporal granularity of neural codes by maximizing the information that the metric preserves about a given stimulus characteristic. Victor and Purpura 1996 found that the distance maximizes information about contrast in V1/V2 between $1/q = 10 - 30ms$ and about texture at around $1/q = 100ms$.

Computationally, this metric is easy to compute for sparse spike trains (even on very long time scales), but harder to compute the more spikes are present in either spike train, since a large number of spike pair combinations has to be checked to find the minimal distance.

3.3.3.3 Van Rossum Distance

The VanRossum Distance (VRD) (Rossum 2001) is very comparabe to the Victor-Purpura distance, as it also has a single parameter for its temporal granularity. But instead of relying on the possibly very calculation intense mapping of close spikes onto each other, VanRossum Distance convolves both input spike trains with causal exponential kernels and then taking the Euclidean distance. For insertion or deletion of spikes in two otherwise identical spike trains, VanRossum Distance gives a fixed penalty of $1/2$, while the distance increases dependent on the timescale parameter when a spike is moved, so it behaves very similar to the Victor-Purpura Distance (the authors relate VanRossum Distance^2 $\approx$ Victor-Purpura Distance). VanRossum Distance with an intermediate temporal parameter depends linearly on noise as can be seen in Figure 3.3.3 (see also Rossum 2001) and can thus be used to quantify the noise in a system.

In terms of computational complexity, the VanRossum Distance depends on the length of the input spike trains. If the spike train is long and very sparse, Victor-Purpura Distance can actually be computed faster than VanRossum Distance, even though the time complexity of Victor-Purpura Distance is higher since it depends on the number of spikes, not time bins. While this is not very relevant when comparing single spike trains, it can add to the already squared complexity of creating distance matrices (see Section 3.3.4).

3.3.3.4 Other Spike Train Distances

While in the current project we mostly use Victor-Purpura Distance or VanRossum Distance, there are other spike train distances we used during the project. We used the multivariate version of the SPIKE and ISI distances, as well as two metrics that are so far unpublished. The *mean-min-distance* was used previously in my Bachelor Thesis to quantify synchrony (Huth 2011), the *firing-rate-independent* distance was devised to be orthogonal to firing rate, since

most spike train distances correlate with firing rate distance or the mean firing rate of both spike trains (meaning that lower firing rates always lead to lower distances).

SPIKE/ISI The ISI distance is defined instantaneously for every time point t as the distances between the last spikes before t in one spike train and the first spike after t of the other spike train. The distance measure is then the sum of all the instantaneous values.

$$t_{\mathrm{P}}^{(n)}(t) = \max(t_i^{(n)} | t_i^{(n)} \leq t) \tag{3.1}$$

$$t_{\mathrm{F}}^{(n)}(t) = \min(t_i^{(n)} | t_i^{(n)} > t) \tag{3.2}$$

$$x_{\mathrm{ISI}}^{(n)}(t) = t_{\mathrm{F}}^{(n)}(t) - t_{\mathrm{P}}^{(n)}(t) \tag{3.3}$$

Mean-Min-Distance is a pseudo distance defined as the mean of the minimal distances of all spikes in one spike train to the nearest spike in the other spike train. If the spike trains have different number of spikes, the result will be asymmetric, ie. the "distance" $A \to B$ is different from $B \to A$. It can be used as an actual distance by computing both directions and taking the mean.

$$mmd(s_a, s_b) = mean_{s_i \in s_a}\left(min(abs(s_i - s_b))\right) \tag{3.4}$$

Firing-Rate Independent Dissimilarity Metric was created to add another dimension to the ability of comparing spike trains. Since most spike distance metrics are correlated either with the difference or the mean of the number of spikes in each spike train (see Figure 3.3.1 for an example), they will be partially redundant to the firing rate distance metric. This is a problem when comparing the temporal patterns in two spike trains of very different firing rates. If we already know that the firing rate is different between the two spike trains, but want to ignore that, most spike train distances will still change due to the number of spikes alone.

The novel metric is bounded between 0 and 1 by a sigmoid function, with 1 meaning the spike trains are very dissimilar. Two empty spike trains have a dissimilarity of 0.5 by definition. With each added spike, the dissimilarity rises, but with each pair of spikes that occur close to each other the dissimilarity drops. The closeness of spikes is determined with a temporal exponential filter f that is applied to each spike train, similar to VanRossum Distance.

$$fis(s_a, s_b) = sig\left(\alpha \cdot \sum(f_\tau(s_a) \cdot f_\tau(s_b)) - \|f_\tau(s_a) - f_\tau(s_b)\|\right) \tag{3.5}$$

The metric has two parameters: α defines the sharpness the sigmoid and a time constant τ defines the length of the temporal filter.

Figure 3.3.2 shows a comparison of different spike train distances comparing either a template spike train to a version of itself that has some spikes added or removed, or a completely unrelated spike train with a similar number of spikes. The line of the unrelated spike train is strongly dependent on absolute firing rate for Victor-Purpura Distance and VanRossum Distance. The *SPIKE* and *ISI* distance become asymptotically independent of firing rate, but do have a high difference if one of the spike trains has very few spikes. The distance based on

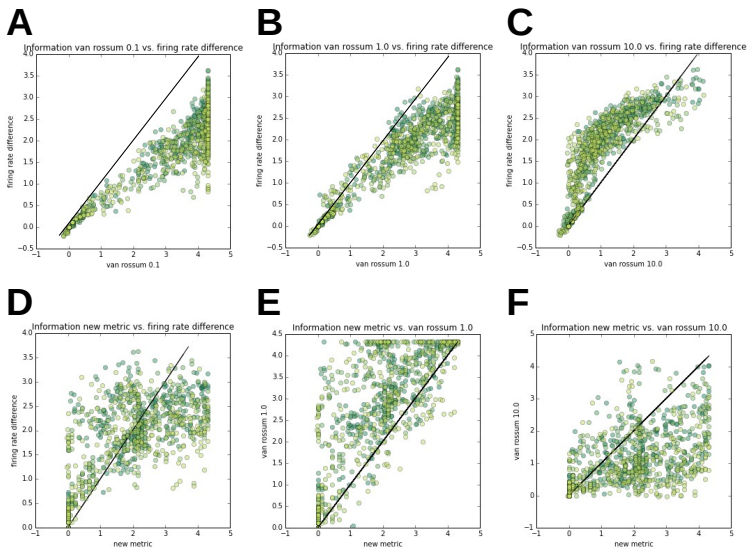

Figure 3.3.1: **Mutual Information of Different Distance Metrics Compared.** Most spike train distances are correlated to firing rate. This data from multi-electrode array (MEA) recordings shows as an example that the VanRossum distance has a linear relationship to the firing rate difference. The firing rate independent dissimilarity (fi) has a much larger spread when correlated to the firing rate difference (**D**).

Schreiber similarity comes closest to independence, but has a slight negative correlation. The Mean-Min-Distance is inadequate for this task. The *firing-rate independent* distance ignores the absolute firing rate completely of the unrelated spike train. For the modified template spike train it shows a region of similarity and for a jittered version a slightly smaller region. The sensitivity parameter α was shown at three different values.

3.3.4 Distance Matrix and Within/Between Distances

Taking the distances of all spike trains produced during an experiment to all others will create a symmetric, square matrix. The diagonal will have the minimal distance and should be ignored for the further analysis. If we sort the matrix by different stimuli that were presented (e.g. directional swipes of a bright bar), we can make out clusters of similar spike trains if and only if the neuron was sensitive to the differences between the stimuli. For two different stimuli (e.g. On and Off transitions), we can split the matrix into four quadrants: On trails to On trails, two On to Off trials Quadrants and Off-to-Off trials. These quadrants fall into two categories: **within**-distances and **between**-distances.

In figure 3.4.2 we can see that in an actual experiment the sensitivity of a neuron can vary. If the cell or its nutrient supply gets damaged during the experiment, it might cease to respond to the stimulus completely. But it is also possible that either because of spike sorting issues or a change in neural circuitry, the neurons recorded responsive properties change towards a different stimulus selectivity.

A measure that can capture how well the responses allow us to decode the stimulus is the ratio of **between** vs. **within** distances, ie. in this case the ratio of the sum of two diagonal

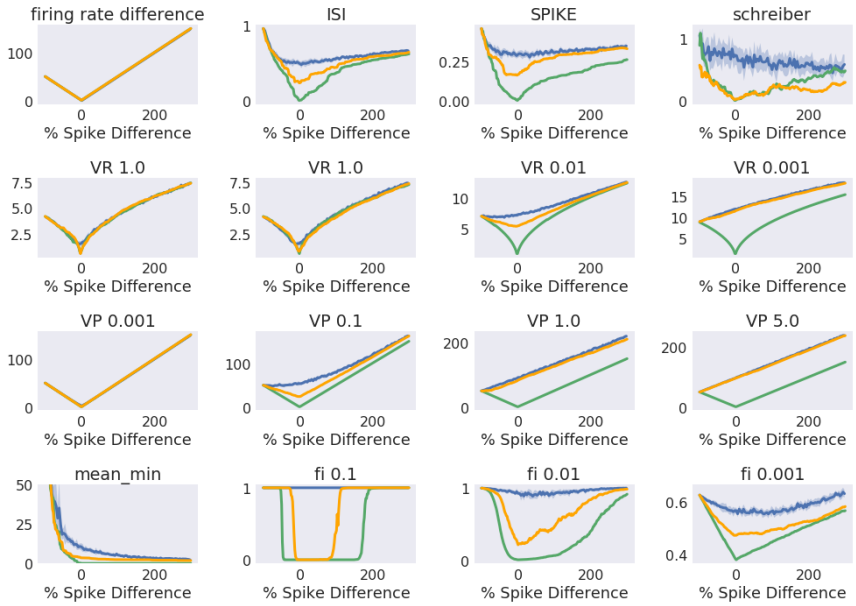

Figure 3.3.2: **Spike Train Metrics in Relation to Firing Rates.** For each plot, a template spike train is compared to spike trains with some spikes added or removed. The *green* line shows the distance if we manipulate the template spike train directly, adding new random spikes or removing spikes. It touches (0,0) in each plot since at that point the template is compared to itself. The *orange* line shows the same process for a jittered version of the template. The *blue* line does not have any temporal structure in common with the template and only varies in the number of spikes.

quadrant pairs of the matrix. The **within** distances can be interpreted as the background noise of the neural code: responses that are "supposed" to be identical, but due to stochastic processes (or other codes in the same spike train) have a distance > 0. The **between**-distance is what can actually be used for decoding. If the **between** distance is larger than the **within** distance, the spike trains can be clustered by the distances and new spike trains recorded from unknown stimuli can be compared to the clusters to make a prediction about which stimulus was shown.

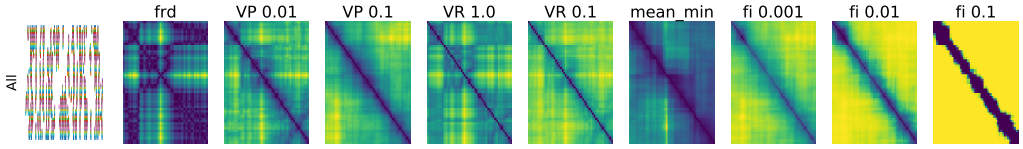

Figure 3.3.3: **Spike Distances under Noise.** In each iteration, spikes are jittered, added and deleted to create a slightly modified spike train. Each matrix compares the progressively changing spike trains to each other.

3.3.5 Information Theory

To quantify how much information a set of spike trains R transmits about a set of stimuli S, we can compute the mutual information $I(R;S)$ with the help of a spike train distance metric that allows us to set a threshold of which spike trains are taken to be the same symbol (Brasselet, Johansson, and Arleo 2011). As we have discussed in the previous sections, we have choices when we calculate if two spike trains are (approximately) identical. While the choice of algorithm is important, the choice of the temporal granularity (which most spike train distance metrics have) is even more important. In addition to our choice of spike distance, we have to set a threshold of when two responses are taken as identical signals. A possible choice would be to use binary word coding with a bin size of e.g. $20ms$ and a threshold of 0, such that only perfect matches are counted. As in the previous section, we compute the distance matrix of all combinations of responses and then apply the threshold.

We defined for a thresholded spike train distance $\phi(r_1, r_2) \in 0, 1$, a set of stimuli $s \in S$ and responses $r \in R$:

$$I(R;S) = H(R) - H(R|S) \tag{3.6}$$
$$H(R) = -\sum_{r\in R} p(r)\log_2 p(r) \tag{3.7}$$
$$\Rightarrow H^*(R) = -\sum_{r\in R} p(r)\log_2\left(\sum_{r'\in R} p(r')\phi(r,r')\right) \tag{3.8}$$
$$H(R|S) = \sum_{s\in S} p(s)\sum_{r\in R} p(r|s)log_2 p(r|s) \tag{3.9}$$
$$\Rightarrow H^*(R|S) = -\sum_{s\in S}\sum_{r\in R} p(r,s)log_2\left(\sum_{r'\in R} p(r'|s)\phi(r,r')\right) \tag{3.10}$$
$$I^*(R;S) = H^*(R) - H^*(R|S) \tag{3.11}$$
$$\Rightarrow I^*(R;S) = \sum_{s\in S}\sum_{r\in R} p(r,s)log_2\left(\frac{\sum_{r'\in R} p(r'|s)\phi(r,r')}{\sum_{r'\in R} p(r')\phi(r,r')}\right) \tag{3.12}$$

The Equation 3.12 can be used to quantify how much information about the stimulus is contained in a neurons response. Since the measure depends on the cut-off threshold that is used by ϕ to convert the distance/similarity into binary similarity, $I^*(R;S)$ is maximized by varying the cut-off.

3.4 Effect of Aging on Retinal Ganglion Cells

The retina as the first neural structure in the visual system already exhibits strong restructuring during aging (see Section 1.7.1.5). How these changes influence the coding properties of the retina is not well understood. We believe that characterizing the changes requires specialized experimental protocols since the characterization that were done so far only establish that some functionality is qualitatively still existent. In this section we will argue for why we think that there are changes, why they are hard to estimate experimentally and what kind of experiment could characterize them.

In addition to the morphological changes, the electrophysiology of the retina changes as well. The electroretinogram (ERG) is e.g. measured to change in age in amplitude as well as recovery rate (Tillman, Panorgias, and Werner 2016). Both *a-* as well as *b-wave* are reduced which Kolesnikov et al. 2010 take as a sign for desensitization due to increased dark noise (spontaneous activity of photoreceptors), which they confirmed in single cell recordings. We ask the question how this increase in noise at the photoreceptor-level affects the rest of the visual system.

3.4.1 Retinal Remodelling Must Have Functional Consequences

It is very unlikely that the change in dendritic structure in age has no effect on the response properties of RGCs. The loss of photoreceptors might be related to the change in bipolar dendritic fields. Figure 3.4.1 shows how a healthy receptive field (3.4.1 **A**) might enlarge its dendritic tree to keep the number of inputs constant in a damaged photoreceptor mosaic

(3.4.1 **B**) or it might grow without changes in the photoreceptors, simply covering a larger area (3.4.1 **C**). On the other hand, the dendritic tree of RGCs shrinks, which would then again decrease the number of photoreceptors that feed one RGC. If we assumed that the increase in bipolar and horizontal cell receptive fields is compensated for the decrease in RGC dendritic tree, there would still be changes (1) in the fovea where one bipolar cell connects to one RGC and (2) in the non-linear properties of the ganglion cell as it receives input from fewer, but larger sub-fields.

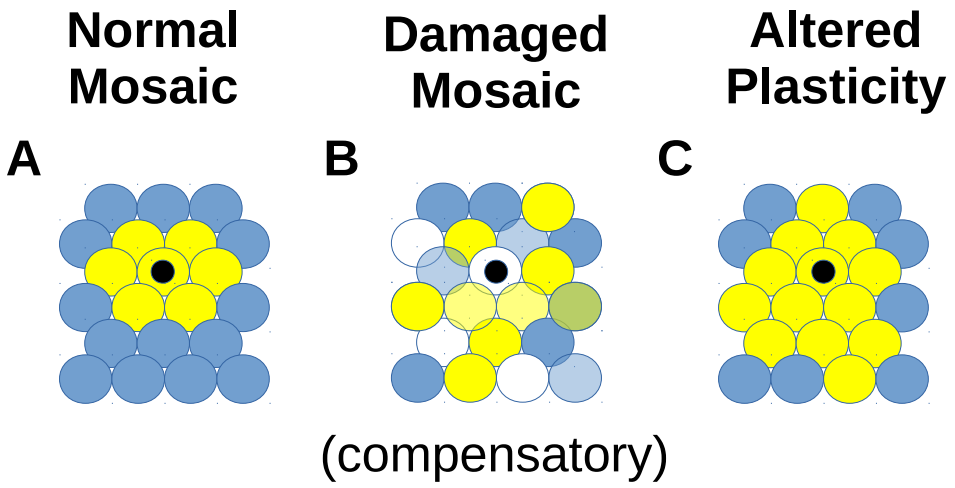

Figure 3.4.1: **Photoreceptor Mosaics.** Enlarged bipolar and horizontal receptive fields could be the result of compensation to damage (**B**) or altered plasticity (**C**). While there is damage in aged retinas, Samuel, Voinescu, et al. 2014 found evidence that remodelling is dependent on a specific intracellular pathway

3.4.2 Project 2: Estimating The Possible Effect Of Aging On Retinal Ganglion Cells

→ see also List of Projects

To estimate the effort to find a small change in receptive field size, we analysed RGC data collected by the lab of Tim Gollisch in Göttingen to estimate the variability and reliability of recordings. We would be interested to find differences in receptive field (RF) size or Receptive Field (RF) structure, reliability of the response and temporal precision.

3.4.2.1 Retinal Activity Recording Using MEA

In the following, we describe a typical recording procedure for mice retina. The work of recording and processing the data was done by the team of Tim Gollisch in Göttingen. At this point I want to thank again Vidhyasankar Krishnamoorthy, Fernando Rozenblit, Norma

Kühn, Mohammad Hossein Khani, Helene-Marianne Schreyer, Jian Liu, Michael Weick and of course Tim Gollisch.

Activity of RGCs was recorded from mice retinas using a multi-electrode array (MEA). A number of different stimuli were shown to the patch of retina and the recorded activity was later spike sorted, resulting in a set of spike trains.

The environment of the experimental rooms is as dimly lit as possible and all monitors are covered with red foil, since mouse retinas are not sensitive to red light. After the mouse is dark adapted for half an hour it is killed and the eyes removed. Each eyeball is cut in half and the lens is removed, leaving only the back part of the eyes, containing the sclera and connective tissue, the retina and the vitreous. They are then left in a nutrient medium for some time, such that they are easier to separate. After the retina is cleared from the vitreous on one side and the RPE on the other, it is placed in a small plastic container mounted on a glass plate with the electrode printed on it. On top of the retina, there is a membrane that keeps the retina in place while allowing nutrients to pass through. During the experiment, a nutrient solution is sucked through the experimental preparation to supply the retina with glucose and oxygen.

The recording setup itself is contained in a Faraday-cage to shield the recording from external electro-magnetic interference. The stimulus is projected on the retina from an oLED screen through a lens to focus it.

During the experiment, the retina is stimulated from the photoreceptor side, which normally is the outer part of the retina, fused with the RPE to supply the large amounts of nutrients that are required by photoreceptors. While we normally see through our ganglion cells (as they are small and transparent enough), it is impossible to record the electric activity of ganglion cells through the photoreceptor and bipolar layer. This is why it is very important that the RPE is removed from the retina, as it blocks the light stimulating the photoreceptors in the experiment. Similarly, vitreous that is not properly removed from the ganglion cell layer will isolate the electrical activity.

After the retina is normalized and shows only small amounts of spontaneous actvity, the recording is started on the data acquisition computer and the stimuli presented. The recording process takes several hours and depends on the health of the retina. A live preview of the band-pass filtered activity indicates if the retina is still responding and the experiment continues for as long as possible.

Spike sorting After a successful recording, the raw data of the MEA has to be processed, such that each recorded action potential can be attributed to a RGC.

Recording channels are pooled according to their similarity and then within each channel group, spikes are detected using a threshold of $4sd$. The voltage trace around each spike gets collected and fitted with a model, such that spike clusters are formed that have a high separability and good characteristics (e.g. similar spike shape). This process is semi-automated, so a person checks the goodness of the detected neurons and tweaks the parameters.

One important constraint of multi-electrode recordings is that if two spikes are simultaneous, only the stronger one will be counted. This means that meaningful cross-correlation can not be computed for cells from the same electrode.

Classification of Cell Types Cell types in the retina can be distinguished in two ways: according to their function (Baden et al. 2016) and their histochemical markers (Huberman

et al. 2009). Usually, RGC and bipolar cells that carry a specific marker also have similar functional characteristics, such as receptive field shape and transiency, and they also tile the retina in regular patterns, keeping a constant distance. Only when cells are lost is the distribution closer to a true random distribution (Esquiva et al. 2017).

Most RGCs have either an On- or an Off- transient response with some of them keeping a sustained response afterwards. A special group of types are direction selective RGCs, which respond stronger to moving stimuli in a specific direction. In the mouse there are three different populations of these cells, ON DSGCs which respond to one of three specific directions (relative to the main axis of the retina), Off DSGCs that respond only to upward motion and On-Off DSGCs, which respond to one of the four cardinal directions (Huberman et al. 2009).

The difficulty in characterizing these cell types and comparing them between different retinal preparations is that currently it is still very hard to specifically label a single cell type and then record from that population only. MEA recordings will always get a random sample of cells which then have to be clustered by functional responses, making it possible that atypical cells (which we would hope to find if we assume there is a difference between young and old retinas) will not be clustered as the same cell types. And even comparing clusters between two recordings is difficult since the functional properties of RGCs is already changing with eccentricity, which can not always be controlled in the experiments due to differences in age and the size of the eye balls between animals. The addition of stochastic sampling makes this process even more complicated. Some small cells e.g. might be under-represented when recording with an MEA.

A possible solution is two-photon microscopy, which can e.g. allow recording of optogenetically labelled cells, making targeting specific populations easier. It can also record the activity of cells (e.g. through Ca^{2+} imaging) with potentially a higher coverage and also capturing part of their morphology. With this technique becoming more accessible and precise in the future, cell classifications and the inter-individual differences across the lifespan could be a lot more certain in a few years.

3.4.2.2 Data Analysis

Receptive fields are traditionally estimated by white-noise checker patterns and a method called spike triggered average (STA). STA estimates the receptive field by averaging over all stimuli that elicited a response. This method works well for cells with a simple receptive field, but fails e.g. for cortical complex cells that respond both to a pattern and its luminance inverse equally. Another drawback of STA analysis is that it takes a lot of data to get a precise estimate of the Receptive Field (RF), but in contrast to Receptive Field (RF) estimation that is performed separate for each cell, the RFs of many cells can be estimated in parallel. To measure the receptive sub-fields of e.g. bipolar cells in the case of RGCs, either spike triggered covariance (STC) or non-negative matrix factorization (NMF) can be used (Liu et al. 2017).

Figure 3.4.2 shows the distance matrix of a typical recording of full-field ON-OFF stimuli. Most notable is that while there is a strong inter-stimulus distance, the within-stimulus distance in the first panel is just as strong. This stems from the fact that the firing rate in the OFF condition is very low and the spike pattern in the ON condition is slowly shifting, creating a large distance between different ON-trials. After 60 trials, the dynamic changes and the distance within the ON condition is now very low, but the distance between the first 60 trials and the remaining trials is very large. This non-stationarity during experiments can

pose a large problem for Receptive Field (RF) estimations.

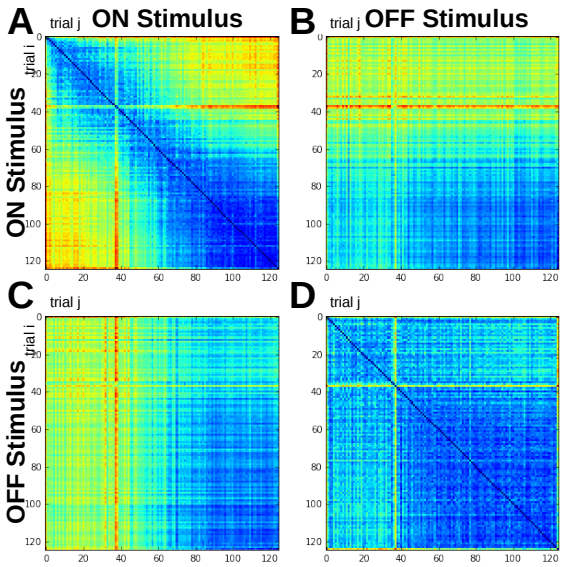

Figure 3.4.2: **Distance Matrix.** The distance matrix shows the change in activity in the different conditions. The upper left and lower right square show the distances within one stimulus condition (**A**, On-On and **D**, Off-Off). The upper right and lower left show the between distances (**B**, **C**). In the first half of the experiment, the On-On distances are quite low and the On-Off distance is high. However, in the second half, the activity looks very different, which we can see in the high distance comparing early On to late On. Late On is a lot closer to the Off condition. This is a sure sign that the cells either changed some characteristic that made it change cluster in the spike sorting phase, or it simply ceased to respond.

The number of cells recorded in each experiment is subject to the experience and skill of the experimenter, but also to a significant amount to chance. Figure 3.4.3 shows the spread of the number of cells recorded, separated by a recording quality rating. Cells with quality 1 and 2 can be included in an analysis, for the others it is not certain that all spikes have been recorded and were sorted to the appropriate neuron. In an optimistic estimation, on average about 20 cells can be recorded in one experiment with quality 1, about 40 including qualities 1 and 2.

3.4.2.3 Temporal Sensitivity

To estimate the number of experiments that need to be performed to get significant results, we needed to verify how many cells in a recording carry enough information to be useful for functional analysis. We took the maximum of temporal selectivity (the mutual information given a spike train distance of a certain temporal resolution, see Figure 3.4.4) and the change in response over the experiment (as seen e.g. in Figure 3.4.2) as indicators for reliability.

In the data we found many cells that had very well defined firing characteristics. Especially when restricting the analysis to the cells labelled as quality “1” during spike sorting (about 12% of the cells, about 40 per experiment), almost all cells had On-, Off- or even On-Off

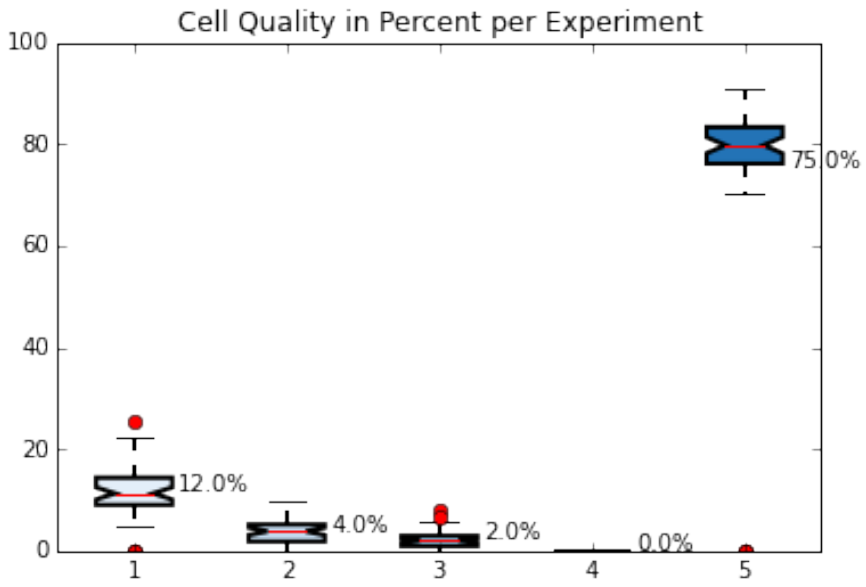

Figure 3.4.3: **Cell Recording Quality.** Over 10 experiments, a large portion of cells found by the clustering algorithm were not actual cells. Only about 12 % had a good quality, 16 % had an acceptable quality. On average about 40 cells would fall into classes "1" and "2".

responses to full field pulse stimuli. If we restricted the analysis to one type that is functionally characterizable, such as direction selective cells, we get another sub-group of these well-captured cells.

To estimate roughly whether the recorded cells gave a reliable answer throughout the experiment, we computed the mutual information between the spike trains and two stimuli (an On- and an Off-Transition) using VPD of different time-scales and the approach used in Brasselet, Johansson, and Arleo 2011 to estimate mutual information. In Figure 3.4.4 the temporal distribution shows that cells do have a preferred temporal scale. For each cell, we chose its most preferred temporal scale. For 10 recording sessions we computed the number of cells with $I*$ (see Equation 3.12) larger than 0.9 bit. Since we only distinguished two stimuli, the maximum possible mutual information would be 1 bit. Since many cells show a decay during the experiment, we additionally counted the cells that had a $I*$ larger than 0.9 bit not only overall, but in that specific time period as well. We found that on average, 34 cells were found that had a $I*$ (see Equation 3.6) larger than 0.9 bit and 30 that were stable until late in the experiment. This matches the estimate from the quality labels applied during spike sorting which would estimate around 40 cells in quality classes 1 and 2.

3.4.2.4 Estimation of Feasibility of Retinal Recordings

The goal of our analysis was to find out if a detection of the magnitude described in Eliasieh, Liets, and Chalupa 2007 and Samuel, Zhang, et al. 2011 is possible with the tool of MEA recordings and functional characterization. Both groups describe sprouting of bipolar and horizontal cells and a degeneration of RGC dendrites. Together the changes could amount to a change in about 10% of receptive field size, or no change in Receptive Field (RF) size, but a change in the structure of excitatory vs. inhibitory sub-fields of the Receptive Field (RF).

Receptive fields can be captured to a precision of one pixel when using a white-noise STA

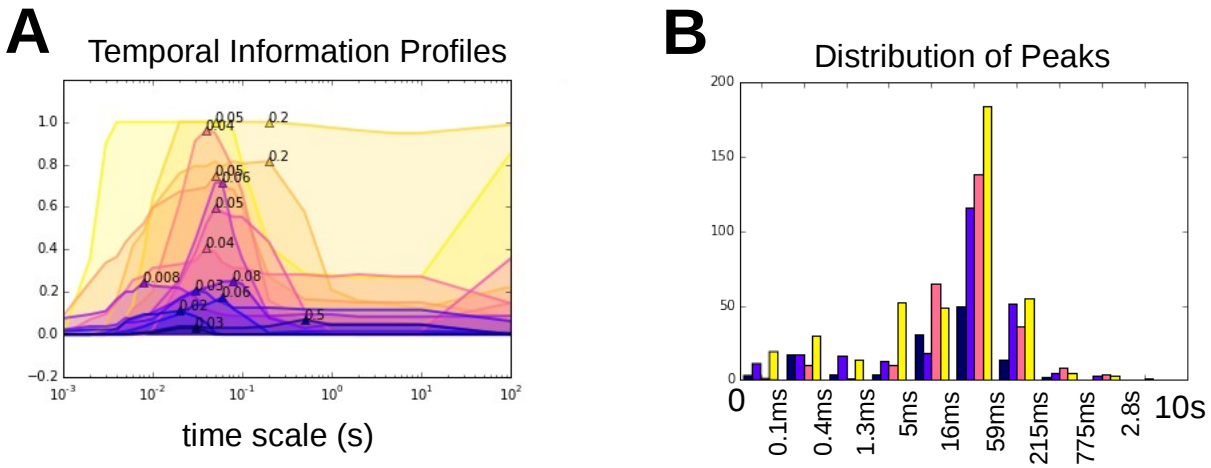

Figure 3.4.4: **Temporal Selectivity.** The mutual information between spike train and stimulus changes depending on the time scale we use to compare spike trains. In **A** it can be seen that a portion of cells have a clear maximum of mutual information. Colours depend on the time in the experiment (purple: early, yellow: late) **B** shows peaks in the temporal selectivity (numbers show the bin edges). Most cells have a maximum between 16 and 59ms.

paradigm. Even though the scale might differ between experiments, let's assume a pixel size of $40\mu m$ similar to Liu et al. 2017. RFs roughly have a spread between $0.1mm$ and $0.5mm$ diameter, depending on eccentricity this spread might shift up or down. This corresponds to between ≈ 6 and 157 pixels that are part of the receptive field.

Going from these assumptions, without sorting cells further, if we assume that the strength with which each pixel acts on the receptive field is given by a spatial Gaussian and the Receptive Field (RF) is strictly linear. Then we can numerically simulate to measure a receptive field with a specific size, converted into a Gaussian, such that the 2σ radius matches the radius of the Receptive Field (RF). We will then throw a biased coin for each pixel, corresponding to its weight. On average we will get the number of pixels that cover the 2σ radius of the receptive field (e.g. 6 for a $0.1mm$ diameter Receptive Field (RF)). For the simulation, we assume that cells have sizes uniformly distributed between $0.1mm$ and $0.5mm$ (to mimic using all available cells) and a change in size by 10%. We simulate measuring N cells (starting from 3 to 150), repeating the simulation 200 times to estimate the likelihood of success[1]. The result is visible in Figure 3.4.5. Given that there is a difference of 10% receptive field size, around 65 cells (in young and old each, 130 cells total) need to be recorded to get a 50% chance of finding a result with a $p < 0.05$ or 150 (300 cells total) to get a $p < 0.01$ with 50% chance or an 80% chance of a result with $p < 0.05$.

The number of cells that have to be recorded depends on the difference between the two means relative to the standard deviation. So if we restrict the Receptive Field (RF) size to a smaller range by e.g. only examining a single cell type, depending on the spread of the Receptive Field (RF) sizes, we might get better results. We will get exactly the same results if e.g. cells are uniformly distributed between $[0.1, 0.2]$ vs. $[0.11, 0.21]$ or between $[0.4, 0.5]$ vs.

[1]We repeated the numerical simulation only to bootstrap the probabilities, we do not actually recommend either recording cells iteratively until significance is reached (which would be "p-hacking" and has a high likelihood of returning false-significant results), or repeating the data acquisition 200 times.

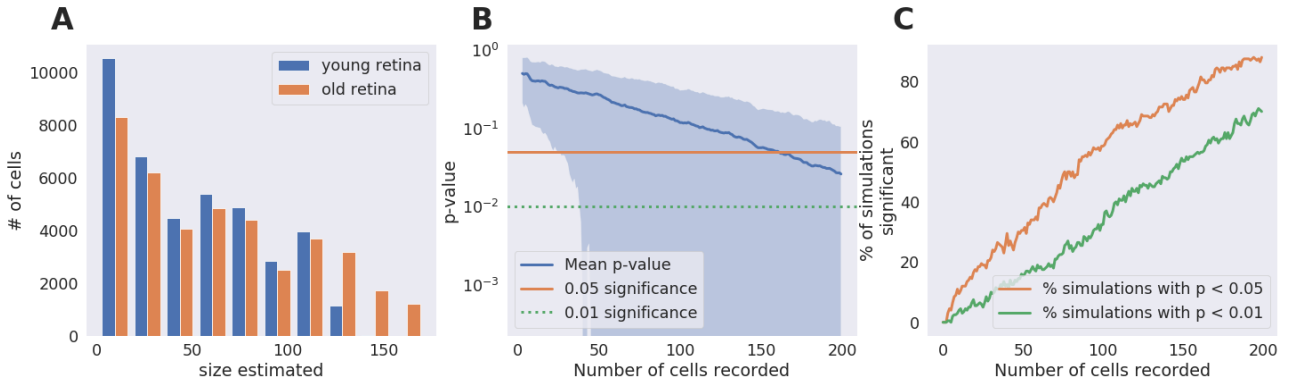

Figure 3.4.5: **Feasibility of MEA Experiments.** In a numerical simulation we estimated the receptive fields of up to 200 neurons in two populations each that differed in Receptive Field (RF) size by 10%. Each simulation was repeated 200 times. **A** shows the size histogram of all RFs measured. It is visible that the two distributions have a different mean. **B** shows the result of subsequent t-tests using an increasing percentage of cells to show which number of cells is necessary to get a significant result. The blue line shows the mean of the simulations and the blue area the 1std confidence interval. **C** shows the percentage of simulations that lead to a significant result. At around 75 cells the probability to get a $p < 0.05$ result is 50%, at 150 cells the probability to get a $p < 0.01$ result is 50%.

$[0.41, 0.51]$. While for the first set of cells this would constitute a 10% change in Receptive Field (RF) size, it's only a 2.5% increase for the larger cells. For a shift from $[0.3, 0.4]$ to $[0.33, 0.44]$, only 25 cells are required to almost guarantee a positive result.

The complications for this approach is that first of all a cell type has to be found that has large, but very predictable Receptive Field (RF) sizes - without having hard data for it, it seems that size variability scales with Receptive Field (RF) size. Then these cells have to be well identifiable and occur with good frequency in recordings. If e.g. we find our type in one out of 10 cells, then on average we might get 4 good cells (out of ≈ 40) in a successful experiment. To get 25 cells we would need 7 experiments, which would give 280 overall recorded cells, making the restriction to one cell type not that much more useful. One abundant, large cell type is the large Off-alpha cell.

In our considerations we also neglected changes in eccentricity, the suppressive surround and potential increased difficulty to get data from old retinas.

3.4.2.5 Conclusion

Our estimates for the best case scenario predict that more than 10 successful experiments (recording 300 cells) need to be performed and analysed for a decent chance of finding a $p < 0.05$ result. Including training, we estimate this project would amount to at least one and a half years of work, just recording and data analysis. Also the very optimistic, clear cut change in receptive field size is not very likely since there are two opposing changes found morphologically in the retina: horizontal and bipolar cell sprouting and a decrease in the RGC dendritic tree. These changes are more likely to affect the surround modulation of cells than the excitatory receptive field.

A big problem for receptive field estimation is the inhibitory surround and non-linearities.

When estimating a receptive field with white noise stimuli, the stimulus space is sampled randomly under the assumption that a linear receptive field can be obtained by averaging over all stimuli that elicited a response (spike triggered average (STA)). The surround is much larger than the center: Deny et al. 2017 found that the surround and non-linear effects were able to influence the firing rate of cells over $900\mu m$ away from the stimulus, while the linear explainable effect reaches $300\mu m$ at the same retinal eccentricity. Methods like non-negative matrix factorization (NMF) (Liu et al. 2017) explicitly exclude inhibitory influences and instead focus on the stimulus correlations that reveal excitatory subunits such as bipolar cells. Estimating the shape and density of the surround inhibition experimentally is still a hard problem. Closed-loop methods have been used to adjust the stimulus according to the online recorded activity from MEAs (see e.g. Gollisch and Herz 2012 or Ferrari et al. 2017). To measure the inhibitory surround, such a closed-loop paradigm could be used to first estimate excitatory parts of the receptive field and then probe neighbouring regions while keeping the center stimulated.

Due to the very high amount of effort involved in recording an adequate amount of RGCs and the relatively slim chance of finding significant differences with current methods, we concentrated our efforts on modelling. On the one hand, we want to investigate if the changes we expect would make a large difference in the sensory process (see sections 3.5.1 and 4.6), but we also suspect that more effective experimental paradigms that are tailored to find the differences have a higher chance for success. On the other hand, we wanted to build a tool that made it possible to design stimuli to specifically find size differences in receptive fields or the inhibitory surround (see Chapter 5).

3.5 Effect of Noise on LGN cells

As we discussed in section 1.3.1, the magnocellular and parvocellular pathway are affected differently in aging. Since the two pathways already differ in response properties at the level of the LGN, we developed the idea that from these differences we can infer how low level mechanisms change in age. We used Virtual Retina, a model that was developed for modelling retinal ganglion cells and LGN cells, which is discussed in section 5.4.2 and analysed the resulting spike trains.

Emilie Mayer, a master student at Ecole de Mines, participated in an internship in the project and wrote her master thesis on the simulations and analysis she performed (see Section 3.5.2 for more details).

3.5.1 Gain Control or Spatial Integration?

Spear et al. 1994 found in rhesus monkey LGN that while magnocellular neurons have significantly higher maximal response rates and signal-to-noise ratios than parvocellular neurons, aging reduces the maximal firing rate in magnocellular slightly and increases it in parvocellular neurons. The signal-to-noise-ratio (SNR) drops in both. How does this translate to visual perception?

Due to the different characteristics of magno- and parvocellular pathways, it is possible to distinguish them in psychophysical experiments simply by choosing the appropriate stimuli. A stimulus with a fast onset will activate the M pathway more than the P pathway. In contrast

the P pathway can be more engaged with a large contrast change. Using saturation, stimuli can be targeted at each of the pathways in isolation (Elliott and Werner 2010).

We know from Bonnel, Mohand-Said, and Sahel 2003; Elliott and Werner 2010 that, although there are strong aging effects in both magnocellular and parvocellular pathways, the parvocellular pathway is more affected with an increase of threshold of 0.2-0.3 log units, while the magnocellular pathways threshold only increased half as much. This differential change can be due to a number of differences between the two pathways, including the aforementioned contrast-gain-control and spatial integration.

Under the assumption that noise at the sensory level increases with age, we examine a model of local gain control and spatial summation that was proposed by Wohrer, Kornprobst, and Vieville 2007 to model retinal ganglion cells and cells in the Lateral Geniculate Nucleus (LGN). We ask two questions: (1) does stronger local gain control - as formulated in our model - filter out incoming noise? And (2) does increased spatial summation filter out incoming noise? Further, we examine if the stochasticity in noise generation would overshadow each effect, making it in irrelevant.

In the first part of the project (section 3.5.2) we find that gain control does not have a strong effect on noisy input, while spatial summation filters out noise depending on the width of spatial filtering. We further expand on these results in section 3.5.3.

We used the VirtualRetina simulator Wohrer and Kornprobst 2009 for the first set of simulations and the `convis` retina model for later simulations to generate biologically plausible LGN spikes from synthetic luminance stimuli of four configurations which were a combination of gain control being enabled or disabled and the final spatial integration stage being enabled or disabled.

Gain Control and Spatial Integration Model The gain control mechanism implemented in VirtualRetina and `convis` follows the model devised by Shapley and Victor 1981. It depends on contrast since the previous stage converted the luminance input into a contrast signal.

While a simple inhibition model would only affect the amplitude of the signal (see Figure 3.5.1), the model defined here also changes the phase of the signal (see Figure 3.5.2) in accordance with electrophysiological observations.

The model is defined as follows:

$$\frac{dV_{Bip}}{dt}(x,y,t) = I(x,y,t) - g_A(x,y,t)dV_{Bip}(x,y,t) \tag{3.13}$$

$$g_A(x,y,t) = G * E * Q(VBip)(x,y,t) \tag{3.14}$$

$$Q(VBip) = g_A^0 + \lambda_A V_{Bip}^2 \tag{3.15}$$

$*$ denoting the convolution operator, G and E spatial Gaussian and temporal exponential filters respectively

Then, the output is processed by a static non-linearity and an optional spatial integration filter (another Gaussian).

$$I_{Gang}(x,y,t) = G * N(eT * V_{Bip}) \tag{3.16}$$

$$N(V) = \begin{cases} \frac{i_G^0}{1-\lambda(V-v_G^0)/i_G^0}, & \text{if } V < v_G^0 \\ i_G^0 + \lambda(V - v_G^0), & \text{otherwise} \end{cases} \tag{3.17}$$

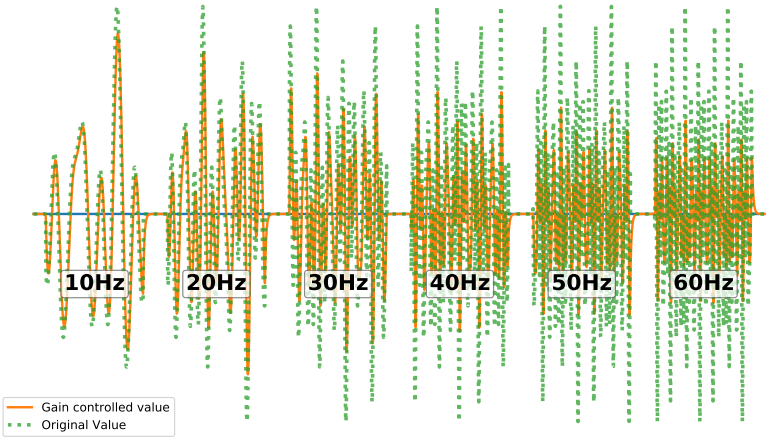

Figure 3.5.1: **Response of the Gain Control.** Stimuli with different frequency content are affected by the contrast gain control in a different way. While the presentation of the "10 Hz" stimulus is almost indistinguishable from the output, the higher frequencies have a much stronger amplitude attenuation. (frequencies of the signals are scaled arbitrarily)

3.5.2 Project 3: Investigating the Noise Hypothesis for Healthy Ageing: the Effect of Noise on Retinal Processing - Master Thesis by Emilie Mayer

→ see also List of Projects

In the following section I will try to summarize the work Emilie did for her Master thesis in 2016 while she was an intern at the *institute de la vision*. The outline of her project was to investigate the effects of noise on the gain control mechanisms of the LGN. For that we prepared a general framework, but left her room to put her own direction on the project. She started getting familiar with the Virtual Retina simulator Wohrer 2008 and modified the software to add noise to different stages and also accept an additional input sequence that can be fed into specific layers. For the final analysis we did not use the modifications, but rather only varied the configuration of the retina model to simulate magnocellular and parvocellular LGN cells. It might seem odd to use a retina model to simulate LGN cells, but the responses can be modelled fairly similar. Even if LGN cells have a lower firing rate and stronger gain control, their receptive fields are similar to RGC cells. Since we use a retina model that includes contrast gain control which has also been used to model gain control in the LGN (Wohrer and Kornprobst 2009), the results are transferable to LGN cells.

Figure 3.5.2: **Phase Advance of Gain Control.** These plots show the in- vs. the output of the contrast gain control mechanism at inputs of different frequencies. The 10 Hz trace at the far left is close to the 1:1 diagonal, but the faster the stimulus becomes, the more the plot rotates clockwise, indicating a temporal shift between in- and output. (frequencies of the signals are scaled arbitrarily)

3.5.2.1 Methods

We calculated the response of a local gain control circuit and a spatial integration layer to a noisy moving grating stimulus over different noise levels. The output of the model were spikes, generated by noisy leaky integrate-and-fire neurons. We then analysed the effect that noise had on the differences of responses by measuring the variability of the produced spike trains.

Stimulus We presented five different stimuli to the model at three noise levels and two filter conditions each.

1. Drifting gratings with static noise (**A1** in Figures 3.5.3 and 3.5.4)
2. Drifting gratings with 10Hz refreshed noise (**A2**)
3. Drifting gratings with 40Hz refreshed noise (**A3**)
4. Larger drifting gratings with 10Hz refreshed noise (**B**)
5. Fast drifting gratings and 40Hz refreshed noise (**C**)

Each stimulus received either Gaussian noise or filtered noise that was truncated to only contain spatial frequencies close to the stimulus.

Retina Configuration We compared three different configurations and manipulated additionally the strength of contrast gain control. Each parameter set and stimulus configuration was fed to VirtualRetina (see Section 5.4.2) at each noise level ten times and the resulting spike trains were analysed.

- **P-Cell:** the parvocellular configuration had no gain control ($\lambda_{amp} = 0$) and no spatial integration.
- **(Magnocellular) X-Cell:** the X-cell had gain control ($\lambda_{amp} = 200$) and a steeper static nonlinearity. It did not have spatial pooling.

- **(Magnocellular) Y-Cell:** the Y-cell had gain control ($\lambda_{amp} = 200$), a steeper static non-linearity and spatial pooling that blurs the rectified input to the ganglion cells by a standard deviation of 0.1 cycles per degree (cpd). This leads to a more non-linear response.

Table 3.1: Parameters that differ between the configuration files. Each configuration is used once with enabled contrast gain control (CGC) and once without.

Parameter	Parvo	Parvo CGC	Magno X	Magno X CGC	Magno Y	Magno Y CGC
lambda_amp	0	200	0	200	0	200
bipolar-amplification_Hz	100	100	400	400	400	400
sigma-pool	0	0	0	0	0.1	0.1

Signal and Spike Train Comparison The output of each simulation was a set of 10 spike trains for each combination of input noise, stimulus image and simulator configuration. To assess the variability, the spike trains of each noise level were compared to a reference simulation in which no noise was present.

3.5.2.2 Results

The results show a general increase in Victor-Purpura Distance in relation to noise, as expected. For the `Parvo` configuration, the increase was most pronounced, for `Magno X` the incline is weaker and for `Magno Y` the relation between noise level and Victor-Purpura Distance is abolished for almost all stimuli configurations. When contrast gain control is enabled, Victor-Purpura Distance drops in all simulations, but keeps the linear relationship with noise level for `Parvo` and `Magno X`, while in `Magno Y` there is an increase in Victor-Purpura Distance from medium to high noise for Gaussian noise in four of the five conditions.

From the results it can be concluded that contrast gain control and the static non-linearity did reduce variability, but not the variability induced by input noise, since the linear relationship between Victor-Purpura Distance and noise level still had the same slope. For the configuration that additionally included spatial pooling, this relation was mostly flat, showing no change in output variability with respect to input noise. Whether this means that spatial pooling generally abolishes noise, or is just less sensitive to noise, such that the externally induced variability is masked by internal variability, is inconclusive from these results.

3.5.3 Project 4: Effect of Gain Control and Spatial Integration (Part II)

→ see also List of Projects

Since the previous project left a number of questions unanswered, we made some additional simulations after the departure of Emilie.

One of our questions was whether the differences between *no gain control*, *gain control* and *gain control and spatial integration* would hold for much higher or lower noise levels. Also we found that the distance to the no-noise condition might not be the best way to quantify the sensitivity to noise.

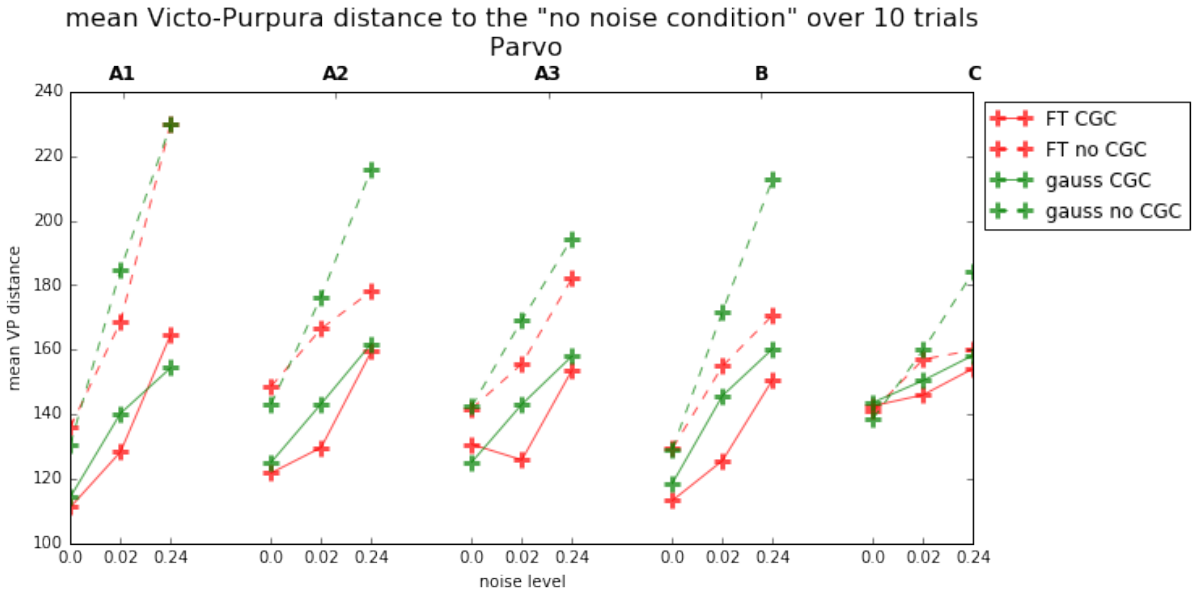

Figure 3.5.3: **Results Parvocellular Pathway. A1-C** reference the stimulus used (see Section 3.5.2.1). The *VP* distance to the noise-free simulation rises with noise level. Enabling contrast gain control (solid lines) reduces the distance. Green lines show results for broad-band noise, red lines for band-pass filtered noise. Courtesy Emilie Mayers Master Thesis.

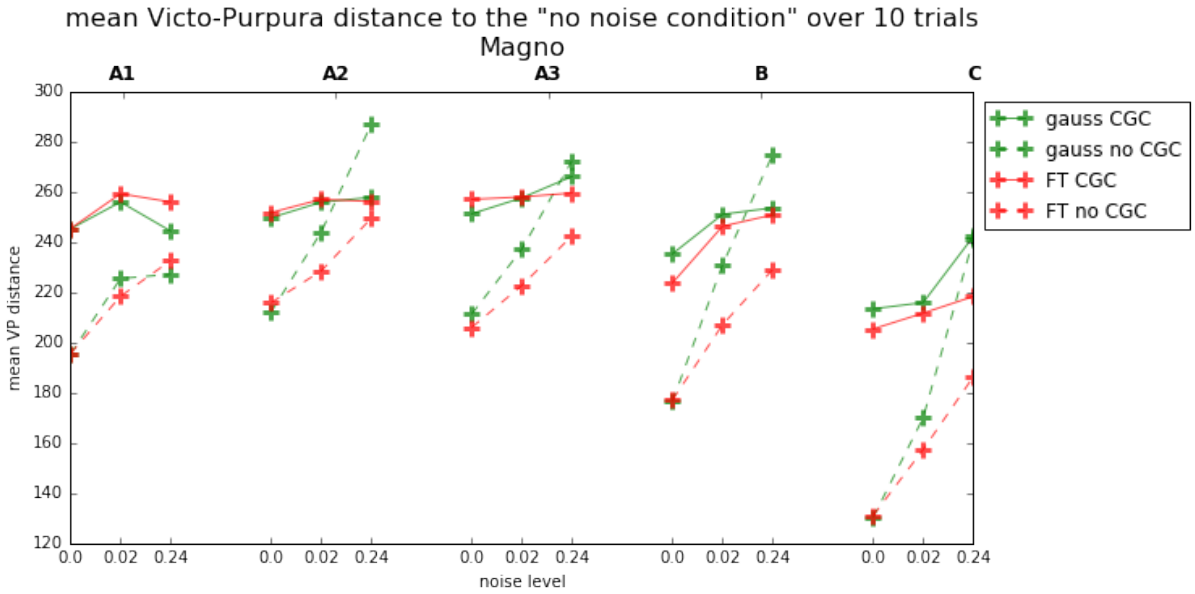

Figure 3.5.4: **Results Y-Cell Magnocellular Pathway. A1-C** reference the stimulus used (see Section 3.5.2.1). The *VP* distance to the noise-free simulation rises with noise level, however less than for parvocellular (see Figure 3.5.3). Enabling contrast gain control (solid lines) increases the distance, but reduces the slope wrt. noise, such that for some stimuli (**A2**,**A3**) the distance is independent of noise level. Green lines show results for broad-band noise, red lines for band-pass filtered noise. Courtesy Emilie Mayers Master Thesis.

We used Convis (Huth, Masquelier, and Arleo 2018, also Chapter 5) to model LGN-like responses to visual stimuli, using a model similar to Wohrer, Kornprobst, and Vieville 2007, but more easily integrated into our Python analysis code.

We measure three Victor-Purpura Distance for each noise level (see Figure 3.5.5):

- **internal variability**: the distance between the spike trains generated from the exact same stimulus
- **noise induced variability**: the distance between two simulations with different instantiations of external noise
- **noise level induced variability**: the distance to a simulation without noise

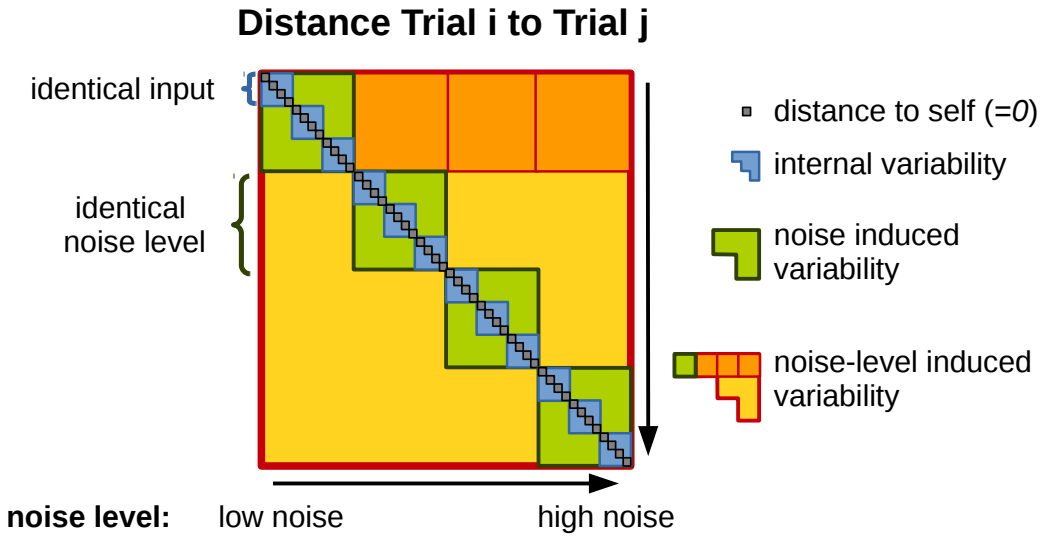

Figure 3.5.5: **Different Forms of Variability in the Distance Matrix.** The simulation at each of the k noise levels was repeated j times (grey pixels in blue squares, here: 4) with exactly the same input (including the same external input noise), then the same was done for i different instantiations of noise (blue squares in green squares, here: 3). The marked areas of the distance matrix can then be summed to get a measure of internal variability and noise induced variability at each noise level, as well as the noise-level induced variability comparing each trial to the noise free condition (the first green and the dark orange boxes).

We did this since the distance within each noise level will usually be smaller than the distance to the noise-free stimulus, but will say more about the actual effect of noise. In contrast to simple linear processing, the noisy stimuli do not generate output that is distributed equally around the output of the noise-free simulation, such that the mean of many noisy trials would equal the non-noisy trial. Rather the addition of noise changes the response enough that we can even think of it as a completely new stimulus that is encoded.

We extended the noise range until we could distinguish two plateaus: a lower noise limit, where external noise has no effect and an upper noise limit where the activity is maximally random, such that an increase in external input noise has no influence on the distances.

In addition to changing the level of noise, we also change the input gain of the stimulus (including noise).

3.5.3.1 Results

Changing the contrast of the stimulus reveals for the gain-control free model a maximal distance that is a combination of input contrast. This maximal distance seems to correlate with the firing rate of the model having a value around 100 Hz. For larger input gain, the firing rate increases, but the *VP* distance decreases since the firing is less temporally coordinated (see Figure 3.5.6).

With Contrast Gain Control, firing rates are generally lower, removing this problem (see Figure 3.5.7).

Figure 3.5.8 shows that firing rates reduce strongly if we use a spatial filter before the spiking mechanism.

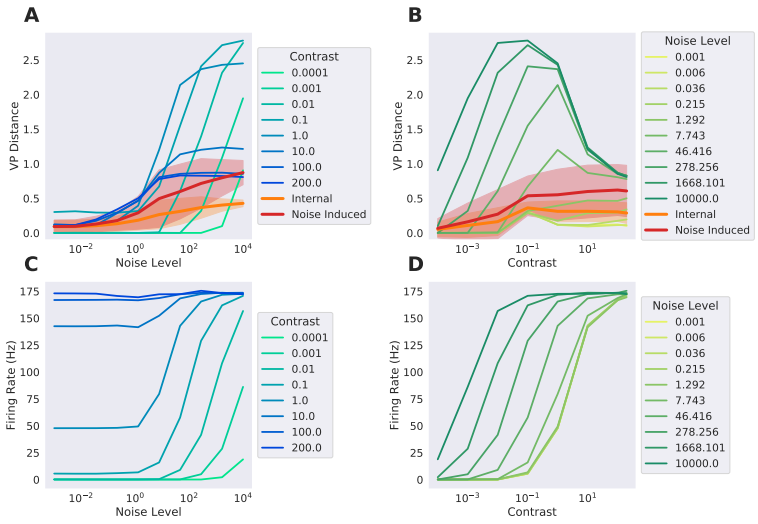

Figure 3.5.6: **Simulations without Contrast Gain Control.** **A** and **B** show how Victor-Purpura Distance changes over external noise level and contrast respectively. The thin lines show distances to a noise-free simulation (*noise-level-induced differences*), the thick orange and red line show the variability due to *internal* variability (orange) and internal and external noise (*noise-induced variability*, red) **C** and **D** show the firing rates of each simulation.

If instead of Victor-Purpura Distance we use the *firing-rate-independent dissimilarity*, we see that ignoring firing-rate, the increased firing rate due to high contrast for the non-gain controlled model results in the lowest dissimilarity. This means that the increase in distance seen by *VP* is mostly due to the firing rate and not variability in temporal structure. For the gain controlled models, we see that the low firing rate at the low end of contrast and noise_level makes the dissimilarity start at 0.5, but then the dissimilarity first increases and then decreases, probably also due to high firing rates. The model with gain control and spatial integration shows almost no difference between the variability that is coming from internal noise sources and the added external variability: simulations that get exactly the same noise instance are exactly as variable as the simulations that get fresh noise each time! This means that while the variability changes with the noise level, the variability does not actually *come* from the noise. Rather the noise changes contrast gain control properties, changing the firing rate, but then the variability comes mainly from the spike generation.

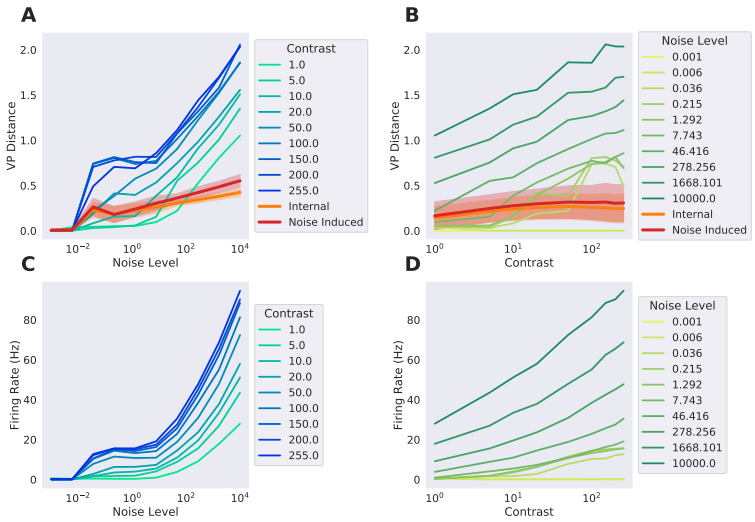

Figure 3.5.7: **Simulations with Contrast Gain Control.** **A** and **B** show how Victor-Purpura Distance changes over external noise level and contrast respectively. The thin lines show distances to a noise-free simulation (*noise-level-induced differences*), the thick orange and red line show the variability due to *internal* variability (orange) and internal and external noise (*noise-induced variability*, red) **C** and **D** show the firing rates of each simulation.

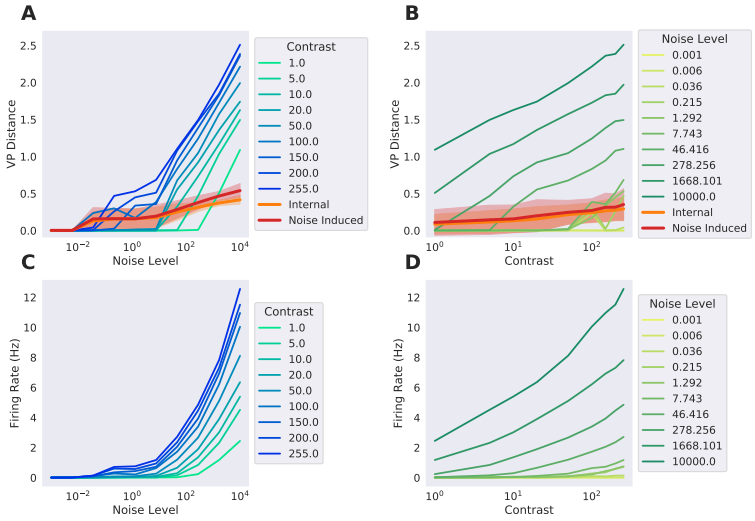

Figure 3.5.8: **Simulations with Contrast Gain Control and Spatial Integration.** **A** and **B** show how Victor-Purpura Distance changes over external noise level and contrast respectively. The thin lines show distances to a noise-free simulation (*noise-level-induced differences*), the thick orange and red line show the variability due to *internal* variability (orange) and internal and external noise (*noise-induced variability*, red) **C** and **D** show the firing rates of each simulation.

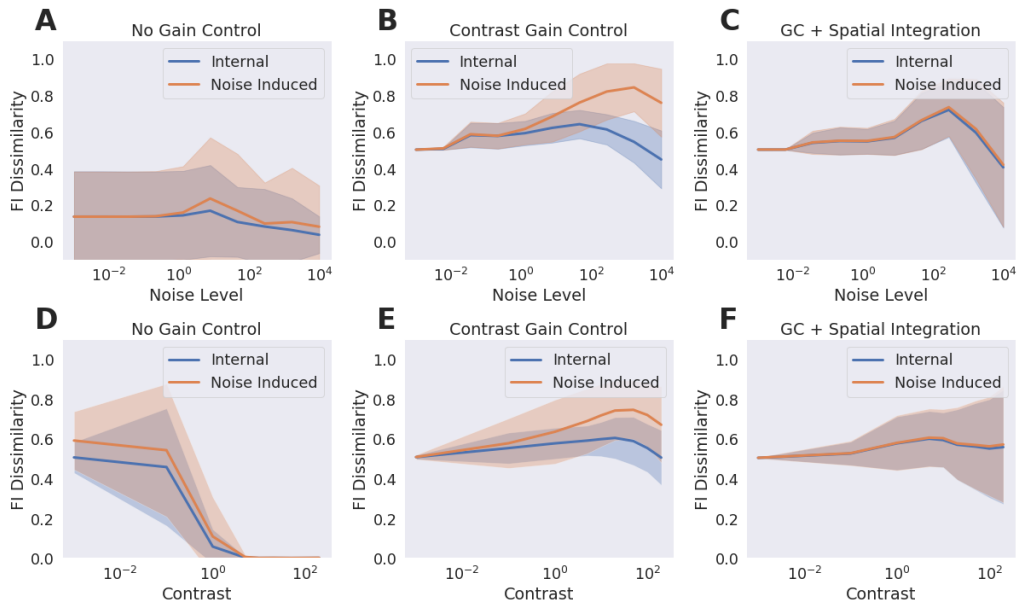

Figure 3.5.9: **Firing-Rate-Independent Dissimilarity.** In contrast to the plots using Victor-Purpura Distance, the distances from the non-gain-controlled model drop to very low dissimilarity with increasing contrast (compare Fig. 3.5.6 **B**). With gain control (compare Fig. 3.5.7 **A,B**) variability rises and then falls over both noise level and contrast. Adding spatial integration (compare Fig. 3.5.8 **A,B**) has a similar effect over noise level, but not stimulus contrast.

3.6 Summary

Photoreceptor noise is increased in age due to optical factors, such as reduced retinal illumination, scatter and inhomogeneities of the ocular medium, or properties of the photoreceptors themselves. In this chapter we started to probe how this increase in input variability is affected by gain control and spatial integration.

Comparing gain control and non-gain control in the first part of the project (Figures 3.5.3) shows that the gain controlled model reduces Victor-Purpura Distance compared to non-gain-controlled. The "Y-Magno" configuration, which additionally has a spatial integration stage (Figure 3.5.4), changes this relation. For some stimuli (**A1**), the distance for the gain controlled stimulus is even higher than for the non-gain controlled. Gain control in general lowers the slope and the stimulus stays more stable, as the gain control constrains the firing rate. It is possible that the flat profile of the "Y-Magno" configuration with gain control shows that either the effect of noise strength was completely removed, or the effect of noise is only visible at higher noise levels.

Exploring a larger noise range shows that the configuration with gain control and spatial integration indeed does have a slope and two plateaus, not just a single plateau as found in the previous simulation. Extremely low and extremely high firing rates result in low Victor-Purpura Distance, which is why the model without contrast gain control has a lower Victor-Purpura Distance for high input noise than intermediate input noise. The gain controlled models have overall a lower firing rate and a slower increase of both firing rate and Victor-Purpura Distance. A comparison of **internal variability** (orange and red curves in Figures

3.5.6, 3.5.7 and 3.5.8) shows that for the no-gain control model the noise induced variability is about twice as strong as the internal variability alone, meaning that internal noise and external noise (at a fixed noise level) has about the same strength. For the gain controlled model, the two curves are much closer together, showing that the internal variability is stronger than the external variability. The internal variability of the model with gain control and spatial integration was similar to the model without spatial integration, even though the between-distances were about 20% higher. Using **firing-rate independent dissimilarity**, the internal variability shows that with increasing contrast, for the no-gain control model drops strongly in dissimilarity as the high firing rate produces very regular firing. A significant difference between internal- and noise-induced variability is only visible in the gain controlled model. The gain controlled and spatial integration model, as well as the non-gain controlled model show similar dissimilarity between simulations that only differ in internal noise and those that also get "fresh" external noise. We found that the current definition of the firing-rate independent dissimilarity has a few flaws, e.g. in contrast to *VP* and other distances, getting a signal-to-noise ratio like quantity is not very informative since high and low values are asymptotically bound by 0 and 1. For future projects, a different formulation of a measure that is orthogonal to firing-rate distance should be investigated.

As a conclusion, both gain control and spatial integration affect the response of our model to increasing input noise, however, the difference on trial-to-trial variability with and without spatial-integration is very similar. This result gives evidence to the hypothesis that if noise at the level of photoreceptors increases, the magnocellular pathway is more capable to deal with increased noise levels than the parvocellular layer due to its stronger gain control. This is in line with findings from Spear et al. 1994 that show that the magnocellular pathway is less affected by detrimental aging effects. It also confirms our idea that the effects of input noise can propagate through the visual system and cause a wide range of aging effects that at the first glance do not seem to be caused by increased input noise.

References

Baden, Tom et al. (2016). "The functional diversity of retinal ganglion cells in the mouse". In: *Nature* 529.7586, pp. 345–350. ISSN: 0028-0836. DOI: 10.1038/nature16468. URL: http://www.nature.com/articles/nature16468.

Bonnel, Sébastien, Saddek Mohand-Said, and José Alain Sahel (2003). "The aging of the retina". In: *Experimental Gerontology* 38.8, pp. 825–831. ISSN: 05315565. DOI: 10.1016/S0531-5565(03)00093-7.

Brasselet, Romain, Roland S Johansson, and Angelo Arleo (2011). "Quantifying neurotransmission reliability through metrics-based information analysis." In: *Neural computation* 23.4, pp. 852–81. ISSN: 1530-888X. DOI: 10.1162/NECO_a_00099. URL: http://www.ncbi.nlm.nih.gov/pubmed/21222522.

Deny, Stéphane et al. (2017). "Multiplexed computations in retinal ganglion cells of a single type". In: *Nature Communications* 8.1, pp. 1–17. ISSN: 20411723. DOI: 10.1038/s41467-017-02159-y.

Eliasieh, Kasra, Lauren C. Liets, and Leo M. Chalupa (2007). "Cellular reorganization in the human retina during normal aging". In: *Investigative Ophthalmology and Visual Science* 48.6, pp. 2824–2830. ISSN: 01460404. DOI: 10.1167/iovs.06-1228.

Elliott, Sarah L and John S Werner (2010). "Age-related changes in contrast gain related to the M and P pathways." In: *Journal of vision* 10.4, pp. 4.1–15. ISSN: 1534-7362. DOI: 10.1167/9.8.1071.

Esquiva, Gema et al. (2017). "Loss of melanopsin-expressing ganglion cell subtypes and dendritic degeneration in the aging human retina". In: *Frontiers in Aging Neuroscience* 9.APR, pp. 1–17. ISSN: 16634365. DOI: 10.3389/fnagi.2017.00079.

Ferrari, Ulisse et al. (2017). "Closed-Loop Estimation of Retinal Network Sensitivity by Local Empirical Linearization". In: *eneuro* 4.6, ENEURO.0166–17.2017. ISSN: 2373-2822. DOI: 10.1523/ENEURO.0166-17.2017. URL: http://eneuro.org/cgi/doi/10.1523/ENEURO.0166-17.2017.

Gollisch, Tim and Andreas V M Herz (2012). "The iso-response method: measuring neuronal stimulus integration with closed-loop experiments." In: *Frontiers in neural circuits* 6.December, p. 104. ISSN: 1662-5110. DOI: 10.3389/fncir.2012.00104. URL: http://www.pubmedcentral.nih.gov/articlerender.fcgi?artid=3525953%7B%5C&%7Dtool=pmcentrez%7B%5C&%7Drendertype=abstract.

Huberman, Andrew D. et al. (2009). "Genetic Identification of an On-Off Direction- Selective Retinal Ganglion Cell Subtype Reveals a Layer-Specific Subcortical Map of Posterior Motion". In: *Neuron* 62.3, pp. 327–334. ISSN: 08966273. DOI: 10.1016/j.neuron.2009.04.014. URL: http://dx.doi.org/10.1016/j.neuron.2009.04.014.

Huth, Jacob (2011). "Bachelor Thesis : Synchrony Binding in Noise Excitable Coherence Resonance Synchrony Binding in Noise Excitable Coherence Resonance Networks". PhD thesis. DOI: 10.13140/RG.2.2.27976.57607.

Huth, Jacob, Timothée Masquelier, and Angelo Arleo (2018). "Convis: A Toolbox to Fit and Simulate Filter-Based Models of Early Visual Processing". In: *Frontiers in Neuroinformatics* 12.March, pp. 1–16. ISSN: 1662-5196. DOI: 10.3389/fninf.2018.00009. URL: http://journal.frontiersin.org/article/10.3389/fninf.2018.00009/full.

Kolesnikov, Alexander V et al. (2010). "Age-related deterioration of rod vision in mice." In: *The Journal of neuroscience : the official journal of the Society for Neuroscience* 30.33, pp. 11222–11231. ISSN: 0270-6474. DOI: 10.1523/JNEUROSCI.4239-09.2010.

Liu, Jian K. et al. (2017). "Inference of neuronal functional circuitry with spike-triggered non-negative matrix factorization". In: *Nature Communications* 8.1. ISSN: 20411723. DOI: 10.1038/s41467-017-00156-9. URL: http://dx.doi.org/10.1038/s41467-017-00156-9.

Masland, R. H. (2001). "Neuronal diversity in the retina". In: *Current Opinion in Neurobiology* 11.4, pp. 431–436. ISSN: 09594388. DOI: 10.1016/S0959-4388(00)00230-0.

Rossum, M C van (2001). "A novel spike distance." In: *Neural computation* 13.4, pp. 751–763. ISSN: 0899-7667. DOI: 10.1162/089976601300014321.

Samuel, Melanie a, P Emanuela Voinescu, et al. (2014). "LKB1 and AMPK regulate synaptic remodeling in old age." In: *Nature neuroscience* 17.August, pp. 1–10. ISSN: 1546-1726. DOI: 10.1038/nn.3772. URL: http://www.ncbi.nlm.nih.gov/pubmed/25086610.

Samuel, Melanie a., Yifeng Zhang, et al. (2011). "Age-Related Alterations in Neurons of the Mouse Retina". In: *Journal of Neuroscience* 31.44, pp. 16033–16044. ISSN: 0270-6474. DOI: 10.1523/JNEUROSCI.3580-11.2011.

Sanes, Joshua R. and Richard H. Masland (2015). "The Types of Retinal Ganglion Cells: Current Status and Implications for Neuronal Classification". In: *Annual Review of Neuroscience* 38.1, pp. 221–246. ISSN: 0147-006X. DOI: 10.1146/annurev-neuro-071714-034120. URL: http://www.annualreviews.org/doi/abs/10.1146/annurev-neuro-071714-034120.

Shapley, Robert M and J. D. Victor (1981). "How the contrast gain control modifies the frequency responses of cat retinal ganglion cells." In: *The Journal of physiology* 318, pp. 161–179. ISSN: 0022-3751, 1469-7793.

Spear, P. D. et al. (1994). "Effects of aging on the primate visual system: spatial and temporal processing by lateral geniculate neurons in young adult and old rhesus monkeys". In: *Journal of Neurophysiology* 72.1, pp. 402–420. ISSN: 0022-3077. DOI: 10.1152/jn.1994.72.1.402. URL: http://www.physiology.org/doi/10.1152/jn.1994.72.1.402.

Strong, S. P. et al. (1998). "Entropy and Information in Neural Spike Trains". In: *Physical Review Letters* 80.1, pp. 197–200. ISSN: 0031-9007. DOI: 10.1103/PhysRevLett.80.197.

arXiv: 9603127 [cond-mat]. URL: http://link.aps.org/doi/10.1103/PhysRevLett.80.197.

Tillman, Megan A., Athanasios Panorgias, and John S. Werner (2016). "Age-related change in fast adaptation mechanisms measured with the scotopic full-field ERG". In: *Documenta Ophthalmologica*, pp. 1–12. ISSN: 15732622. DOI: 10.1007/s10633-016-9541-2. URL: http://link.springer.com/10.1007/s10633-016-9541-2.

Victor, J D and K P Purpura (1996). "Nature and precision of temporal coding in visual cortex: a metric-space analysis." In: *Journal of Neurophysiology* 76.2, pp. 1310–1326. ISSN: 0022-3077. URL: http://eutils.ncbi.nlm.nih.gov/entrez/eutils/elink.fcgi?dbfrom=pubmed%7B%5C&%7Did=8871238%7B%5C&%7Dretmode=ref%7B%5C&%7Dcmd=prlinks%7B%5C%%7D5Cnpapers2://publication/uuid/AB4FACE8-C94C-486E-9EDC-FAABA32E1EAF.

Wohrer, Adrien (2008). "Model and large-scale simulator of a biological retina, with contrast gain control". PhD Thesis. University of Nice-Sophia Antipolis.

Wohrer, Adrien and Pierre Kornprobst (2009). "Virtual Retina: a biological retina model and simulator, with contrast gain control." In: *Journal of computational neuroscience* 26.2, pp. 219–49. ISSN: 1573-6873. DOI: 10.1007/s10827-008-0108-4. URL: http://www.ncbi.nlm.nih.gov/pubmed/18670870.

Wohrer, Adrien, Pierre Kornprobst, and Thierry Vieville (2007). "Virtual Retina : a biological retina model and simulator, with contrast gain control [Research Report]". In: *RR-6243*, 32 <inria–00160716v2>.

Chapter 4

Investigating Aging by Modelling Psychophysics

> Everything you see or hear or experience in any way at all is specific to you. You create a universe by perceiving it, so everything in the universe you perceive is specific to you.
>
> *Douglas Adams* in "Mostly Harmless"

4.1 Introduction

While the previous chapter modelled neural data, most of electrophysiological data is bound to come from non-human animals. But the goal of aging research is primarily concerned with human aging, since humans are the ones with increasing life-span and the resulting increase in age-related pathologies and the ultimate goal is to improve the quality of life of humans in old age.

With human subjects of course we are limited non-invasive methods such as psychophysical measurements. Invasive neural recordings are only possible in rare cases (such as during necessary neuro-surgery) and thus don't allow us to adequately sample the population to the same degree as we can do in non-human animals. Some electro-physiological findings might transfer between species, while some may not. It would be very helpful to know which changes in e.g. rhesus monkeys also occur in humans without having to repeat the same experiments. A method to approach this problem is to use computational models of the aging effects we find in other species and verify these models with data we can collect from humans without ethical concerns.

We already reviewed some psychophysical results of aging changes in chapter 1. One of the largest changes is a decrease in contrast sensitivity. Importantly, contrast sensitivity does not change homogeneously over spatial frequency and if we also measure contrast sensitivity in noise, the changes become even more diverse. To explain these changes with computational aging and disease mechanisms, we used a simple computational model and a decoding approach to measure a perceptual threshold in our model, which can then be compared to

the psychophysical findings. We specifically looked at aging effects due to the number and receptive field size of cortical cells spanning the visual field and lateral inhibition.

From Section 4.4 on we present a framework to integrate neuro-computational and psychophyiscal methods by measuring perceptional thresholds in computational models that try to encode a visual stimulus. Our goal was to find a very simple model that incorporates possible aging mechanisms (see Section 1.9) that can replicate psychophysical data and thus reveal something about the internal changes in the aging visual system.

We will first present the psychophysical methodologies and data that we want to model, then we present the neurological basis for our model. We simulated two models, a two-layer model which one of my students ran in a number of configurations, changing the number of cells and the size of receptive fields, and later a three-layer model with a lateral inhibition parameter.

4.2 Contrast Sensitivity of the Primary Visual Cortex

An axis of insight we use in our group to investigate the aging process is the change in contrast sensitivity (CS) in noise between young versus old human subjects observed in (Allard et al. 2013) and (Silvestre, Cavanagh, et al. 2017; Silvestre, Arleo, and Allard 2018b). Contrast of visual stimuli is more important to our perception than absolute luminance as shown in e.g. Cornsweet stimuli (see Figure 4.2.1) where a shaded edge can change our estimation of the brightness of a whole shape. While luminance is normalized very early in the visual system, increase in contrast is still detectable in the firing rates of neurons in the primary visual cortex, but the feature tuning of their responses are already contrast invariant Carandini 2007.

A stimulus with a strong contrast is easily perceivable by a subject in an experiment, which we can test by presenting either vertical or horizontal stripes of alternating bright and dark patches and asking the subject to report whether the stimulus was vertical or horizontal. Decreasing the contrast below a certain point makes this task harder and the subject will have to make uninformed guesses when the stimulus becomes imperceptible. This allows us to measure a threshold between fully invisible, ie. random guessing, and fully visible with a performance of close to 100% correct (baring occasional mistakes made in reporting the orientation). The contrast sensitivity (CS) is the inverse of the threshold $CS = 1/C_{thresh}$

This threshold is very stable for each subject, but changes with the spatial frequency of the stimulus. In our notation, the contrast sensitivity function (CSF) is always the CS over spatial frequency. Figure 4.2.4 shows a CSF measured by Watson and Ahumada 2005 over a range of spatial frequencies from 0.1 to 25 cycles per degree (cpd). It is interesting to note, that there is an optimum at around 3cpd (see Figure 4.2.2 A) where performance is best, while for both higher and lower frequencies the performance deteriorates until the threshold becomes technically infinite for high spatial frequencies (very small objects beyond the subjects acuity) and very large spatial frequencies (larger than the screen used to project the stimuli).

If we add noise to the stimulus, we can observe that the threshold is increasing. Increasing noise has a roughly linear effect on the threshold, as an increase of n noise contrast units will result in $k \cdot n$ contrast units of increase of the threshold. The linear factor (here k) is related to the calculation efficiency (CE) (in our case $k = 1/\sqrt{CE}$). However, at very low noise levels this no longer holds: if the noise added to the stimulus is close to zero, there are still internal

Figure 4.2.1: **The Cornsweet Illusion**: The left part of the image appears darker, even though the color values at both sides are exactly the same. The only difference is the two ramps in the middle that generate an impression of a contrast edge. In the lower part of the image, the change in brightness is shown as a line graph.

noise sources that give a limit to performance. We can measure these internal sources by finding the external noise level that starts to impact the threshold. This point is called the Equivalent Internal Noise (EIN) (also sometimes σ_{int}). It is called "equivalent" since it is measured in equivalent units to the external noise we used to find it.

The relation between threshold, CE, EIN and CS relative to the external noise level σ can be summarized by the following formula:

$$c_{thesh}(\sigma) = \frac{1}{CS} = \sqrt{\frac{EIN^2 + \sigma^2}{CE}} \tag{4.1}$$

The relation of CS to spatial frequency is more complex and we chose a possible fit in section 4.2.1

Allard et al. 2013 measured contrast sensitivity, EIN and CE of young and old subjects. They found a decrease in sensitivity over all spatial frequencies, however for each of the investigated spatial frequencies (1, 3 and 9 cpd) this sensitivity decrease is caused by a different combination of CE decrease and EIN increase.

Figure 4.2.3 shows the age related change in CS, EIN and CE.

Daphne Silvestre extended the work of Allard et al. 2013 and measured across more spatial frequencies, in higher noise levels and with a correction for the optical transfer function in Silvestre, Arleo, and Allard 2018b and another paper is in preparation that compares old and young subjects with the updated methodology (Silvestre, Arleo, and Allard 2018a).

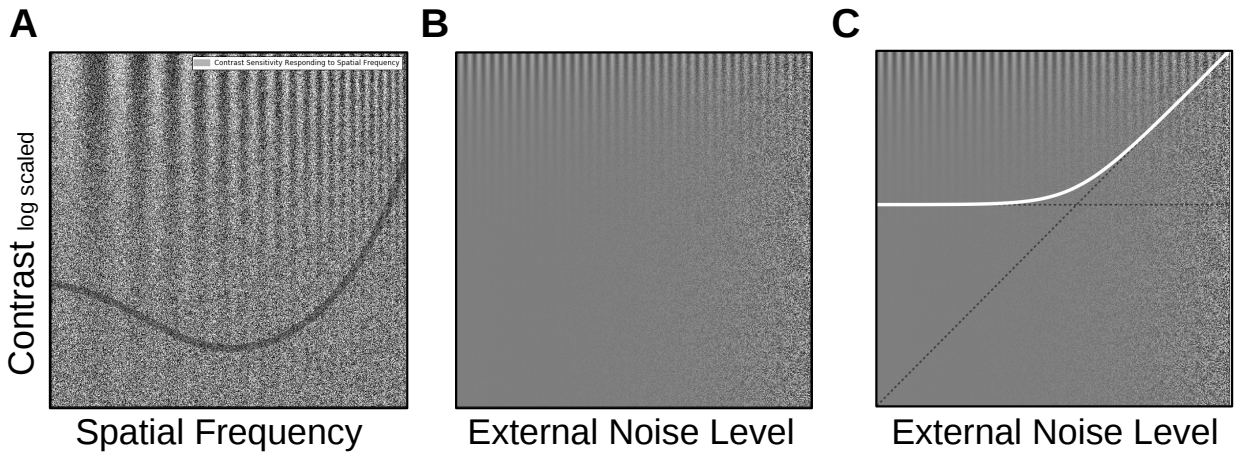

Figure 4.2.2: **Contrast Sensitivity**: **A:** The dark band shows a typical CS function over spatial frequency. There is an optimal sensitivity at intermediate spatial frequencies, while very fine and very large patterns become increasingly hard to see. **B:** This plot shows different combinations of signal and noise contrast. Even without a marked threshold line the observer is able to see their very own threshold varying over noise levels. The apparent plateau at low noise levels stems from the noise being masked by the noise in both the display or print quality of the image and the observers internal noise sources (dependent on viewing distance) **C:** A typical CS curve over noise with the asymptotes of the external noise limited and internal noise limited parts of the CS curve shown as dashed lines.

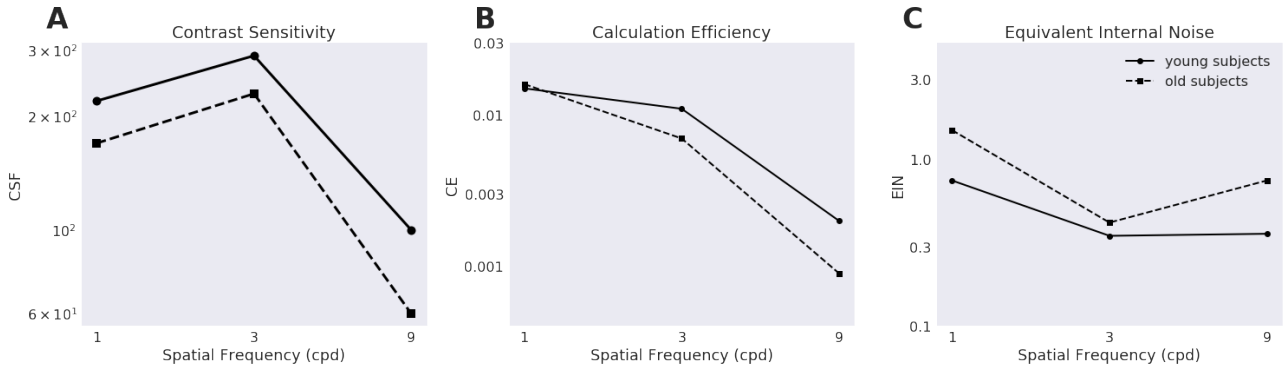

Figure 4.2.3: **Contrast Sensitivity in Aging**: Change of **A** CSF, **B** CE and **C** EIN due to age. Solid lines show data from young subjects, dashed lines show data from old subjects. Adapted from Allard et al. 2013

4.2.1 Interpolated Data of Contrast Sensitivity in Noise

To get a better idea of what the complete contrast sensitivity profile in noise could look like, we combined data from two sources. The work from Allard et al. 2013 builds the basis for our investigation since it provides data for young and old subjects in different noise conditions. We used their data from their dynamic noise condition and used the values of calculation efficiency and internal noise to replicate the contrast sensitivity curve over noise.

Since Allard et al. 2013 only investigated a small set of spatial frequencies, we used a continuous CSF used by Watson and Ahumada 2005 to fit to their data, which had more measurement points of spatial frequency, yet no change in age or noise conditions. Out of the multiple continuous CSF that Watson and Ahumada 2005 considered, we chose the S_{YQM} function (adapted from Yang, Qi, & Makous (1995)), since it has a good fit to their data and does not feature a discontinuity when going to very low spatial frequencies. Figure 4.2.4 shows the (arbitrarily scaled) CSF of both data sources combined.

4.2.1.1 Methods and Results of Allard 2013

Two groups of subjects (20 young, mean age 24; 20 old, mean age 69) were shown noisy sine wave gratings of 1, 3 and 9 cpd in a circular window of 4 visual degree with randomized orientation (horizontal or vertical) and phase. At each presentation the stimulus is shown for 500ms with an additional on- and off-ramp of 125ms. Three different noise conditions were used: no noise, static local noise that was only added to the stimulus area and global dynamic noise that was applied to the whole image. Since Allard et al. 2013 showed that only the dynamic, extended noise gave ecological results, we only consider this data. Using a 2-down-1-up contrast staircase the threshold for each subject was determined for a no-noise and high-noise condition and CE and EIN were computed from these thresholds.

4.2.1.2 Methods and Results of Watson2005

Watson and Ahumada 2005 used a library of static stimuli (the "modelfest-stimuli") of natural and synthetic stimuli of varying second order statistics and spatial frequency content. They included a series of gabor function stimuli with a fixed number of cycles and others with fixed extend. They collected contrast thresholds for all stimuli for 16 observers in 10 different labs.

They then tested a number of different CSF models on their ability to predict the contrast threshold from the input image. They evaluated the CSF in a pipeline of fixed elements that model well known effects, such as the "oblique effect" and aperture effects.

Of the multitude of CSF functions, we chose to use S_{YQM}, since it was the best performing model with a low number of parameters. It is defined as follows:

$$S_{YQM} = \frac{exp[-f/f_0]}{1 + \frac{a}{1+(f/f_1)^2}} \tag{4.2}$$

```
def S_YQM(_f,f_0=7.0,f_1=0.6951,a=7.7712):
    # our implementation of the S_YQM function
    # default parameters correspond to the fit from Watson2015
    return np.exp(-(_f/f_0)) / (1+ a / (1+(_f/f_1)**2))
```

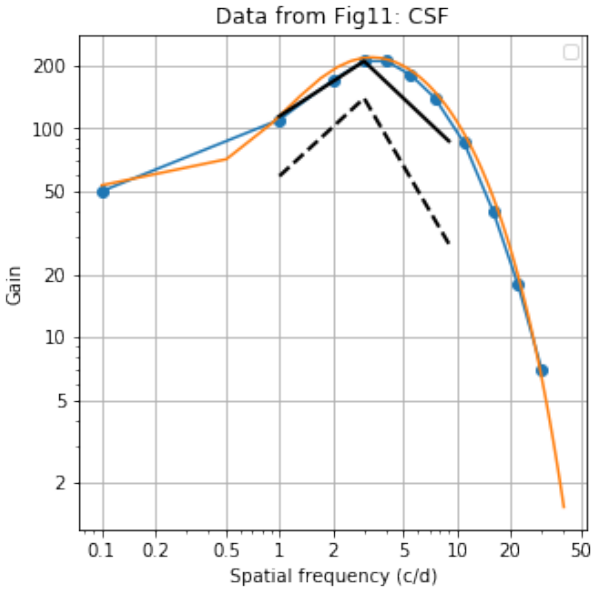

Figure 4.2.4: **Scaled CSF data with continuous CSF fit**: **blue**: data from Watson and Ahumada 2005, **orange**: fit from Watson and Ahumada 2005 using the YQM sensitivity function, **black**: data from Allard et al. 2013: the solid line is the CSF of young participants, the dashed from old participants

4.2.1.3 Merging the Data Sources

We then fitted the CSF from Watson and Ahumada 2005 to the different noise conditions from Allard et al. 2013 and thus created two CSF surfaces that show the CSF at each noise level and spatial frequency continuously for young resp. old participants (see Figure 4.2.5).

Looking at the data from Allard et al. 2013 alone, the effects of aging at each spatial frequency do not show a homogeneous direction of change (see Table 4.1). While the decrease in CS is universal at all spatial frequencies, the increase in EIN is strong in both 1 and 9 cpd but not at 3 cpd. CE even changes in opposite directions for 1 and 9 cpd, even if only very slightly. We take this as a strong indicator, that for each spatial frequency, the mechanisms are distinct, leading to differential outcomes of the aging process. We have summarized the changes in Table 4.1. In section 4.7.1 we use only the differences of CS, CE and EIN to test hypotheses about changes in the receptive field mosaic of the visual system.

Table 4.1: **Changes in calculation efficiency (CE), equivalent internal noise (EIN) and contrast sensitivity (CS) with age**

SF	Calculation Efficiency	Equivalent Internal Noise	**Contrast Sensitivity**
1	CE →	EIN ↗	CS ↘
3	CE ↘	EIN ⇝	CS ↘
9	CE ↘	EIN ↗	CS ↓↓

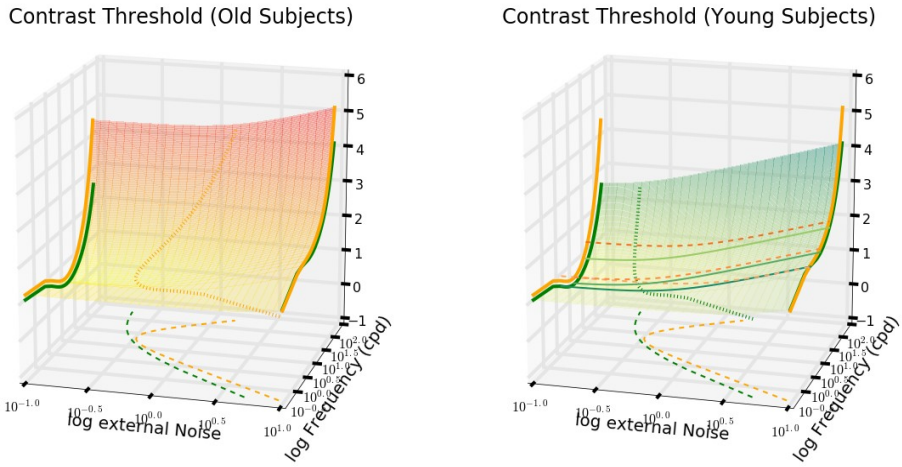

Figure 4.2.5: **CSF threshold surfaces**: for young and old participants (green: young, orange: old). The surfaces are generated from a fusion of data from Watson and Ahumada 2005 and Allard et al. 2013. Dashed lines on the x-z plane represent the internal noise curves. The finely dashed line on the surface gives the projection of the internal noise curve onto the surface. On the surface of young participants, the CSF over noise curves are marked as well: they connect the CSF at no noise to the CSF curve at high noise at each of the spatial frequencies 1, 3 and 9.

4.3 Decomposition of Noise Sources

In more recent publications Silvestre, Arleo, and Allard 2018b used multiple luminance levels and modulation transfer function (MTF) measurements to get cleaner, more interpretable data, also using a modified stimulus that has a constant number of cycles. The MTF can be measured directly or approximated by a Lorentzian function (see Equation 4.3). Since luminance has different effects on different internal noise sources, the measured EIN was modelled as the sum of three components: (1) photon noise, which is inversely proportional to luminance as less photons means a more noisy signal, (2) early noise and (3) late noise that occurs after contrast normalization. Photon noise is independent of spatial frequency, while both early and late noise sources have characteristic curves, the shape of which becomes apparent when the corresponding noise source is limiting perception.

$$MTF(f) = \left(a + \left(\frac{f}{u(d)}\right)^2\right)^{-a} \sqrt{D(f, d, 555)} \tag{4.3}$$

$$N_{eq}(L, f) \times L = \frac{1}{MTF^2(f)} \times \left(N_{photon} + \frac{N_{early(f)}}{L} + L \times N_{late}(f)\right) \tag{4.4}$$

While this extension is very promising for future efforts to convert the psychophysical models into neuro-computational models, the procedure was so far only performed and analysed on subjects under 40, so the aging effects shown in Allard et al. 2013 are pending to be re-evaluated as well. However, the considerations and simulations that are presented in sections 4.2.1, 4.7.1 and 4.7.2 can be extended to new data and more fine grained to specific noise sources.

4.4 Decision Model of LIP Neurons

To model a biologically plausible, neural decoding mechanism, we took inspiration from a model for a perceptual decision making task performed developed by the lab of Michael Shadlen (e.g. Mazurek et al. 2003) on monkeys while recording neural activity in the middle temporal visual area (V5 or MT) and the lateral intraparietal cortex (LIP).

The task for the monkey was to judge the direction of random dot motion which has a varying degree of coherence. The direction of the majority of the dots then has to be indicated by a saccade. The monkeys were able to learn the task and their performance depended on the coherence of the dot motion, ie. the percentage of dots that move in the same direction. If the coherence is high, the monkeys also answer faster and more reliably than if the coherence is low. The neural recordings from MT give responses that correspond to the direct sensory input. Each cell is sensitive to motion in a specific direction and the firing rate is correlated to the coherence of dot motion: complete random motion will create activity at noise level and if all dots are moving in the preferred direction, the response is maximal.

From these cells we can already say something about the performance of the monkey and the decision in each trial: if the firing rate averaged over one trial of the population sensitive to rightward motion is higher than the firing rate of the population sensitive to leftward motion, the monkey will be more likely to answer that the stimulus contains rightward motion.

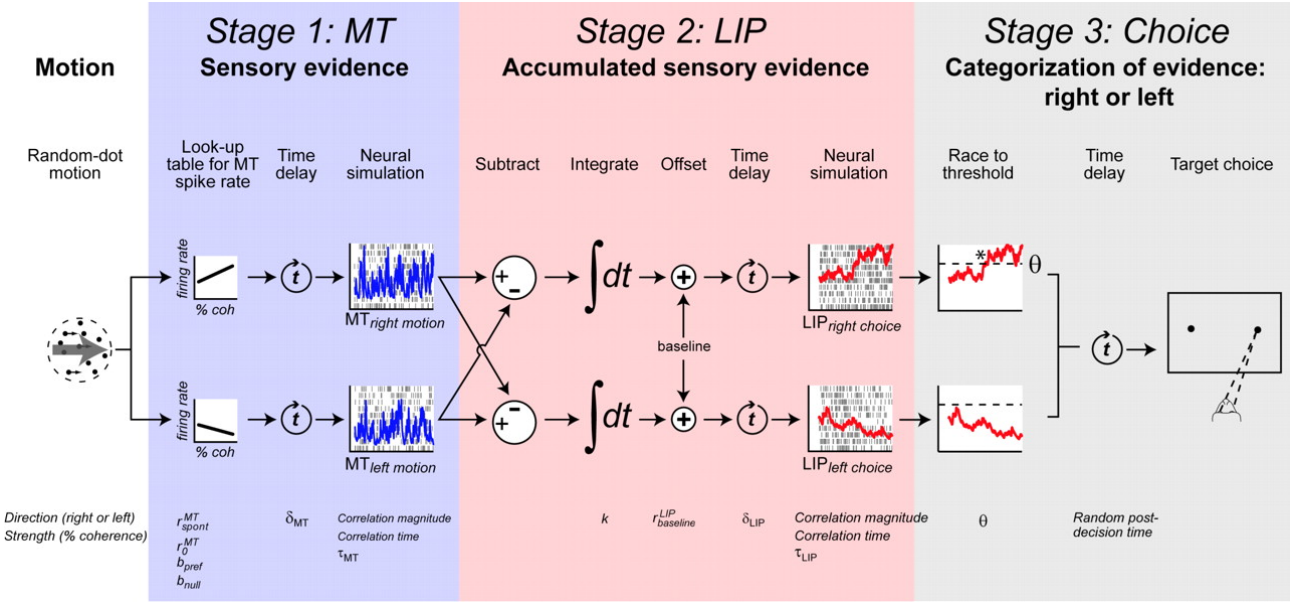

Figure 4.4.1: A model for perceptual decision making based on data recorded from MT and LIP neurons. The first stage filters specific patterns from sensory information (here: motion direction). The activity is directly related to the strength of the detected pattern. The second stage integrates sensory evidence and subtracts counter-evidence. Once the units in this stage cross a specific threshold, an action e.g. a saccade is performed. From: Mazurek et al. 2003

The maximal performance is dependent on the direction selectivity of the neurons and their signal-to-noise-ratio (SNR), ie. their firing rate for preferred vs. non-preferred stimuli.

But the model doesn't end there: the recordings in LIP give more insight into *how* the sensory information is processed to come to a decision. The firing rate of LIP neurons is increasing over the course of a trial, giving the impression that they act as integrators of the sensory information from MT. The rise in firing rate over time is directly related to the strength of coherence of the dot motion. In the model, these cells are taken to be "integrators of evidence": strong coherence results in a strong rise, weak coherence in a slow rise; when the direction of dots reverses, the firing rate drops in accordance to the coherence in the new direction. Once the firing rate of the population representing a specific decision (e.g. a saccade to the right) reaches a specific threshold, the corresponding action is taken.

The model discussed in Mazurek et al. 2003 fits well to the response data of the monkeys for accuracy as well as response time over a range of motion coherence. It is also a very simple model that combines basic neural operations to perform a decision based on perceptual information. In a more general framework we can describe the model as (1) representing sensory information by specialized neurons that give a noisy representation of their "best guess" as to the current state of the perceived stimulus; then (2) the sensory information is e.g. integrated in neurons with slow time constants or recurrent connections; positive evidence increases the activity while contrary evidence has an inhibitory effect and decreases the activity. Finally (3) either an action is performed as soon as a threshold is reached, or at the end of the trial the activity of the different integrators is compared.

While the models we present in section 4.7.1 and 4.7.2 will not have exactly the same architecture, they use the key concept of temporal integration of sensory evidence to model perceptual thresholds.

4.5 Decoding Directional Population Codes

We extended the model introduced in section 4.4 with a decoding method that takes into account the activity of cells sensitive to *all* directions, not only the ones with the most active firing rate. We used a *population vector* approach that computes the most likely direction given the activity of a population of direction sensitive neurons. In our special case we extended this method to orientation instead of direction, but we first want to introduce the concept as it was used in e.g. Salinas and Abbott 1994 to decode wind sensitive neurons in crickets. Given a population of neurons of which we know for each neuron a preferred stimulus direction that maximizes the firing rate, we can represent the population activity as a set of scaled vectors, each having a length proportional to the firing rate and pointing in the preferred direction of the neuron (Figure 4.5.1 gives an illustration). We can then add all of the vectors, which can be imagined as laying them end to end as shown in the Figure. But mathematically this can be done separately for the x and y dimension simply by adding up all the x components and y components of the vectors separately. The resulting vector will give us two interesting quantities: we have decoded a direction that the population codes for in their joint activity and we have the length of the vector which corresponds to the relative certainty about the direction. If all neurons are very active and their activity does not differ by much, the resulting vector will be very close to the origin, showing a strong disagreement in the population. If one the other hand all neurons are silent except one, the length of the vector will be the same as the vector of this one neuron.

In our model we code orientation which wraps around not at 360 degree, but at 180 degrees. The population vector method can still be used, however we multiply the preferred orientations by 2 and divide the decoded orientation by 2 to get a sensible result.

$$2 \cdot \theta_{est} = angle\left(\sum r_\theta * \mathbf{u}_{2\theta}\right) \tag{4.5}$$

\begin{explain} $\mathbf{u}_\theta$ is a unit vector in the direction θ, $angle$ is a function that returns the angle of the resulting vector and θ_{est} is the estimated orientation. \begin{end}

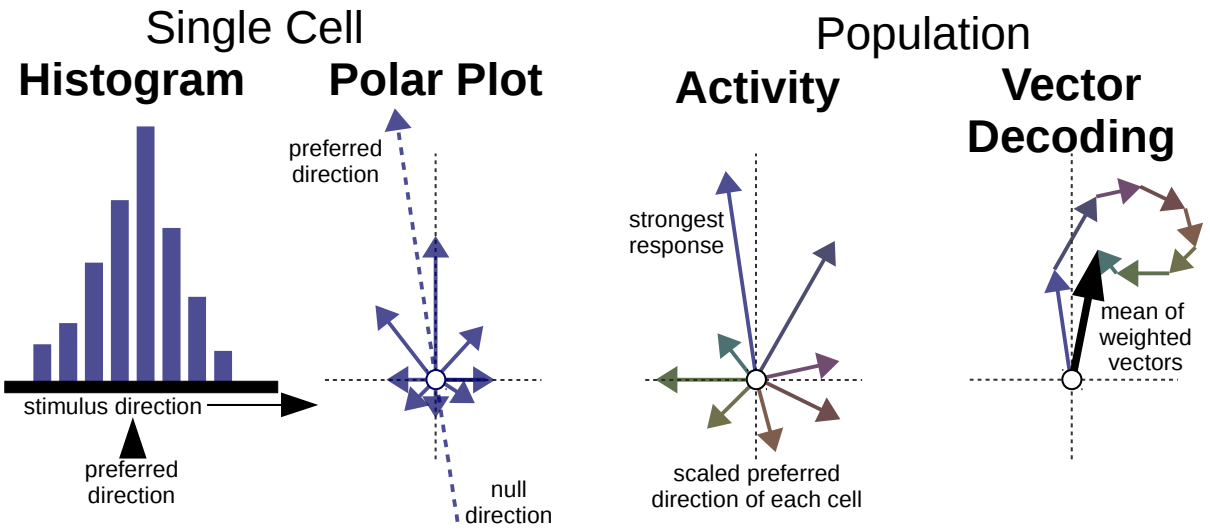

Figure 4.5.1: **Population Vector Decoding**: On the **left** the process for determining the preferred direction of a single cell is shown. For different stimulus directions the response of the cell is recorded and the resulting tuning curve is fitted e.g. with a Gaussian to estimate the *preferred direction* of this cell. On the **right**, the activity of a population of cells, each of which had its preferred direction estimated before, is shown as scaled vectors pointing in the preferred direction. The vector decoding method then simply takes the mean of these vectors to obtain the

4.6 Aging Effects on Contrast Sensitivity

Silvestre, Arleo, and Allard 2018a investigated the change in CS with respect to aging using the model defined in Equation 4.4. They found significant aging changes in the MTF at very high spatial frequencies, Calculation efficiency was found to be almost flat, with a significant, but small change due to age.

4.7 Simulations

4.7.1 Project 5: Investigating the Parameter Space of Cortical Representation - Internship of Atle Eskeland Rimehaug

→ see also List of Projects

Neurons tune themselves to represent patterns, that are helpful to code the environment. For the primary visual cortex these patterns are usually thought to be spatial gabor patches that differ in orientation, spatial frequency, size and phase.

Together with Master student Atle Eskeland Rimehaug, I created a simple model of the primary visual cortex that can capture two important dimensions of neural representations that are suspected to change with age: the size d and the number n of receptive fields.

In Chapter 2, we show that the change in the size of receptive fields is a possible anti-noise mechanism. While we did not count general cell loss as a process that is bound to occur

in the normal aging, we do change the number of receptive fields in this simulation. This could either represent changes due to neuro-degenerative disease, or a reorganization of the cortex, in which the visual field is tiled with fewer receptive fields (compare Figure 2.3.1 and Section 2.3.1).

We measure the size d relative to the spatial frequency the receptive field is sensitive to by counting the cycles contained in the gabor patch. The number of receptive fields we simulate is very small, compared to the actual visual system, however the results are extendible to larger numbers easily.

4.7.1.1 Data and Hypothesis

The goal of the model is to explain the differences between data from young and old subjects in Allard et al. 2013 with a simple neuro-computational model. In that work the authors found that while CS decreases very uniformly across the spatial frequencies presented, equivalent internal noise and calculation efficiency behaves differently for high vs. low spatial frequencies. We summarize the changes simplified in table 4.1.

4.7.1.2 Method

In each simulation we determine the 75% contrast threshold of our model to detect horizontal versus vertical stripes over a range of stimuli that differ in spatial frequency and noise parameters. The threshold is determined by running the model and comparing a decoded orientation to the actual orientation and varying the contrast in a staircase scheme (increasing contrast when the task is too hard, reducing contrast when the task is too easy), such that we can measure the 75% threshold by averaging over the last 20 trials.

4.7.1.3 The Model

The model consists of noisy, leaky integrators that receive the input filtered with a linear Gabor receptive field. Their output is passed through a non-linearity and then decoded by linearly weighting a vector aligned with twice the optimal orientation of each receptive field (to represent orientation values from 0-180 instead of 0-360 as would be done for directional decoding) with the activity elicited by the stimulus and taking the spatial average of these vectors. The resulting vector points to twice the predicted orientation and can be compared to the ground truth to determine the error of the model.

Varying the contrast of the stimulus gives a sigmoidal psychometric function, making the staircase method a valid instrument to find the 75% threshold.

In this part of the project we examined the effect of the number of receptive fields and their size relative to their spatial frequency. Figure 4.7.1 shows this parameterspace.

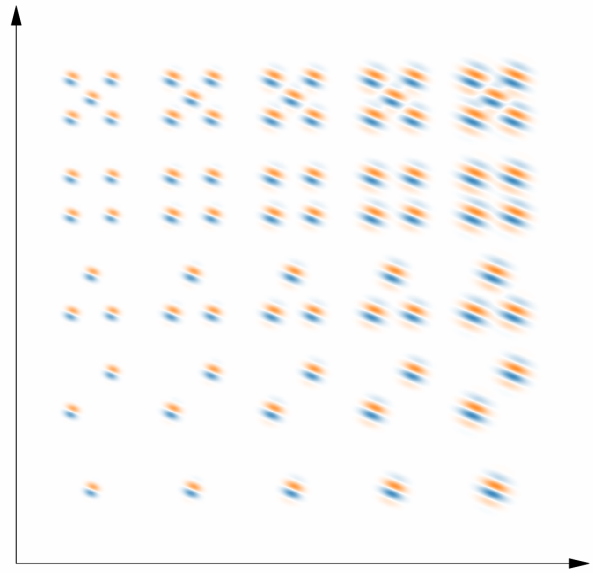

Figure 4.7.1: **Parameter Space of the Two Layer Model** The *y* axis shows an increase in the number of receptive fields while the *y* axis shows an increasing size of the gabor patch with constant spatial frequency selectivity

Two Layer Model (Atles Project)

$$\frac{\mathrm{d}r^1_{x,y,\theta,\phi,f}}{\mathrm{d}t} = -0.9 * r_{x,y,\theta,\phi,f} + N(gabor_{x,y,\theta,\phi,f} \cdot \left(image + \eta_{ext}\right)^T + \eta_{int}) \tag{4.6}$$

$$\frac{\mathrm{d}r^2_{\theta,f}}{\mathrm{d}t} = -0.9 * r^2_{\theta,f} + N\left(\sum_{x,y,\phi} r^1_{*,*,\theta,*,f} + \eta_{int}\right) \tag{4.7}$$

$$\theta_{est} = angle\left(\sum r^2_{\theta,f} * \mathbf{u}_\theta\right) \tag{4.8}$$

The input of a neuron at position x, y (with orientation θ and phase ϕ and spatial frequency f) is the linear response of a Gabor receptive field passed through a non-linear function (for the shown simulations simple rectification). η_{int} is a small, internal noise source. Each neuron low pass filters the input to get its response r. The population estimate of the decoded response is the angle of the sum of the response of all cells, multiplied by a unit vector $\mathbf{u}_\theta$ in the corresponding direction θ for each neuron.

Neurons were created for 16 orientations and 8 spatial frequencies. Each neuron had its receptive field placed at a random position. So our minimal number of cells of 3 actually creates 384 cells and our maximum of 7 creates 896.

Table 4.2: **Parameters of the two layer model**

Parameter	Value(s)
Spatial Frequencies	$[0.5, 1.0, 2.0, 3.0, 5.0, 7.0, 12.0, 16.0]$
Orientations	$0..180°$
Positions	random for each receptive field
leak	0.9

Parameter	Value(s)
noise_level	Normal distributed noise with $sd = 2.0$

4.7.1.4 Results

The results in Figure 4.7.2 show that there is a clear optimal spatial frequency range in which our model is able to perfectly perceive the stimulus: The CSF has an inverted U-shape. Apart from the lowest spatial frequency, the CE has a linear slope that declines with spatial frequency of the stimulus.

The decline in CE with spatial frequency might be explained by the fact that even though the receptive fields (RFs) are smaller for higher spatial frequencies, we kept the number of cells for each spatial frequency constant.

We hoped to find that along the two dimensions n and d, CS, CE and EIN behave differently, making it possible to control CE and EIN arbitrarily to emulate the change observed between young and old. However, under closer inspection only the effect of the number of cells produced significant changes. For the most representative spatial frequency of 2.7 cpd Figure 4.7.3 shows the changes in CSF, CE and EIN over both parameters. In Figure 4.7.2 it is visible that over all spatial frequencies, the receptive field size (number of cycles) has almost no effect (**A-C**), while the number of cells has a well-defined slope (**D-F**).

It is possible that the change in receptive field size was to small. It is also possible that overlap of the receptive fields is detrimental to contrast sensitivity since it can introduce noise correlations into the activity of the encoder neurons. This detrimental effect could then cancel the beneficial effect of larger receptive fields. However, it could also be the case that the effect of cell numbers so strong that, while for the internal and external noise levels we chose the effect of cell numbers was robust (varying the amount of cells from 300s to 800s), while the effect of receptive field size was masked by the variability of the simulations.

The range of both the number of cycles and the number of cells was very constrained since the simulated visual field was not very large and receptive fields span a range of spatial frequencies (from 0.5 to 16 cpd). The highest spatial frequencies run the risk of coming close to a size of only a few pixels, while the largest spatial frequencies risk to partially lie outside of the simulated visual field. Running the simulations with a larger visual field or a more restricted set of spatial frequencies could also lead to more insights. Also it could be possible to remove cells instead of adding them, allowing for more nuance in the number of cells.

4.7.2 Project 6: Effect of Lateral Inhibition on Cortical Selectivity

→ see also List of Projects

We created a three stage model to simulate successive cortical stages that become more and more specific to a pattern, but less specific to precise location. Each stage was simulated by leaky integrate and fire neurons with lateral inhibition creating a winner-take-all mechanism if the inhibition had sufficient strength. The stimuli were converted to spiking activity using VirtualRetina (Wohrer 2008). The spike trains were then loaded in Python and fed into the network implemented *brian2* (Goodman and Brette 2009).

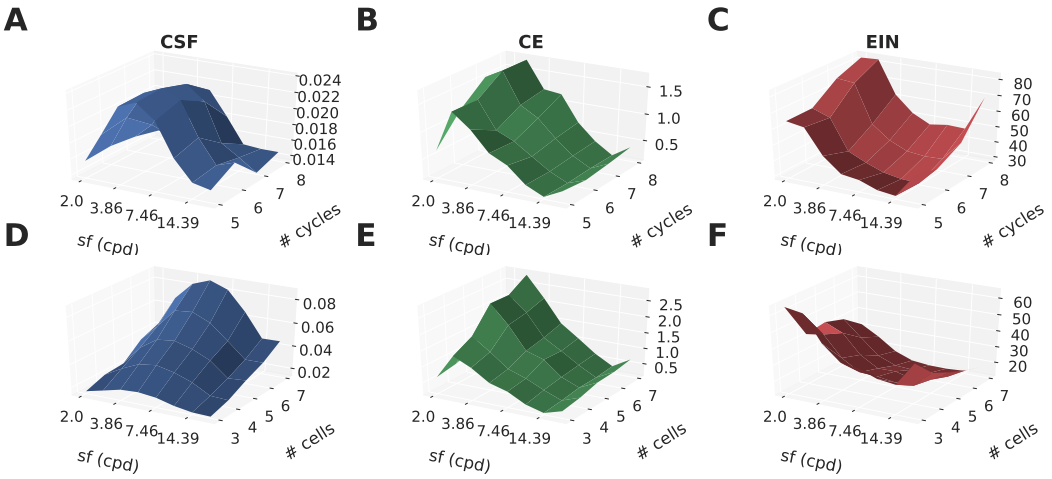

Figure 4.7.2: **Results of Project 4.7.1 over spatial frequencies**: The plot shows the effect of different cell numbers and Gabor cycles each on CSF (**A**, **D**), CE (**B**, **E**) and EIN (**C**, **F**) over spatial frequencies.

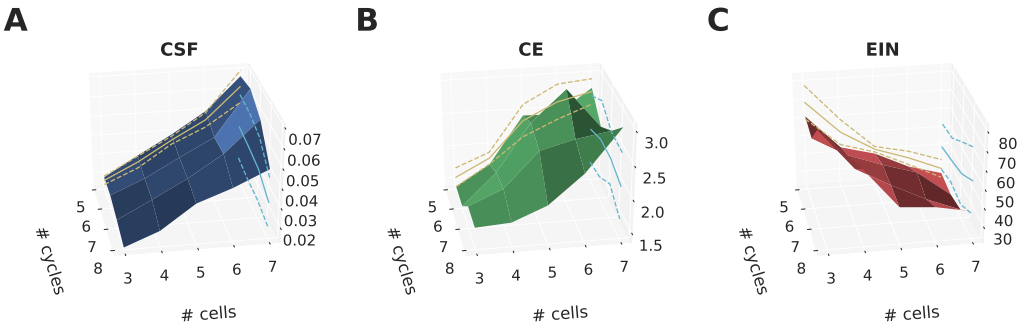

Figure 4.7.3: **Results of Project 4.7.1**: The plot shows the effect of different cell numbers and Gabor cycles on CSF, CE and EIN (at spatial frequency 2.7cpd) as 3d surface plots. The number of cells has a strong effect on the contrast sensitivity (CS), which is not surprising, since CE and EIN are both strongly influenced by the number of cells. The lines projected at the sides give the mean and standard deviation over cycle resp. cell numbers. Figure 4.7.4 shows a contour plot of the same data.

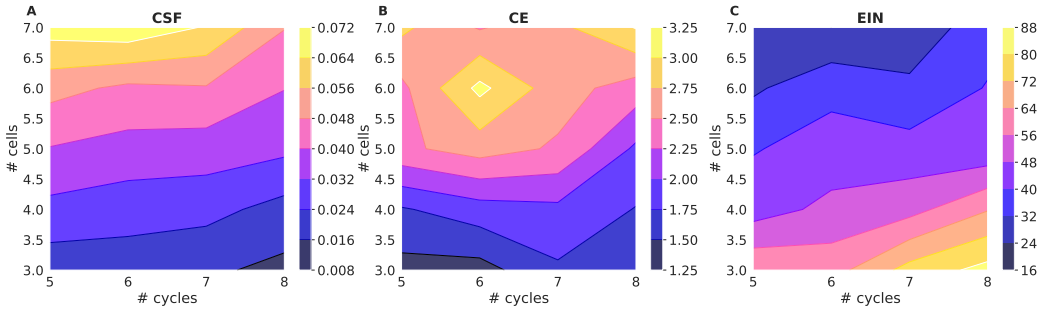

Figure 4.7.4: **Results of Project 4.7.1**: The plot shows the effect of different cell numbers and Gabor cycles on CSF, CE and EIN (at spatial frequency 2.7cpd) as contour plots. The number of cells has a strong effect on the contrast sensitivity (CS), which is not surprising, since CE and EIN are both strongly influenced by the number of cells. The lines projected at the sides give the mean and standard deviation over cycle resp. cell numbers. Figure 4.7.3 shows a 3d surface plot of the same data.

4.7.2.1 Architecture

The network receives input from On and Off ganglion cells simulated by VirtualRetina in a retinotopic grid. To simulate the response of V1-like cells in the first layer **L1**, a number of Gabor shaped projection fields were generated that determined the synaptic weights between ganglion cells and cortical cells. The responses of these cells were selective for spatial frequency and orientation and phase of the stimulus. Since the output of the cortical cells is again spiking activity, their response is rectified as all responses are positive. Each stimulus position, orientation and phase combination is coded by a group of neurons redundantly. The next two layers (**L2** and **L3**) integrate the response of multiple **L1** cells with similar orientation and phase with increasing spatial extend. The final layer sums up **all** responses that correspond to a specific orientation, irrespective of phase, such that its activity is a direct readout of the estimated orientation. In contrast to 4.7.1.3, we did not perform population decoding, but judged the firing rate difference between the true orientation and all other orientations as a measure for performance calculating the Signal-to-Noise-Ratio signal-to-noise-ratio (SNR).

Table 4.3: Parameters of the three layer model. The parameters differ between layers to keep firing rates in physiological ranges.

Parameter	Value(s)
Simulation duration	500 ms
Inhibition inh	[0, 0.5, 1, 2, 4, 8, 16] mV
Neuron type	Leaky integrate and fire
- threshold	10 mV
- reset	0 mV
- refractory period	2 ms
Number of Inpuy Neurons	12800 (On and Off layers of 6400 pixel)
Synaptic strength Input $\rightarrow$ **L1**	5 mV
L1 Number of Neurons	960 (10 per feature combination)
L1 τ	50 ms

Parameter	Value(s)
L1 noise std	10 mV
L1 self-inhibition	$inh * 0.5$ mV
Synaptic strength **L1** $\rightarrow$ **L2**	5 mV
L2 Number of Neurons	96
L2 τ	20 ms
L2 noise std	10 mV
L2 self-inhibition	$inh * 1.0$ mV
Synaptic strength **L2** $\rightarrow$ **L3**	20 mV
L3 Number of Neurons	8 (2 per orientation)
L3 τ	100 ms
L3 noise std	10 mV
L3 self-inhibition	$inh * 1.0$ mV

4.7.2.2 Results

At a constant contrast, the addition of targeted lateral inhibition shows a clear improvement of signal-to-noise-ratio (SNR) (Figure 4.7.7) before signal-to-noise-ratio (SNR) for very high inhibition values. The effect accumulates through hierarchical layers as the improved signal-to-noise-ratio (SNR) at one layer enables the next one to further suppress noise and get a cleaner winner signal. Figure 4.7.6 shows the inhibitory currents of the network in one simulation and a raster plot for the first layer. Without inhibition, the firing rate of the purple and blue cells is slightly higher than the firing rate of other neurons, coding the stimulus correctly, but allowing for a lot of spontaneous activity.
In the case of excessive inhibition, each layer becomes a stable multi-attractor system that ignores inputs as soon as one cell starts to spike. This affects for one the firing rate which will be lower for large inhibition values and the network will also be unable to react to switches in the stimuli (see arrows in Figure 4.7.6).

4.7.2.3 Discussion

The change of signal-to-noise-ratio (SNR) observed in this part of the project relates to the CE of the first part, as the CE is proportional to the signal-to-noise-ratio (SNR) needed to successfully perceive the stimulus (Pelli 1990). Since in the first part the EIN and CE were affected almost anti-proportionally by the number of cells, the inhibition mechanism can be used affect them both differentially. We are planning to extend the simulated psychophysical paradigm to the dimension of lateral inhibition (in different strengths and possibly in different operational modi, see figure 4.7.5) to test this intuition. The next steps are then to find the parameter combinations for each spatial frequency that correspond to the curves on the surface of figure 4.2.5.

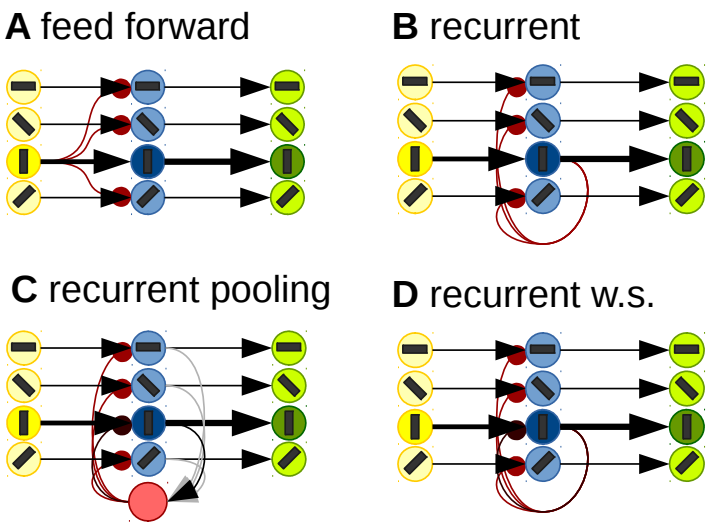

Figure 4.7.5: **Inhibition Mechanisms** Lateral inhibition can be implemented several ways. A feed forward inhibition as in **A** would transmit targeted inhibition from a previous layer in the hierarchy. This scheme requires some histochemical targeting of synapses as e.g. can happen in the retina. **B** instead shows recurrent inhibition that affects neighbouring neurons (which in turn can inhibit the original neuron). This system can already exhibit self-amplification since the strongest neuron will suppress all others, which makes it harder for the other neurons to inhibit the original neuron. **C** shows a collective inhibition pool (e.g. a large inhibitory interneuron) that indiscriminately inhibits alls cells. But since the activity of all cells will still remain proportional, the cell with the strongest activity will remain the most active one. In the retina, the horizontal cells are very large and form gap junctions. Their activity is not targeted. **D** shows inhibition without pooling with self-connections. This could be possible if inhibitory interneurons have only a small dendritic tree but still target many other neurons. This scheme is similar to **D**, except that each neuron can also inhibit its own activity.

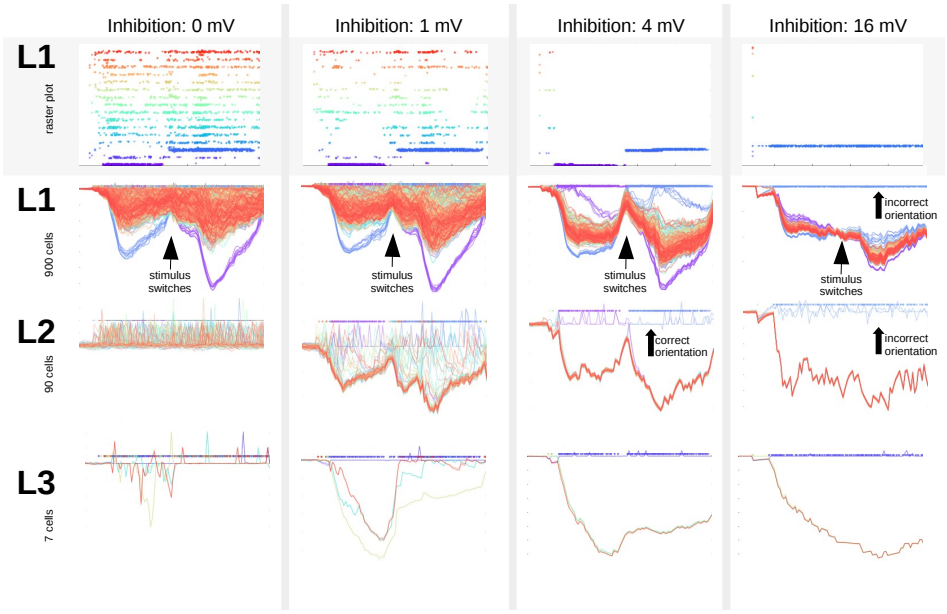

Figure 4.7.6: **Inhibition Affecting Three Layer Model** With increasing lateral inhibition, each stage functions more like a winner-take-all mechanism. The stimulus inverts at the half way point of the simulation, indicated by arrows. For each Layer, a plot shows the inhibitory current being applied to all other neurons. For the first layer **L1**, additionally a raster plot is shown at the very top. Colours correspond to the number of each neuron, the correctly encoded stimulus corresponds to neurons that are coded purple in the first half and later blue in **L1** and **L2**, and only blue in layer **L3**. At the very highest inhibition level the inhibition is so strong that each layer functions as a stable attractor that ignores new inputs.

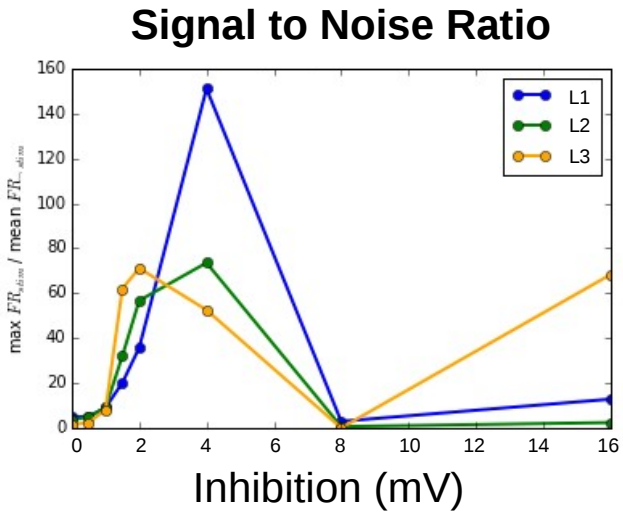

Figure 4.7.7: **Inhibition Affecting Signal to Noise Ratio** The signal to noise ratios of each layer over different inhibition strengths. High-level layers have an optimum at lower inhibition values due to the accumulative effect of lateral inhibition.

4.8 Summary

In this chapter we showed a method to model psychophysical thresholds with neuromimetic models. We simulated a simple cortical model and varied parameters of the model and compared them to expected contrast thresholds in noise. Contrast thresholds in noise can be decomposed into EIN and CE, which we do by fitting psychometric functions to the raw thresholds. EIN and CE vary over spatial frequency and with age. In his M1 project, Atle Eskeland Rimehaug varied receptive field size and number, first separately, then as a grid search. He found that the number of cells had strong influence on EIN as well as CE while the size of receptive fields relative to their spatial frequency selectivity had almost no effect. Overall the strong effect of cell number was affecting CE and EIN similarly, but in opposite directions, increasing CE and decreasing EIN. This is unfortunate since the age-related changes have a more diverse effect on CE and EIN. In a follow-up project we found that lateral inhibition can increase the signal-to-noise-ratio (SNR) in a single processing stage and that with subsequent processing stages this mechanism becomes stronger. As we discussed in section 1.9.4, inhibition undergoes major changes in old age. With this mechanism it might be possible to recreate the exact changes that occur at each spatial frequency. In following projects this relationship will be studied further.

References

Allard, Rémy et al. (2013). "Contrast sensitivity, healthy aging and noise." In: *Vision research* 92, pp. 47–52. ISSN: 1878-5646. DOI: 10.1016/j.visres.2013.09.004. URL: http://www.ncbi.nlm.nih.gov/pubmed/24070688.

Carandini, Matteo (2007). "Melting the Iceberg: Contrast Invariance in Visual Cortex". In: *Neuron* 54.1, pp. 11–13. ISSN: 08966273. DOI: 10.1016/j.neuron.2007.03.019.

Goodman, Dan F M and Romain Brette (2009). "The brian simulator". In: *Frontiers in Neuroscience* 3.SEP, pp. 192–197. ISSN: 16624548. DOI: 10.3389/neuro.01.026.2009.

Mazurek, Mark E. et al. (2003). "A Role for Neural Integrators in Perceptual Decision Making". In: *Cerebral Cortex* 13.11, pp. 1257–1269. ISSN: 10473211. DOI: 10.1093/cercor/bhg097.

Pelli, Denis G (1990). "The quantum efficiency of vision". In: *Vision: Coding and efficiency*, pp. 3–24. URL: http://www.ncbi.nlm.nih.gov/entrez/query.fcgi?db=pubmed%7B%5C&%7Dcmd=Retrieve%7B%5C&%7Ddopt=AbstractPlus%7B%5C&%7Dlist_uids=10484997723605962 97related:SZuh3vwEjQ4J.

Salinas, Emilio and L. F. Abbott (1994). "Vector reconstruction from firing rates". In: *Journal of Computational Neuroscience* 1.1-2, pp. 89–107. ISSN: 09295313. DOI: 10.1007/BF00962720.

Silvestre, Daphné, Angelo Arleo, and Rémy Allard (2018a). "Healthy aging impairs photon absorption efficiency of cones". In: *in press*.

— (2018b). "Internal noise sources limiting contrast sensitivity". In: *Scientific Reports* 8.1, pp. 1–11. ISSN: 20452322. DOI: 10.1038/s41598-018-20619-3.

Silvestre, Daphné, Patrick Cavanagh, et al. (2017). "Adding temporally localized noise can enhance the contribution of target knowledge on contrast detection". In: *Journal of Vision* 17.2017, pp. 1–10. ISSN: 15347362. DOI: 10.1167/17.2.5.doi.

Watson, Andrew B and Albert J Ahumada (2005). "A standard model for foveal detection of spatial contrast." In: *Journal of vision* 5.9, pp. 717–740. ISSN: 1534-7362. DOI: 10.1167/5.9.6.

Wohrer, Adrien (2008). "Model and large-scale simulator of a biological retina, with contrast gain control". PhD Thesis. University of Nice-Sophia Antipolis.

Chapter 5

The `convis` Toolbox for Convolutional Vision Modelling

There must be a better way! And there is.

Raymond Hettinger Python core developer

Beautiful is better than ugly.
Explicit is better than implicit.
Simple is better than complex.
Complex is better than complicated.

PEP 20, The Zen of Python

5.1 Introduction

In this chapter we present `convis`, a Python toolbox for modelling the visual system using convolutional vision models. Out of our groups' usage of the VirtualRetina simulator, we started to extend the software (Section 5.1.1), but had to find an alternative when we wanted to use arbitrary receptive fields within the simulator.

The `convis` toolbox is based on `PyTorch` and features ready built models (see Section 5.4) from the reimplementation of VirtualRetina, basic *LN-cascade* models, up to convolutional neural nets. All of the models can be automatically differentiated and thus optimized with gradient based optimization algorithms. The toolbox has a dual emphasis on efficient, large scale simulation and model fitting to electrophysiological recordings.

In this chapter we will discuss the architecture of the toolbox as an extension to `PyTorch` (Section 5.3), some aspects of the usage (Section 5.3.2.1-5.4.5) and finally the advantages and challenges of gradient based optimization (Section 5.5).

5.1.1 Project 7: The Inofficial VirtualRetina Repository

→ see also List of Projects

Together with Emilie Mayer, I extended VirtualRetina (Wohrer 2008) with some custom functions for use in Project 3.5.2. During this process we found a few minor bugs. To make these bug fixes available to the general public, I created a github repository under https://github.com/jahuth/virtualretina that contains the last version of VirtualRetina that was under *CeCill-C open-source licence* which permits modification and (re-)distribution. Since opening the repository, another researcher contributed a bug fix and a number of users have used the *Issue* forum to ask questions about VirtualRetina.

The official distribution of VirtualRetina is now part of the *PRANAS* software package (http://pranas.inria.fr/) with the source code requestable at https://team.inria.fr/biovision/virtualretina/.

5.2 A Convolutional Vision Model to Model Retina, LGN and the Primary Visual Cortex

What started as a re-implementation of VirtualRetina has turned into a flexible toolbox that supports a range of different models, from *LN* cascade models, to bio-mimetic mechanistic models like VirtualRetina, up to deep convolutional approaches.

The VirtualRetina implementation of its retina model is very efficient since it uses recursive filters wherever possible. These filters can be computed very efficiently on single thread systems, but are limited in their shape. Initially, the only change we wanted to make to the model was to replace the spatial filters with 2d convolutions, which would allow for receptive fields with a more sophisticated internal structure.

To be more flexible in the implementation, we implemented a prototype in `Theano`, a python computation library. To our pleasant surprise, most of the implementation could be done directly from the mathematical formulas, rather than reimplementing the algorithms of the C++ version. The prototype was then extended into a toolbox that allows vision models to be created in `Theano`. With `Theano` one can create a computational graph of abstract variables and operations that can be optimized and compiled to run on either CPUs or GPUs. More complex operations on the graph itself allow for symbolic differentiation to create expressions of the gradient of the output with respect to any of the inputs. This can be used to optimize the parameters of the model, such that the output becomes close to a training signal and is one of the ingredients that made deep learning so successful. No matter, how complex the model becomes, as long as each step is differentiable, an expression for the gradient can be generated. The gradient in `Theano` is itself an expression, i.e. a graph, which can be hard to derive and to turn into code, which is why `Theano` has much longer compile times than e.g. Torch. But conversely, this also easily allows for higher order derivatives, since the process to create a gradient of a gradient is exactly the same as for any other output variable. In PyTorch, the gradient is computed by adding to a buffer attached to each Variable in a separated backwards pass. The graph for this operation is created during the forward computations on the fly by simply memorizing which operations were done to create the Variable that has just been computed. While this graph is less flexible

than the one used in `Theano`, e.g. it can not be optimized, it is computed a lot faster, which makes optimization almost irrelevant. PyTorch builds on the rapid execution of just-in-time compiled code snippets. While each operation is optimized, there is no global optimization to check for redundant computations or unused results.

The toolbox was then ported to PyTorch which increased performance and made the toolbox more flexible.

The outcome was a flexible toolbox that can calculate and also fit models of the retina, lgn, primary visual cortex and even higher visual areas, e.g. a V2 model.

5.2.1 Project 8: Creating Convis

→ see also List of Projects

Initially `convis` was written using `Theano` as the computational backend. But for multiple reasons the toolbox was rewritten for `PyTorch` and as a consequence is much more concise and easy to maintain. An internal change in PyTorch further simplified `convis`, as the distinction between *Tensors* and *Variables* was removed.

The source code of the toolbox was published as a repository on github[1] under GPL-3.0 license. GPL-3.0 is a strong "copy-left" license, which allows users (commercial or private) to copy, distribute and modify the software. However it is required that derivative software is also published under GPL-3.0.

The documentation and an issue tracker are also hosted on github. Through pull-requests contributions from other developers can be integrated into the main distribution. travis-ci.org, a free *continuous integration* service runs automated tests with every revision done to the toolbox to check that the code still runs on both Python 2 ($\geq$ 2.7) and Python 3 ($\geq$ 3.5).

Releases are published on the "Python Package Index" (PyPI), so that package managers such as *pip* or *conda* can install the latest stable version directly. To use GPU acceleration on an Nvidia GPU, the *CUDA* library has to be installed.

5.3 PyTorch Implementation

The last iteration of the toolbox was published as a method paper in Huth, Masquelier, and Arleo 2018. We switched from Theano to PyTorch because the lead team of the Theano project was announced to discontinue their support of the package in autumn 2018 [2]. Although another project has stepped up to continue the support of Theano, the future uncertainty and a number of "hacks" that were necessary to make convis work well with Theano made it advisable to switch to a simpler codebase. The current implementation is an extension to PyTorch in that it creates subclasses of some of their classes with added functionality, while the underlying structure is kept intact such that any package written for the use of PyTorch can also be used for `convis`.

[1] https://github.com/jahuth/convis

[2] See the discussion on https://groups.google.com/forum/#!topic/theano-users/7Poq8BZutbY

5.3.1 PyTorch

To give some context to the features we added to PyTorch, a small introduction to the usage of PyTorch can be helpfull.

Data in the RAM or on the GPU of a computer is manged by `Tensor` objects, which know the location, dimensionality and data type of their associated data and can call the appropriate methods when they are asked to combine themselves with other data.

As an example, two tensors on a GPU can be added together, resulting in a new tensor. Or alternatively, one of the tensors can be asked to add the other Tensor in-place, such that only its own value changes and no new tensor is created. All operations on these tensors are accelerated depending on the location they are in and which acceleration libraries are available. To do a complex computation, one can write a Python function that calls the operations sequentially, very similar to processing data in numpy arrays. While in Theano, any iterative loops require special attention, in PyTorch they do not look different than any other loop in Python.

On top of this basic functionality, PyTorch comes with an add-on module called `autograd`. To be able to use automated differentitation on the output of these computations, `Tensor`s are wrapped in `autograd.Variable` objects, which create new `Variable` objects on each operation with an attached graph of all computations that were done to create this variable and a buffer that stores the accumulated gradient on the backwards pass.

Further PyTorch adds the `nn` sub-module, which as the name suggests makes it easier to create neural networks, such as convolutional neural nets or LSTMs. This module adds `Parameter`s and `Module`s classes. Parameters are special Variables, that by default expect to be optimized. Modules contain a function performing a computation, but they are themselves combinable into larger computations. A Module can for example be a single operation (e.g. convolution), a more complex layer (combining convolution and a non-linearity) or a neural network as a whole.

To use PyTorch in practice to e.g. create a convolutional neural net, one would write a class that inherits from `Module` which has all ingredients of the network as attributes (Convolution and ReLU Modules) and a method `forward` in which the computation is performed. To use the model, it can be called like a function with a `Variable` containing the input images as a parameter.

```
class MyNet(torch.nn.Module):
    def __init__(self):
        self.c1 = torch.nn.Conv2d(1,1,(5,5))
        self.n1 = torch.nn.ReLU()
        self.c2 = torch.nn.Conv2d(1,1,(5,5))
        self.n2 = torch.nn.ReLU()
    def forward(self, inp):
        return self.n2(self.c2(self.n1(self.c1(inp))))
net = MyNet()
things = torch.autograd.Variable(torch.ones(10,10))
outputs = net(things)
```

All variables that were created as `Parameters` can be collected recursively for the complete model to generate update routines for optimizers in a few steps.

5.3.2 Extensions to PyTorch

We extended PyTorch with a `Layer` class, which is similar to the `nn.Module`, but adds some functionality. We chose to call it `Layer`, rather than `Module`, since module already has a specific meaning for python packages. Also we created `Variable` and `Parameter` classes that can contain more custom information, such as doc strings and initializer functions.

To make it possible to process continuous video input and generate continuous streaming output, an additional method had to be added that receives a long video stream or numpy array and chops it into smaller chunks that can be processed sequentially. PyTorch objects by default perform their computation (e.g. executing their forward method or calling a pre-compiled library) when they are called as a function. To maintain compatibility with other PyTorch packages, this method of calling a computation was kept in place and the new functionality was added to Layer objects as a method called `run` that accepts the input as well as a chunk length `dt`. Also we added a method `optimize` to the Layer class that performs all of the boilerplate steps necessary to perform automated parameter optimization with any of the optimizers available from `torch.optim` to approximate a given target output. A specific optimizer can be selected by calling `layer.set_optimizer(...)`, which will then be used for any `optimize` calls.

```
my_model = convis.models.LN()
my_model.set_optimizer.SGD(lr=0.001)
my_model.optimize(some_input, some_output, dt=500)
```

This very simple process can be customized by choosing different optimizers, adjusting their parameters and also replacing the loss metric that is used to compare the current and the desired output. By default, this is root-mean-squared, but for e.g. spiking output the log-likelihood is more appropriate.

5.3.2.1 Tab Completion and Self-Documentation

As a general rule for usability, most features of the toolbox and the models created with it should be discoverable interactively when using a *REPL* interactive command line[3] or *Jupyter* notebook environment. To make all internal parameters of a model discoverable by tab-completion, we added special attributes to the `Layer` class which dynamically collect all internal variables, states and parameters - similar to what `param()` is doing for `nn.modules`, but without requiring the user to actually execute a statement. The variables can be inspected hierarchically in the nested structure of the `Layers` and `Functions` that call each other, or as a flat list.

In *Jupyter* notebooks, `Layers` also have a special handler that will create a more useful representation of the contained model, including a link to the online documentation should the `Layer` be one of the `convis` operations or models. On a text console, printing will create a text representation of sub-modules (similar to `nn.Modules`).

5.3.2.2 Special Layers

`convis` implements a set of layers specialized for dynamic vision models. All layers also inherit methods for parameter loading and saving and running chunked input.

[3] Read-Evaluate-Print Loop, e.g. the default *Python* interactive shell

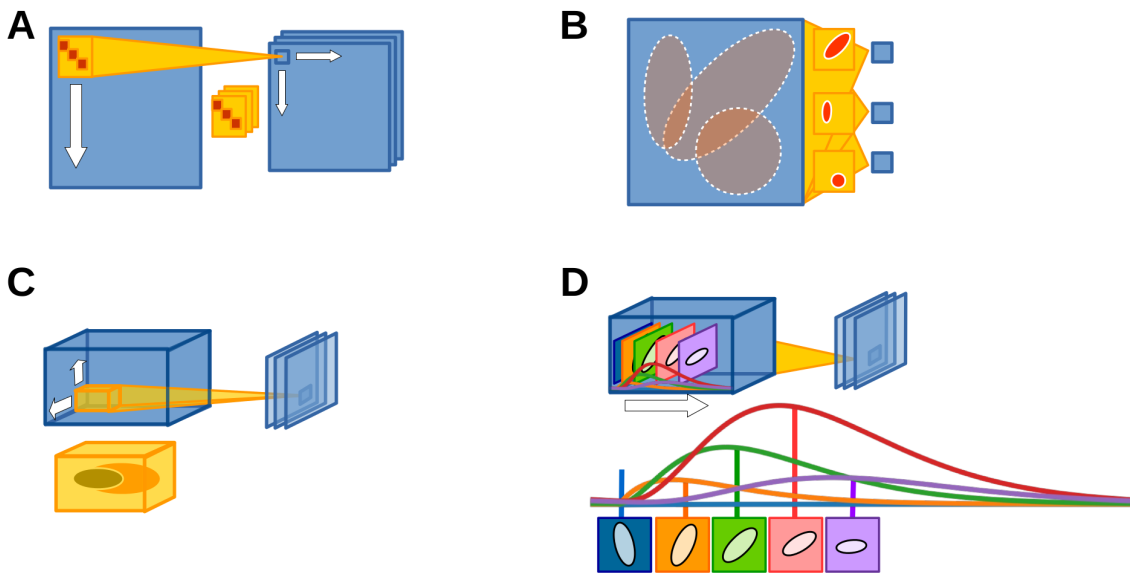

Figure 5.3.1: **Linear Filters A** shows a 2d convolution filter. A set of filters is applied to each location on the image and a set of images is generated as output. Not pictured here is the padding process (Section 5.3.2.2). **B** shows a fully connected filter that connects each output through a weight map to the whole image. **C** shows a 3d convolution: each filter has extend in space and time and is multiplied with the input at each spatio-temporal position. Again, multiple filters can generate multiple outputs. **D** A `SmoothConv` filter that can reduce the number of parameters for very long filters drastically. It uses recursive filters to convolve the input in time with increasing delays and then applies a number of spatial filters (here: 5) to different delays. The result is a smooth, spatio-temporally inseparable filter that can be several hundred or thousands of bins long without taking up much memory or increasing the running time of the model.

Convolution Layer One of the most basic, but powerful layers is the convolution layer. The `Conv3d` layer of `convis` performs linear filtering by multiplying a linear kernel at each position in space and time with the input (see Figure 5.3.1 **A** for a 2d and **C** for a 3d convolution).

`convis` internally uses five-dimensional tensors as in- and outputs since the `Conv3d` operation accepts five-dimensional inputs and filters. The two additional dimensions of the input are interpreted as "batch" and "channel" dimensions, while the two additional channels of the filter are "in-channel" and "out-channel" respectively. This means that if we have more than one "batch", each "batch" will be treated independently (potentially with speed-up due to parallelization). If there is more than one "channel", e.g. 3 for RGB colour coded input video, the filter is required to have a matching "in-channel" dimension, so that a filter is defined for each "channel". The "out-channel" allows for an output with multiple "channels".

The dimensions are in order: [*batch* $\times$ *channel* $\times$ *time* $\times$ x $\times$ y] for the input and [*in-channel* $\times$ *out-channel* $\times$ *time* $\times$ x $\times$ y] for the filter.

If we want, e.g. to process RGB coded video and produce grey scale output, we need a filter with 3 "in-channels" and one "out-channel". If we want to preserve colour separately, we either need a filter with 3 in- and 3 out-channels (which means the kernel is 9 times its original size), or if the processing is independent, we can switch the colour dimensions from "channel" into "batch" dimensions. In CNNs, the channels play an important role, since throughout the processing chain, the image tends to become smaller, but the number of channels increases, projecting the visual information into a more and more position invariant and conceptual representation. For vision models in convis, the channels can e.g. be produced from different orientation selective filters.

Implementing orientation selective, or even motion direction selective filters as a convolution is straight forward since the filter can mimic the preferred stimulus, so that even very complex motion patterns can be implemented as a 3d-filter.

The time complexity of executing a convolution operation can increase rapidly with the size of the filter if executed on a CPU, however since the operation is very parallelizable, it can be executed a lot faster on a GPU. For simple shapes, such as Gaussian or exponential filters, recursive filters are more effective (see Section 5.3.2.2), but for more complex shapes, or even arbitrary receptive fields (RFs) obtained from electro-physiological recordings, numerical convolutions are necessary.

In its most basic definition, convolution operation compute output that is smaller than the input since there are less positions for the kernel to fit inside the input than there are pixels in the input. To avoid inconsistent output sizes when any of the internal filters are changed, convis uses two different padding strategies to guarantee that the output has the same size as the input independent of filter size. In the two spatial dimensions, a border is added to the input, by default by mirroring the input at its edges, so that pixels in the border have a similar mean and contrast as the pixels in the input. In the temporal dimension, the padding has to use a different strategy since `convis` processes input stimuli in chunks of a user defined length (e.g. 500 frames at a time). To get the convolution to work on continuous streaming input, a part of the previous input has to be remembered between runs so that the output is perfectly independent of chunk size. The length of the input that needs to be remembered is the temporal length of the filter minus one.

Recursive Layers Similar to the recursive filtering operations used in VirtualRetina, the recursive Gaussian and exponential filters are very efficient. The Gaussian filter is implemented

according to Deriche 1993 and operates separately on the vertical and horizontal dimensions. This limits the filter to Gaussian filters that are either circular, or ellipsoid and aligned either with the horizontal or vertical axis. The temporal exponential filters are implemented similar to Clifford and Langley 2000, including high-pass, low-pass and cascaded exponentials.

Temporally Smoothed 3d Convolution Since convolutions can be expensive to compute for very long filter lengths, we implemented a hybrid filter between recursive and convolutional filters. The layer is initialized with the number of basis functions that should be used. Each basis function has a smooth temporal profile (which is computed recursively) and is multiplied with a spatial filter (see Figure 5.3.1 **D**). The different filters are staggered in time, either with equal or increasing distance to model a spatio-temporal receptive field that smoothly changes over time. This filter has the advantage over a full spatio-temporal convolution that it has less parameters. When fitting sparse experimental data that is expected to have slow dynamics it needs less data to be fitted.

Receptive Field Layer Similar to a convolution, the `RF` layer uses a 3d linear filter, but produces only a single output pixel (see Figure 5.3.1 **B**). In terms of implementation it is actually a convolution, but with a filter that matches the spatial extend of the input. In time, the filter still works as a convolution filter with the same padding strategy as the `Conv3d` layer. It is possible to create multiple outputs by using the *out-channel* dimension of the filter, e.g. by concatenating a set of receptive fields such that they are joined at the second dimension.

Spiking Layers Spiking mechanisms introduce a serious non-linearity into a model. In many cases, a firing probability will be the output of a model rather than an actual spike train. However, to generate data from a model either for simulating downstream mechanisms or to validate an analysis method, it can be important to produce plausible spikes from the prediction of the model.

The simplest assumption is that of a **Poisson** spike train. Each spike is temporally independent and the firing probability over time can be interpreted directly as the probability of observing a spike at each time point.

If we assume that membrane potential is accumulated over time, we can model this instead with a leaky integrate and fire model, which will spike if the accumulated membrane potential crosses a set threshold. The layer that implements this spiking mechanism in `convis` also has an optional refractory period that will prevent the neuron from firing for a short amount of time.

To give the user even more options for spike generation, we implemented the **Hodgkin-Huxley**, the **Fitz-Hugh Nagumo** and the **Izhikevich** model, which together cover a large range of dynamics. Figure 5.3.2 shows the output of different spiking mechanisms to the same input.

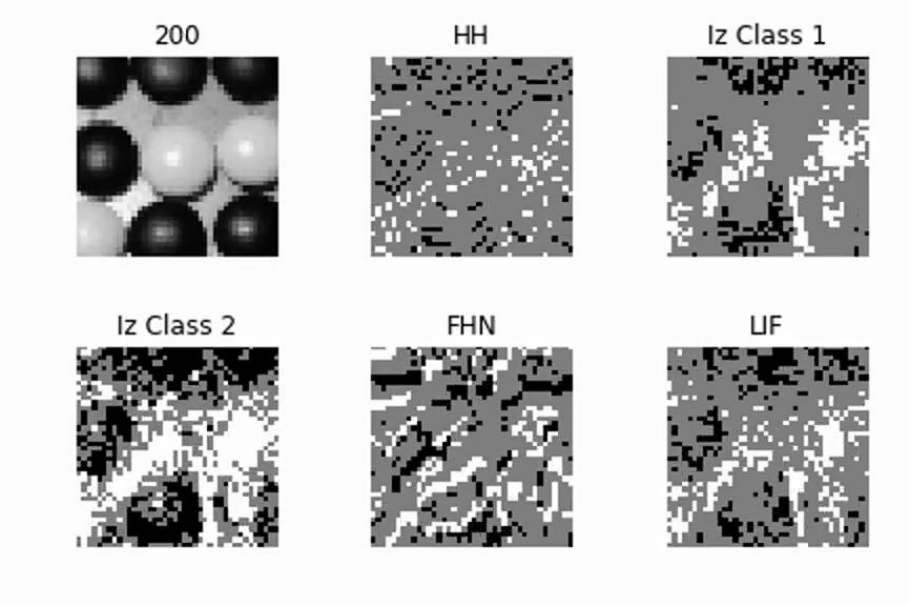

Figure 5.3.2: **Different Spiking Mechanisms** This figure illustrates that with the same input, different spiking mechanisms can generate very diverse patterns. White pixel signify a spike in an On-layer, black pixel spikes in an Off-layer.

5.4 Models Implemented

Next to the retina model from Wohrer 2008 (section 5.4.2), we implemented a range of linear-nonlinear cascade models as described in Real et al. 2017, which offer a range of complexity from the most simple linear-nonlinear model to a subunit model with per-subunit feedback and delays (section 5.4.1).

In Mcintosh et al. 2016, the authors used a convolutional neural network to model retina data. Since this seemed like the optimal application for the toolbox, we implemented their architecture (details in section 5.4.3). While they published their code, the convis implementation has the advantage of processing continuous streaming input instead of processing isolated chunks. Also, depending on the precise complexity and quality of retinal ganglion cell data, their model might have to be adapted slightly to fit other datasets by e.g. changing the number of subunits assumed. While it is possible to change that in their code, the class implementing their model in convis is very short, making a reimplementation very easy.

We also implemented a V2 model which was proposed by Rowekamp and Sharpee 2017 (section 5.4.4). Since V2 is mostly interested in delicate patterns, but less in their exact position or polarity, the model is a quadratic model capturing the spatial correlations between input pixels, which is then turned into a convolutional model by adding the response at different spatial positions. As an advantage over the implementation from Rowekamp and Sharpee 2017, we could create the model in a very short code segment. The pure numpy implementation by Rowekamp and Sharpee 2017 is a file with over 900 lines of code (not counting the custom gradient descent mechanism) with each gradient being implemented by hand. With our implementation we were able to create larger correlation maps and positional invariance. We could also try out different fitting methods, such as the limited-memory Broyden–Fletcher–Goldfarb–Shanno optimization algorithm (LBFGS), which found correla-

tion structures very similar to the ones published in Rowekamp and Sharpee 2017 in only a few seconds as opposed to several thousand iterations of the slow, hand-tuned gradient descent mechanism used in Rowekamp and Sharpee 2017.

5.4.1 LN Cascade Models

A commonly used model for the visual system is the combination of linear and non-linear filters. In the simplest case a single linear Receptive Field (RF) is combined with a rectifying non-linearity to formalize the intuition of what the measured Receptive Field (RF) represents: a linear filter of the stimulus that governs the response, while negative responses are not possible. Figure 5.4.1 **A** shows a schematic for this case.

The implementation in `convis` is straight forward: a linear layer and a non-linear layer are applied sequentially. For the linear stage e.g. a convolution operation can be used to create a set of local responses over the whole visual field, or a simple multiplicative filter that will create a specific set of responses. The non-linearity can be a simple expression such as rectification or squaring.

An *LN cascade model* is a sequence of linear and non-linear operations. These models allow more complex responses and also create more complicated *error surfaces* (see Section 5.5)

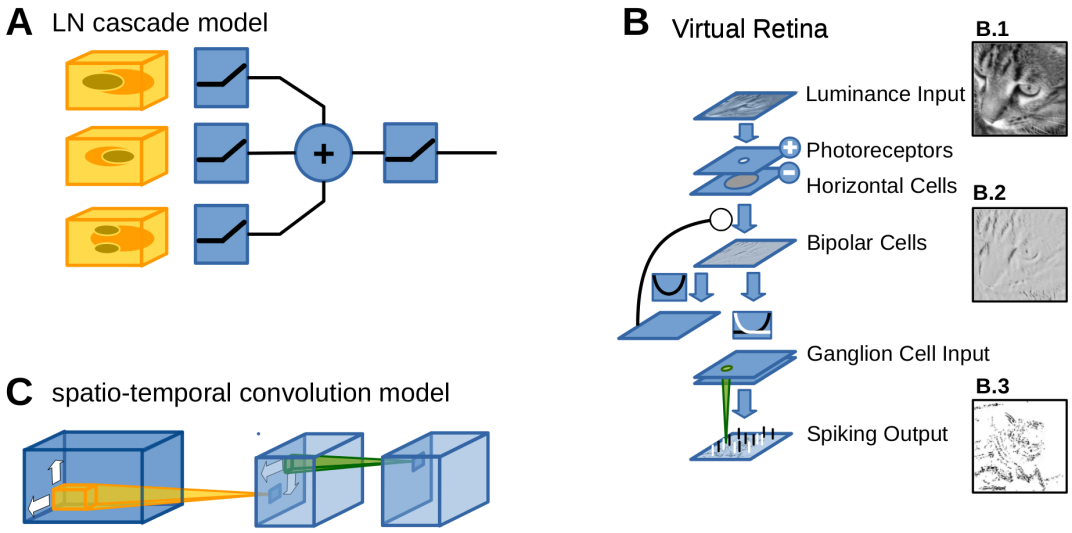

Figure 5.4.1: **Three kinds of `convis` models.** **A** shows a LN-LN model that uses three different convolution filters, rectifies and sums their responses. Instead of a sum, another convolution could be used and the cascade can be repeated multiple times. **B** shows a simplified schema of the retina model (section 5.4.2) *B.1* shows an example stimulus, *B.2* shows the effect of the OPL layer and *B.3* shows an example of spiking activity. **C** shows an almost conventional convolutional neural network. Each layer is comprised of a 3d convolution (and implied rectification). The number of layers and their channel-width determines the complexity of the model (see section 5.4.3 for an example).

5.4.2 The VirtualRetina Model

We implemented a version of the retina model published as VirtualRetina (Wohrer 2008) (see Figure 5.4.1 **B**). Our version has the advantage that all spatial filters can be replaced by 2d convolutions with arbitrary filters, the OPL can even be replaced with a full spatio-temporal convolution filter.

The retina model contains a linear stage in which the input is bandpass filtered with an a-causal spatio-temporally inseparable filter to create a contrast signal corresponding to the OPL. This contrast signal is then gain controlled with a highly non-linear local-gain control mechanism that replicates the phase-advance seen in the gain control dynamics of LGN recordings and finally a spike generation stage.

The linear "Outer Plexiform Layer" stage models the photon absorption at the level of photoreceptors and the lateral inhibition of horizontal cells which create a center-surround receptive field. To achieve this, VirtualRetina uses spatial gaussian filters and temporal exponential filters to first create a center signal by linearly filtering the input. This center signal is then filtered by another spatial and another temporal filter to create a surround signal which is then subtracted from the center signal. The linear weight between center and surround determines if the luminance input is converted to a pure contrast image (transient in space as well as time), or whether the amount of luminance will create a sustained response as well.

In the "Bipolar" stage provides contrast gain control, similar to the feedback that amacrine cells cells give to bipolar cells. It is implemented with a spatial map samples the local contrast and provides the leak current to the shunting inhibition on the bipolar cell.

In the biological retina, computations up to this point are (mainly) performed by non-spiking neurons. However, the retinal ganglion cells, the output neurons of the retina, create spikes to transmit visual information through their axons and the optic nerve. Spiking is inherently a highly non-linear process in which low or negative levels of input will result in no activity at all and a sufficiently positive input might create a roughly linearly proportional amount of spikes until a limit of refractory time is reached in which no increase in firing rate is possible. The model contains a static non-linearity which models the strictly positive response of the neuron and a leaky integrate-and-fire neuron model with refractory period. The rectified input is integrated over time, while a leak current drives the neuron back to its resting potential should the input be too weak. But once enough input is accumulated to cross a predefined threshold, a spike is recorded and the neuron is set to be in its refractory period, which will last a certain number of milliseconds. Only once the refractory period is over can the neuron start again to integrate more input.

Some ganglion cell types show an additional level of non-linearity, which stems from their dendritic tree integrating spatially over many non-linearly rectified signals. In the model this is done by having an optional spatial filter stage between the static spiking non-linearity and the spike generation.

5.4.2.1 Linear Filtering in the OPL

The first stage of the model is linear and models the combined response of photo-receptors and horizontal cells. Together they form a center-surround receptive field with the inhibitory surround slightly delayed in time. In VirtualRetina, this filter is created using recursive spatial and temporal filtering separately. By subtracting the delayed, inhibitory response from the excitatory response a spatio-temporally inseparable receptive field is created.

$L(x, y, t)$ is the luminance input.

$$C(x, y, t) = G * T * E_n * L(x, y, t) \tag{5.1}$$
$$S(x, y, t) = G * E * C(x, y, t) \tag{5.2}$$
$$I_{OLP}(x, y, t) = \lambda_{OPL}(C(x, y, t) - w_{OPL}S(x, y, t)_) \tag{5.3}$$

Our model also offers a fully recursive implementation. Alternatively, a half-recursive filter is available that replaces the spatial filters of center and surround with convolutions, but keeps the temporal filters recursive. Another implementation allows for convolution filters for each of the separated filters (spatial and temporal) and another one allows for a convolutional 3d receptive field. All implementations take the same parameters. The 3d receptive field, can be initialized using the parameters, however changes in the kernel can not be translated back into the input parameters.

5.4.2.2 Contrast Gain Control

The contrast-gain-control stage is implemented as a iteratively evaluated differential equation:

$$\frac{dV_{Bip}}{dt}(x, y, t) = I_{OLP}(x, y, t) - g_A(x, y, t)dV_{Bip}(x, y, t) \tag{5.4}$$
$$g_A(x, y, t) = G * E * Q(VBip)(x, y, t) \tag{5.5}$$

with $Q(VBip) = g_A^0 + \lambda_A V_{Bip}^2$

5.4.2.3 Spike Generation

The spike generation is done using numerical integration of a leaky integrate-and-fire model with refractory period. But first, the input is processed by a spatial filter and a static nonlinearity:

$$I_{Gang}(x, y, t) = G * N(eT * V_{Bip}) \tag{5.6}$$

with G being a spatial Gaussian kernel and the static nonlinearity $N(V)$ being:

$$N(V) = \begin{cases} \frac{i_G^0}{1-\lambda(V-v_G^0)/i_G^0} & \text{if } V < v_G^0 \\ i_G^0 + \lambda(V - v_G^0) & \text{if } V > v_G^0 \end{cases} \tag{5.7}$$

The actual *LIF* then has the equation:

$$\frac{dV_n}{dt} = I_{Gang}(x_n, y_n, t) - g^L V_n(t) + \eta_v(t) \tag{5.8}$$

If the neuron is in the refractory period, V is clamped at 0. When V crosses a certain threshold, V is reset to 0 and a random refractory time is chosen from a normal distribution of specified mean and standard deviation.

5.4.2.4 Other Features

Our retina model can load *xml* files that contain VirtualRetina configurations, however some options are ignored. Additionally, the parameters of the model can be saved and loaded as *json* files.

There is a number of features which we didn't implement. The output spike trains in our model are computed per pixel, not from explicitly positioned neurons. Also the spiking neuron model is not event driven, so the spikes are produced with the resolution of the internal frame rate (usually 1kHz). We did not implement a microsaccade generator since most of our stimuli already contain motion.

5.4.3 Convolutional Models

Deep convolutional networks (see Figure 5.4.1 **C** for a simple example schematic) are generating a lot of scientific interest due to their successful application in visual object classification, speech recognition, translation and game playing.

To model responses of retinal ganglion cells (RGC) Mcintosh et al. 2016 created a convolutional model with three stages. The first layer of the model has 8 subunits and sums over an area of 5×5 pixel and 10 time bins. The 8-channel output is fed into the second layer that has 16 subunits and uses spatio-temporal RFs of the same size as the first layer. The last layer then fully connects the 16-channel output to however many output units are supposed to be fitted. See section 7.3 for our reimplementation.

In contrast to VirtualRetina, this model does not come with exemplary parameters and is meant mostly for data-fitting. Recently, Maheswaranathan et al. 2018 compared the subunits of the fitted model to the receptive fields of bipolar cells and found that the internal structure of the retina matches the internal filters of the model fitted only to RGC responses. This more recent extension of the model has normalization and two 8-channel layers. A poster from the group hinted at an LSTM at the last stage (McIntosh et al. 2016).

5.4.4 V2 Model

A very intersting model that is challenging to fit was proposed by Rowekamp and Sharpee 2017 to model *V2* cells recorded in macaque viewing natural stimuli (Willmore, Prenger, and Gallant 2010). Since *V2* cells both are slightly location invariant and respond to the cross-correlation of the input rather than a fixed pattern, the model is a mix between a convolutional model and a quadratic model. The quadratic parameter of the model can be decomposed into the different subunits which can then be analysed. Rowekamp and Sharpee 2017 showed that these subunits are forming cross-orientation suppression patterns, i.e. the orientation of positive and negative subunits tended to be orthogonal.

Our implementation of the model is not particularly long (see Appendix 7.3.1) and there is no need to write special code for the fitting procedures, as all gradients can be derived automatically. Unfortunately the models complexity requires a very slow gradient descent, both for the original implementation and ours, that is initialized with a solution found by a simpler model earlier. However, when using LBFGS, after only a few iterations a model is found that - while it doesn't replicate the firing rates of the data - found quadratic parameters that had very similar principal components to the one that was found by the slow gradient

descent method, which lets us to believe that information about the stimulus cross-correlation is found in the curvature of the error surface. It is possible, that a more sophisticated fitting procedure could improve drastically on the slow gradient descent procedure and find the correct model faster.

5.4.5 Run-Time and Comparison to Other Software

We compared the features of convis to other software packages that also provide models for retinal or early cortical responses (see Table 5.1). We examined for each software whether they provided luminance gain control and contrast gain control. Most packages provide luminance gain control as some form of high-pass filter, e.g. VirtualRetina and other software built on it's theoretical foundation (COREM and convis) adapt to luminance in the outer plexiform layer stage. Contrast gain control is much less common and all but one of the examined software packages use the same formulation as VirtualRetina. Only topographica implemented an alternative contrast gain control stage after Naka and Rushton 1966.

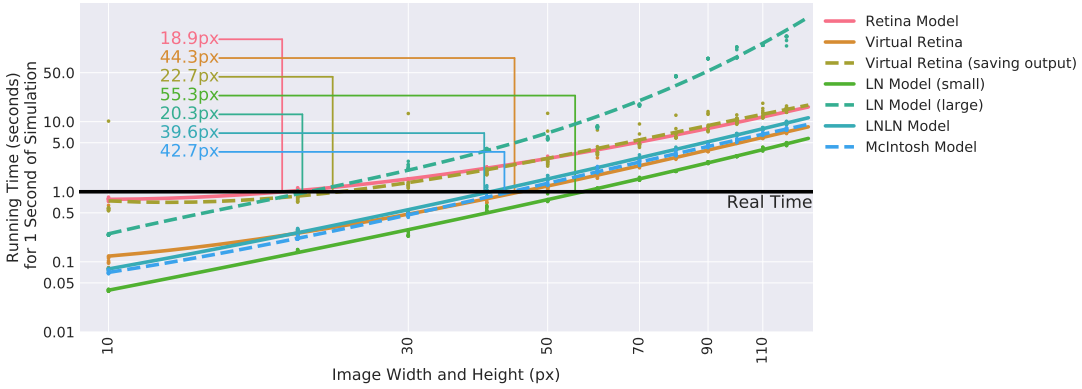

Figure 5.4.2: **Run-time of different models** Each line shows the time it takes to compute 1 second of 1kHz sampled output at a specific image size of different convis models and VirtualRetina as a comparison. The intersections with the real-time line (one second computed in one second) is marked for each model and the image size at the real-time intersection is shown in the corresponding colour.

Computing convolutions is slower than recursive filters, so computation speed is not a natural strength of the models implemented in convis. The run-time depends strongly on the size of the image that is processed. In Figure 5.4.2 we plotted the run-time to compute 1 second of output of different convis models over the width of a square input image. We compared the run-time to VirtualRetina, in one run only saving the generated spikes, in another saving the output of each layer to a hard-disk. We included the second run, since the only way to analyse the output of each layer of VirtualRetina is to save it to a file, while in convis all outputs can remain in memory to be analysed with common scientific Python tools. Not surprisingly, the convis implementation (using separate convolutions in the outer plexiform layer layer) ran slower than VirtualRetina on the same computer. It uses convolutions, which are slower to compute than recursive filters and it performs Also the image size that still allows to run the model in real time was only 18×18 for the convis

retina model, compared to 44×44 for VirtualRetina. If VirtualRetina saves all outputs on a hard-disk, it has about the same speed as the `convis` retina model. But more interesting is the comparison to the simpler *LN* and *LNLN* model, as well as the *McIntosh* model. The small *LN* model had a filter size of $20, 10, 10$, i.e. 20 time steps times a 10×10 filter at each time step. The large *LN* model had a filter that was twice the size in each direction $(40, 20, 20)$, which increased the run time dramatically. All other models were faster to compute than even VirtualRetina, since they only had up to three, relatively small linear convolution stages. Despite the small filter size, the *McIntosh* model was shown to be able to fit RGC responses very well (Mcintosh et al. 2016).

Table 5.1: Comparing different retina simulation software: VirtualRetina (Wohrer and Kornprobst 2009), Topographica (Bednar 2012), Virtual Retina++ (continued development of VR in the ENAS / PRANAS package Cessac and Palacios 2013), Lorach et al. (Lorach et al. 2012), and RetinaStudio (Martínez-Álvarez et al. 2013) . ≈VR signifies that the gain control was implemented similarly to VirtualRetina: Contrast gain control through shunting inhibition, using a local estimate of spatio-temporal contrast (Wohrer, Kornprobst, and Vieville 2007).

Name / Application	Luminance Gain Control	Contrast Gain Control	Language of Source Code, Configuration	Open Source	Filters	continuous in/output	Optimization/ Plasticity
VirtualRetina (Wohrer and Kornprobst 2009) RGC responses	Yes	Local Shunting	C++, xml	Yes (CeCILL-C)	recursive	No	No
Lorach et al. 2012 Neuroprosthetics	Yes	No	hardware DVS, Matlab	No	convolution	No	No
Topographica (Bednar 2012) PVC / Neural Maps	Yes	Naka-Rushton (Naka and Rushton 1966)	C, Python	Yes (BSD 3)	convolution		Yes
ENAS (Cessac and Palacios 2013) Model Verification	Yes	≈VR	C++, xml/GUI	No	recursive	No	No
iModel Ret_Mesh (Baker and Bair 2013) RGC responses	Yes	No	C/OpenGL / Java	code available from imodel.org website	hexagonal grid RFs	No	No
RetinaStudio (Martínez-Álvarez et al. 2013) Neuroprosthetics			C#/Flowlang	Flowlang		No	No
COREM (Martínez-Cañada et al. 2016) RGC responses	Yes	≈VR	C++, scripts	Yes (CeCILL-C)	recursive	Yes	No
deepretina (Mcintosh et al. 2016) RGC responses	HP filters possible	No	Python / Theano	available on github (no license specified)	convolution	No	Yes
isetbio (Brainard et al. 2017) Perceptual thresholds optical aberations photoreceptor sampling		-	Matlab /	Yes (MIT)	hexagonal grid	No	No
pulse2percept (Beyeler et al. 2017) Perceptual thresholds of RGCs for implant assessment		-	Python / Scipy	Yes (BSD 3-clause)	square or gaussian RFs, radial current spread	No	No
Convis (Huth, Masquelier, and Arleo 2018) RGC responses	Yes	≈VR	Python / PyTorch	Yes (GPL-3)	recursive or convolution	Yes	Yes

5.5 Fitting of Models

The *backpropagation* mechanism of `PyTorch` allows for efficient parameter fitting using a number of different gradient based optimization mechanisms. The goal of every parameter optimization is to minimize a *loss function* by changing the values of a set of parameters. The values of the parameters form the *parameter space* and the *error surface* is the loss associated with each position in the parameter space. This surface can be very smooth with a unique minimum, or it can be arbitrarily "peaky" with many local minima. What gradient based optimization is doing is using the local information of the error slope to make a more informed guess about where to look next.

An algorithm that makes fairly few assumptions is naive gradient descent. It simply follows the gradient scaled by a learning rate: Each parameters value changes proportional to the gradient of the error with respect to that parameter. Since the gradient at the optimum is 0 in all directions, the algorithm stops once the minimum is reached.

The following code listing **??** illustrates how to manually do gradient descent in `PyTorch`. The `outp` goal variable was created by an `LN` model with a randomized weight and the `LN` model called `model` uses the mean squared distance of its output to `outp` to get a gradient to adapt its weight. The Figure 5.5.1 shows the loss during the optimization as well as the distance between the weights of the two models.

```
import numpy as np
import convis, torch
model = convis.models.LN()
model.conv.set_weight(np.ones((5,5,5)),normalize=True)
for i in range(50):
    o = model(inp)
    loss = ((outp-o)**2).mean()
    loss.backward(retain_graph=True)
    model.conv.weight.data = (model.conv.weight.data
                      - 0.1 * model.conv.weight.grad.data)
    model.conv.weight.grad.zero_()
```

PyTorch offers optimizer objects that perform the optimization steps and hold hyperparameters and e.g. momentum terms. In `convis`, the boilerplate for optimization can be omitted making optimization as easy as:

```
model = convis.models.LN()
model.set_optimizer.SGD(lr=0.01)
for i in range(50):
    model.optimize(inp, outp)
```

The approach makes one assumption that is easily violated: that there are no local minima. And even *if* there is only one minimum, the algorithm could be trapped in a cycle around the minimum and never reach it as a large learning rate will cause an optimization step to overshoot the minimum, potentially ending up at a symmetric position on the other side. Because of these shortcomings, a number of extensions can help gradient descent to find the global minimum faster and to avoid local minima. One is stochastic gradient descent (SGD) which adds a small noise term to jump out of local minima. Another is a "scheduler" that changes the learning rate over the course of the optimization: in the beginning, it makes

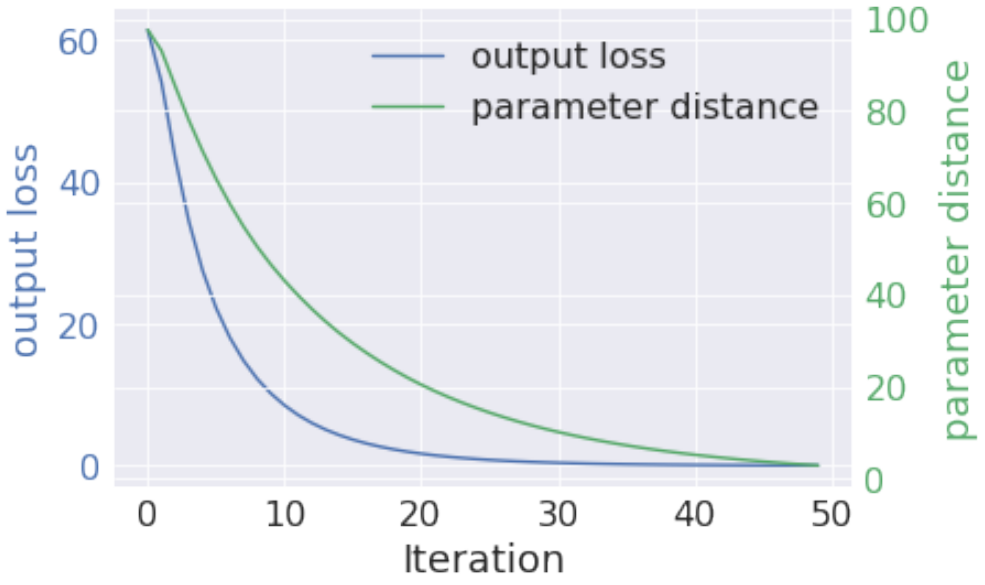

Figure 5.5.1: **Trace of the loss and weight distance of the example in 5.5.** Both, output loss and the distance of the parameters to the ground-truth parameters decrease. However, as the parameters get closer to the true parameters, the error gets smaller and thus the gradient gets smaller as well. This leads naive gradient descent to slow down more and more the closer we are to the solution.

a lot of sense to have a high learning rate to get close to the minimum, later the learning rate has to be lowered, so that the minimum can actually be reached. Alternatively, a *momentum* term can be used to accelerate the learning if the gradient has been in the same direction for multiple steps and to decrease it if one has passed the minimum.

Since the error change depends strongly on what the parameter that was changed is doing, different algorithms can be better suited for different models. For the models we implemented in the `convis` toolbox, some have a very convex error surface and are thus relatively easy to fit. Others have a more complex behaviour.

5.5.1 Gradient Descent Methods

The simplest group of gradient guided optimizers are gradient descent algorithms. Stochastic gradient descent (SGD) for example simply subtracts the gradient linearly scaled from each parameter. While this method literally goes in the right direction, it will not reach a minimum rapidly for small learning rates and it will overshoot beyond the minimum for large learning rates, causing it sometimes to oscillate around the minimum. In the case of quadratically decreasing gradient toward the minimum, SGD will slow down more and more the closer it is to the minimum, making it impossible to actually reach it. To counter that, one can add a momentum term, which will add a bias such that the gradient is followed more strongly if it is pointing in the same direction as in the past. The learning rate and momentum term can be fixed by hand, but it is more common to use learning rate schedulers to use large steps initially and then gradually decreasing learning rates, the more iterations were already performed.

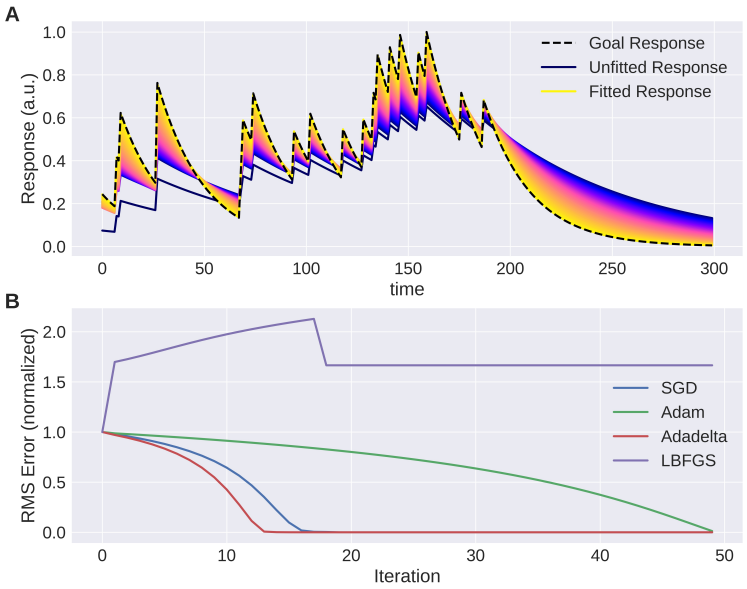

Figure 5.5.2: **Fitting an exponential filter** Similar to the example in section 5.5, we can also optimize the parameters of recursive filters. **A** shows how the target voltage trace is approximated after successive iterations (colours from purple to yellow show the number of iterations). **B** shows how different optimizers can deal with this problem. Simple gradient descent methods are robust and can handle a parameter like the recursive time-constant well, while the more sophisticated LBFGS algorithm fails.

Advanced gradient descent methods like Adadelta Zeiler 2012 have a dynamic learning rate. Adadelta is more robust to noisy gradients than standard SGD. *AdaGrad* can work with sparse gradients, *RMSProp* can deal with non-stationary objectives. The *Adam* optimizerKingma and Ba 2014 uses two moment terms and combines the advantages of *AdaGrad* and *RMSProp*.

Figure 5.5.2 shows a fast convergence of SGD and Adadelta.

5.5.1.1 LBFGS

Newton methods and pseudo-Newton methods also use information about the change in gradient with respect to the parameters, i.e. the curvature of the error landscape. In the simplest case of a linear filter and a quadratic error function, this allows to find the global minimum instantaneously, since the local curvature of a quadratic function uniquely determines the minimum. As long as the error landscape has a quadratic Taylor expansion close to a minimum, the curvature can be used to directly jump to the minimum. For large convolutional filters, this can even be performed for all parameters in the same step. The limited-memory Broyden–Fletcher–Goldfarb–Shanno optimization algorithm (LBFGS) optimizer implements a pseudo-Newton method and estimates the curvature by evaluating the error function at different points in the parameter space. While this can make the parameters converge very fast to an optimal solution, this algorithm has a weakness when the parameters are too close to a local solution and so the gradient and its curvature is weak. In this cases it might be more successful to initialize a model multiple times with completely random parameters and performing only a few LBFGS iterations each and then choosing the parameter combination

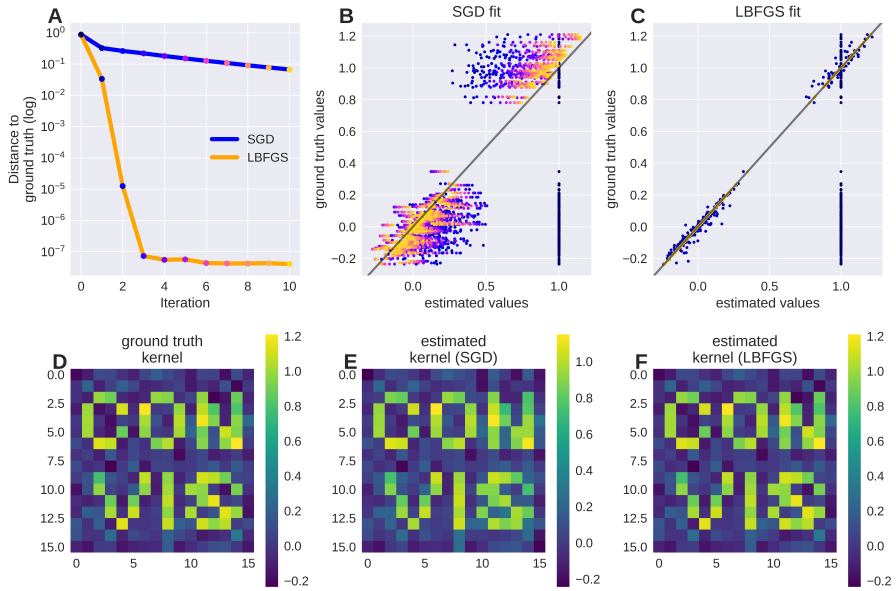

Figure 5.5.3: **Fitting a spatial filter** Repeating a similar optimization to Figure 5.5.1, we now optimize a spatial filter of an *LN* model to replicate another *LN* model using two different optimization algorithms: SGD and LBFGS. **A** shows the loss of each optimizer for the first 10 iterations. **B** shows that SGD slowly approaches the true values (shown in D) (colours from purple to yellow show the number of iterations). LBFGS in contrast achieves a very low loss after only three iterations. **C** shows that almost immediately a solution close to the goal is reached and then subsequently improved upon. **E** and **F** show the recovered linear filters after 10 iterations. Compared to *D**, both filters look fairly similar.

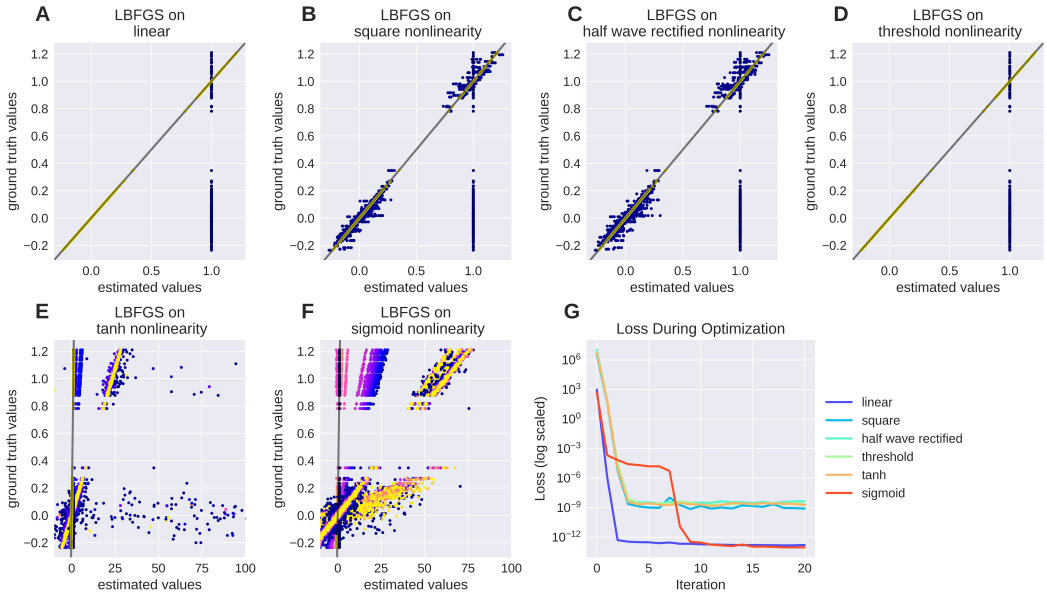

Figure 5.5.4: **Fitting LN model.** **A-F** show the parameter values during the optimization process when a specific non-linearity is used for the *LN* models. **A** and **D** pose no difficulty at all, **B** and *C **prolong the fitting process slightly and** E **and** F **are more difficult to fit. In** G** the loss decreases after only few iterations for all non-linearities. The plot averages multiple initial conditions.

with the lowest loss, rather than trying to improve a solution iteratively.

Figure 5.5.2 shows how LBFGS can fail, in contrast Figures 5.5.3 and 5.5.4 show that LBFGS can converge almost immediately to a solution very close to the optimum, even if non-linearities are used that flatten out a large part of the parameter space (e.g. a sigmoid far from 0).

5.5.1.2 Fitting multi-stage models

Once one of the linear stages of a two-stage subunit model is fixed, fitting the other one is no longer a problem. To test whether `convis` can fit both stages at once we created a model with a convolution with a vertical bar, then a rectification and then a convolution with a horizontal bar. Then we created a second model that also had two convolutions and two non-linearities, but the convolutions were initialized to random filters. Using stochastic gradient descent or *Adagrad*, the error is decreasing over time, but the shape of the receptive fields does not look in any way satisfying. Using LBFGS instead, a solution very close to the ground truth is found after only two iterations. This means that the curvature of the gradient is smooth enough for this problem to make the global minimum easy to find.

The situation is slightly more complicated if we have multiple subunits which are combined. In this case, LBFGS from random initial positions might become trapped in local minima, hinting at a "peaky" error landscape. Using random initialization points for LBFGS seems to work well in that case.

Good and Bad Input A stimulus used in an experiment has to explore the dynamics of the system in question sufficiently to make it possible to build a model that captures this mechanism afterwards. For the very simple *LNLN* model discussed, the non-linearity cascade requires the stimulus to have certain properties such that we can recover the model parameters by the input-output relationship. If we e.g. use an input, that is spatially homogeneous, we will not be able to see any spatial structure in the output. Also if we use a stimulus that has many, strongly negative values, since all weights in the ground truth model are positive the non-linearity will remove any information and the model will be completely silent. In the previous simulations we used spatio-temporal noise from a normal distribution with a mean of 0 - which coincidentally is the threshold of the non-linearity. In a physical experiment, we can only model neurons that respond to the stimulus at some point, but not others, taking care of at least one rectification of which we explore both sides. But there can be many more non-linearities that we will only notice if we explore the stimulus space sufficiently. In the example above, we can change the mean of the input distribution gradually. For very negative input, we can observe that we can not recover the internal structure of the model, since it is silent always. For very positive values, we can also not recover the structure, since the rectification we use behaves linearly at very high values, combining the filters of both layers into one linear filter. Closer to the threshold of the non-linearity, we can see a gradual improvement in final loss from high values to smaller positive values. On the negative side, we see that *sometimes* we can fit the model really well, even with a negative mean, but other times we fail, leading to a gradual increase in the probability that the final loss will be very small, however the distribution is bimodal. This effect comes from the sparseness, introduced by the non-linearity on negatively biased values. Sparseness itself is very helpful to investigate non-linearities between spatial integration layers - however a sparse stimulus will need more

time to explore the parameter space. The thresholded negative values from the first Layer have a high sparseness and so sometimes they will explore the second filter enough for the optimization process to infer it, in other runs it will fail to do so.

5.6 Conclusion

We presented convis, a Python toolbox for modelling visual responses based on PyTorch. The toolbox allows for efficient simulation of models as well as gradient based model fitting. Among the models that are implemented in convis are *LN*-cascade models, convolution models, and a detailed retina model.

In addition to the already implemented models, new models can be created by combining layers. The design of convis allows for models to be defined in only few lines of code with expressions similar to Matlab or numpy. All models inherit the ability for gradient descent, processing of very long (potentially infinite) input sequences, self-documentation and parameter management.

Gradient descent methods can speed up model fitting drastically, however their use is not always straight forward. The reason why deep neural networks need so much data and have such a slow convergence is that the combination of linear and non-linear operations creates a highly peaky error landscape. Many models used to model e.g. RGC responses are much simpler than these models. They can still require special strategies to fit (see the Section 5.4.4 as an example), but having access to the gradient helps fitting these models immensely.

convis also implements spiking neuron models, such as LIFs, Hodgkin-Huxley, Fitz-Hugh Nagumo and Izhikevich models, which each also provide a gradient. But since these models are highly state dependent and usually have some form of discontinuity that implements their spiking behaviour, the gradient is less useful for fitting these models. Still convis gives the opportunity to explore the gradient of spiking models which might at some point give better insights into how to fit complex spiking models to data since today this is still a hard problem (see e.g. Rossant et al. 2011).

convis is available under *GPL-3* license at https://github.com/jahuth/convis.

References

Baker, Pamela M and Wyeth Bair (2013). "WM: an integrated framework for modeling the visual system". In: *Frontiers in Neuroinformatics* 84. ISSN: 1662-5196. DOI: 10.3389/conf.fninf.2013.09.00084.

Bednar, James a. (2012). "Building a mechanistic model of the development and function of the primary visual cortex". In: *Journal of Physiology-Paris* 106.5-6, pp. 194–211. ISSN: 09284257. DOI: 10.1016/j.jphysparis.2011.12.001. URL: http://www.ncbi.nlm.nih.gov/pubmed/22343520.

Beyeler, Michael et al. (2017). "pulse2percept: A Python-based simulation framework for bionic vision". In: *bioRxiv*. DOI: 10.1101/148015. eprint: https://www.biorxiv.org/content/early/2017/07/10/148015.full.pdf. URL: https://www.biorxiv.org/content/early/2017/07/10/148015.

Brainard, David H. et al. (2017). *Pytorch github repository*. https://github.com/isetbio/isetbio. URL: https://github.com/isetbio/isetbio (visited on 10/10/2017).

Cessac, Bruno and Adrian G. Palacios (2013). "Spike train statistics from empirical facts to theory: The case of the retina". In: *Modeling in Computational Biology and Biomedicine: A Multidisciplinary Endeavor* 9783642312, pp. 261–302. DOI: 10.1007/978-3-642-31208-3_8.

Clifford, C W and K Langley (2000). "Recursive implementations of temporal filters for image motion computation." In: *Biological cybernetics* 82.5, pp. 383–390. ISSN: 0340-1200. DOI: 10.1007/s004220050592.

Deriche, Rachid (1993). "Recursively implementating the Gaussian and its derivatives". In: *Rapports de recherche INRIA* {RR}-1893, p. 24. URL: http://hal.inria.fr/inria-00074778/PDF/RR-1893.pdf.

Huth, Jacob, Timothée Masquelier, and Angelo Arleo (2018). "Convis: A Toolbox to Fit and Simulate Filter-Based Models of Early Visual Processing". In: *Frontiers in Neuroinformatics* 12.March, pp. 1–16. ISSN: 1662-5196. DOI: 10.3389/fninf.2018.00009. URL: http://journal.frontiersin.org/article/10.3389/fninf.2018.00009/full.

Kingma, Diederik P. and Jimmy Ba (2014). "Adam: A Method for Stochastic Optimization". In: pp. 1–15. ISSN: 09252312. DOI: http://doi.acm.org.ezproxy.lib.ucf.edu/10.1145/1830483.1830503. arXiv: 1412.6980. URL: http://arxiv.org/abs/1412.6980.

Lorach, Henri et al. (2012). "Artificial retina: the multichannel processing of the mammalian retina achieved with a neuromorphic asynchronous light acquisition device". In: *Journal of Neural Engineering* 9.6, p. 066004. ISSN: 1741-2560, 1741-2552. DOI: 10.1088/1741-2560/9/6/066004. URL: http://iopscience.iop.org/1741-2560/9/6/066004%7B%5C%%7D5Cnhttp://iopscience.iop.org/1741-2552/9/6/066004/pdf/1741-2552_9_6_066004.pdf.

Maheswaranathan, Niru et al. (2018). "Deep learning models reveal internal structure and diverse computations in the retina under natural scenes". In: *bioRxiv*. DOI: 10.1101/340943. URL: https://www.biorxiv.org/content/early/2018/06/08/340943.

Martínez-Álvarez, Antonio et al. (2013). "RetinaStudio: A bioinspired framework to encode visual information". In: *Neurocomputing* 114, pp. 45–53. ISSN: 09252312. DOI: 10.1016/j.neucom.2012.07.035.

Martínez-Cañada, Pablo et al. (2016). "A Computational Framework for Realistic Retina Modeling". In: *International Journal of Neural Systems* 26.7, p. 1650030. ISSN: 0129-0657. DOI: 10.1142/S0129065716500301. URL: http://www.worldscientific.com/doi/10.1142/S0129065716500301.

Mcintosh, Lane T et al. (2016). "Deep Learning Models of the Retinal Response to Natural Scenes". In: *Advances in Neural Information Processing Systems 29 (NIPS)* Nips, pp. 1–9.

McIntosh, Lane et al. (2016). *Convolutional Neural Network Models of the Retina*.

Naka, KI and WAH Rushton (1966). "S-potentials from colour units in the retina of fish (Cyprinidae)". In: *The Journal of physiology* 185.3, pp. 536–555.

Real, Esteban et al. (2017). "Neural Circuit Inference from Function to Structure". In: *Current Biology* 27.2, pp. 189–198. ISSN: 09609822. DOI: 10.1016/j.cub.2016.11.040. URL: http://linkinghub.elsevier.com/retrieve/pii/S0960982216313938.

Rossant, Cyrille et al. (2011). "Fitting Neuron Models to Spike Trains". In: *Frontiers in Neuroscience* 5.February, pp. 1–8. ISSN: 1662-4548. DOI: 10.3389/fnins.2011.00009. URL: http://journal.frontiersin.org/article/10.3389/fnins.2011.00009/abstract.

Rowekamp, Ryan J. and Tatyana O. Sharpee (2017). "Cross-orientation suppression in visual area V2". In: *Nature Communications* 8, pp. 1–9. ISSN: 20411723. DOI: 10.1038/ncomms15739. URL: http://dx.doi.org/10.1038/ncomms15739.

Willmore, Ben D B, Ryan J Prenger, and Jack L Gallant (2010). "Neural representation of natural images in visual area V2." In: *The Journal of neuroscience : the official journal of the Society for Neuroscience* 30.6, pp. 2102–14. ISSN: 1529-2401. DOI: 10.1523/JNEUROSCI.4099-09.2010. URL: http://www.ncbi.nlm.nih.gov/pubmed/20147538%7B%5C%%7D5Cnhttp://www.pubmedcentral.nih.gov/articlerender.fcgi?artid=PMC2994536%7B%5C%%7D5Cnhttp://www.pubmedcentral.nih.gov/articlerender.fcgi?artid=2994536%7B%5C&%7Dtool=pmcentrez%7B%5C&%7Drendertype=abstract.

Wohrer, Adrien (2008). "Model and large-scale simulator of a biological retina, with contrast gain control". PhD Thesis. University of Nice-Sophia Antipolis.

Wohrer, Adrien and Pierre Kornprobst (2009). "Virtual Retina: a biological retina model and simulator, with contrast gain control." In: *Journal of computational neuroscience* 26.2, pp. 219–49. ISSN: 1573-6873. DOI: 10.1007/s10827-008-0108-4. URL: http://www.ncbi.nlm.nih.gov/pubmed/18670870.

Wohrer, Adrien, Pierre Kornprobst, and Thierry Vieville (2007). "Virtual Retina : a biological retina model and simulator, with contrast gain control [Research Report]". In: *RR-6243*, 32 <inria–00160716v2>.

Zeiler, Matthew D. (2012). "ADADELTA: An Adaptive Learning Rate Method". In: ISSN: 09252312. DOI: http://doi.acm.org.ezproxy.lib.ucf.edu/10.1145/1830483.1830503. arXiv: 1212.5701. URL: http://arxiv.org/abs/1212.5701.

Chapter 6

Concluding Remarks

In this thesis we started the first steps in an effort to understand the multi-faceted neural changes that occur due to aging. We started out from a discussion of observed aging effects and developed four *minimal aging hypotheses* (Section 1.9). We will quickly outline the approaches that grew out of this framework in this introduction before discussing possible extensions to the work in the following sections.

One approach, outlined in chapter 2, connected the observed increase in receptive field size in aging to the *input noise hypothesis* using a side-effect of spike-time dependent plasticity (STDP). We might even consider this a compensatory mechanism that is triggered by increased input noise and leads to larger, more noise robust receptive fields. In the scope of a planned cooperation with an experimental lab in Göttingen, we analysed retinal ganglion cell (RGC) data to estimate the likelihood of successfully proving a change in the size of RGCs caused by bipolar cell sprouting (Section 3.4.2.4). Unfortunately we concluded that the project was not feasible with the methods we had in mind. We will describe some possible future projects that have a better chance of success than the planned project. Since gain control and normalization is a repeated motive in the visual system (Carandini and Heeger 2012), we examined the effect of input noise on a contrast gain control circuit, first across a small range of input noise, yielding inconclusive results, then across a larger range and finally using a modified spike train distance that compensates for the firing rates of the inputs. To connect our theoretical models to psychophysical data that was available to our group, we developed a method based on decoding and psychophysical threshold estimation to measure calculation efficiency (CE) and Equivalent Internal Noise (EIN) in models of the visual system. We explored two dimensions: receptive field (RF) size and number, which can both be expected to change in age.

As a methodological advance, we have presented `convis`, the convolutional vision model toolbox that supported some of the simulations, but more importantly offers approaches for experimental data fitting and efficient simulation in an integrated, easily extensible framework.

6.1 Aging Hypotheses

We presented a framework of minimal hypotheses of aging effects that reduce the large number of age associated changes to single, causal origins. Not all minimal hypothesis developed in chapter 1 could be tested in the short span of our work. We mostly explored the *input noise*

hypothesis. The increase of cortical receptive fields as suggested by the increase of population receptive fields (pRFs) could be shown in chapter 2 to be caused by the effect of input noise on plasticity mechanisms. The other projects were so far also explored from the perspective of input noise, but they also offer opportunities to explore some of the other hypotheses. Still, there are many questions remaining to be answered. We will discuss issues specific to one of the projects in the following sections. In addition, there are still approaches we could not examine within this thesis.

The *plasticity hypothesis* could be tested in simulations similar to 2.6.1. Instead of changing input noise, the ratio of facilitation and depression can be changed. As we discussed in section 1.8.3, plasticity might very well be biased towards depression. This will evidently not lead to an enlargement of receptive fields as we defined them in section 2.6.1. However, if the decrease in the numbers of synapses is combined with lateral inhibition that normalizes the activity of the cortical neurons, the overall activity levels will stay constant, but the patterns that activate neurons will come from less afferents. This sparser connectivity pattern might lead to simpler computational structures or it might result in more stochastic behaviour since there is less opportunity for redundant processing that could keep timing constant. There is a large number of possible follow-up hypothesis that give rise to interesting theoretical models that could be tested. Is a decrease in synaptic connections necessarily detrimental? Is it necessary for the brain to recruit more neurons to do the same computations if each of them has less connections? Would a network with a strong bias for depression stabilize at some point or would it lose all synapses in specific circumstances?

For the *inhibition hypothesis* (section 1.9.4), a suitable experiment is already set up in section 4.7.1. The model we proposed is using lateral inhibition, although we so far kept it at a constant level in these simulations, but varied inhibition in section 4.7.2. In section 6.5, we give an outline on how to extend the full project to lateral inhibition.

The *white matter hypothesis* can be tested in theoretical models or experimentally. Modelling approaches can focus either on increased noisiness of transmitted signals by adding noise to a multi-stage model, or on the decreased bandwidth of cortical connectivity that can lead to stronger information bottle-necks, resulting potentially in a decrease in the complexity of the information that can be transmitted. However, it is also possible that changes in coding strategy could compensate for a loss of white matter fibers. E.g. temporal multiplexing can reduce the number of channels needed to transmit the same information at the cost of reaction time. Whether the brain can actively switch between different coding schemes depending on available bandwidth has not been widely discussed and would be a remarkable discovery. It is more likely that if a neural code is a mix of synchronous/parallel and temporal/sequential coding, it could adapt flexibly to either be more distributed across white matter fibers or adapt more sequential cognitive strategies. This would still imply that cognition changes drastically with a loss of white matter fibers, which might be in line with a general increase in reaction time associated with old subjects. Whether and how the brain can cope with a loss of long-range connections is a fascinating topic that we would have loved to explore in much more detail. On the experimental side, correlation studies between specific cognitive functions and white matter anisotropy can differentiate between white matter and other anatomical changes, such as eg. cortical thickness as was done in Ziegler et al. 2010. Approaches to link white matter defects at specific locations to specific cognitive functions could be possible, but we do not know of specific evidence that white matter degradation could be a localized phenomenon. Diseases that specifically target retinal

ganglion cells, the axons of which form the optic nerve, could be considered a localized white matter loss, however the effects tend to be disruptive only locally and result simply in a loss of visual perception.

6.2 Receptive Fields and Noise

The positive effect of noise on receptive field size is a fortunate coincidence. If our pilot simulations had yielded negative results, we would have to devise a much more complicated mechanism that could relate the change in receptive field size to regularities of the input. It is still possible that the brain uses a different mechanism for this task since the size of receptive fields does seem to be constrained by the two forces: the desire to be large enough such that noise can be reasonably compensated and the desire to still provide information with as high resolution as possible.

It still remains to be explored if there is an asymmetry between the temporal and spatial aspects of receptive fields.

The internal structure of receptive fields was so far not in the scope of this particular project - we only considered the number of non-zero weights, but not their configuration. Yet, we would assume that even though there are neurons with circular receptive fields and others with intricate patterns, some only responding to a single stimulus while others will respond to a class of objects, that still all of these neurons locally use the same strategy to choose their inputs. If this is an effect of a hierarchical increase in complexity along the visual pathways, we can expect insights from deep neural networks and the visual system to complement each other, as both show this hierarchical increase in complexity.

6.3 Retinal Data Analysis

Early on in the project, we approached the group of Tim Gollisch for a possible collaboration on the aging effects in retinal circuits. We had considered to add a 6-9 month data acquisition period to the thesis in which multi-electrode array (MEA) recordings could be performed on retinas of young and old mice to examine possible differences. Even though, robust evidence exists that the dendrites of bipolar-, horizontal- and ganglion cells in the retina reconfigure in mice and men (Eliasieh, Liets, and Chalupa 2007, Samuel et al. 2011), functional characterizations of these changes were very limited. Samuel et al. 2011 only confirmed that cells are still in principle functional and that direction selective cells still exist. A change in the dendritic tree would result in a change of receptive field, which Samuel et al. 2011 estimate as a 10% decrease for ganglion cells, which however might be compensated by a similar increase at the level of bipolar cells. The shift of receptive field integration from ganglion cells to bipolar cells can change the coding properties of retinal cells even without changing the overall extent of the receptive field, since then most of the spatial integration happens before rather than after the bipolar-amacrine-ganglion cell synapse non-linearity.

But examining these changes experimentally is not trivial since receptive field sizes vary between retinal ganglion cell types and with eccentricity. Since only a limited number of RGCs can be recorded in a single experiment using the proposed method of MEA recordings, a statistical analysis comparing cell populations from young and old animals require a certain number of experiments to be performed. We did a simulation of the Receptive Field

(RF) estimation procedure assuming an optimistic effect of 10 % Receptive Field (RF) size change and calculated the number of cells that had to be recorded for a certain likelihood of statistically significant results. Our conclusion in section 3.4.2.4 was that the number of experiments that needed to be performed would be too high to add the experimental data acquisition as a side-project to the thesis. Restricting the population of cells to a single type, eg. direction selective *RGCs*, would not alleviate this problem, since the decreased spread in possible receptive field size (which should make the comparison easier) is compensated by the decreased yield in analysable cells. MEAs are not able to target specific cells, rather the recorded cells have to be filtered by functional analysis to differentiate between cell types.

The experiments could still be carried out in the future. As the sole goal of a PhD thesis it might be feasible to record enough data. A more targetable recording technique might also improve the odds of finding a result, as would a technique that yields a larger number of recorded cells, eg. using larger MEAs or Calcium imaging. If no change in Receptive Field (RF) size is notable, single cell recordings and current injection into bipolar cells might be necessary, as was eg. done in Liu et al. 2017, to explore the changes in non-linearity. However, these experiments are very difficult to perform even on retinas of young animals and might be even more difficult if done on old animals.

While it is not clear if the change in RGC receptive fields can be characterized and whether it has a notable effect on retinal coding of different RGC types, the mechanisms that cause these changes are posing interesting questions in their own right. Is it possible that these changes are input-driven, eg. by a decay of photo-receptors? Are they a side effect of changes in Calcium buffering dynamics, similar to what is speculated in Ashok and Foster 2007 but in this case causing a proliferation rather than a depression of dendritic development? The answers to this questions can reveal the remodelling possibilities of the retina that could help in integrating iPCs or retinal implants to combat degenerative diseases such as RP, AMD and Stargardt.

6.4 Gain Control and Noise

Closely related to the VirtualRetina retina model, we investigated the interaction between gain control and noise. Gain control can emphasize or diminish the ratio between signal and noise, depending on the dynamic range that is projected onto the output range. Since gain control can be implemented by recurrent or lateral inhibition, our *inhibition hypothesis* would predict decreased gain control throughout the visual system which would result in a large repertoire of changes. However, a much simpler effect can be observed in the very early visual system: in the lateral geniculate nucleus (LGN) a number of pathways are separated which each have different properties. The magnocellular and parvocellular pathways both project to the visual cortex, however they carry complementary information (see 1.3.1). Of interest to us was foremost that the parvocellular pathway is more affected by aging (Bonnel, Mohand-Said, and Sahel 2003; Elliott and Werner 2010). This might suggest that a property of the magnocellular pathway is responsible for the increased resistance to aging. The magnocellular pathway is more heavily gain-controlled and can contain a spatial integration stage after the initial non-linearity. Both can work as anit-noise mechanisms, which fits well with our *input noise hypothesis*: If we assume that the only difference between young and old is an increase in receptor noise, we would expect that pathways featuring computations that

combat noise are more resistant to this change.

We created two iterations of simulations and analysis to validate the intuitive assumptions and to disentangle whether spatial integration or gain control has a greater effect on noise reduction.

The method we demonstrate in sections 3.5.2 and 3.5.3 to quantify the relation between input and output variability can be translated to other mechanisms as well that are assumed to affect the processing of noisy signals. Moving away from the distance-to-noise-free measure to the difference between noise induced and internal variability gives us the insight that both, The observation that with increasing noise level the output firing rate increases, similar as it does in response to an increase in contrast, leads us to the definition of a spiking difference that normalizes over firing rate.

The results from section 3.5.3 were computed with the `convis` implementation of contrast gain control rather than the VirtualRetina simulator used in section 3.5.2. The `convis` implementation made integrating the model into the analysis code easier, since no data had to be written to a file on disk.

The results leave some room for interpretation. Using the Victor-Purpura Distance (VPD), there is a large difference between non-gain-controlled and gain-controlled simulations in that non-gain-controlled show a larger noise induced variability than internal variability. The gain-controlled simulation shows almost the same values, indicating that for a constant noise level, all noise induced variability is masked by internal variability. However, if we control for firing rate by using a firing-rate independent distance measure (Figure **??**), the effect vanishes, i.e. the increase in variability was mostly due to the large increase in firing rate due to the increase in noise-induced contrast. Using this distance measure, the difference between gain-controlled simulations with and without spatial integration becomes more pronounced.

6.5 Receptive Fields Affecting Psychophysical Measurements

In this project, there are many avenues wide open for exploration. While we did test a range of numbers and sizes, the simulations were limited strongly for the smallest and largest sizes possible. In the visual system the size of receptive fields scales from minutes of arc, for acuities close to 30cpd, to tens of degrees with numbers of cells per visual area varying inversely to the size of receptive fields. From Brewer and Barton 2012 and other pRF studies, we know that cortical regions coding for the very high density areas of the visual field which would cover only 0.5 degree in young subjects, covers 4 times as much visual space in old subjects, more similar to more peripheral pRF. At the same time, the surface area that corresponds to the central 0.5 degree shrinks to a third of its size in aging[1]. The notes in section 2.3.1 about pRF still apply here, so the very central, high-resolution receptive fields might be masked in the change size of the population RFs and the underlying change for those cells might be even higher. In the project we laid out in section 4.7.1, we aimed to examine the whole spectrum of spatial frequencies visible to humans to compare the measures of internal noise and calculation efficiency with our models. But we could not emulate the spatial frequency spectrum adequately due to the constraints on image size and resolution: if we cover the high-spatial-frequency end, we have to increase the resolution, but to cover the low end, we have to increase the image size. Both scales together result in large demands

[1] see specifically Fig. 2 in Brewer and Barton 2012

for memory during the simulations and consequently, the simulations only cover very few cells per spatial frequency, as opposed to the large number of overlapping cells in the cortex. A method that circumvents this issue by appropriately adjusting resolution and noise strength by downscaling or cropping input images could extend the results to more appropriate number of neurons. Another option could be to investigate a single spatial frequency channel at a time, however this would remove effects of harmonics and interference between spatial frequency channels which could be an important factor that affects cells with high and low spatial frequency selectivity very differently. Reimplementing the pure Python code in `convis` can bring some improvement, since convolution is a more natural approach to simulating receptive fields over the whole visual space. The issues of image scale still plays a role for `convis`, requiring the same constraints as discussed before.

Another extension of this project, which has less to do with its method and more with the scientific scope, is to investigate the effect of lateral inhibition. We introduced the inhibition hypothesis in chapter 1 and listed evidence that inhibition is altered in high aging. Inhibition can function as a gain control, anti-noise mechanism, soft winner-take-all circuit and guide attention. We already included lateral inhibition in the model to enhance the cross-orientation suppression leading to a lower contrast threshold. But so far we did not include the parameter for lateral inhibition as an independent variable that can have an effect on EIN and CE. We did do preliminary simulations that showed lateral inhibition suppressing input noise up to a point where the recurrent part of the network becomes a stable attractor and no longer responds to changes in the input. The combination of all three variables can then be used to fit the characteristics of different points of the spatial-frequency spectrum in terms of contrast sensitivity (CS), CE and EIN. Since it is unlikely that lateral inhibition in the cortex would change heterogeneously, but systematically for different parts of the primary visual cortex, it should be noted that even with constant lateral inhibition profiles, which depend to some part on the physical cortical distance, a change in the spacing between cortical positions that code for certain visual positions will result in changes of lateral inhibition.

This project is far from concluded, which might seem unfortunate for this thesis, but we are certain that with the ground work laid in section 4.7.1, many changes in the visual system can be characterized more deeply than descriptive models used traditionally in psychophysics.

6.6 Further Applications of Convis

Convis proved to become a versatile tool that grew beyond it's original intended scope. As originally intended, it can replace VirtualRetina with a comparable model that offers more flexible spatio-temporal filters - at a cost of processing speed depending on the resolution used in the simulation. Further, we also implemented alternative retina and V1 models on a spectrum of simple to complex linear-nonlinear cascade models, including Convolutional Neural Networks such as the model discussed in Mcintosh et al. 2016. The collection of all of these diverse models in the same framework makes it easy for experimentalists to change from one model to another only by switching out the name of the instantiated model class. It is also a novel development that models meant primarily for data generation, such as VirtualRetina, and models used primarily to fit experimental data are provided in the same framework. This allows to generate synthetic data either from a model that provides high

level parameters (eg. the size of receptive fields) or from a model replicating the behaviour of a specific recorded cell. Conversely, both types of models can be fit to data more effectively than MonteCarlo methods or parameter grid searches. The architecture of the toolbox allows for automated differentiation for almost any type of processing which opens the door for a wide range of gradient based optimization methods - most of which are already implemented for the PyTorch ecosystem. This advance in the ability to rapidly fit any of a set of well established models using a wide range of gradient based optimisation routines in very few lines of code (see examples in section ref{sec:pytorch_extensions} for a three line example) helps with achieving results that are consistent with other research groups and avoid the danger of introducing reimplementation errors.

Evidence is emerging[2], that 1d convolutions might enable better performance than the much more complicated, but widely used Long Short Term Memory (LSTM)s. Convolution kernels are also more easily interpretable than LSTM parameters. Convis offers temporal convolutions of continuous video streams by adding an overlap between chunks that are computed separately. While other approaches such as Bai, Kolter, and Koltun 2018 use diluted convolution in a deep architecture, `convis` can combine simple recursive temporal filtering with convolution to achieve long history sizes with continuous, smooth convolution using a small amount of parameters (eg. with logarithmic temporal spacing) and a very small memory footprint of a memory single value per coefficient.

The discontinuities of spiking models are an inherent problem for their differentiability. Some tentative approaches exist that try to circumvent this problem by defining a proxy gradient that ignores discontinuity. These approaches make use of computational frameworks such as PyTorch just like convis. Still, most of these approaches use large batches of small sequences instead of the continuous processing that convis is based on. Convis is an ideal testbed for backpropagation in spiking models. Data generators for the neuromorphic MNIST task are included in the framework[3] and a range of spiking mechanisms are implemented in their forward pass, including a Leaky-Integrate-and-Fire model, random Poisson spiking, Hodgkin-Huxley, Fitz-Hugh Nagumo and the Izhikevich model. To our knowledge only the Leaky-Integrate-and-Fire model was so far integrated into Deep Spiking Networks (Deep Neural Networks which use spiking neurons and adapt either through STDP or backpropagation) and this was also the only model where attempts were made to create a custom backwards pass. Since some of the other models offer a richer temporal dynamic, they might have advantages for Deep Spiking Networks which were so far not explored by any research group.

6.7 Conclusions on Aging

In this thesis we demonstrated in a range of different simulations and considerations how fruitful the approach of following a minimal hypothesis can be. We started with the hypothesis that noise at the level of photoreceptors is increased in high age. We could relate this increase of input noise to an increase in Receptive Field (RF) size in a compensatory mechanism that only relies on the well established mechanism of STDP. We could explain the differential aging effects in the magnocellular and parvocellular pathways, even if we could

[2] see Bai, Kolter, and Koltun 2018 or http://www.offconvex.org/2018/07/27/approximating-recurrent/

[3] see https://jahuth.github.io/convis/docs_streams.html or search for 'MNIST' in the 'convis' documentation

not definitely conclude so far whether the increased noise resistance in the magnocellular pathway is due to gain control or spatial integration. In addition to this first hypothesis, we also tentatively discussed the consequences of changes in inhibitory circuits as well as plasticity mechanisms. Since evidence for each of these hypothesis exist, it is likely that these effects occur simultaneously and interact. Aging remains a complex phenomenon, but extracting possible cause-effect relations using theoretical tools as we have done here, can help in structuring our knowledge about this multifaceted process. In the earlier sections of this chapter we outlined possible future projects that can further deepen our understanding of the underlying mechanisms of aging. While we did not carry out an electro-physiological experiment, we estimated the effort that would go into a project like this from existing data and have prepared analysis methods to infer the size of receptive fields (spike triggered average (STA) or direct fitting with `convis`) as well as the temporal and stimulus related reliability, quantified as *mutual information*. A tool that was helpful in quickly setting up simulations and fitting procedures is the `convis` toolbox we developed during the project. It has numerous applications outside the discussed projects which we hope to evaluate in future studies as well.

Much still remains to be investigated, but using the right methods, some of which we hope to have presented in this thesis, understanding the neural basis of aging will become only an question of time.

References

Ashok, Kumar and Thomas C Foster (2007). "Neurophysiology of Old Neurons and Synapses". In: *Brain Aging: Models, Methods, and Mechanisms*, pp. 1–19. URL: http://www.ncbi.nlm.nih.gov/books/NBK3882/.

Bai, Shaojie, J. Zico Kolter, and Vladlen Koltun (2018). *An Empirical Evaluation of Generic Convolutional and Recurrent Networks for Sequence Modeling*. arXiv: 1803.01271 [cs.LG].

Bonnel, Sébastien, Saddek Mohand-Said, and José Alain Sahel (2003). "The aging of the retina". In: *Experimental Gerontology* 38.8, pp. 825–831. ISSN: 05315565. DOI: 10.1016/S0531-5565(03)00093-7.

Brewer, Alyssa a. and Brian Barton (2012). "Effects of healthy aging on human primary visual cortex". In: *Health* 04.09, pp. 695–702. ISSN: 1949-4998. DOI: 10.4236/health.2012.429109. URL: http://www.scirp.org/journal/PaperInformation.aspx?PaperID=23240.

Carandini, Matteo and David J Dj Heeger (2012). "Normalization as a canonical neural computation." In: *Nature Reviews Neuroscience* November, pp. 1–12. ISSN: 1471-003X. DOI: 10.1038/nrn3136. arXiv: NIHMS150003. URL: http://discovery.ucl.ac.uk/1332718/.

Eliasieh, Kasra, Lauren C. Liets, and Leo M. Chalupa (2007). "Cellular reorganization in the human retina during normal aging". In: *Investigative Ophthalmology and Visual Science* 48.6, pp. 2824–2830. ISSN: 01460404. DOI: 10.1167/iovs.06-1228.

Elliott, Sarah L and John S Werner (2010). "Age-related changes in contrast gain related to the M and P pathways." In: *Journal of vision* 10.4, pp. 4.1–15. ISSN: 1534-7362. DOI: 10.1167/9.8.1071.

Liu, Jian K. et al. (2017). "Inference of neuronal functional circuitry with spike-triggered non-negative matrix factorization". In: *Nature Communications* 8.1. ISSN: 20411723. DOI: 10.1038/s41467-017-00156-9. URL: http://dx.doi.org/10.1038/s41467-017-00156-9.

Mcintosh, Lane T et al. (2016). "Deep Learning Models of the Retinal Response to Natural Scenes". In: *Advances in Neural Information Processing Systems 29 (NIPS)* Nips, pp. 1–9.

Samuel, Melanie a. et al. (2011). "Age-Related Alterations in Neurons of the Mouse Retina". In: *Journal of Neuroscience* 31.44, pp. 16033–16044. ISSN: 0270-6474. DOI: 10.1523/JNEUROSCI.3580-11.2011.

Ziegler, David A. et al. (2010). "Cognition in healthy aging is related to regional white matter integrity, but not cortical thickness". In: *Neurobiology of Aging* 31.11, pp. 1912–1926. ISSN: 01974580. DOI: 10.1016/j.neurobiolaging.2008.10.015. URL: http://dx.doi.org/10.1016/j.neurobiolaging.2008.10.015.

Chapter 7

Appendix

Glossary

Adadelta

Gradient based optimization algorithm, see Zeiler 2012. 114

Adenosine Monophosphate (AMP)

The "uncharged" version of the energy molecules *ADP* and ATP. 127

Adenosine Triphosphate (ATP)

A molecule that provides energy for intracellular processes. When it is used up, it reverts to AMP. 127

After Hyper Polarization (AHP)

A depression of the membrane potential following neural activity. Section 1.8.3 discusses how this influences plasticity in aging. 19, 26

Age-related Macular Degeneration (AMD)

Age-related neurodegenerative disease that affects the centre of the retina. See Section 1.7.2.1. 23, 24, 122

AMP-activated protein kinase (AMPK)

A protein kinase that creates ATP. 18

Bipolar cell

A cell type in the retina that is bipolar cell. Section 3.2.1 gives an introduction to cells in the retina. 59

Calcium (Ca^{2+})

Calcium (Ca) is the 20th element of the periodic table. In cellular medium it acts primarily as the positively charged ion Ca^{2+}. 18–20, 44, 59

Calculation Efficiency (CE)

A constituent component of contrast sensitivity. See formula 4.1. 77–81, 89–92, 95, 119, 124

Cataract

see section 1.7.1.1. 21, 28

Contrast Sensitivity (CS)

1 over the contrast threshold (lowest contrast a subject is able to perceive). 13, 24, 77–79, 81, 86, 87, 90, 91, 124

Contrast Sensitivity Dunction (CSF)

The curve of contrast sensitivity (1/threshold) usually over the range of spatial frequencies. 77, 79–82, 89–91

Convis

A Python toolbox for creating convolutional vision models which I implemented during my PhD studies. 2, 6, 8, 65, 96, 98, 100, 102, 103, 105, 109, 110, 112, 113, 116, 117, 135, 138

convolutional neural network (CNN)

An architecture for neural networks that allows to process images very efficiently. 102

Cycles Per Degree (cpd)

a unit signifying the spatial extent of a stimulus in the visual field (independent of distance). 68, 77, 78, 80, 81, 89

Electroretinogram (ERG)

The response of the retina can be measured with an electrode attached near the eye. The recording is non-invasive and allows an analysis of photoreceptor and retinal health. 56

Equivalent Internal Noise (EIN)

A constituent component of contrast sensitivity. See formula 4.1. 78–81, 83, 89–92, 95, 119, 124

Firing-Rate Difference (FRD)

Spike train distance that consists of the difference in spikes (normalized by time). 50

Gabor Filter/Gabor Patch

A linear filter that is created by multiplying a spatial cosine wave with a Gaussian envelope. 50, 88

Lateral Geniculate Nucleus (LGN)

A neural hub in the brain stem that receives input from the optic nerve and outputs to the visual cortices. 34, 36, 47, 49, 64, 66, 70, 122, 128

Lateral Intra-Parietal cortex (LIP)

An area of the cerebral cortex involved in eye movements and working memory, located in the intraparietal sulcus. 83, 84

LBFGS optimization algorithm

The limited-memory Broyden – Fletcher – Goldfarb – Shanno optimization algorithm is a pseudo-Newton method that uses the curvature of the error surface to find the minimum of an error surface. 104, 108, 114–116

Long Short Term Memory (LSTM)

a recurrent deep learning method. 125

Long Term Depression (LTD)

a sustained weakening of a synaptic connection. 26, 29, 44

Long Term Potentiation (LTP)

a sustained strengthening of a synaptic connection, eg. caused by regular stimulation of a certain frequency. 26, 29, 44

Magnocellular Pathway

A pathway in the visual system that distinguishes itself from the parvocellular pathway in the lateral geniculate nucleus (LGN). See Sections 2.2.4 and 3.2.2.1. . 6, 8, 13, 34, 36, 38, 44, 45, 47, 49, 64–66, 74, 122, 125, 126, 128

Middle temporal visual area (V5 or MT)

An area of the extrastriate cortex of involved in vision, specifically in the perception of motion. 14, 40, 83, 84

Modulation Transfer Function (MTF)

The modulation transfer function describes the change in frequency spectrum before and after a filtering operation. 83, 86

Multi-Electrode Array (MEA)

a device used for recording many neurons simultaneously, eg. in the retina. *MEA*s can have between a few dozen to thousands of independent electrodes. 8, 23, 53, 58, 59, 61, 64, 121, 122

Non-Negative Matrix Factorization (NMF)

matrix factorization with the constraint that all factors are positive. 59, 64

outer plexiform layer (OPL)

The outer layer of the retina that houses the photoreceptors. 22, 48, 109

Parvocellular Pathway

A pathway in the visual system that distinguishes itself from the magnocellular pathway in the LGN. See Sections 2.2.4 and 3.2.2.1. . 6, 13, 34, 36, 38, 44, 47, 49, 64–67, 74, 122, 125, 128

Population Receptive Field (pRF)

A receptive field measured for a voxel, rather a specific cell. See section 2.3.1. 14, 39, 45, 120, 123

PyTorch

A computational library for Python, based on Torch, that is used among other applications for DeepLearning. 7, 96, 98, 112, 117

Reactive Oxygen Species (ROS)

A family of molecules that contain oxygen and are highly reactive (see Section 1.5.2). 18

Receptive Field (RF)

A portion of the sensory space that elicits a response in a neurons. 22, 30, 34–36, 38–42, 44, 57, 59–63, 89, 102, 105, 108, 119, 121, 122, 125

Retinal Pigment Epithelium (RPE)

A cell layer of the retina that (among other functions) supplies the photoreceptors with nutrients and is closely linked to photoreceptor health. 22, 23, 48, 58

Retinitis Pigmentosa (RP)

Neurodegenerative disease that affects the periphery of the retina. See Section 1.7.2.2. 23, 24, 122

RGC

Retinal Ganglion Cell. Section 3.2.1 gives an introduction to cells in the retina. 8, 22, 24, 47, 49, 56–59, 61, 63, 64, 66, 108, 110, 117, 119, 121, 122

Saccade

A rapid eye movement. 83

signal-to-noise-ratio (SNR)

The ratio of signal strength relative to the strength of the noise competing with the signal. 28, 30, 34, 64, 84, 91, 92, 95

Spike Triggered Average (STA)

a method to estimate the receptive field of a neuron by averaging over all stimuli that elicited a spike. 59, 61, 64, 126

Spike Triggered Covariance (STC)

a method to estimate the receptive field of a neuron by averaging over the cross-correlations of each stimuli that elicited a spike. 59

Stargardt Macular Distrophy

Neurodegenerative disease that affects the centre of the retina. See Section 1.7.2.1. 23, 24, 122

STDP

A plasticity mechanism that modifies synaptic weights according to the relative delays at which spikes are received and emitted. 2, 6, 30, 34, 41, 45, 119, 125, 133

Stochastic Gradient Descent (SGD)

A simple optimization algorithm using random motion to avoid local minima. 112–115

Superior Colliculus (SC)

A part of the mid brain that (among others) controls saccadic eye movements. 49

Theano

A computational library for Python that is used among other applications for DeepLearning. 97, 98

VanRossum Distance

A spike distance defined in Rossum 2001. 51, 52

VEP

visual evoked potential. 14, 39

Victor-Purpura Distance

Victor-Purpura Distance. 51, 52, 68, 70–73, 123

VirtualRetina

The VirtualRetina retina simulator described in Wohrer 2008. 65, 96, 97, 102, 106, 108–110, 122, 123

7.1 Extended Table of Age Ranges

Table 7.1: Age limits of different species of a selection of scientific studies that separate subjects into young and old groups (and optionally an intermediate group). Another table lists correlation studies that have more than three or no age groups (Table 7.2). X-Y: range from X to Y, X +/- Y: mean of X with standard deviation Y.

Animal	Young Age	Intermediate	Old age	Study
Human	(years)	(years)	(years)	
	26-35	36-45	45-60	Brozek and Keys 1945
			54 - 79	Friede 1962
	18-28		64-81	Salthouse and Somberg 1982
	20-29		53-77	Schlotterer, Moscovitch, and Crapper-McLachlan 1983
	18-28		62-72	Ball and Sekuler 1986
	18-30		59-76	Cremer and Zeef 1987
	21-27		66-77	Goggin and Stelmach 1990
	18-33	41-63	66-91	Stevens 1992
	18-23		62-83	Gilmore et al. 1992 (1)
	17-23		63-91	Gilmore et al. 1992 (2)
	23 +/- 6		72 +/- 7.5	Porciatti et al. 1992
	20-33	37-61	65-84	Huaman and Sharpe 1993
	18-28		60-74	Kramer et al. 1994
	17-27		55 to 90	Stuart et al. 2003
	17-27		55 to 90	Stuart et al. 2003
	mean 23		mean 66	Riecker et al. 2006
	19-25	65-72	76-92	Poliakoff et al. 2006
			74.4 +/- 5.6	Kalisch, Tegenthoff, and Dinse 2008
	19-25		64 - 82	Elliott and Werner 2010
	mean 30		mean 66	Sebastián and Ballesteros 2012
	21 +/- 1.83		69.53 +/-4.05	Bernard and Seidler 2012
			60-94	Kattenstroth et al. 2013
	20-33		60-82	Cheng and Lin 2013
	20-40	40-60	60-90	Heise et al. 2013

Animal	Young Age	Intermediate	Old age	Study
	20-29		65-76	Allard et al. 2013
	22-36		66-95	Strömmer, Tarkka, and Astikainen 2014
Monkey	(years)	(years)	(years)	
- Rhesus Monkey	5 - 16		25-28	Spear et al. 1994
	6-15.2		17.5-26.5	Koo et al. 2012
		21-22	28-32	Yu 2005; Wang et al. 2005
	5-13		21-26	Luebke et al. 2015
Mouse				
- C57BL/6J	40 weeks		100 weeks	Zerweck, Mitchell, and Anthony 1981
Rat	(months)	(months)	(months)	
- Long Evans rats			20	Connor and Diamond 1982:
- BN TNO/IVEG	5		33-35	Fliers, De Vries, and Swaab 1985
- WAG/Rij	3	19	25	Ravid et al. 1987 (Pilot)
- BN/BiRij	3 and 7		32-33	Ravid et al. 1987
- BN/BiRij	7-8		32-32	Van Gool et al. 1987
- FBNF1 hybrid	4-7		27-32	Hickmott and Dinse 2013
Aplysia californica			>240 days	Zolman and Peretz 1987

Table 7.2: Age range of a selection of correlation studies (human subjects, age in years). For studies that include group analyses, we included the number of groups as well as the range of the oldest group in the analysis.

Minimum	Number of groups (age span)	Highest age group	Maximum	Study
18	4 groups (7 years)	45-60	60	Brozek and Keys 1945
7	17 groups (4 years)	87-91	91	Misiak 1951
20	6 groups (10 years)	70-79	79	Coppinger 1955
	2 groups (>50, <50)	50-80	80	Sokol, Moskowitz, and Towle 1981
4	(every 7 years)		90	Snyder, Dustman, and Shearer 1981
19			87	Owsley, Sekuler, and Siemsen 1983

Minimum	Number of groups (age span)	Highest age group	Maximum	Study
15			89	Morrison and McGrath 1985
24			100	Terry, DeTeresa, and Hansen 1987
22	4 groups (20 years)	80-92	92	Kline et al. 1992
19			84	Tobimatsu et al. 1993
6		61-80	80	Emmerson-Hanover et al. 1994

7.2 Additional Results For Receptive Field Increase Due To Noise

In section 2.6.1 we show that spike-time dependent plasticity (STDP) can enlarge receptive fields in response to jittered input. To show that this effect is not dependent on the specific parameters of the simulation we show other parameter constellations. We varied each parameter and took the difference of the number of weights < 0.01 of a low noise (0.5ms jitter) and high noise (100ms jitter) simulation.

At multiple points the plots cross 0, showing that in that specific simulation there is no decrease in small weights: When the firing rate of the pattern (*p_pattern*) is too low or the firing rate of the poisson neurons (*p_poisson*) is too high, there is no difference between the jittered and unjittered patterns, resulting in similar weight distributions. More interesting is the effect of high *taupre* or low *taupost*, which both abolish the difference between high and low jitter: When *taupre* is larger than 30ms or *taupost* is 10ms (all other time constants being 20ms), the mechanism is biased towards facilitation, so all weights are driven to high values, leaving no weights < 0.01. The inhibition parameter also seems crucial, but that effect is only related to the firing rates of the simulation.

Table 7.3: Parameters of STDP simulations

	E 10	E 11	E 12
fr p pattern	5%	5%	10%
fr p noise	5%	5%	0%
taupre	40ms	60ms	20ms
taupost	40ms	10ms	20ms

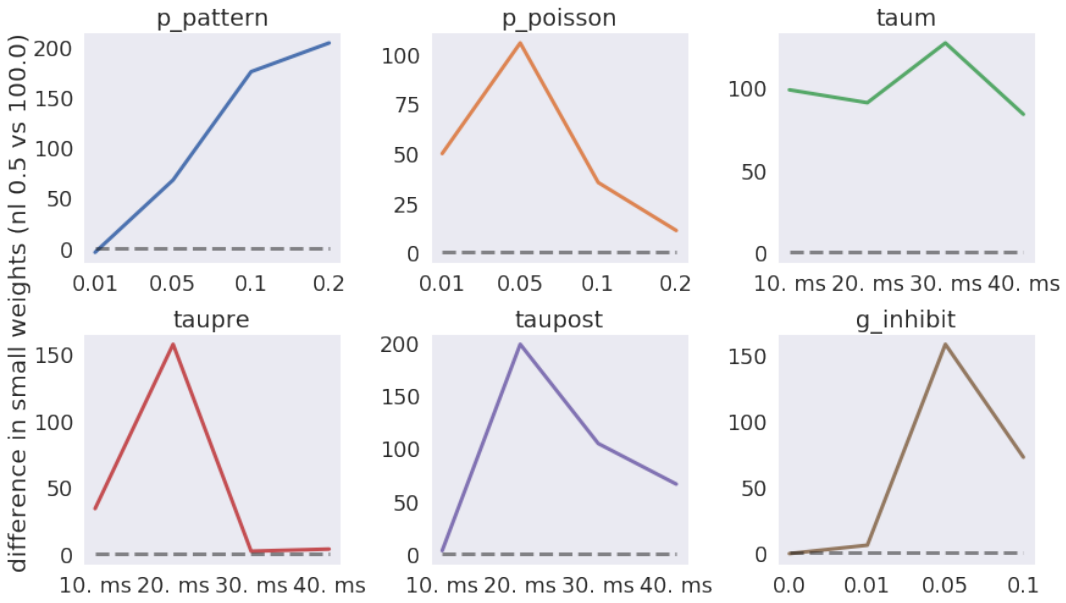

Figure 7.2.1: **Parameter Exploration**

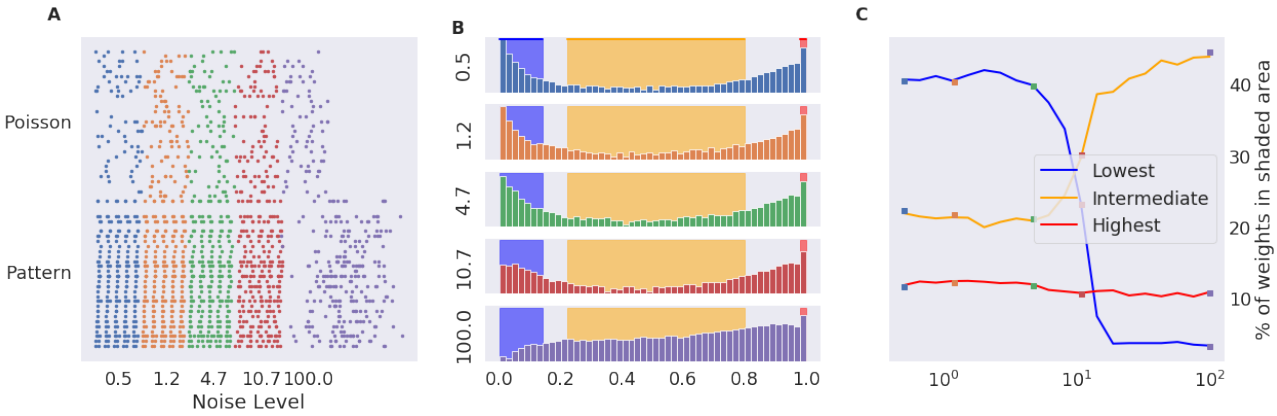

Figure 7.2.2: **Experiment with plasticity bias:** Using longer time constants for presynaptic spikes, the effect gets even more pronounced. **A**: raster plot of different noise levels, **B** histogram of weights. **C** number of weights in the coloured areas in C.

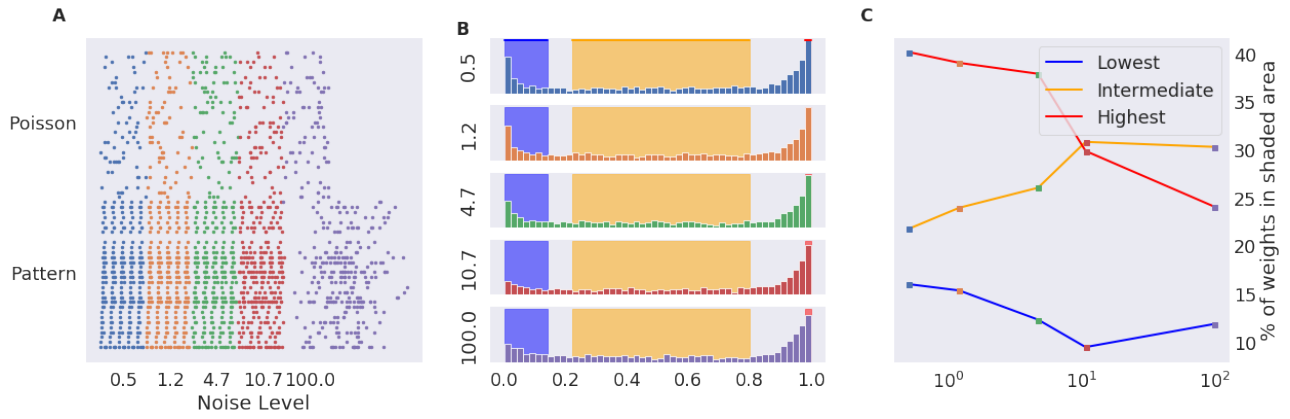

Figure 7.2.3: **Experiment with symmetric plasticity** and long time constants. The simulation is very similar to the one discussed in section 2.6.1.2.

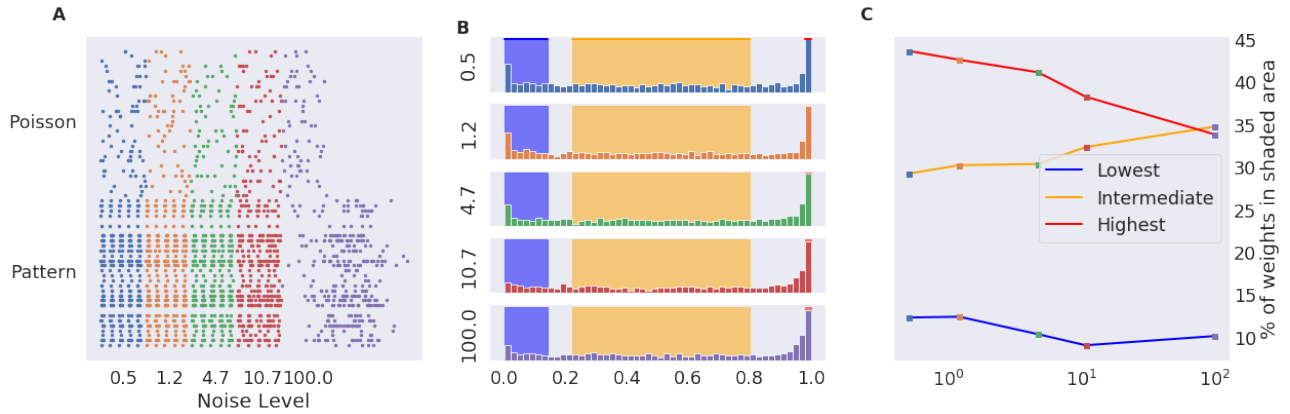

Figure 7.2.4: **Experiment with stronger pattern and decreased, symmetric time constants** the increased firing rate of the pattern is compensated by a decrease in noise spikes. Overall, less non-zero weights are generated compared to the other experiments, but a decrease is still notable.

7.3 Convis: McIntosh Model

This code fully implements the convolutional retina model from Mcintosh et al. 2016 in `convis`. The model is also included in the toolbox as `convis.models.McIntosh`.

```
class McIntosh(Layer):
    """
        Convolutional Retina Model
        Contains two convolutional layers and one readout layer.
        The first convolutional layer has 8 channels.
        The second convolutional layer has 16 channels.
        The readout is a linear combination over all space
        and all channels of layer 2, resulting in 'out_channels'
        many output channels.
        To set the weights individually::
            m = convis.models.McIntosh(out_channels=5)
```

```
        m.layer1.set_weight(np.random.randn(8,1,20,10,10))
        # mapping from 1 to 8 channels
        m.layer2.set_weight(np.random.randn(16,8,10,50,50))
        # mapping from 8 to 16 channels
        # the readout needs some number of outputs
        # and 16 x the number of pixels of the image as inputs
        m.readout.set_weight(np.random.randn(5,16*input.shape[-2]
                                             *input.shape[-1]))
        # plotting the parameters:
        m.plot()
    [1] Mcintosh, L. T., Maheswaranathan, N., Nayebi, A., Ganguli, S.,
    & Baccus, S. A. (2016). Deep Learning Models of the Retinal Response
    to Natural Scenes. Advances in Neural Information Processing Systems
    29 (NIPS), (Nips), 1-9. Also: arXiv:1702.01825 [q-bio.NC]
"""
verbose = False
def __init__(self,filter_size=(10,5,5), random_init=True, out_channels=1,
             filter_2_size=(1,1,1), layer1_channels = 8,layer2_channels = 16):
    super(McIntosh,self).__init__()
    layer1 = Conv3d(1,layer1_channels,filter_size,time_pad=True,autopad=True)
    self.add_module('layer1',layer1)
    self.layer1.set_weight(1.0,normalize=True)
    if random_init:
        self.layer1.set_weight(np.random.rand(
                                    layer1_channels,
                                    1,
                                    filter_size[0],
                                    filter_size[1],
                                    filter_size[2]
                                ), normalize=True)
    layer2 = Conv3d(layer1_channels,
                    layer2_channels,
                    filter_2_size,
                    time_pad=True,
                    autopad=True)
    self.add_module('layer2',layer2)
    self.layer2.set_weight(1.0,normalize=True)
    if random_init:
        self.layer2.set_weight(np.random.rand(
                        layer2_channels,
                        layer1_channels,
                        filter_2_size[0],
                        filter_2_size[1],
                        filter_2_size[2]
                    ), normalize=True)
    self.readout = torch.nn.Linear(1,out_channels,bias=False)
def forward(self, the_input):
    a = torch.nn.functional.relu(self.layer1(the_input))
    a = torch.nn.functional.relu(self.layer2(a))
```

```
        self._last_processed_image = a.size()
        # The readout should consider all channels and all locations
        # so we need to reshape the Tensor such that the 4th dimension
        # contains dimensions 1,3 and 4
        #  - moving dimension 3 to 4:
        a = torch.cat(a.split(1,dim=3),dim=4)
        #  - moving dimension 1 to 4:
        a = torch.cat(a.split(1,dim=1),dim=4)
        if self.readout.weight.size()[-1] != a.size()[-1]:
            if self.verbose:
                print('Resetting weight')
            if self._use_cuda:
                self.readout.weight = torch.nn.Parameter(
                    torch.ones((self.readout.weight.size()[0],a.size()[-1])))
                self.readout.cuda()
            else:
                self.readout.weight = torch.nn.Parameter(
                    torch.ones((self.readout.weight.size()[0],a.size()[-1])))
        a = self.readout(a)
        return a
```

7.3.1 Convis: Rowekamp Model

This code implements the quadratic-convolutional V2 model from Mcintosh et al. 2016 in convis.

```
class V2(convis.base.Layer):
    """
        V2 model From Rowekamp & Sharpee 2017
        doi: 10.1038/ncomms15739
    """
    def __init__(self,
                 im_shape=(20,20),
                 subunit_shape=(16,16),
                 delays=[0,1,2,3,4,5,6,7,8,9]):
        self.dims = 5
        super(V2, self).__init__()
        self.subunit_shape = subunit_shape
        self.subunit_len = np.prod(subunit_shape)
        self.a1 = Parameter(0.0,doc="")
        self.a2 = Parameter(0.0)
        self.d = Parameter(1.0)
        self.v = Parameter(np.random.rand(*(subunit_shape)))
        self.J = Parameter(1.0*(np.random.rand(*(
                    np.prod(subunit_shape),np.prod(subunit_shape)))<0.01))
        self.subunit_weight = Parameter(np.ones((10,5,5)))
        self.delay = []
        for d in delays:
            self.delay.append(convis.filters.Delay(delay=d))
    def forward(self, inp):
        sub_unit_responses = []
        x_positions = inp.shape[-2]-self.subunit_shape[0]+1
        y_positions = inp.shape[-1]-self.subunit_shape[1]+1
        if self.subunit_weight.shape == (1,1,1):
            self.subunit_weight.set(np.ones((len(self.delay),
                x_positions,y_positions)))
        for t in range(len(self.delay)):
            t_inp = self.delay[t](inp)
            for x_pos in range(x_positions):
                for y_pos in range(y_positions):
                    x = t_inp[:,:,:,
                              x_pos:x_pos+self.subunit_shape[0],
                              y_pos:y_pos+self.subunit_shape[1]
                             ].contiguous()
                    x_flat = x.view(x.size()[0],
                                    x.size()[1],
                                    x.size()[2],
                                    self.subunit_len)
                    y = ((self.v[None,None,None,:,:] * x).sum(-1).sum(-1)
                        + torch.mul(
                            x_flat,torch.matmul(x_flat,self.J)
```

```
                    ).sum(-1)+self.a1)
                sub_unit_responses.append(sigmoid(y))
        sub_unit_responses = torch.mul(
            self.subunit_weight.view(self.subunit_weight.size()[0]*
                        self.subunit_weight.size()[1]*
                        self.subunit_weight.size()[2]).contiguous()[:,None,None],
                torch.cat(sub_unit_responses,dim=0))+self.a2
        r = torch.sum(sub_unit_responses,dim=0)[None,:,:,None,None]
        return self.d*softplus(r)
```

The code that is required to fit this model to data contains the steps to initialize the parameters, load the data, choosing an optimizer and calling `optimize`:

```
centered_stimulus = np.load('e0040.p1.stimulus.centered.npz').items()[0][1]
psth = np.load('e0040.p1.psth.npz').items()[0][1]
psth[np.isnan(psth)] = 0.0

v = V2(delays=np.arange(10))
v.p.J.set(0.0*np.ones((256,256)))
v.p.v.set(np.zeros((16,16)))
v.p.subunit_weight.set(np.ones((10,5,5)))
loss_func = lambda x,y: torch.nn.functional.poisson_nll_loss(x,y,log_input=False)
v.set_optimizer.LBFGS()
t_init = np.random.randint(5000)
loss = v.optimize(centered_stimulus[t_init:6000][:-1],
                  1.0*psth[t_init:6000][1:,None,None],
                  dt=200,
                  loss_fn=loss_func)
```

References

Allard, Rémy et al. (2013). "Contrast sensitivity, healthy aging and noise." In: *Vision research* 92, pp. 47–52. ISSN: 1878-5646. DOI: 10.1016/j.visres.2013.09.004. URL: http://www.ncbi.nlm.nih.gov/pubmed/24070688.

Ball, K and R Sekuler (1986). "Improving visual perception in older observers." In: *Journal of gerontology* 41.2, pp. 176–182. ISSN: 0022-1422 (Print)0022-1422. DOI: 10.1093/geronj/41.2.176.

Bernard, Jessica A. and Rachael D. Seidler (2012). "Evidence for motor cortex dedifferentiation in older adults". In: *Neurobiology of Aging* 33.9, pp. 1890–1899. ISSN: 01974580. DOI: 10.1016/j.neurobiolaging.2011.06.021. URL: http://dx.doi.org/10.1016/j.neurobiolaging.2011.06.021.

Brozek, J. and A. Keys (1945). "Changes in flicker-fusion frequency with age." In: *Journal of Consulting Psychology* 9.2, pp. 87–90. ISSN: 0095-8891. DOI: 10.1037/h0053488. URL: http://content.apa.org/journals/ccp/9/2/87.

Cheng, Chia Hsiung and Yung Yang Lin (2013). "Aging-related decline in somatosensory inhibition of the human cerebral cortex". In: *Experimental Brain Research* 226.1, pp. 145–152. ISSN: 00144819. DOI: 10.1007/s00221-013-3420-9.

Connor, James R. and Marian C. Diamond (1982). "A Comparison of dendritic spine number and type on pyramidal neurons of the visual cortex of old adult rats from social or isolated environments". In: *Journal of Comparative Neurology* 210.1, pp. 99–106. ISSN: 10969861. DOI: 10.1002/cne.902100111.

Coppinger, N W (1955). "The relationship between critical flicker frequency and chronologic age for varying levels of stimulus brightness." In: *Journal of gerontology* 10.1, pp. 48–52. ISSN: 0022-1422.

Cremer, R and E J Zeef (1987). "What kind of noise increases with age?" In: *Journal of gerontology* 42.5, pp. 515–518. ISSN: 0022-1422.

Elliott, Sarah L and John S Werner (2010). "Age-related changes in contrast gain related to the M and P pathways." In: *Journal of vision* 10.4, pp. 4.1–15. ISSN: 1534-7362. DOI: 10.1167/9.8.1071.

Emmerson-Hanover, R. et al. (1994). "Pattern reversal evoked potentials: Gender differences and age-related changes in amplitude and latency". In: *Electroencephalography and Clinical Neurophysiology - Evoked Potentials* 92.2, pp. 93–101. ISSN: 01685597. DOI: 10.1016/0168-5597(94)90049-3.

Fliers, E., G.J. De Vries, and D.F. Swaab (1985). "Changes with aging in the vasopressin and oxytocin innervation of the rat brain". In: *Brain Research* 348.1, pp. 1–8. ISSN: 00068993. DOI: 10.1016/0006-8993(85)90351-8. URL: http://linkinghub.elsevier.com/retrieve/pii/0006899385903518.

Friede, Reinhard L. (1962). "The relation of the formation of lipofuscin to the distribution of oxidative enzymes in the human brain". In: *Acta Neuropathologica* 2.2, pp. 113–125. ISSN: 00016322. DOI: 10.1007/BF00685170.

Gilmore, G C et al. (1992). "Motion perception and aging." In: *Psychology and aging* 7.4, pp. 654–660. ISSN: 0882-7974. DOI: 10.1037/0882-7974.7.4.654.

Goggin, Noreen L. and George E. Stelmach (1990). "Age-Related Differences in a Kinematic Analysis of Precued Movements". In: *Canadian Journal on Aging / La Revue canadienne du vieillissement* 9.4, pp. 371–385. ISSN: 17101107. DOI: 10.1017/S0714980800007480.

Heise, K.-F. et al. (2013). "The Aging Motor System as a Model for Plastic Changes of GABA-Mediated Intracortical Inhibition and Their Behavioral Relevance". In: *Journal of Neuroscience* 33.21, pp. 9039–9049. ISSN: 0270-6474. DOI: 10.1523/JNEUROSCI.4094-12.2013. URL: http://www.jneurosci.org/cgi/doi/10.1523/JNEUROSCI.4094-12.2013.

Hickmott, Peter and Hubert Dinse (2013). "Effects of aging on properties of the local circuit in rat primary somatosensory cortex (S1) in vitro". In: *Cerebral Cortex* 23.10, pp. 2500–2513. ISSN: 10473211. DOI: 10.1093/cercor/bhs248.

Huaman, a. G. and J. a. Sharpe (1993). "Vertical saccades in senescence". In: *Investigative Ophthalmology and Visual Science* 34.8, pp. 2588–2595. ISSN: 01460404.

Kalisch, Tobias, Martin Tegenthoff, and Hubert R. Dinse (2008). "Improvement of sensorimotor functions in old age by passive sensory stimulation". In: *Clinical Interventions in Aging* 3.4, pp. 673–690. ISSN: 11769092. DOI: 10.2144/000113917.

Kattenstroth, Jan Christoph et al. (2013). "Six months of dance intervention enhances postural, sensorimotor, and cognitive performance in elderly without affecting cardiorespiratory functions". In: *Frontiers in Aging Neuroscience* 5.FEB, pp. 1–16. ISSN: 16634365. DOI: 10.3389/fnagi.2013.00005. arXiv: fnagi.2013.00005 [10.3389].

Kline, D W et al. (1992). "Vision, aging, and driving: the problems of older drivers." In: *Journal of gerontology* 47.1, P27–P34. ISSN: 0022-1422. DOI: 10.1093/geronj/47.1.P27.

Koo, Bang Bon et al. (2012). "Age-related effects on cortical thickness patterns of the Rhesus monkey brain". In: *Neurobiology of Aging* 33.1, 200.e23–200.e31. ISSN: 01974580. DOI: 10.1016/j.neurobiolaging.2010.07.010. URL: http://dx.doi.org/10.1016/j.neurobiolaging.2010.07.010.

Kramer, a F et al. (1994). "Aging and inhibition: beyond a unitary view of inhibitory processing in attention." In: *Psychology and aging* 9.4, pp. 491–512. ISSN: 0882-7974. DOI: 10.1037/0882-7974.9.4.491.

Luebke, Jennifer I. et al. (2015). "Age-related changes to layer 3 pyramidal cells in the rhesus monkey visual cortex". In: *Cerebral Cortex* 25.6, pp. 1454–1468. ISSN: 14602199. DOI: 10.1093/cercor/bht336.

Mcintosh, Lane T et al. (2016). "Deep Learning Models of the Retinal Response to Natural Scenes". In: *Advances in Neural Information Processing Systems 29 (NIPS)* Nips, pp. 1–9.

Misiak, H. (1951). "The Decrease of Critical Flicker Frequency with Age". In: *Science* 113.2941, pp. 551–552. ISSN: 0036-8075. DOI: 10.1126/science.113.2941.551. URL: http://www.sciencemag.org/cgi/doi/10.1126/science.113.2941.551%20http://www.ncbi.nlm.nih.gov/pubmed/14834857.

Morrison, J D and C McGrath (1985). "Assessment of the optical contributions to the age-related deterioration in vision." In: *Quarterly Journal of Experimental Psychologyhysiology* 70, pp. 249–269. ISSN: 0144-8757.

Owsley, Cynthia Cyxthia, Robert Sekuler, and Dennis Siemsen (1983). "Contrast sensitivity throughout adulthood". In: *Vision research* 23.7, pp. 689–699. URL: http://www.sciencedirect.com/science/article/pii/0042698983902109.

Poliakoff, E. et al. (2006). "Vision and touch in ageing: Crossmodal selective attention and visuotactile spatial interactions". In: *Neuropsychologia* 44.4, pp. 507–517. ISSN: 00283932. DOI: 10.1016/j.neuropsychologia.2005.07.004.

Porciatti, V et al. (1992). "The effects of aging on the pattern electroretinogram and visual evoked potential in humans." In: *Vision research* 32.7, pp. 1199–1209. ISSN: 0042-6989.

Ravid, R. et al. (1987). "Changes in Vasopressin and Testosterone in the Senescent Brown-Norway (BN/BiRij) Rat". In: *Gerontology* 33.2, pp. 87–98. ISSN: 1423-0003. DOI: 10.1159/000212858. URL: https://www.karger.com/Article/FullText/212858.

Riecker, Axel et al. (2006). "Functional significance of age-related differences in motor activation patterns". In: *NeuroImage* 32.3, pp. 1345–1354. ISSN: 10538119. DOI: 10.1016/j.neuroimage.2006.05.021.

Rossum, M C van (2001). "A novel spike distance." In: *Neural computation* 13.4, pp. 751–763. ISSN: 0899-7667. DOI: 10.1162/089976601300014321.

Salthouse, T. A. and B. L. Somberg (1982). "Isolating the age deficit in speeded performance". In: *Journals of Gerontology* 37.1, pp. 59–63. ISSN: 00221422. DOI: 10.1093/geronj/37.1.59.

Schlotterer, G, M Moscovitch, and D Crapper-McLachlan (1983). "Visual processing deficits as assessed by spatial frequency contrast sensitivity and backward masking in normal ageing and Alzheimer's disease". In: *Brain*, pp. 309–324. URL: http://brain.oxfordjournals.org/content/107/1/309.short.

Sebastián, Manuel and Soledad Ballesteros (2012). "Effects of normal aging on event-related potentials and oscillatory brain activity during a haptic repetition priming task". In: *NeuroImage* 60.1, pp. 7–20. ISSN: 10538119. DOI: 10.1016/j.neuroimage.2011.11.060. URL: http://dx.doi.org/10.1016/j.neuroimage.2011.11.060.

Snyder, E. W., R. E. Dustman, and D. E. Shearer (1981). "Pattern reversal evoked potential amplitudes: Life span changes". In: *Electroencephalography and Clinical Neurophysiology* 52.5, pp. 429–434. ISSN: 00134694. DOI: 10.1016/0013-4694(81)90026-2.

Sokol, S, a Moskowitz, and V.L Towle (1981). "Age-related changes in the latency of the visual evoked potential: Influences of check size". In: *Electroencephalography and Clinical Neurophysiology* 51.5, pp. 559–562. ISSN: 00134694. DOI: 10.1016/0013-4694(81)90232-7.

Spear, P. D. et al. (1994). "Effects of aging on the primate visual system: spatial and temporal processing by lateral geniculate neurons in young adult and old rhesus monkeys". In: *Journal of Neurophysiology* 72.1, pp. 402–420. ISSN: 0022-3077. DOI: 10.1152/jn.1994.72.1.402. URL: http://www.physiology.org/doi/10.1152/jn.1994.72.1.402.

Stevens, J. C. (1992). "Aging and spatial acuity of touch". In: *Journals of Gerontology* 47.1, pp. 35–40. ISSN: 00221422. DOI: 10.1093/geronj/47.1.P35.

Strömmer, Juho M., Ina M. Tarkka, and Piia Astikainen (2014). "Somatosensory mismatch response in young and elderly adults". In: *Frontiers in Aging Neuroscience* 6.OCT, pp. 1–9. ISSN: 16634365. DOI: 10.3389/fnagi.2014.00293.

Stuart, Meg et al. (2003). "Effects of aging on vibration detection thresholds at various body regions". In: *BMC Geriatrics* 3, pp. 1–10. ISSN: 14712318. DOI: 10.1186/1471-2318-3-1.

Terry, Robert D., Richard DeTeresa, and Lawrence A. Hansen (1987). "Neocortical cell counts in normal human adult aging". In: *Annals of Neurology* 21.6, pp. 530–539. ISSN: 15318249. DOI: 10.1002/ana.410210603.

Tobimatsu, Shozo et al. (1993). "Age-related changes in pattern visual evoked potentials : differential effects of luminance , contrast and check size". In: 88, pp. 12–19.

Van Gool, W.A. et al. (1987). "Effect of housing in an enriched environment on the size of the cerebral cortex in young and old rats". In: *Experimental Neurology* 96.1, pp. 225–232. ISSN: 00144886. DOI: 10.1016/0014-4886(87)90185-3. URL: http://www.ncbi.nlm.nih.gov/pubmed/7269789%20http://linkinghub.elsevier.com/retrieve/pii/0014488687901853.

Wang, Yongchang et al. (2005). "Degradation of signal timing in cortical areas V1 and V2 of senescent monkeys." In: *Cerebral cortex (New York, N.Y. : 1991)* 15.4, pp. 403–8. ISSN: 1047-3211. DOI: 10.1093/cercor/bhh143. URL: http://www.ncbi.nlm.nih.gov/pubmed/15749984.

Wohrer, Adrien (2008). "Model and large-scale simulator of a biological retina, with contrast gain control". PhD Thesis. University of Nice-Sophia Antipolis.

Yu, Shan (2005). "Effects of age on latency and variability of visual response in monkeys". In: *Chin Sci Bull* 50.11, pp. 1163–1165. ISSN: 1001-6538. DOI: 10.1360/982005-572. URL: http://219.238.6.200/article?code=982005-572%7B%5C&%7Djccode=98.

Zeiler, Matthew D. (2012). "ADADELTA: An Adaptive Learning Rate Method". In: ISSN: 09252312. DOI: http://doi.acm.org.ezproxy.lib.ucf.edu/10.1145/1830483.1830503. arXiv: 1212.5701. URL: http://arxiv.org/abs/1212.5701.

Zerweck, Charles R., Robert B. Mitchell, and Adam Anthony (1981). "Age-related changes in brain RNA of noise stressed mice". In: *Neurobiology of Aging* 2.2, pp. 143–147. ISSN: 01974580. DOI: 10.1016/0197-4580(81)90012-9.

Zolman, James F and Bertram Peretz (1987). "Motor neuronal function in old Aplysia is improved by long-term stimulation of the siphon/gill reflex." In: *Behavioral neuroscience* 101.4, p. 524.